ADA 274 931

REPORT DOCUMENTATION PAGE

Form Approved
OMB No. 0704-0188

1. AGENCY USE ONLY (Leave blank)	2. REPORT DATE	3. REPORT TYPE AND DATES COVERED
	August 1993	Final Report: August 87-September 1989

4. TITLE AND SUBTITLE A Site Characterization Methodology for Aquifers in Support of Bioreclamation Activities Volume II. Borehole Flowmeter Technique, Tracer Tests, Geostatistics and Geology

5. FUNDING NUMBERS
MIPR N88-28
N88-54, N88-79
TVA CONTRACT TV-72467A

6. AUTHOR(S)

Steven C. Young

7. PERFORMING ORGANIZATION NAME(S) AND ADDRESS(ES)

Tennessee Valley Authority
Engineering Labcratory
P. O. Drawer E.
Norris, TN 37828

8. PERFORMING ORGANIZATION REPORT NUMBER

TVA Engineering Laboratory
WR 28-3-520-142

9. SPONSORING/MONITORING AGENCY NAME(S) AND ADDRESS(ES)

Air Force Engineering and Services Center
Engineering and Services Laboratory
Tyndall Air Force Base, Florida 32405

10. SPONSORING/MONITORING AGENCY REPORT NUMBER

ESL-TR-90-19

11. SUPPLEMENTARY NOTES

Air Force Project Officer: Bruce Nielsen

12a. DISTRIBUTION/AVAILABILITY STATEMENT

Approved for Public Release. Distribution Unlimited

12b. DISTRIBUTION CODE

A

13. ABSTRACT *(Maximum 200 words)*

This report discusses a field demcnstration of a methodology for characterizing an aquifer's geohydrology in the detail required to design an optimum network of wells and/or infiltration galleries for bioreclamation systems. The project work was conducted on a 1-hectare test site at Columbus AFB, Mississippi. The technical report is divided into two volumes. Volume I describes the test site and the well network, the assumptions, and the application of equations that define groundwater flow to a well, the results of three large-scale aquifer tests, and the results of 160 single-pump tests. Volume II describes the bore hole flowmeter tests, the tracer tests, the geological investigations, the geostatistical analysis and the guidelines for using groundwater models to design bioreclamation systems.

14. SUBJECT TERMS	15. NUMBER OF PAGES
Site Characterization, Hydraulic Conductivity, Groundwater Flow, Geostatistics, Geohydrology, Monitoring Wells	227
	16. PRICE CODE

17. SECURITY CLASSIFICATION OF REPORT	18. SECURITY CLASSIFICATION OF THIS PAGE	19. SECURITY CLASSIFICATION OF ABSTRACT	20. LIMITATION OF ABSTRACT
U	U	U	Unlimited

(The reverse of this page is blank.)

EXECUTIVE SUMMARY

In order to successfully provide aquifer remediation, bioreclamation systems need to deliver the proper nutrient concentrations to the areas of contamination. The project's primary objective was to develop and to demonstrate a methodology for characterizing an aquifer's geohydrology in the detail required to design an optimum network of wells and/or infiltration galleries for bioreclamation systems. The project work included performing and analyzing a series of aquifer tests and recirculating tracer tests on a 1-hectare test site located at Columbus Air Force Base, Mississippi. The tests' results demonstrate that bioreclamation systems can not be adequately designed without first characterizating the spatial variability in the hydraulic conductivity field. The recommended methodology includes multiwell aquifer tests and geological investigations and focuses on borehole flowmeter tests to measure the vertical variation in the horizontal hydraulic conductivity values at each well location.

A borehole flowmeter test involves measuring the incremental discharges along the fully screened wells during small-scale pumping/injecting tests. Within the well, vertical zones having high horizontal flow rates indicate zones of high horizontal hydraulic conductivity, and vice versa. The method is quick and simple to implement. At many well locations, the horizontal hydraulic conductivity values measured at 0.3-meter vertical intervals varied over a 3 to 5 order of magnitude range. At some of the well locations, the variation in the hydraulic conductivity field caused approximately 70 percent of the groundwater flow to occur within less than 10 percent of the aquifer thickness.

The accuracy of the borehole flowmeter results were compared with the results of fourteen small-scale tracer tests and one large-scale tracer test. The fourteen small-scale tracer tests were uniformly distributed over a 3,000 m^2 area. These tracer tests typically had distances of 4 to 7 meters between the injection and the withdrawal wells. The one large-scale tracer test included four withdrawal wells and one injection well and covered the entire 3,000 m^2 area. Given the uncertainty

associated with interpolating among the hydraulic conductivity values at the wells used during the tracer tests, good agreement was shown between the hydraulic conductivity values calculated from the tracer breakthrough curves and the borehole flowmeter tests.

The statistical and structural properties of the hydraulic conductivity field at the test site indicate that the aquifer is heterogeneous. A measure of heterogeneity is the variance of the natural logarithm of the hydraulic conductivity measurements, lnK. At the test site lnK is 4.7. The estimates of lnK for an aquifer composed of coastal sands in Cape Cod, Massachusetts, studied by the United States Geological Survey and for an aquifer composed of glacial till in Borden, Canada, studied by Stanford and Waterloo Universities, are less than 0.5. The demonstration of the site characterization methodology in a very heterogeneous aquifer insures that the procedures should be valid for a variety of aquifer types ranging from uniform sands to a complex mixture of gravel, sand, and clay.

In order to demonstrate and document the effectiveness of the site characterization methodology, two reports were written. Volume I describes the test site and the well network, the assumptions and the application of equations that define groundwater flow to a well, the results of three large-scale aquifer tests, and the results of 160 single-well pump tests. Volume II describes the borehole flowmeter tests, the tracer tests, the geological investigations, the geostatistical analyses, and the guidelines for using groundwater models to design bioreclamation systems.

SUMMARY OF THE SITE CHARACTERIZATION METHODOLOGY

The flowchart and Tables 1 and 2 describe the major tasks that comprise the site characterization methodology. The site characterization methodology includes designing a well network, preparing a preliminary assessment of the site's heterogeneity, measuring the vertical variation in the horizontal hydraulic conductivity, and collecting calibration data for groundwater flow models. Deviations from the flowchart can be expected to result from having prior information of

the geohydrological conditions, an existing well network, and/or concerns related to the geochemistry or microbiology. The detailed documentation concerning the site methodology development provides information from which alternative approaches can be prepared. An objective of the site characterization is to characterize the aquifer heterogeneity. If the aquifer is very heterogeneous, two problems may arise.

The first problem related to heterogeneity occurs when the vertical profiles of horizontal hydraulic conductivity at the well locations are very different. In these instances, no validated procedures exist for the proper interpolation among the profiles. As a result, the representativeness of the interpolated three-dimensional hydraulic conductivity field is unknown. This uncertainty becomes embedded into the groundwater modeling results and leads to uncertainty in the evaluation of the hydraulic design of the bioreclamation system. The second problem related to heterogeneity occurs where the variations among the hydraulic conductivity of the aquifer materials are very large. There it may be too costly to install a system of wells and/or infiltration galleries to deliver an adequate flow rate to less permeable target zones of the aquifer material.

FLOWCHART OF THE MAJOR TASKS IN THE SITE CHARACTERIZATION METHODOLOGY

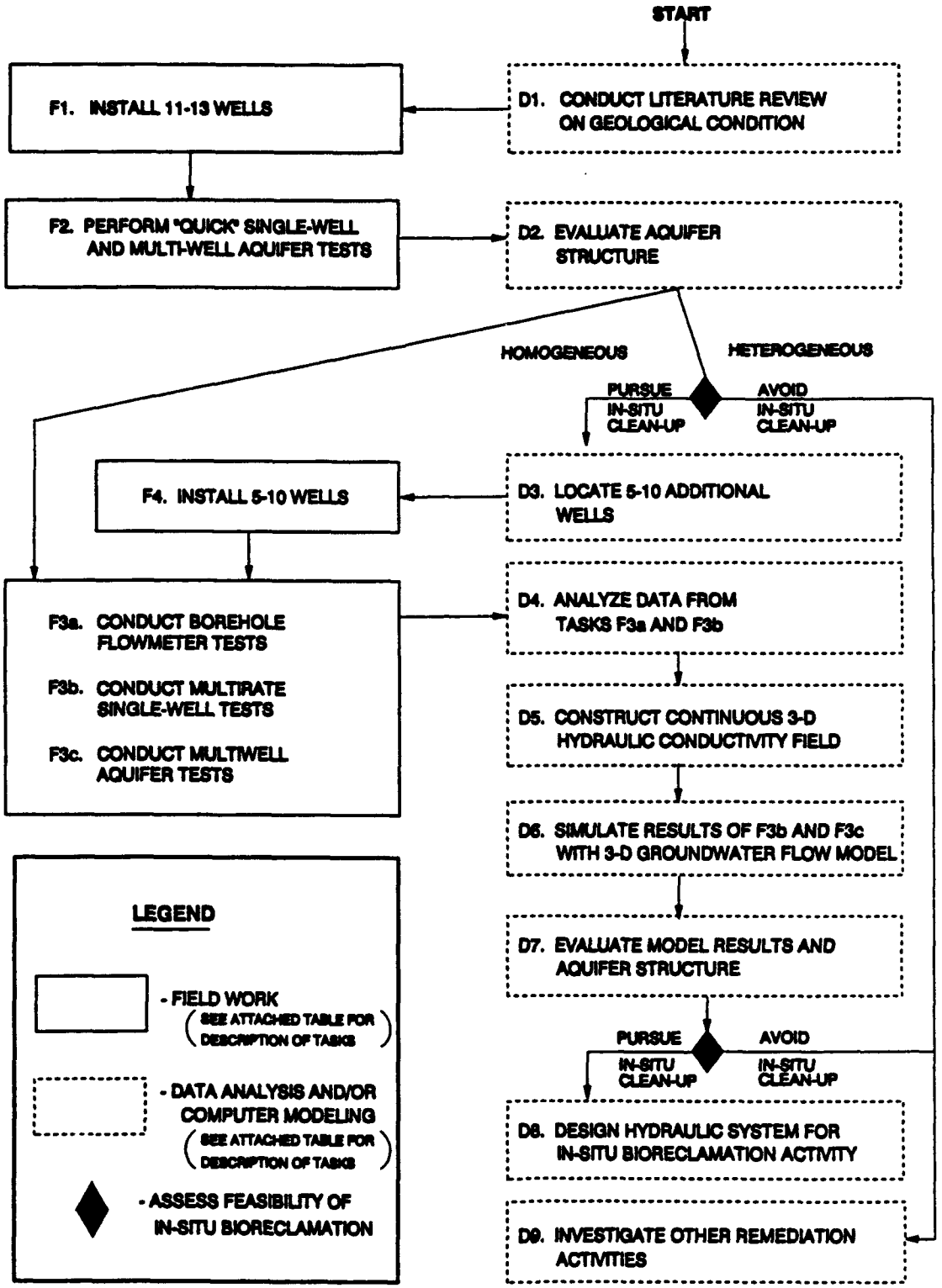

TABLE 1. DESCRIPTION OF THE TASKS ASSOCIATED WITH FIELDWORK

Task		Description
F1.	Install 11-13 wells	Use a Hollow-Stem Auger to install 11 to 13 fully screened wells. Nine of these wells should be placed on a regular grid; the remaining wells should be placed 2 to 4 meters from a well near the interior of the well network. (Volume I, Section II)
F2.	Perform "Quick" Single-Well and Multiwell Aquifer Tests	Conduct 10- to 40-minute moderate to low flow single-well tests at each well to determine the transmissivity pattern. Slug-tests should not be conducted because they are strongly affected by the disturbed zone around the wells. During the single-well tests monitor the drawdown in any close wells to determine values for storage coefficients and hydraulic conductivity. Note whether large vertical variations of hydraulic conductivity exist. (Volume I, Sections V, VI, VII, and VIII)
F3a.	Conduct Borehole Flowmeter Tests	While pumping/injecting at a low rate, perform borehole flowmeter tests to determine transmissivity and three-dimensional hydraulic conductivity patterns. Conduct a separate borehole flowmeter test at high injection rates if large portions of the unsaturated zone need to be characterized. Each test should last 40 to 90 minutes. (Volume II, Section III)
F3b.	Conduct Multirate Single-Well Tests	Conduct the necessary single-well tests to determine how sensitive the calculated transmissivity value is to the pumping rate. Results from the borehole flowmeter tests may be acceptable for inclusion in the data base. If the aquifer is rather homogeneous only several of these tests are needed. (Volume I, Sections VII and VIII)
F3c.	Conduct Multiwell Aquifer Tests	During Tasks F3a and F3b, monitor the drawdown in nearby wells. (Volume I, Sections V and VI)

TABLE 2. DESCRIPTION OF TASKS ASSOCIATED WITH DATA ANALYSIS AND/OR COMPUTER MODELING

	Task	Description
D1.	Conduct Literature Review on Geological Conditions	Obtain information on the type of depositional environments responsible for the aquifer material. Extract any information about the structure of the hydraulic conductivity field. (Volume II, Section IV)
D2.	Evaluate Aquifer Structure	Determine whether bioreclamation appears to be a viable remediation approach, given the known trends in the hydraulic conductivity field. (Volume I, Sections VI and VIII, and Volume II, Section III)
D3.	Install 5-10 Additional Wells	Install wells in areas where the greatest differences occur in the transmissivity field and/or where improvements can be made in the variogram calculations. Use program similar to WELPLAN. (Volume I, Section II)
D4.	Analyze Data from Tasks F3a and F3b	Determine vertical variations of hydraulic conductivity at each well site. Determine whether calculated transmissivities are sensitive to pumping rate. (Volume I, Sections V, VI, VII, and VIII, and Volume II, Section III)
D5.	Construct Continuous 3-D Hydraulic Conductivity Field	From three-dimensional hydraulic conductivity data, construct a continuous three-dimensional grid. The method for doing this is beyond scope of this report. (Volume II, Sections VI and VII, discusses some options)
D6.	Simulate Results of F3b and F3c with Three-Dimensional Groundwater Flow Model	If the aquifer is heterogeneous, transmissivities and storage coefficients will be sensitive to the pumping rates, test duration, and orientation/distance between the pumped and the observation well. The appropriateness of a groundwater flow model's accuracy is to reproduce the drawdowns observed during Tasks F3a and F3b (Volume I, Section VI, and Volume II, Section VIII)
D7.	Evaluate Model Results and Aquifer Structure	Based on the comparison between the predicted and the observed well responses determine whether to pursue in-situ bioreclamation.

TABLE 2. DESCRIPTION OF TASKS ASSOCIATED WITH DATA ANALYSIS AND/OR COMPUTER MODELING (CONCLUDED)

Task	Description
D8. Design Hydraulic System for In-Situ Bioreclamation	Use groundwater model to evaluate alternative designs for bioreclamation systems. (Volume II, Section VIII discusses some approaches)

(The reverse of this page is blank.)

PREFACE

This report was prepared by the Tennessee Valley Authority, Engineering Laboratory, 129 Pine Road, Norris, Tennessee 37828 under Military Interdepartmental Purchase Request (MIPR) N88-28 for the Air Force Engineering and Services Center (HQ AFESC/RD), Air Force Engineering and Services Laboratory, Tyndall Air Force Base, Florida, 32403-5323.

The report discusses a field demonstration of a methodology for characterizing an aquifer's geohydrology in the detail required to design an optimum network of wells and/or infiltration galleries for bioreclamation systems. The project work was conducted on a 1-hectare test site located at Columbus AFB, Mississippi. The field work occurred between August 1987 and September 1989.

The technical report is divided into two volumes. Volume I describes the test site and the well network, the assumptions, and the application of equations that define groundwater flow to a well, the results of three large-scale aquifer tests, and the results of 160 single-well pump tests. Volume II describes the bore hole flowmeter tests, the tracer tests, the geological investigations, the geostatistical analyses, and the guidelines for using groundwater models to design bioreclamation systems.

The report discusses a methodology that includes field procedures and data analysis methods advocated by the Tennessee Valley Authority. The publication of the report by the Air Force does not constitute an endorsement of the methodology by the Air Force.

This technical report has been reviewed by the Public Affairs Office (PA) and is releasable to the National Technical Information Service (NTIS). At NTIS, it will be available to the general public, including foreign nationals.

This technical report has been reviewed and is approved for publication.

BRUCE J. NIELSEN
Project Officer

NEIL J. LAMB, Colonel, USAF, BSC
Director, Environics Directorate

ROBERT G. LAPOE, Major, USAF, BSC
Chief, Site Remediation
Division

(The reverse of this page is blank.)

TABLE OF CONTENTS

TABLE OF CONTENTS
(CONTINUED)

TABLE OF CONTENTS
(CONTINUED)

TABLE OF CONTENTS
(CONCLUDED)

LIST OF FIGURES

LIST OF FIGURES
(CONTINUED)

LIST OF FIGURES
(CONTINUED)

LIST OF FIGURES
(CONTINUED)

LIST OF FIGURES
(CONTINUED)

LIST OF FIGURES
(CONTINUED)

LIST OF FIGURES
(CONCLUDED)

LIST OF TABLES

LIST OF TABLES
(CONCLUDED)

LIST OF SYMBOLS

z = depth (L)

Δz_i = the thickness of layer i (L)

h = hydraulic head (L)

h_R = hydraulic head in the aquifer prior to pumping (L)

$h(r,t)$ = hydraulic head in the aquifer at radius r and time t (L)

H = total aquifer thickness (L)

K = aquifer hydraulic conductivity (L/T)

K_i = hydraulic conductivity for layer i (L/T)

K_s = hydraulic conductivity of skin effect (L/T)

K_c = calculated hydraulic conductivity for aquifer (L/T)

$T = \int_H K\,dz = \bar{K}H$ = transmissivity (L^2/T)

$S = \int_H S_o\,dz + S_y = S_oH + S_y$ = storage coefficient (-)

S_i = storage coefficient for layer i (-)

S_y = drainable porosity = specific yield (-)

S_o = specific storage coefficient (1/L)

D = diffusivity = T/S (L^2/T)

r = radial distance from the center of the well (L)

$R = \sqrt{\frac{2.25Tt}{S}}$ = radius of influence (L)

r_w = radius of well (L)

r_s = radius of skin effect (L)

t = elapsed time (T)

t_o = time intercept on a semilogarithmic plot where drawdown equals zero (T)

Q = discharge rate (L^3/T)

ΔQ_i = the flow to (or from) layer i (L^3/T)

$W(u) = \ln\left(\frac{1}{1.781 \cdot u}\right) \sum_{n=1}^{\infty} (-u)^n \frac{1}{n \cdot n!}$ = well function

$u = \frac{r^2 S}{4\,Tt}$ = dimensionless time

s = drawdown in the aquifer after pumping (L)

Δs_i = drawdown for layer i (L)

s' = drawdown adjusted by the Jacob correction factor (L)

B = aquifer thickness (L)

$c = Q/2\pi Kb^2$ [Theis correction factor] (-)

θ = angular direction (-)

V_d = the cumulative volume of water discharged from a well during an aquifer test (L^3)

V_i = the estimated volume of groundwater removed from within the cone-of-depression at some time, t, during an aquifer test (L^3)

σ^2 = variance

λ = correlation length

(The reverse of this page is blank.)

SECTION I

INTRODUCTION

A. OBJECTIVE

The goal of this project is to develop and demonstrate a methodology for characterizing an aquifer's geohydrology. Site characterization is to be sufficient for designing a system of wells and/or infiltration galleries that optimize the transport of nutrients to targeted zones during in-situ bioreclamation activities. The methodology includes the procedures required to: (1) properly design and install a groundwater well network for site characterization activities; and (2) properly design, conduct, and analyze aquifer well tests to measure horizontal hydraulic conductivity variation in three dimensions. Numerous field test results from Columbus Air Force Base (CAFB), Mississippi, demonstrate that three-dimensional characterization data are a prerequisite to accurate prediction of advective transport in heterogeneous aquifers. The methodology also provides guidelines for the application of groundwater transport models in the design of an effective network of wells and/or infiltration galleries for bioreclamation activities.

B. BACKGROUND

An alternative to waste extraction and conventional pumping and treatment methods at spill sites and hazardous waste sites is to treat the wastes in situ. In situ biodegradation, commonly referred to as bioreclamation, is based on the concept of stimulating bacteria to metabolize the contaminants. Over the last 25 years, laboratory degradation of organics has been extensively studied and has become well understood. In general, the application of bioremediation technology to full-scale field experiments has not met with the success that laboratory data would suggest. One of the problems associated with designing and operating in situ bioreclamation is characterizing the properties of the aquifer that determine advective transport of an injected nutrient solution.

In an aquifer, the three-dimensional structure of the hydraulic conductivity field will control the groundwater flow patterns. The advection of the nutrient solution will be controlled by the hydraulic conductivity of the different aquifer materials. The rate at which the nutrient solution disperses is controlled by the interconnectiveness among the different hydraulic conductivity zones. Thus, proper characterization of the spatial variability in the hydraulic conductivity field is essential to accurate groundwater transport predictions of the effectiveness of different withdrawal pumping schemes for bioreclamation and pump-and-treat activities.

Proper characterization of an aquifer's hydraulic properties requires an effective method for measuring the spatial variability in the hydraulic conductivity field. The Tennessee Valley Authority (TVA) and the Massachusetts Institute of Technology (MIT) have demonstrated that a borehole flowmeter can be used during a single-well pumping test to measure the discharge rate from any specified vertical interval within a fully screened well (Rehfeldt, et al., 1990). The methodology developed by TVA uses a borehole flowmeter to calculate horizontal hydraulic conductivity variations in three dimensions. The overall methodology includes significant advancements in the design, construction, and use of borehole flowmeters and in the design, implementation, and data analysis of multiwell and single-well aquifer tests.

C. SCOPE

1. Description of Tasks

The project centered on conducting and analyzing a series of pump and tracer tests at an uncontaminated area of the terrace aquifer at Columbus Air Force Base (CAFB). The test site is situated on the youngest terrace in a series of Pleistocene and Holocene Age deposits associated with the Tombigbee and Buttahatchee Rivers. The sand, gravel, silt, and clay deposits occur in irregular lenses and layers.

The test site covers 1 hectare and has 37 fully screened groundwater wells. Well locations were based on several considerations

including: (1) characterizing the statistical properties of the hydraulic conductivity field; and (2) conducting small (1-5 meters) and large (5-50 meters) pump and tracer tests. Site characterization activities included multiwell aquifer tests, single-well pumping and injection tests, and two sets of borehole flowmeter measurements. The site characterization results and methodology were validated by comparison with the results from a series of small-scale and one large-scale tracer test. A summary of the project activities is listed in Tables 3 and 4.

TABLE 3. SUMMARY OF PROJECT ACTIVITIES: SITE CHARACTERIZATION PROJECTS

	Project	Result
1.	5-Day Large-Scale Aquifer Tests With a Constant 68 L/min Discharge Rate	T at 27 wells , S at 9 wells
2.	5-Day Pulsing Large-Scale Aquifer Tests With an Average Pumping Rate of 68 L/min	T at 27 wells , S at 27 wells
3.	8-Day Large-Scale Aquifer Tests With a Constant 110 L/min Discharge Rate	T at 27 wells, S at 12 wells
4.	Seven Small-Scale Aquifer Tests (1 hour to 3 hours) With Pumping Rates From 34 to 81 L/min	T at 35 wells, S at 35 wells
5.	34-Liter Slug Tests	T at 37 wells
6.	2-Minute 34 L/min Pumping Tests	T at 37 wells
7.	Single-Well Injection Tests at 22 L/min	T at 37 wells
8.	One Hundred Forty-Nine Multiple Rate (6 L/min to 80 L/min) 115 Pumping Tests at the Same Well	149 values of T at 37 wells (an average of about 3 tests per well)
9.	Borehole Flowmeter Measurements During 22 L/min Injection Tests	881 K_s at 37 wells
10.	Borehole Flowmeter Measurements During 30 L/min Withdrawal	362 K_s at 21 wells
11.	Borehole Flowmeter Measurements During 15 L/min Withdrawal	380 K_s at 21 wells

TABLE 3. SUMMARY OF PROJECT ACTIVITIES: SITE CHARACTERIZATION PROJECTS (CONCLUDED)

Notes: (1) T = transmissivity
S = storage coefficient
K = hydraulic conductivity
(2) Drawdown data sets consisted of manual measurements and/or automatic measurements made by a data logging system connected to a pressure transducer. Storage coefficients were calculated only for the data from the pressure transducers.
(3) Each hydraulic conductivity measurement is based on the average discharge across a 0.3 meter vertical section of a well screen. An average of 21 measurements was made at each well. The number of measurements at each well varied because of the different thicknesses of the saturated zone during pumping at each well.

TABLE 4. SUMMARY OF PROJECT ACTIVITIES: TRACER TESTS

	Tracer Test	
1.	8-hour five-spot tracer test for wells spaced 3.6 to 4.6 meters apart with a 31 L/min injection rate	Breakthrough curves at four wells
2.	25-hour five-spot tracer test for wells spaced 3.6 to 6.3 meters apart with a 38 L/min injection rate	Breakthrough curves at four wells
3.	Three 36-hour doublet tracer tests conducted at 3 well pairs with spacings of 5.2, 6.7, and 6.2 meters with injection rates between 11.5 and 14.2 L/min	Breakthrough curves at three wells
4.	Four 70-hour doublet tracer tests conducted at 4 well pairs with spacings of 7.3, 8.9, 15.2, and 15.8 meters with injection rates between 15.1 and 34.1 L/min	Breakthrough curves at four wells
5.	One 168-hour five-spot tracer test with injection and pumping wells 31 meters apart and with 27 monitoring wells at distances from 4.8 to 31.1 meters from the injection well with an injection rate of 106 L/min	Breakthrough curves at 27 wells

2. Description of the Report

The project results are contained in two volumes. Volume I contains the description of the test site, the data and results for the multiwell aquifer tests and the single-well hydraulic tests. Volume II contains the results for the borehole flowmeter measurements, the tracer tests, the geological investigations, and recommendations for applying groundwater models to effectively design a network of wells and/or infiltration galleries for bioreclamation activities.

Volume I includes nine major sections. Section I is the introduction. Section II describes the site location, the methods used to design the well network, and the methods used to install and develop the wells. Sections III and IV summarize the most relevant well equations and the limitations associated with their applications to heterogeneous aquifers. Sections V and VI provide the data and analysis of the multiwell aquifer tests. Sections VII and VIII provide the data and analysis of the single-well hydraulic tests. Section IX summarizes the important results in Section I to Section VIII.

This volume includes eight major sections. Section I is the introduction. Section II summarizes the results of the large-scale aquifer and single-well tests discussed in Volume I. Section III describes the development and application of the borehole flowmeter technique for measuring horizontal hydraulic conductivity variation in three dimensions. Section IV provides explanations for the complexity of the site and trends in the hydraulic conductivity data based on geological investigations. Sections V and VI describe the tracer tests and compares the borehole flowmeter results with the tracer test results. Section VII presents a geostatistical analysis of the hydraulic conductivity data. Section VIII provides guidelines and recommendations on how to characterize the geohydrology of a site and to apply groundwater transport models to a test site for the design of an effective network of wells and/or infiltration galleries for any pump-and-treat bioreclamation scheme.

(The reverse of this page is blank.)

SECTION II

BRIEF OVERVIEW OF THE RESULTS OF THE SINGLE-WELL AND MULTIWELL AQUIFER TESTS DISCUSSED IN VOLUME I

A. TEST SITE AND WELL NETWORK

The 1-hectare test site is approximately 6 km east of the Tombigbee River and 2.5 km south of the Buttahatchee River. The 11-meter thick terrace aquifer consists of a mixture of gravel, sand, and clay lenses and is underlain by the Cretaceous Age Eutaw Formation. The Eutaw Formation consists primarily of marine clay, silt, and sand. Compared to unconsolidated aquifers found in coastal, glacial, and lacustrine settings the alluvial aquifer at CAFB is very heterogeneous. A network of 37 fully screened wells was designed to meet multiple objectives which include small- and large-scale pump and tracer tests. Given the limitations of satisfying the constraints of the multiple objectives, the well network was optimized with regard to geostatistical analyses by using the ideas presented by Warrick, et al. (1987), and by Olea (1975) on the optimal location of data for semivariogram analyses and kriging analyses, respectively. Figure 1 shows the location of the 37 wells.

B. RESULTS FROM THE LARGE-SCALE AQUIFER TESTS

Three large-scale multiwell aquifer tests were conducted at the test site between May and July 1989. Aquifer Test 1 involved pumping Well 5 (the center well) at a constant rate of about 68 L/min. Aquifer Test 2 involved pumping Well 5 at regulated cyclic intervals producing an average pumping rate of about 68 L/min. In Aquifer Test 3 Well 5 was pumped at a constant rate of about 113 L/min. The small-scale pumping tests required pumping a series of wells at rates between 34 and 81 L/min and monitoring the water table in wells that were 4 to 7 meters from the pumping well. The durations of the small-scale pumping tests were between 1 and 2 hours.

For each of the large-scale aquifer tests, transmissivity values were calculated for almost all of the 27 interior wells. Analyses of the

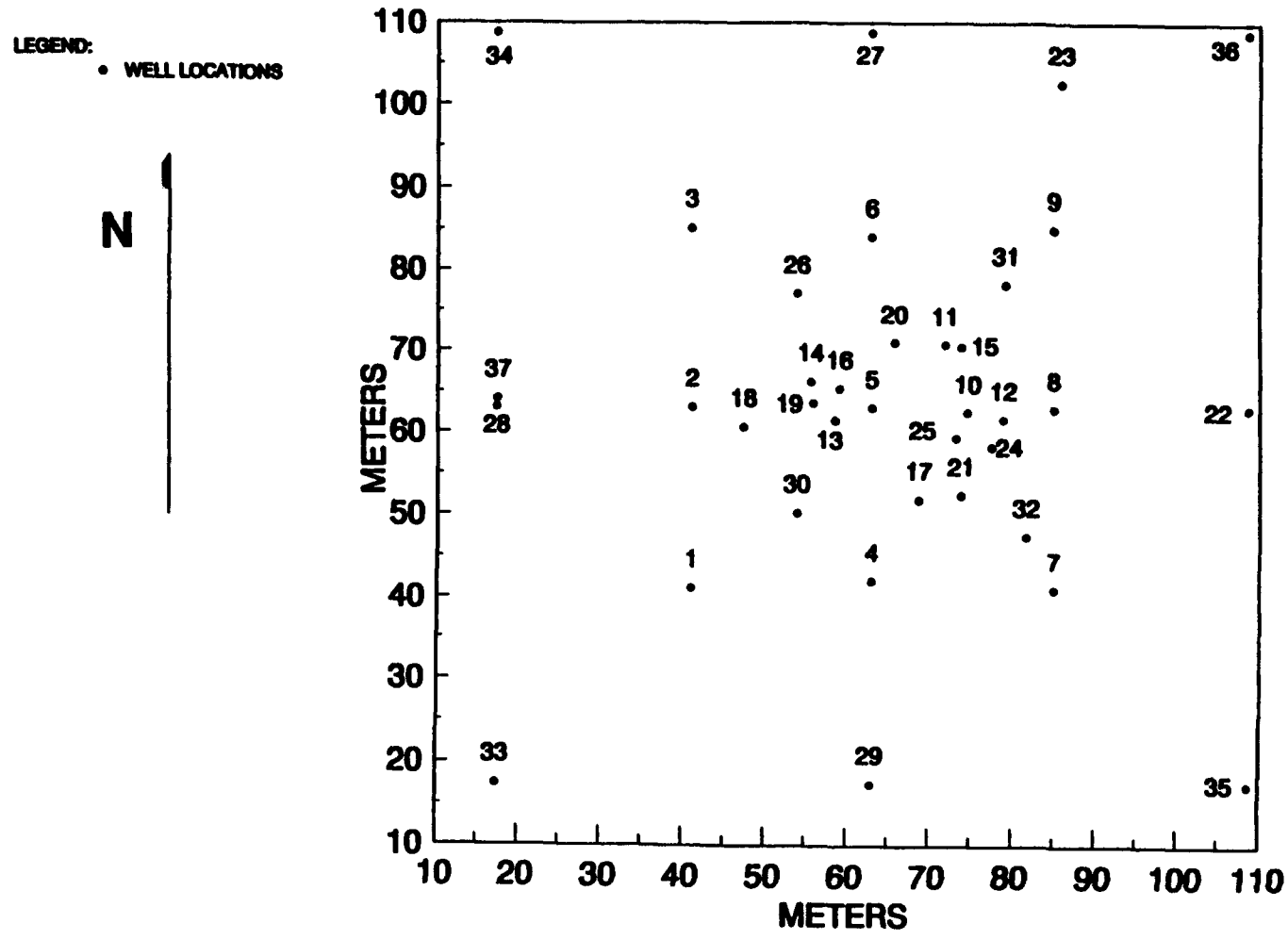

Figure 1. Well Network at the CAFB Test Site.

transmissivity and the storage coefficient values show that the values typically ranged between 10 and 200 cm/s and 0.1 and 0.00001, respectively. For each of the three large-scale aquifer tests the standard deviation for the calculated transmissivity values ranged between 7.5 and 13.0 cm/s. The average transmissivity for the aquifer was estimated between 30 and 40 cm/s. For Aquifer Test 2, storage coefficients were calculated for 24 of the interior wells. The average and the standard deviation for the storage coefficient values are 0.03 and 0.024, respectively.

Figures 2 and 3 show that the calculated transmissivity and the storage coefficient values decrease and increase over time, respectively. These trends can be attributed to how an aquifer responds to stress caused by pumping. When an aquifer is stressed, the initial pressure response is first transmitted into and through the zones of high diffusivity. Initially, hydraulic pressure in the well will more closely represent the pressure in the zones of high diffusivities rather than the average pressure in the aquifer. Therefore, an analysis of well data, at early times, will lead to estimates of transmissivity and storage coefficients more representative of the zones of high diffusivity rather than of the total thickness of the aquifer. Because cross flow causes the pressure gradients between the zones of high and low diffusivity to dissipate over time, the hydraulic pressure in the well will more closely represent the pressure in the total aquifer than in the zones of high diffusivity at late times. Consequently, an analysis of the well data, at late times, will lead to estimates of transmissivity and storage coefficients more representative of the all the aquifer material than the material of high diffusivity.

Figure 4 shows a correlation between the distance between the pumping and the observation wells and the value of the storage coefficient. The data in Figure 4 is based on the results of the pumping tests listed in Table 3 and discussed in Volume 1. The storage coefficients ranged between 10^{-6} to 10^{-2} for distances between 0 and 10 meters, 10^{-4} to 10^{-2} for distances between 10 and 20 meters, and 10^{-2} to 10^{-1} for distances greater than 20 meters. A plausible

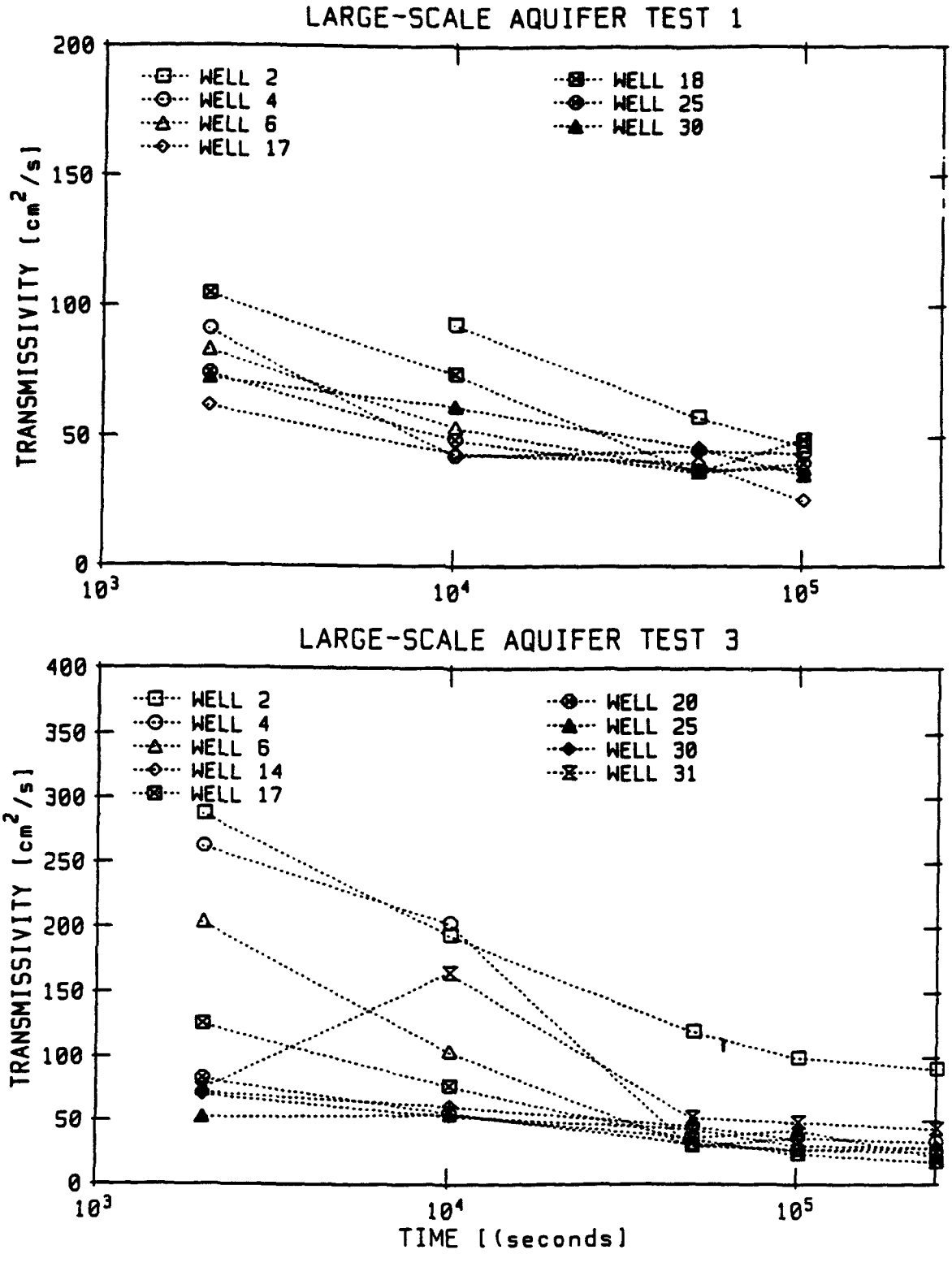

Figure 2. Transmissivities as a Function of Time for Large-Scale Aquifer Tests 1 and 3.

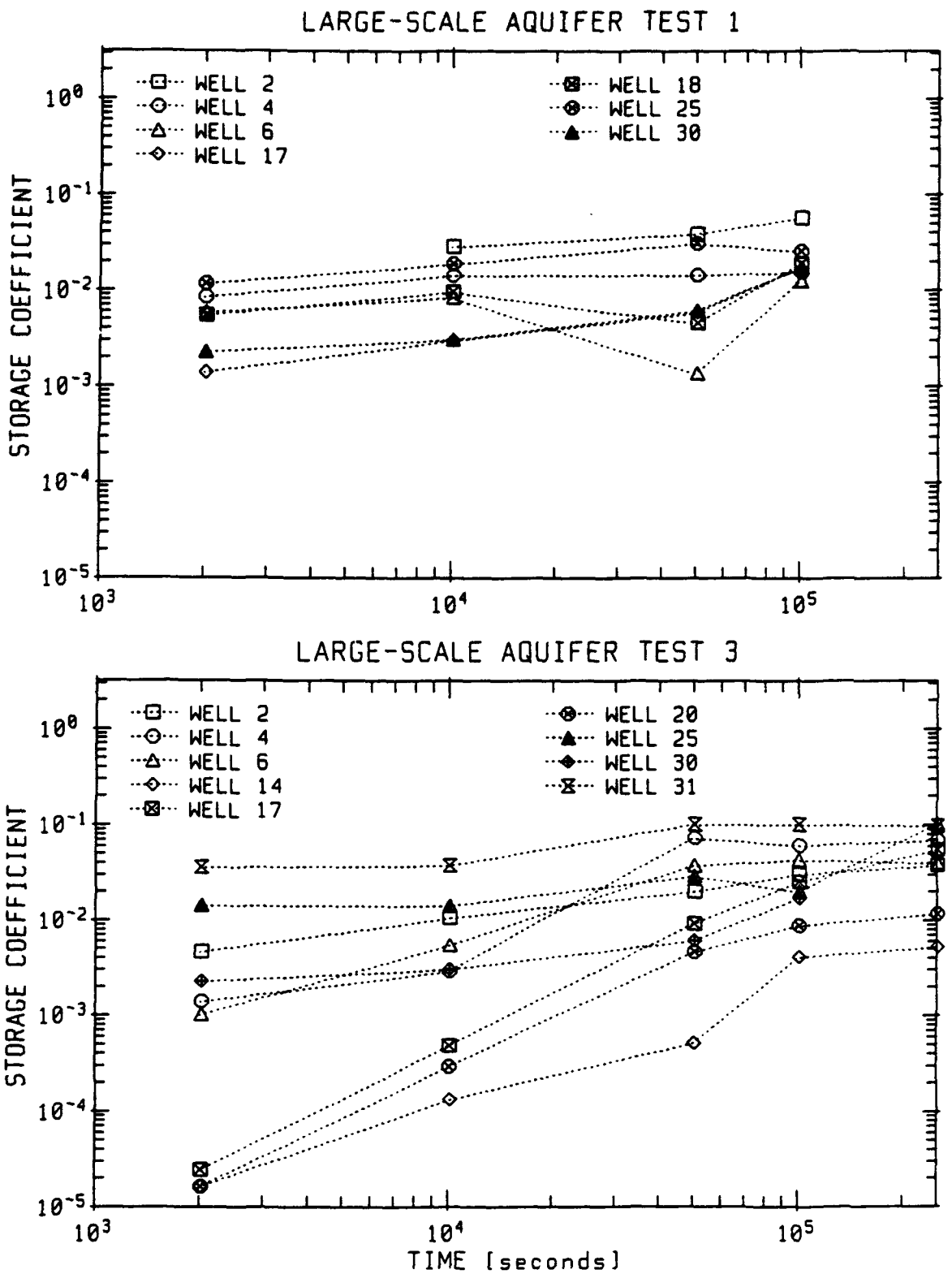

Figure 3. Storage Coefficients as a Function of Time for Large-Scale Aquifer Tests 1 and 3.

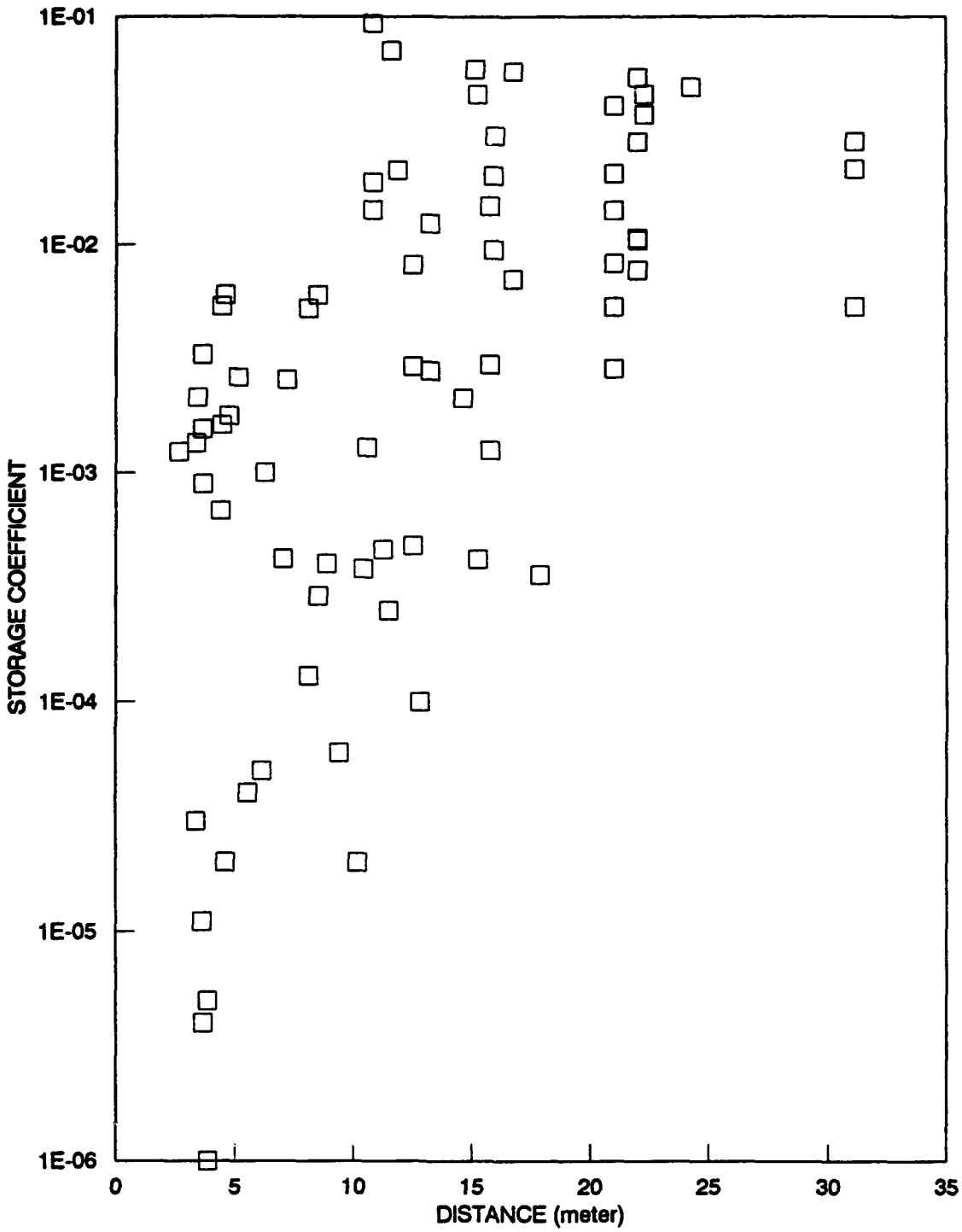

Figure 4. Storage Coefficients as a Function of Distance Between the Observation and the Pumping Well.

explanation for this trend is the existence of discrete highly permeable lenses scattered throughout the aquifer (an occurrence verified by the results in Section III).

The lower values of storage coefficients occur when highly transmissive, thin lenses (or a single lens) which are interbedded in material of lower hydraulic conductivity, intersect both the pumping and the observation well. Higher values of storage coefficients occur when the aquifer material between the pumping and the observation well is less heterogeneous and does not have continuous lenses that intersect both wells. The data indicate that the correlation between storage coefficients and distance is likely to be typical of heterogeneous aquifers.

C. RESULTS FROM THE SINGLE-WELL PUMP TESTS

At each well, a series of single-well pump tests was conducted to determine the aquifer's transmissivity. The pump tests included slug tests, short-duration (2-minute) pump tests, low-rate (15 L/min) pumping tests, moderate-rate (20-30 L/min) injection and/or pumping tests, and high rate (60 L/min) pumping tests. At 27 of the 37 well locations, the transmissivities from the single-well tests ranged over an order of magnitude. The test results show that the design of a single-well test affects the transmissivity calculated at the pumped well. Important design features are the pumping rate and the test duration.

The analysis of the single-well data indicates that significant skin effects exist at most of the wells. Skin effects represent the disturbed zone around a well created during the well installation. A negative skin effect means that the hydraulic conductivity of the natural aquifer material near the well has been reduced. Negative skin effects can be caused by the smearing of clay particles, the compaction of sediments during the advancement of the drill casing, and/or the intrusion of fines into coarse sediments because of improper well development.

One of the important implications of negative skin effects is that the Cooper-Jacob equation (1946), which has been used by numerous

researchers (Rehfeldt, et al., 1989; Hess, 1989; Boggs, et al., 1990; and Morin, 1988), is not valid for calculating transmissivity values from single-well pump tests data. As discussed in Volume I, skin effects can be accounted for in the data analysis by using the Cooper-Jacob straight-line analysis. This analysis requires the geohydrologist to determine the transmissivity from the slope of the most appropriate straight-line through the drawdown-time data. One of the advantages of the Cooper-Jacob straight-line analyses is that an assumed storage coefficient is not required as is the case with the Cooper-Jacob analysis. Figure 5 illustrates the method used to determine the slope for all of the drawdown-time plots. In Figure 5, the time at which the straight-line behavior begins is called, for convenience, the inflection point.

Figure 6 shows the difference in the transmissivity values calculated from the Cooper-Jacob equation (no skin effects assumed) and the Cooper-Jacob straight-line analysis (skin effects accounted for). As previously stated, the Cooper-Jacob equation requires an assumed value for the storage coefficient. Because the storage coefficient varies over from 10^{-1} to 10^{-6} at the test site (see Figure 4), Figure 6 includes two comparisons. Comparison 6(a) uses the Cooper-Jacob transmissivities based on an assumed storage coefficient of 10^{-1}. Figure 6(b) uses Cooper-Jacob transmissivities based on an assumed storage coefficient of 10^{-6}. The analysis of the pumping tests showed that, on the average, the Cooper-Jacob straight-line analysis gave transmissivity values about an order of magnitude higher than the Cooper-Jacob equation.

The trends shown in Figure 6 are based on the analysis of multiple pump tests conducted at each of the 37 wells. The numerous pump tests were conducted to investigate the sensitivity of the calculated transmissivity values at each well location to different pumping rates. This sensitivity was anticipated because the hydraulic properties of the aquifer change with distance from the well. The tests' results showed that at all the wells, the calculated transmissivity was sensitive to the pumping rate. At some of the wells (2, 18, 19, 16, 28, 37, and 26), the calculated transmissivity values increased over an order of magnitude

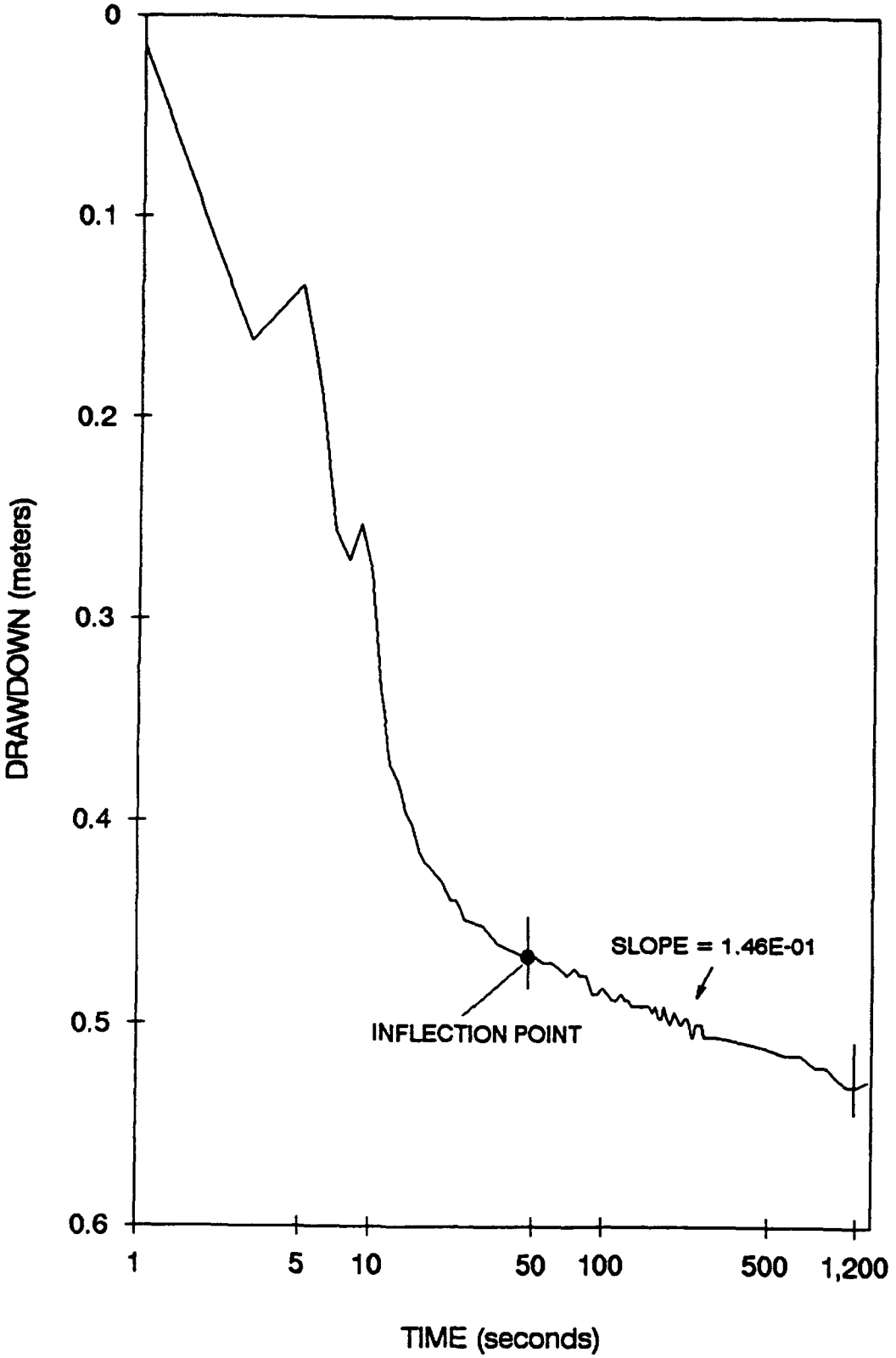

Figure 5. An Example Drawdown Curve (from Well 16) for the Single-Well Pump Tests.

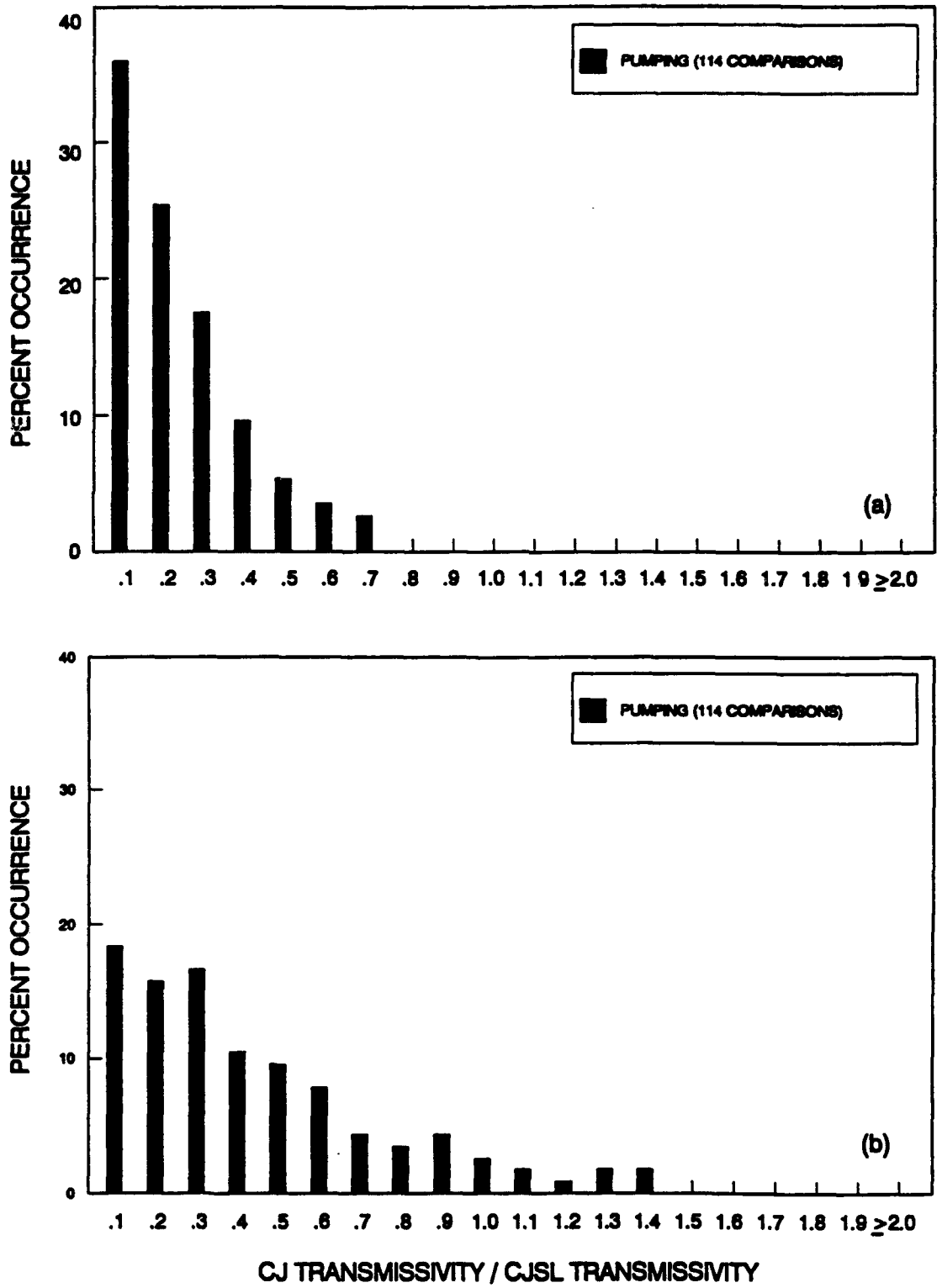

Figure 6. Comparison Between the Transmissivities Calculated by the Cooper-Jacob (CJ) and the Cooper-Jacob Straight Line (CJSL) Equations, (a) Storage Coefficient is 0.1; (b) Storage Coefficient is 0.00001.

with increases in the pumping rate. At other wells (4, 36, 8, and 34) the transmissivity values decreased over an order of magnitude. At about one-half of the wells, the increase in the pumping rate changed the calculated transmissivities by less than a factor of 4.

The sensitivity of the calculated transmissivity to the pumping rate, at an observation well, indicates whether a well is located in a region of relatively low or high transmissivity. When this indirect type of information on transmissivity trends is examined collectively, as in Figure 7, qualitative trends in the transmissivity field are produced. The trends in Figure 7 compare well with the trends shown in Figures 8 and 9, which show the transmissivity field for the injection and the low-rate single-well pump tests. All three figures indicate a highly transmissive material in the west and the north and a moderately transmissive material in the east.

Table 5 lists the mean and the standard deviation for the transmissivity values calculated from the single-well and the aquifer pump tests. The statistics indicate that significant differences exist among the different test results. Table 5 shows that the single-well test types with the smallest radius of influence (i.e., the slug test and the short-duration pump test) have mean transmissivity values considerably smaller than the mean transmissivity values for the aquifer tests. This is likely a result of skin effects. Table 5 also shows that the single-well tests with the largest radius of influence (i.e., the high-rate pumping test and the injection test) have mean transmissivity values that closely match the mean transmissivity values of the aquifer tests. Overall, the tests' results show that the pumping rates and the type of well test affect the calculated transmissivities from a well test.

D. RECOMMENDED METHOD FOR CHARACTERIZING A TRANSMISSIVITY FIELD

The different values for the means and the standard deviations in Table 5 show that calculated transmissivity values depend on the type of pump test. The correctness of the different transmissivity fields was evaluated against two sources of information. The first source of information was a 1956 aerial photograph (Figure 10) of the site that

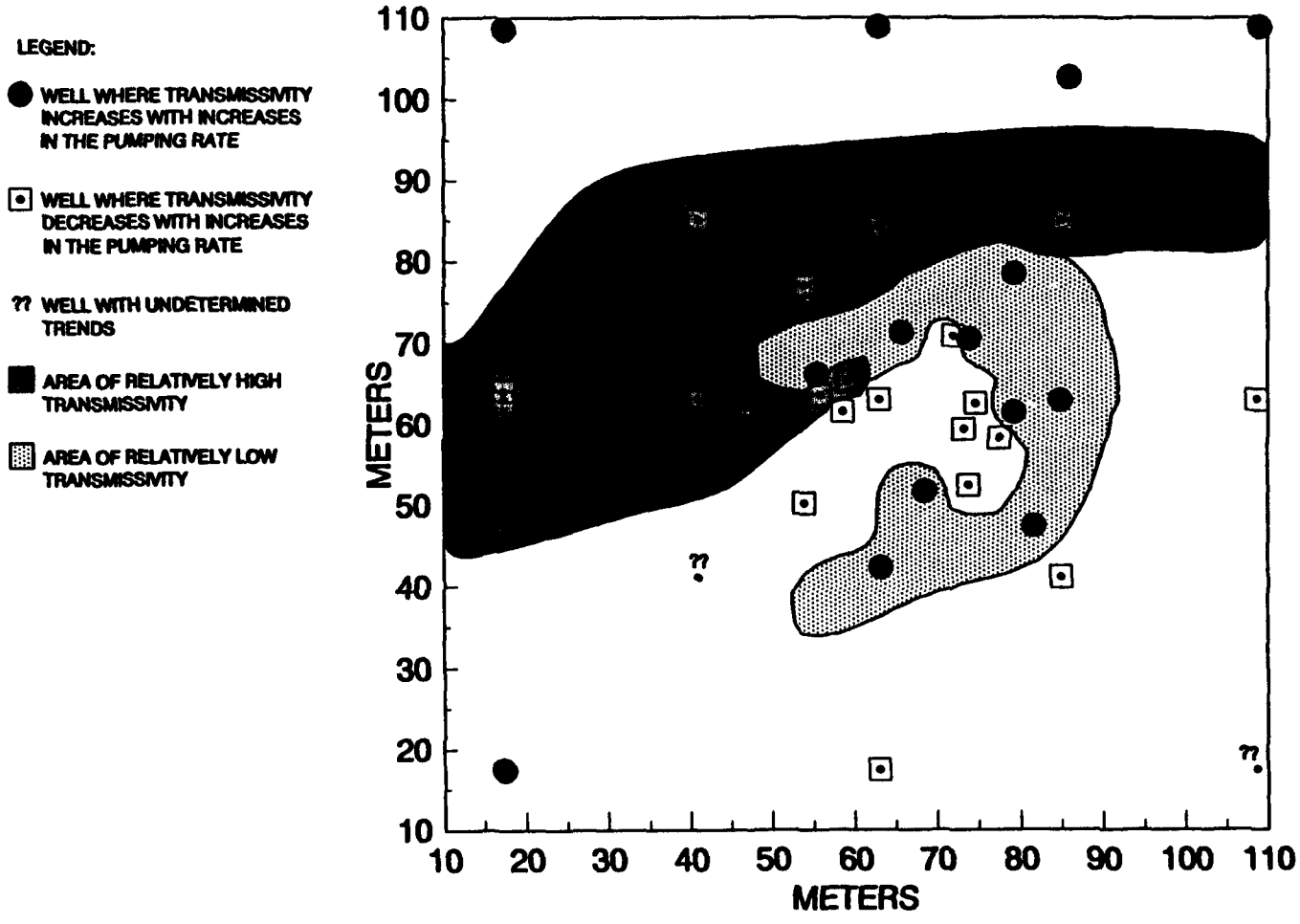

Figure 7. Areas of High Transmissivity and Low Transmissivity Determined From the Effects That the Pumping Rate Has on the Calculated Transmissivity at Each Well.

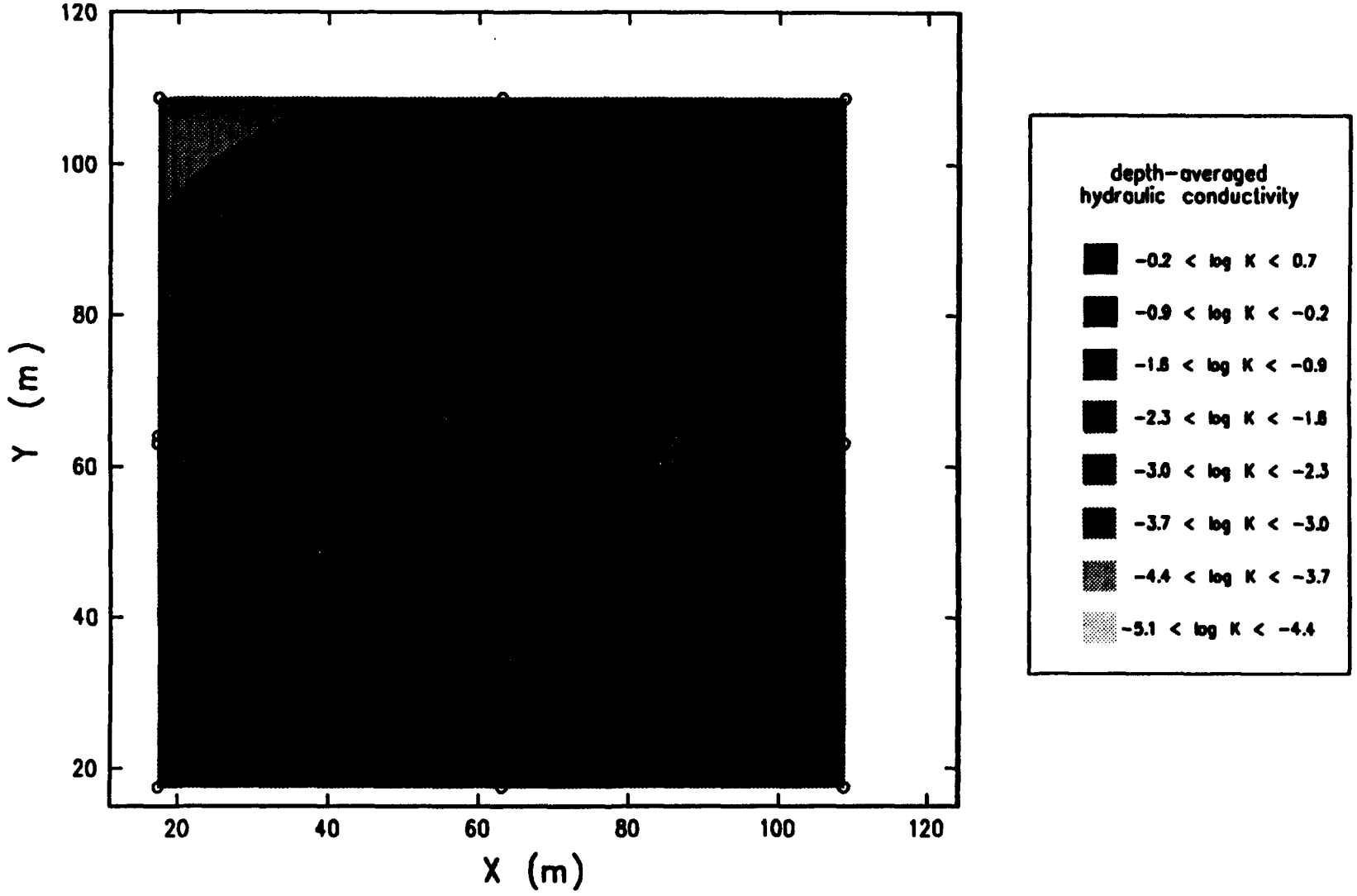

Figure 8. Transmissivity Field Based on the Moderate-Rate Injecting Test Results From the 37 Wells.

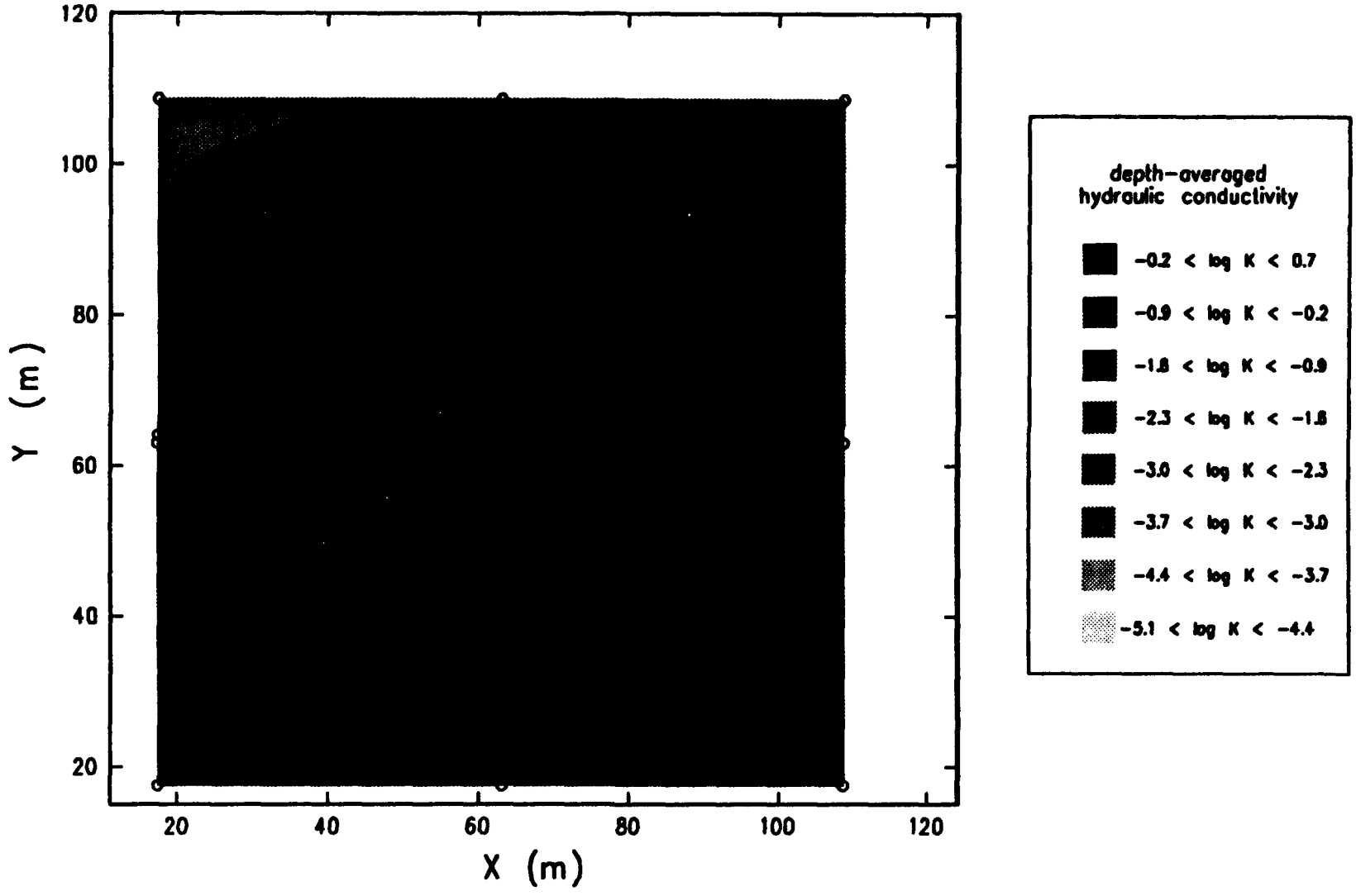

Figure 9. Transmissivity Field Based on the Low-Rate Pumping Test Results From the 37 Wells.

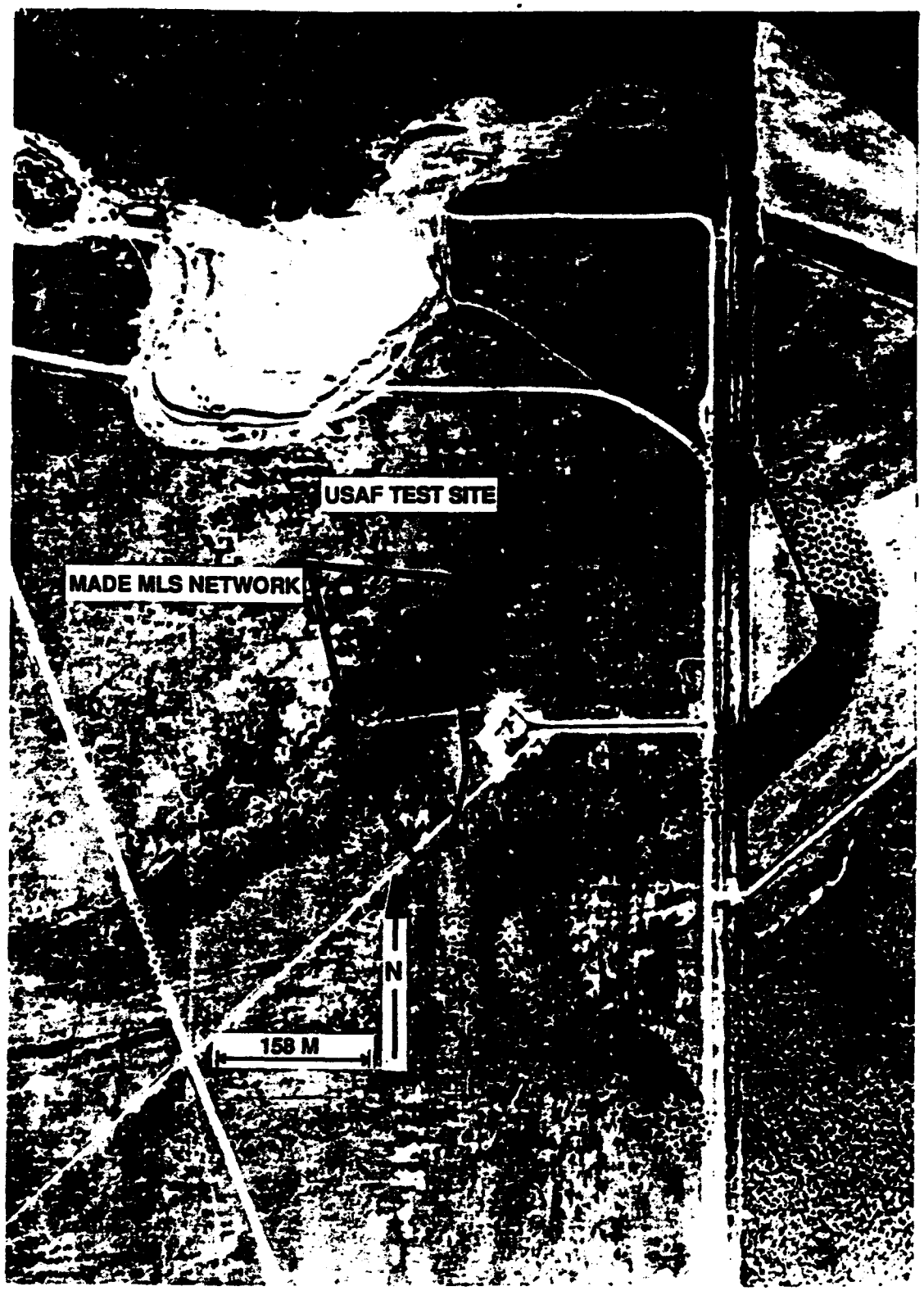

Figure 10. Ox Bow Meander at the CAFB Test Site as Shown in a 1956 Aerial Photograph.

shows a former river channel in the northwestern and the northern regions and a presumed point bar in the southeastern region of the well network. The second source of information was a map of the high and low regions of transmissivity based on the trends between the calculated transmissivity values and the pumping rate, shown in Figure 7. Based on the information in these two figures, the best site characterization method for defining a transmissivity field was determined to be low-rate single-well pumping tests.

TABLE 5. SUMMARY OF THE TRANSMISSIVITY VALUES CALCULATED FOR THE SINGLE-WELL AND THE AQUIFER TESTS

	ARITHMETIC VALUES		LOGARITHMIC VALUES	
DATA SET	MEAN	SD	MEAN	SD
SLUG TEST	3.5	2.0	2.7	2.3
SHORT DUR. PUMP TEST	10.1	12.6	4.1	5.0
INJECT. TEST	32.7	31.7	21.1	2.9
PUMP TEST (LOW-RATE)	75.5	97.0	39.3	3.8
PUMP TEST (HIGH-RATE)	37.6	20.3	31.2	2.0
AQUIFER TEST 1	36.7	7.5		
AQUIFER TEST 2*	31.3	9.4		
AQUIFER TEST 3	32.7	12.9		

SD = standard deviation

* based on 24 of the 27 interior wells

note: durations of the single-well tests are: short-duration pump tests, 2 minutes; low-rate pump tests, 20 minutes, high-rate pump tests, 20 minutes; and injection tests, 40 minutes.

SECTION III

HYDRAULIC CONDUCTIVITIES FROM THE BOREHOLE FLOWMETER METHOD

A. OVERALL OBJECTIVES

Borehole flowmeter tests involve measuring the incremental discharges along a fully screened well during small-scale pumping tests. By assuming the flow of groundwater to the well is horizontal and unbounded, the hydraulic conductivity of each layer in the aquifer is calculated with the well equations developed by Cooper and Jacob (1946). Figure 11 provides a schematic of horizontal flow to a well and the corresponding profiles for cumulative discharge and calculated hydraulic conductivities.

The borehole flowmeter method relies on the capability to accurately measure the drawdown rate and the vertical flow distribution in a fully screened pumped well. The method is summarized by the following five steps. First, the borehole flowmeter is lowered close to the bottom of the well. Second, a pressure transducer is lowered below the water table. Third, a constant and known flow rate is withdrawn from or injected into the groundwater well. Fourth, after the rate of drawdown in the well has stabilized, the flowmeter is used to make flow measurements at selected depths in the well. Fifth, the pressure transducer data is downloaded approximately 5 to 10 minutes after the pumping or injecting of the water has ceased.

In the analysis of borehole flowmeter data, one should account for ambient flow in the well and head losses associated with the well pipe and screen. To account for any ambient vertical flow (vertical hydraulic gradients), one should perform a borehole flowmeter survey before the pump test and/or perform two pumping tests at different flow rates. Rehfeldt, et al. (1989), provide a good discussion of these options. To account for head losses associated with the well pipe and screen, one can use semi-empirical equations. Hufschmied (1983) and Rehfeldt, et al. (1989), provide a detailed discussion on the use of these equations.

Boggs, et al. (1990), Molz, et al. (1989), and Rehfeldt, et al. (1989) compare the borehole flowmeter method with alternative methods for

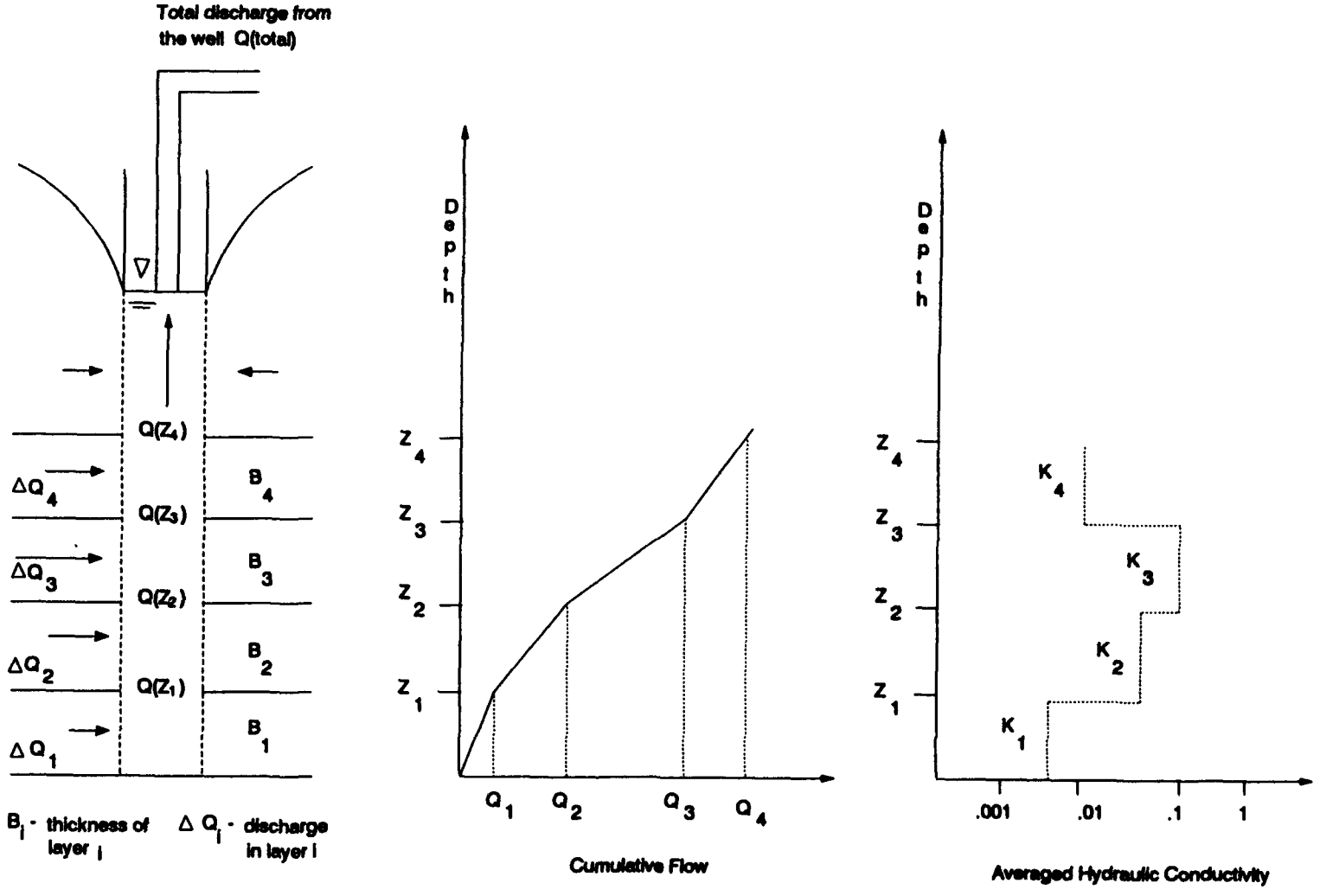

Figure 11. Schematic of Horizontal Flow to a Well and the Profiles of the Cumulative Flow and the Calculated Hydraulic Conductivities.

measuring spatial variations in hydraulic conductivity. The alternative methods include small-scale tracer tests, multilevel slug tests, laboratory permeameter tests, and empirical equations for calculating hydraulic conductivity from grain-size distributions. The researchers conclude that the borehole flowmeter method is the most promising for measuring spatial variations in an aquifer's hydraulic conductivity field.

Although the borehole flowmeter method has greater potential than comparable methods for measuring the spatial variability of hydraulic conductivity, the method is not well established. Rehfeldt, et al. (1989) and Molz, et al. (1990) provide the well equations with which to calculate hydraulic conductivity values. However, neither group thoroughly demonstrates the applicability of the well equations and/or the representativeness of the calculated hydraulic conductivity values. The representativeness of calculated conductivities depends on the susceptibility of the aquifer sediments to collapse, the zone of disturbance around a well, the method of well development, the variability in the permeabilities of the aquifer's sediments, the reliability and resolution of the flowmeter, and the method by which the data are analyzed. Table 6 lists the objectives for the laboratory and field borehole flowmeter tests.

TABLE 6. OBJECTIVES FOR THE BOREHOLE FLOWMETER TESTS

1. Characterize the spatial variability of the hydraulic conductivity field at the test site.
2. Evaluate existing methods for analyzing borehole flowmeter data and, if needed, develop new methods.
3. Evaluate existing methods for collecting borehole flowmeter data and, if needed, develop new methods.
4. Determine the reproducibility of the flowmeter test results.
5. Determine the sensitivity of the test results to different flow rates.
6. Evaluate the impact of well installation methods and skin effects on the borehole flowmeter results.

B. GENERAL APPROACH

Borehole flowmeter surveys were conducted at the test site during July 1988, December 1988, and April 1989. The July 1988 survey included the five reconnaissance wells shown in Figure 1 of Volume I. The December 1988 survey included Wells 1 to 23. The April 1989 survey included all 37 wells. Although each of the surveys was similar, several important differences existed. These differences included the type of flowmeter used, the pumping rates, and the method used to measure the drawdown-response in a well.

In July 1988, an impeller flowmeter from Haferland Geophysical was used. The primary objectives for this survey were to provide the information necessary to select a test site and determine the feasibility of injecting instead of pumping water during a borehole flowmeter technique. Problems with the impeller meter during the July field tests and with prior laboratory tests provided the impetus for TVA to investigate an alternative flowmeter design. After a review of several different methods to measure flow rates, TVA decided to develop an electromagnetic (EM) flowmeter.

In December 1988, a prototype EM flowmeter was used. The EM flowmeter provided greater than an order of magnitude lower detection limit than the impeller meter. Appendix A describes the testing on both the impeller and the EM flowmeter. At each of the 23 wells, the borehole flowmeter measurements were taken during a moderate pumping rate (26 to 38 L/min) and a low pumping rate (15 to 22 L/min). At selected wells, vertical gradients were measured at the tube locations shown in Figure 6, Volume I. The vertical gradients were measured with the vacuum manifold developed as part of the EPRI-MADE project (Young and Boggs, 1988; Boggs, et al., 1989).

In April 1989, borehole flowmeter tests were conducted at all 37 wells by injecting water at a rate near 22 L/min. The well responses were measured using an EM flowmeter and a Druck pressure transducer. Injection tests were used to provide a maximum saturated aquifer thickness for the flow measurements. The EM flowmeter was used because

it is more accurate, precise, and durable than the impeller meter. The pressure transducer was used to accurately measure the drawdown response at 1-second intervals. A summary of the differences among the three borehole flowmeter surveys is given in Table 7.

TABLE 7. SUMMARY OF ACTIVITIES FOR EACH BOREHOLE FLOWMETER SURVEY

Borehole Flowmeter Survey	Wells	Field Method	Major Objectives
July 1988	R1-R5	Impeller Flowmeter Moderate Pumping Rates Moderate Injection Rates Manual Head Measurements	-conduct reconnaissance -locate test site -evaluate impeller meter -evaluate feasibility of injection tests
December 1988	1-3,5 6-23	Electromagnetic Flowmeter Moderate Pumping Rates Low Pumping Rates Manual Head Measurements Vacuum Manometer	-evaluate electromagnetic flowmeter -quantify effect of different pumping rates -measure vertical gradients outside of well casing
April 1989	1-37	Electromagnetic Flowmeter Moderate Injection Rates Manual Head Measurements Transducer Head Measurements	-evaluate skin effects -increase vertical coverage as much as possible

C. METHOD OF ANALYSIS

Appendix B describes in detail the method used to determine hydraulic conductivity profiles from the borehole flowmeter data. The method includes three steps. The first step is to determine the ratio of the hydraulic conductivity values at each layer, K_i, to the depth-averaged hydraulic conductivity value. This ratio is calculated from the borehole flowmeter measurements of groundwater flow in the well before and during pumping and estimates of well head losses. The second step is to determine the value of the depth-average hydraulic conductivity K from a Cooper-Jacob straight-line analysis of the drawdown curve. The third step is to determine the hydraulic conductivity for each layer by multiplying the value of K_i by K.

Implicit in the borehole flowmeter data analysis is that given negligible headlosses, the vertical distribution of horizontal flow to the well is unaffected by the pumping rates. Appendix C presents the vertical distribution of horizontal flows obtained at 20 wells for the April injection test and the two December pumping tests. The comparison of the distributions shows very good agreement between the two pump tests when the drawdown is similar. These comparisons typically show flow distribution values within 30 percent. Some of the other comparisons, though few, had flow distribution values that were typically within a factor of 100 percent. These comparisons occurred when the drawdown value for the tests was greater than 0.8 meter.

At CAFB converging and diverging groundwater can be inferred from the vertical flowmeters up to 3 L/min (Table B1) in the fully screened wells under ambient conditions and the significant vertical gradients (up to 10 percent) alongside the outside of the well during pumping conditions. The complex flow patterns to the well are affected by the amount of drawdown, flow rate, skin effects, and natural soil heterogeneity. Changes in vertical flow distribution, with the rate and the direction of pumping, are possible (given the very heterogeneous conditions at CAFB).

If vertical flow near the well is the primary reason for the differences in the distribution of flow, then the largest differences should occur between the injection and the high-rate pumping tests. Figures C1 to C4 show this trend. Because vertical flow occurs during some of the pumping tests, one may argue that the data analysis method presented in Appendix B should be changed to accommodate vertical flow. Theoretically, a data analysis approach with two-dimensional flow can be achieved using optimization techniques. However, the development of such a method exceeded the resources of the project and does not promise significant improvements over the method listed in Appendix B.

The analytical solution for two-dimensional flow to a well with a skin effect in a multilayered aquifer would require numerous assumptions about the aquifer. In many cases, if not most, the uncertainty associated with these assumptions would offset benefits gained from a more complex analytical solution. Although Appendix C shows that the

flow distribution changes with the pumping rate and direction, the uncertainty associated with these changes averages near a factor of 2. From a practical viewpoint, this amount of uncertainty is acceptable and expected because of the numerous uncertainties associated with the three-dimensional structure of the aquifer, the three-dimensional flow patterns in the aquifer, and the simplification of conceptually dividing the aquifer into discrete horizontal layers to analyze the flowmeter data.

D. BOREHOLE FLOWMETER RESULTS

Before the April injection borehole flowmeter tests, the sensitivity of the calculated depth-averaged hydraulic conductivity to the pumping rate was not known. In fact, the analyses of the April time-drawdown curves led to the series of multirate pumping tests at each of the wells. As shown in Table 27 of Volume I, large differences exist at most of the wells for the calculated depth-averaged hydraulic conductivity values for the low-rate pumping tests, which typically had flow rates between 10 and 20 L/min, and for the injection tests, which typically had flow rates between 21 and 23 L/min.

Because the results of the low-rate pumping tests provide a better estimate of the depth-averaged hydraulic conductivity with regard to the aquifer material near the well than the results of the injection tests, the April borehole flowmeter results were modified to include the information from the low-rate pumping tests. From the April borehole flowmeter injection tests, a second set of hydraulic conductivity measurements were created. This set, shown in Figures 12 to 14, are the relative hydraulic conductivity distributions as determined by the April borehole flowmeter results scaled to the depth-averaged hydraulic conductivity values for the low-rate pumping tests.

E. GENERAL STATISTICS

1. The Complete 37-Well Data Set

Table 8 summarizes the statistical properties of the borehole flowmeter hydraulic conductivity distributions. By applying the

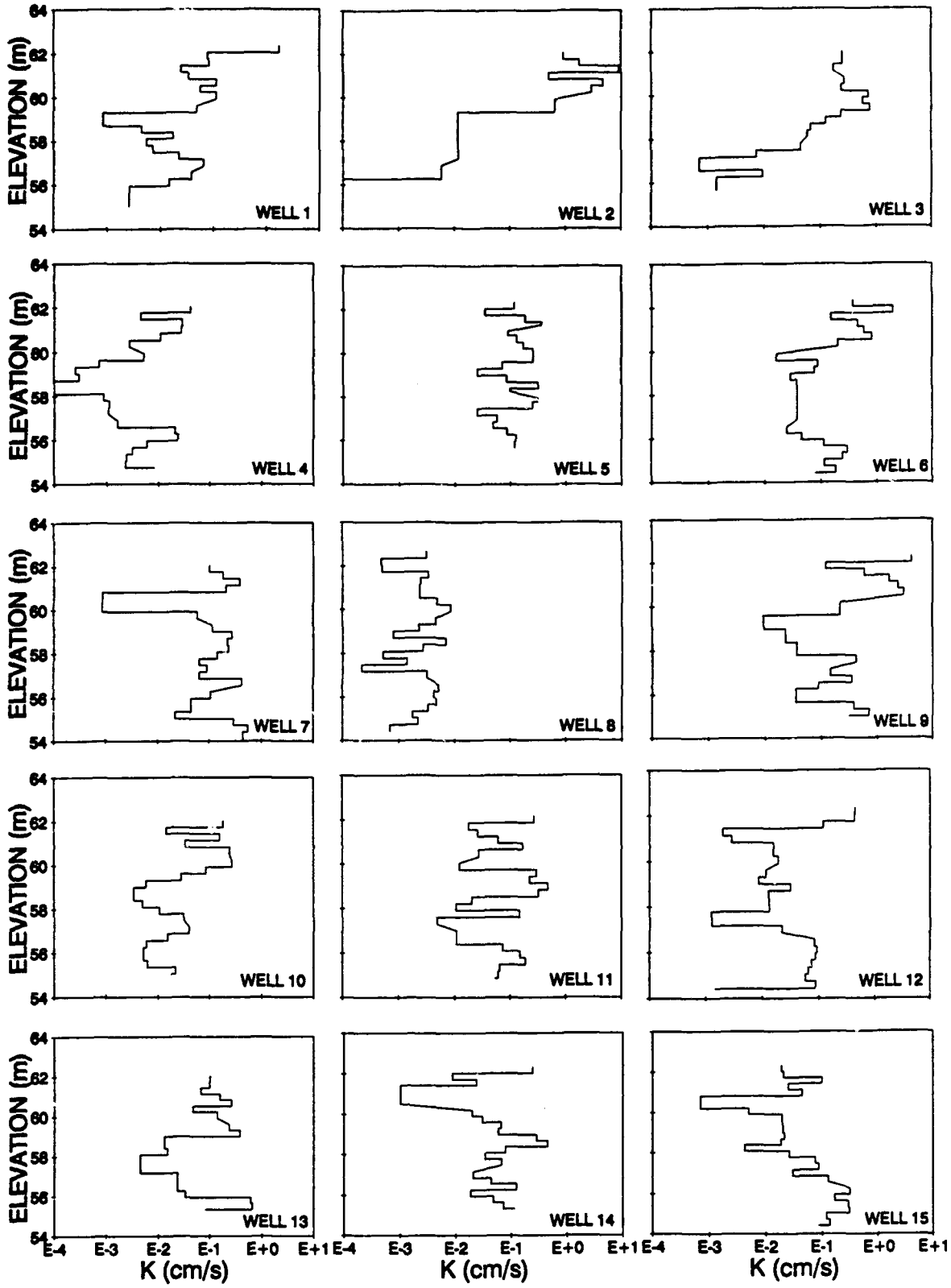

Figure 12. Vertical Profiles of Hydraulic Conductivity for Wells 1 - 15.

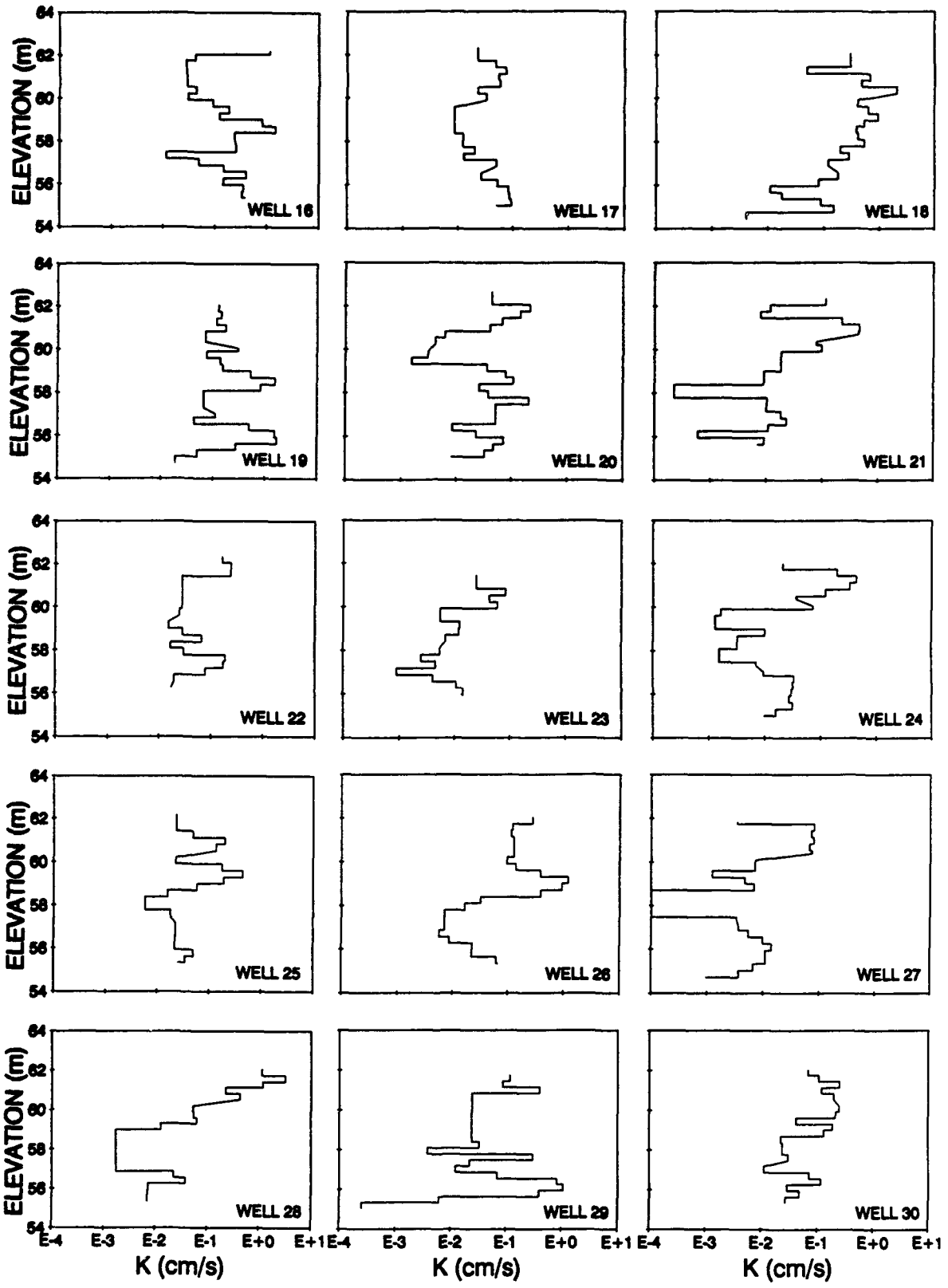

Figure 13. Vertical Profiles of Hydraulic Conductivity for Wells 16 - 30.

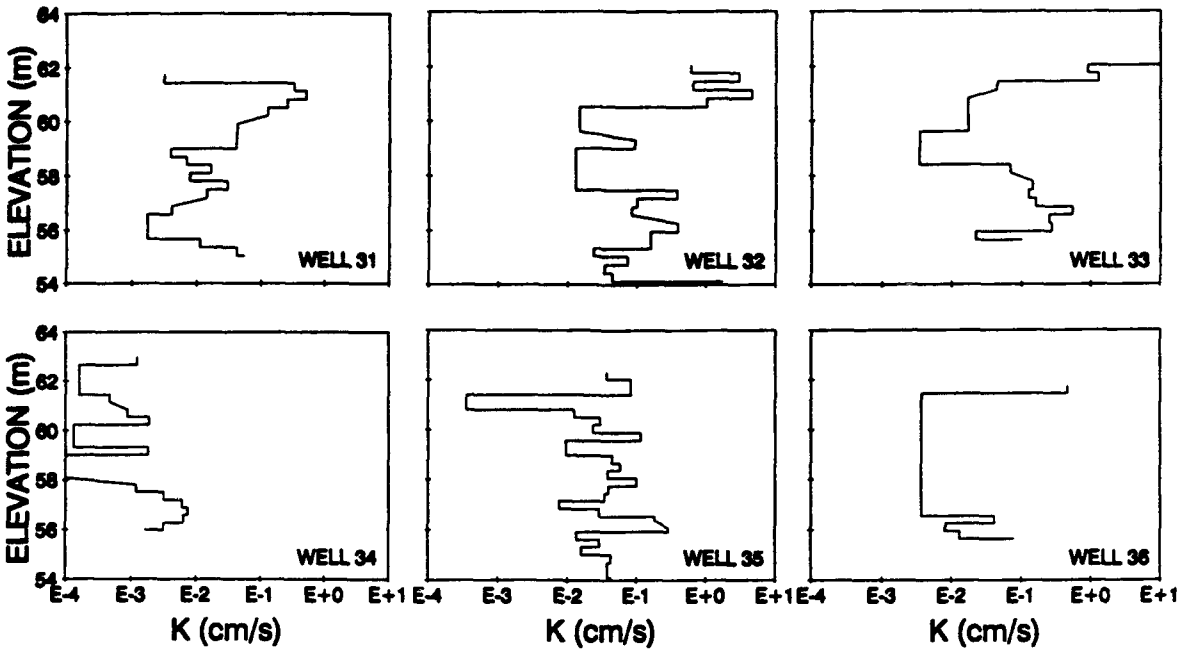

Figure 14. Vertical Profiles of Hydraulic Conductivity for Wells 31 - 36.

Kolmorgorov-Smirnov Test (Liffifors, 1967) both normality and log normality can be rejected at the 99 percent confidence limit for the data set. One possible criticism of applying the Kolmorgorov-Smirnov test is that the 881 sample points are not random; consequently, a bias exists in the data set. Indeed this is the case, but because of the rather large "KS" values in Table 8, it appears that most, if not all, of the random samples taken from the 881 hydraulic conductivity measurements would be neither normally nor log-normally distributed.

TABLE 8. ARITHMETIC AND GEOMETRIC MEANS FOR 881 HYDRAULIC CONDUCTIVITY DATA POINTS

	Normal	Log_{10}	LN
Arithmetic Average (cm/s)	0.261	-1.49	-3.42
Variance	2.54	.889	4.71
KS	0.483	0.143	0.143

KS = value calculated to check for normality based on the Kolmorgorov-Smirnov Test (Liffifors, 1967). Normality can be rejected at the 99 percent and/or 95 percent confidence limits if KS is greater than 0.034 and 0.030, respectively.

The lack of normality or log-normality is very significant in relation to stochastic theories that have this assumption as one of their premises. These stochastic theories have been receiving considerable attention in the literature. Two applications of stochastic theories are the prediction of macrodispersivities (Gelhar and Axness, 1983) and the development of optimized well networks for pump-and-treat remediations (Wagner and Gorelick, 1989).

2. Probability Density Functions (PDF)

Although the PDF of the hydraulic conductivity field for the entire region is of interest, the usefulness of this PDF for interpreting the data set is dependent on the representativeness of the PDF to each different region in the entire region. Hence, whenever a global PDF is developed from a group of spatially oriented data points, one should

compare it to regional PDFs to determine the potential usefulness of the global PDF for interpreting among the original data points or simulating alternative realizations of the original data points.

Several methods exist to compare the statistical properties of different data sets, but all of these methods assume that the data sets are composed of independent and identically distributed samples. As with the Kolmorgorov-Smirnov test, this assumption is not possible with any designed experiment. Nevertheless, these methods will provide useful information about the potential difference between the global PDF and the regional PDFs. One method that makes no assumption of the distribution function for the data sets centers on the Kolmorgorov-Smirnov limiting distribution (Smirnov). Given a sample of n i.i.d. (independent and identically distributed) random variables X, and a sample of m i.i.d. random variables Y, this method evaluates the differences between the two empirical distribution functions Fn(x) and Gm(x) using Kolmorgorov-Smirnov's limiting distribution. The method provides the probability that the two empirical distributions were created from the same probability density function.

From the comprehensive borehole flowmeter data set, six smaller data sets were created by partitioning the comprehensive data set into a top zone and a bottom zone, by partitioning the comprehensive data set into an east zone and a west zone, and by partitioning the comprehensive data set into a north zone and a south zone. Table 8 provides the detailed criteria used to partition the comprehensive data base. To use the Kolmorgorov-Smirnov's limiting distribution to compare data sets, each data set should have at least 100 points. As shown in Table 9, none of the data sets have less than 320 points.

Table 9 lists the average and the variance for both the normal and the logarithmic values for each of the data sets. For the normal values, the averages and the variances range from .089 to .413 cm/s and from .036 to 6.55 cm^2/s^2, respectively. For the logarithmic values, the averages and the variances range from .021 to .046 cm/s and from .742 to 1.14 cm^2/s^2, respectively. The wide range of values for the first two moments of the data sets and the plots (Figure 15) of

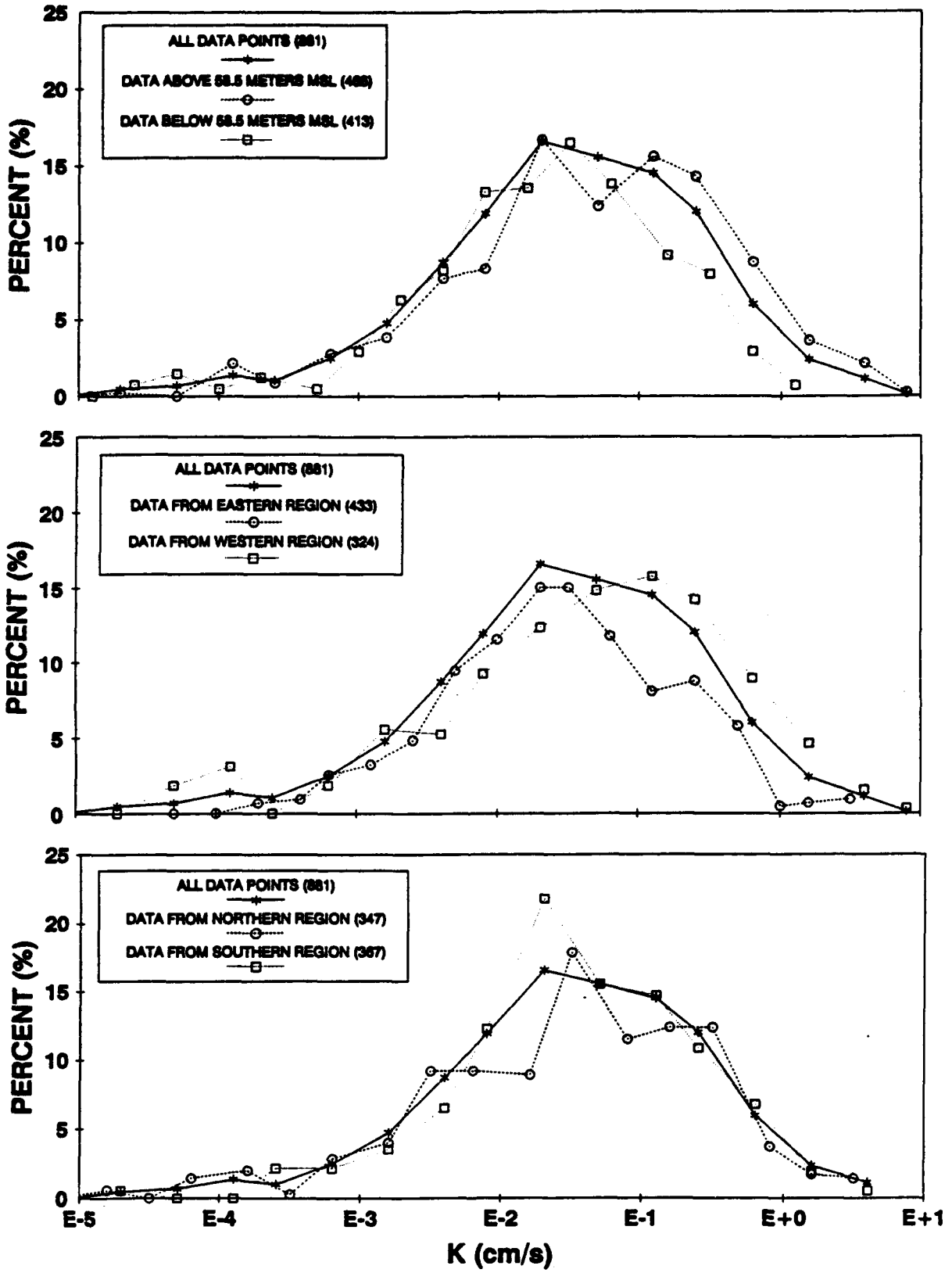

Figure 15. The Probability Density Function for the Hydraulic Conductivity Values at Different Regions Across the Test Site.

the frequency distribution for each data set indicates that trends (different PDFs) may exist in different zones of the test site.

TABLE 9. COMPARISON OF THE STATISTICAL PROPERTIES FOR SELECTED DATA SETS FROM THE 881 HYDRAULIC CONDUCTIVITY DATA POINTS

	Hydraulic Conductivity Data Sets*						
	All	Upper	Lower	East	West	North	South
Number of Points	881	468	413	433	324	347	367
Arithmetic Mean	.261	.413	.089	.137	.483	.195	.319
Variance	2.54	4.71	.036	.120	6.55	.312	5.45
Logarithmic Mean	.0319	.0458	.0212	.0276	.0450	.0383	.0349
Logarithmic Variance	.889	.962	.749	.619	1.14	.941	.742
Probability*		<1%	<1%	4.0%	<1%	89%	22%

* The percent likelihood that the regional and the complete data sets are realizations of the same probability density function (PDF) based on the Kolmorgorv-Smirnov's limiting distribution (Feller, 1948; Smirnov, 1948)

Note: 1. The hydraulic conductivities included in the data sets are as follows: Top - values above 58.5 meters MSL; Bottom - values below 58.5 meters MSL; East - values from Wells 7,8,9,10,11,12,15,17,20,21,22,23,24,25,31, 32,35, and 36; West - values from Wells 1,2,3,13,14,16, 18,19,26,28,30,33,34, and 37; North - values from Wells 3,6,9,11,14,15,16,20,23,26,27,31,34,36, and 37; South - values from Wells 1,4,7,12,13,17,18,21,24,25,29,30,32,33, and 35.

2. Based on the Kolmorgorv-Smirnov's limiting distribution the probability that the 'upper' and the 'lower' data sets are realizations of the same PDF is <1%; the probability that the 'east' and the 'west' data sets are realizations of the same PDF is <1%; the probability that the 'north' and the 'south' data sets are realizations of the same PDF is <5.8%.

As shown in Table 9, the Kolmorgorov-Smirnov limiting distribution states that there is less than a 1 percent chance that the same probability density function could have produced both the "comprehensive" and the "upper" data sets, the "comprehensive" and the

"lower" data sets, the "comprehensive" and the "west" data sets, the "lower" and the "upper" data sets, and the "east" and the "west" data sets. The low probabilities associated with comparison above indicate that significant regional differences exist in the structure of the hydraulic conductivity field. These differences are related to the site geology which is discussed in Section VI.

F. THREE-DIMENSIONAL HYDRAULIC CONDUCTIVITY FIELD

1. Stacked Two-Dimensional Plots

Figure 16 shows areal plots of the hydraulic conductivity patterns based on averaged values over the intervals 54-56 meters MSL, 56-58 meters MSL, 58-60 meters MSL, and 60-62 meters MSL. These plots were generated by the program GCONT, which uses a finite-element interpolation scheme (Harper, 1990).

At the deepest interval (54-56 meters MSL), only the central portion of the test site has measured hydraulic conductivity values. The deeper coverage in the central portion of the test site occurred because the Eutaw clay has a depression. Away from the central portion of the test site, the predominant material in the 54-56 meter interval is the Eutaw clay. Each well was installed about 0.5 meters into the Eutaw clay. The Eutaw clay has a horizontal hydraulic conductivity less than 10^{-5} cm/s.

Across the vertical interval of 54 to 56 meters MSL, a zone of high hydraulic conductivity cuts north-south through an area of moderate to low hydraulic conductivity. Given its sinuosity and stream-like configuration, the high hydraulic conductivity zone appears to have been created by a meandering stream. Across the vertical interval of 60 to 62 meters MSL, a striking feature is the configuration of the highest hydraulic conductivity zones that occur in the northern and western regions of the site. This configuration matches the configuration of the ox bow meander shown in Figure 10. Although potential geological features are definable at the upper and the lower regions of the saturated

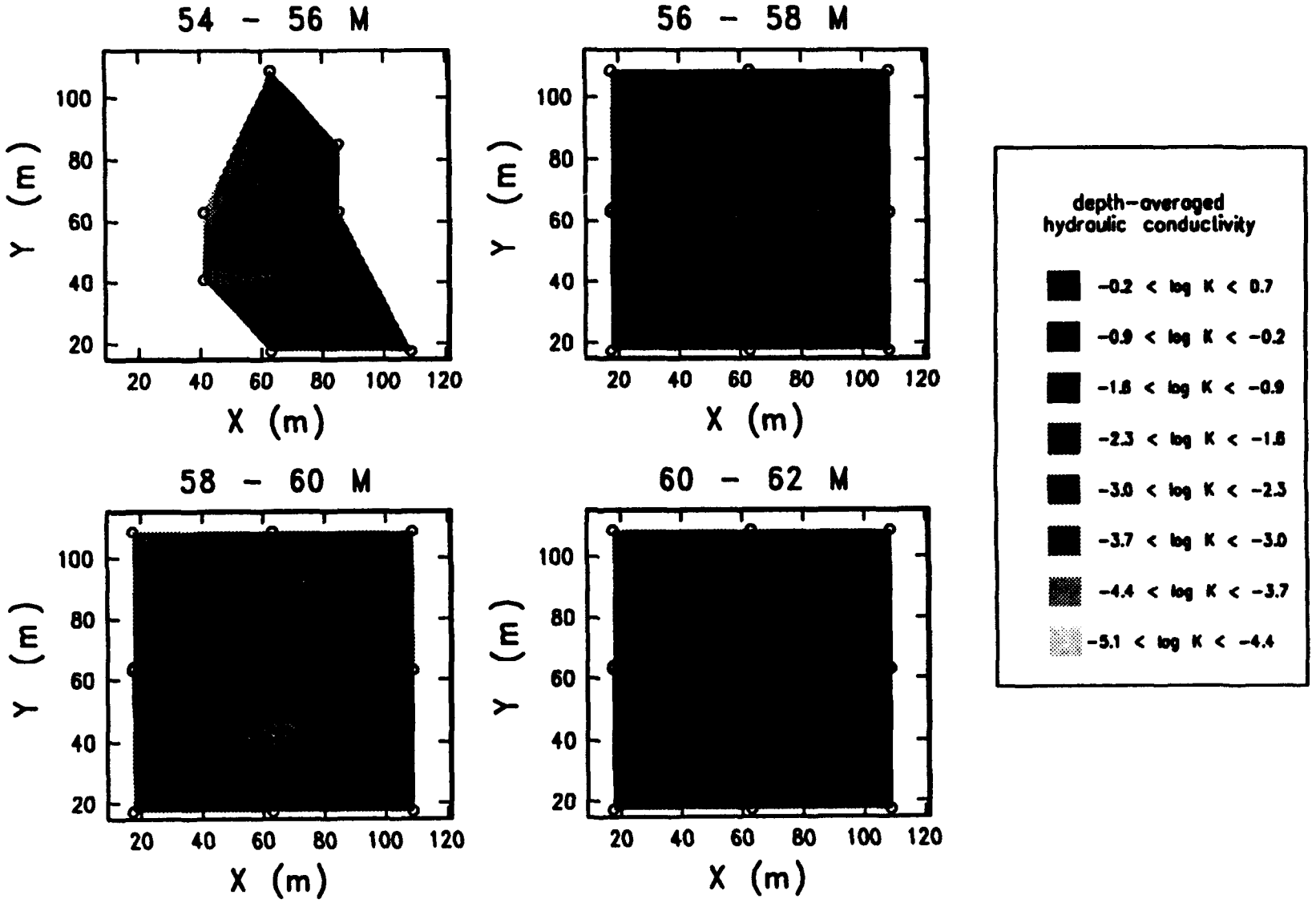

Figure 16. Depth-Averaged Hydraulic Conductivity Cross Sections of the Hydraulic Conductivity Field.

aquifer, no clear geological features are evident over the intervals from 56 to 60 meters MSL.

Overall, Figure 16 shows recognizable features and/or patterns in the hydraulic conductivity field. Based on the available information, it appears that these patterns have been produced by two different river systems. The first river system (i.e., the deepest) flowed primarily north-south and the second river system (i.e., the shallowest) flowed primarily east-west.

2. Fence Diagrams

Figures 17 and 18 are fence diagrams of hydraulic conductivity values greater and less than 0.07 cm/s at selected wells, respectively. The figures were created to assist in identifying the structure within the hydraulic conductivity field. The patterns of interest include information related to the orientation, shape, and size of the different hydraulic units in the aquifer. This information will improve the understanding of hydrogeological processes that created the aquifer. In turn, this will improve the methods for interpolating the hydraulic conductivity data points.

In Figure 17, the high hydraulic conductivity zones appear to fall into one of two categories. One group of lenses is about 1 meter thick, appears to be randomly distributed in the vertical, and occurs predominantly in the central and eastern section of the aquifer. A second group of lenses is from 1 to 3 meters thick, appears to be oriented in a southwest to northeast direction, and occurs predominantly along the transect from Well 28 to Well 36. Based on the known geology of the site, the first group of lenses was likely created by a braided stream environment and the second group of lenses was probably created by a meandering stream/river environment.

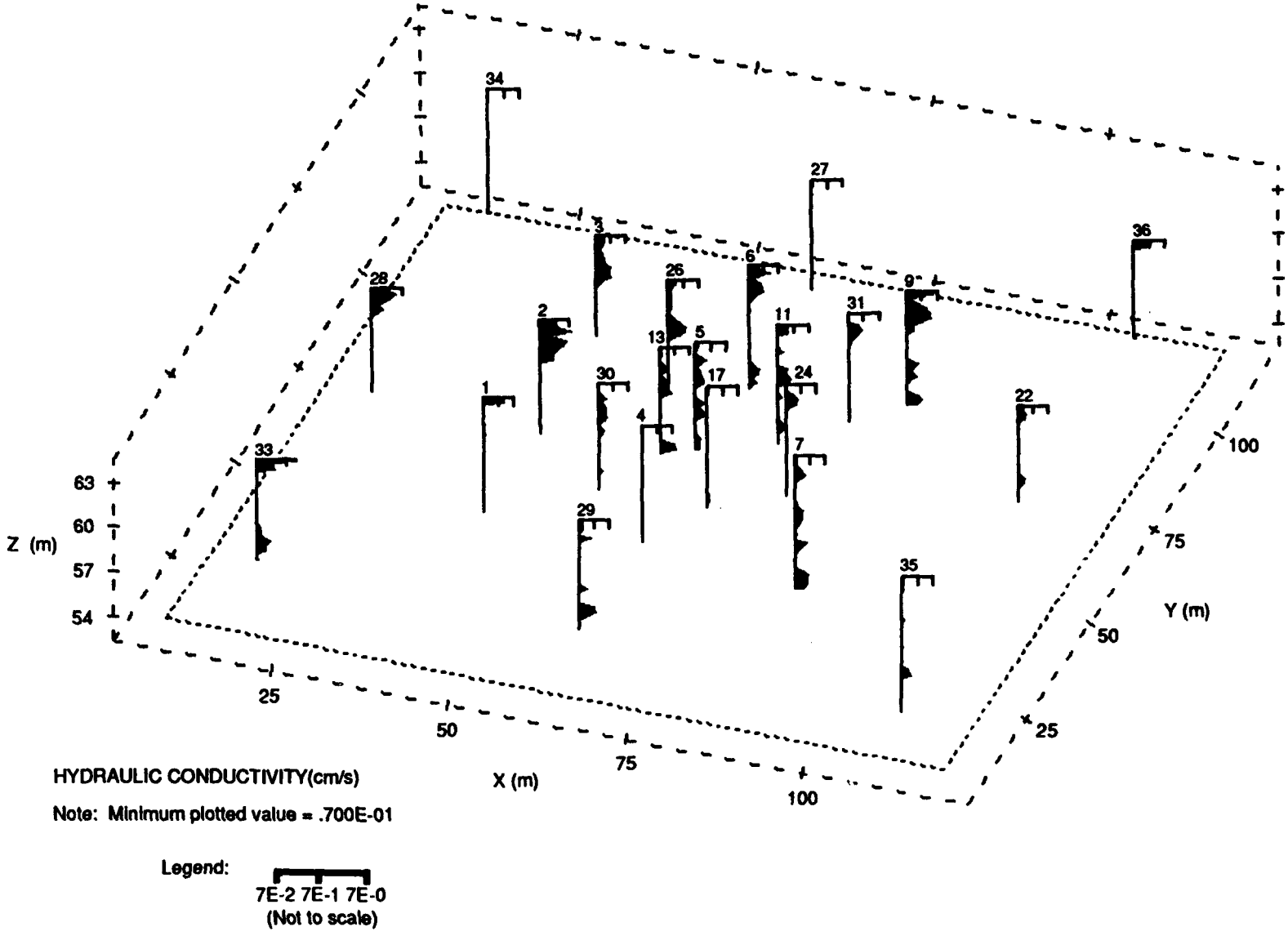

Figure 17. Fence Diagram of Hydraulic Conductivity Values Greater Than 0.07 cm/s at Selected Wells.

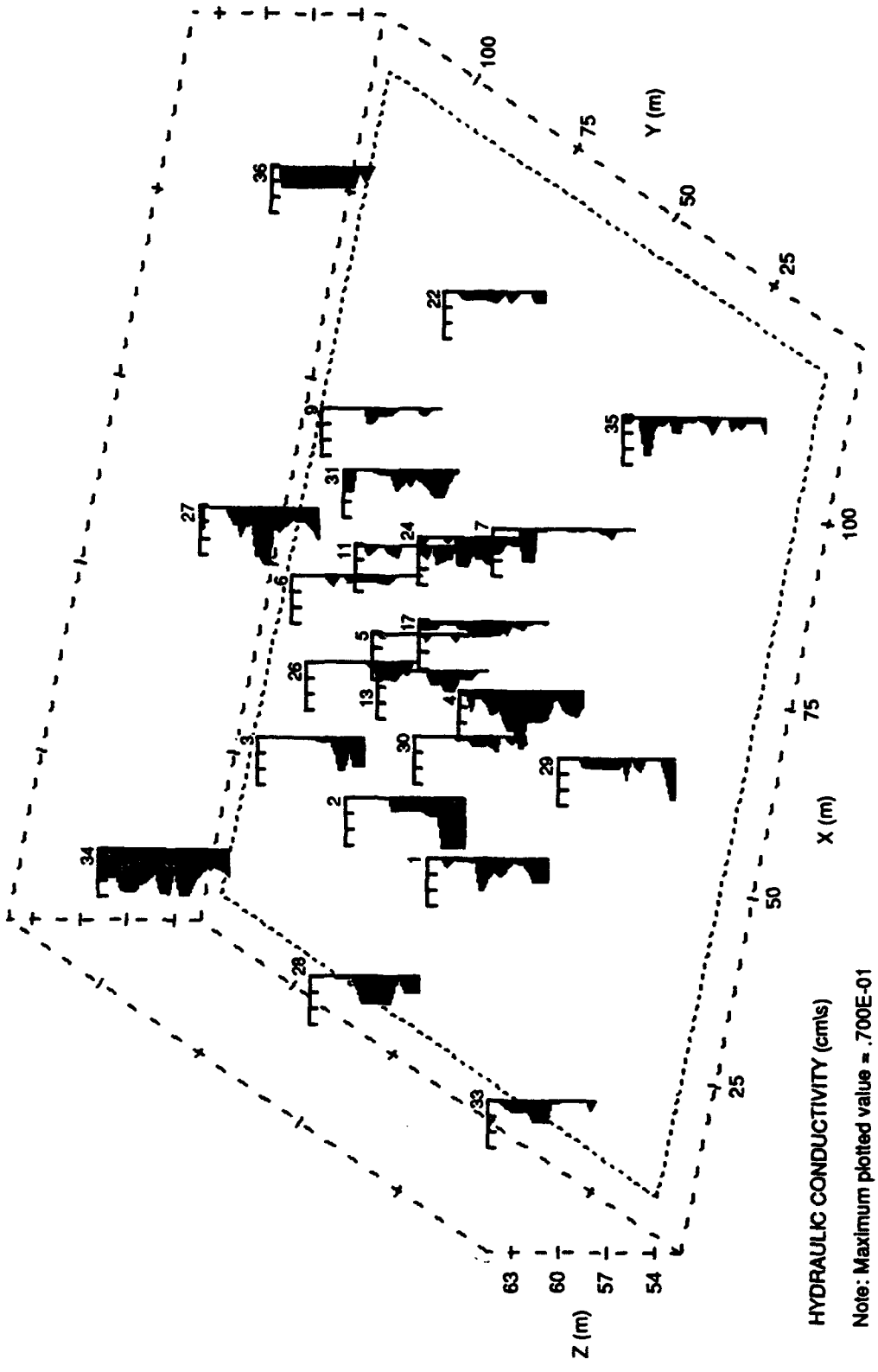

Figure 18. Fence Diagram of Hydraulic Conductivity Values Less Than 0.07 cm/s at Selected Wells.

(The reverse of this page is blank.)

SECTION IV

THE GEOLOGY OF THE COLUMBUS AIR FORCE BASE TEST SITE

A. GENERAL OVERVIEW

1. Importance of Depositional Environments

The borehole flowmeter results illustrated in Figures 12, 13, and 14 represent a heterogeneous aquifer. Hydraulic conductivity values vary orders of magnitude over vertical distances as small as 0.3 meter and over horizontal distances as small as 3 meters. A prerequisite to solute transport modeling is the interpolation of two- or three-dimensional continuous hydraulic conductivity fields from point measurements. Considerable debate exists within the groundwater literature for interpolating hydraulic conductivity data. Different interpolation methods include geostatistical methods, regression analyses, polynomial fits, fractal patterns, and different inverse weighting approaches. To a large degree, the selection of the method to create the three-dimensional grid will determine the representativeness of the solute transport predictions. Consequently, considerable care should be exercised in the selection and the application of the interpolation method.

Knowledge concerning an aquifer's depositional environments is valuable when developing a methodology for interpreting hydraulic conductivity values in three dimensions. This knowledge includes information related to the type, dimensions, and properties of the different facies (e.g., geological units) that compose the aquifer. An example of a depositional environment is a meandering stream; an example of a facies in a meandering stream environment is a point bar. Knowledge regarding the history of the depositional environments includes information concerning the geological period over which the different facies were deposited.

The importance of depositional environments can be readily seen in comparing coastal and fluvial aquifers. Coastal aquifers consist of sediments deposited from large-scale oceanic forces that change relatively slowly with respect to geological time. As a result, coastal

aquifers are homogeneous and relatively void of interfaces between sediments having significantly different hydraulic properties. Fluvial aquifers, on the other hand, consist of sediments deposited from small-scale fluvial forces that change relatively quickly with respect to geological time. As a result, fluvial aquifers are heterogeneous and contain distinct interfaces between different geologic facies.

2. Local Geology

a. Fluvial System

The upper aquifer at the Columbus Air Force Base test site consists of fluvial sand, gravel and clay deposited during the Quaternary Period (last 40,000 years, Pleistocene and Holocene) by the Tombigbee River and its tributaries. The aquifer is composed of approximately 11 meters of terrace deposits consisting primarily of poorly sorted to well-sorted sandy gravel and gravelly sand. The deposits often occur in irregular lenses and layers. Quaternary deposits unconformly overlie the Cretaceous Age Eutaw Formation consisting of marine clay, silt, and sand.

Two major categories of fluvial systems are meandering systems and braided systems. Both types can occur in one river in different locations at the same time, or at the same location at different times. Factors that control fluvial systems include bedrock composition physiography, climatological conditions, and topography.

b. Meandering Systems

Experiments and theory have shown that a stream in equilibrium will meander. The important facies associated with meandering streams/rivers are listed in Table 10 and shown in Figures 19 to 21. In a meandering-stream environment, both erosion of the cutbank and scouring in the deeper portions of the river channel produce sharp lower boundary interfaces between facies. Often the erosional surface is beneath the coarsest material present, typically channel-lag gravel and coarse sand. The grading of the material types becomes finer grained toward the top of the point bar, with primary structures changing from

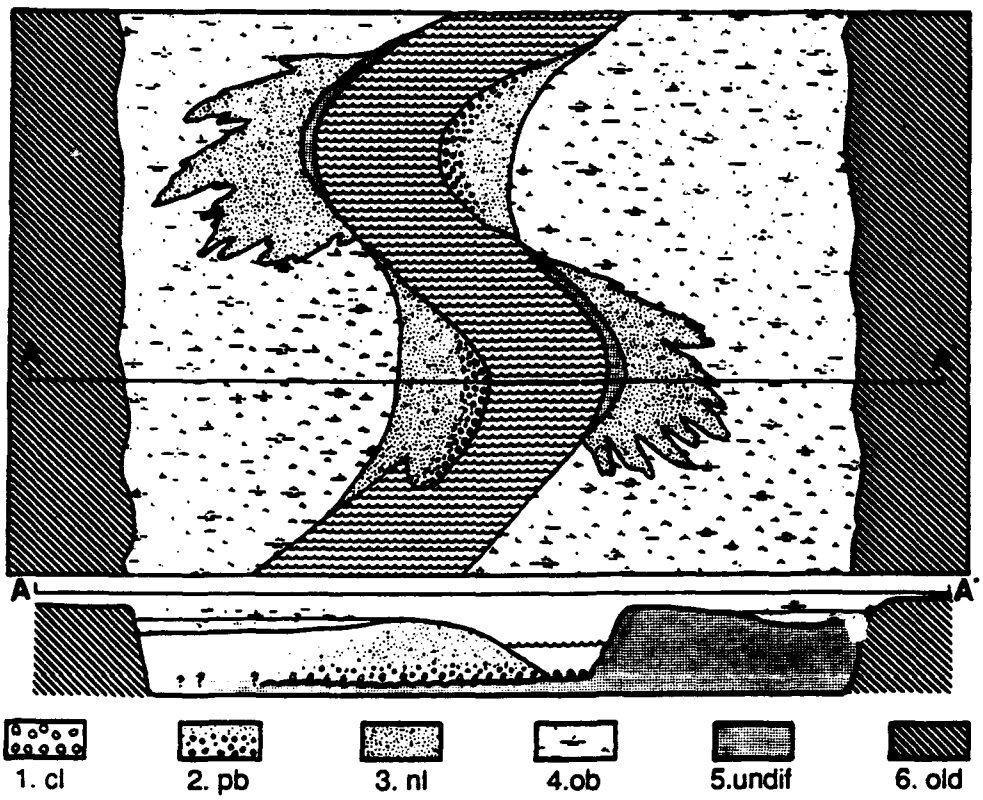

(1) Channel-Lag Deposits, Commonly Gravel
(2) Point-Bar Deposits
(3) Natural Levee (May Be Poorly Sorted)
(4) Overbank or Swamp Deposit
(5) Undifferentiated, Previously Deposited, Meandering-Stream Sediments, Now Subjected to Erosion and Resedimentation Downstream
(6) Older Sediments or Rock

Figure 19. Schematic Map and Cross Section Indicating Idealized Facies Relationships Within Meandering-Stream Deposits (after Matthews, 1974, p. 157).

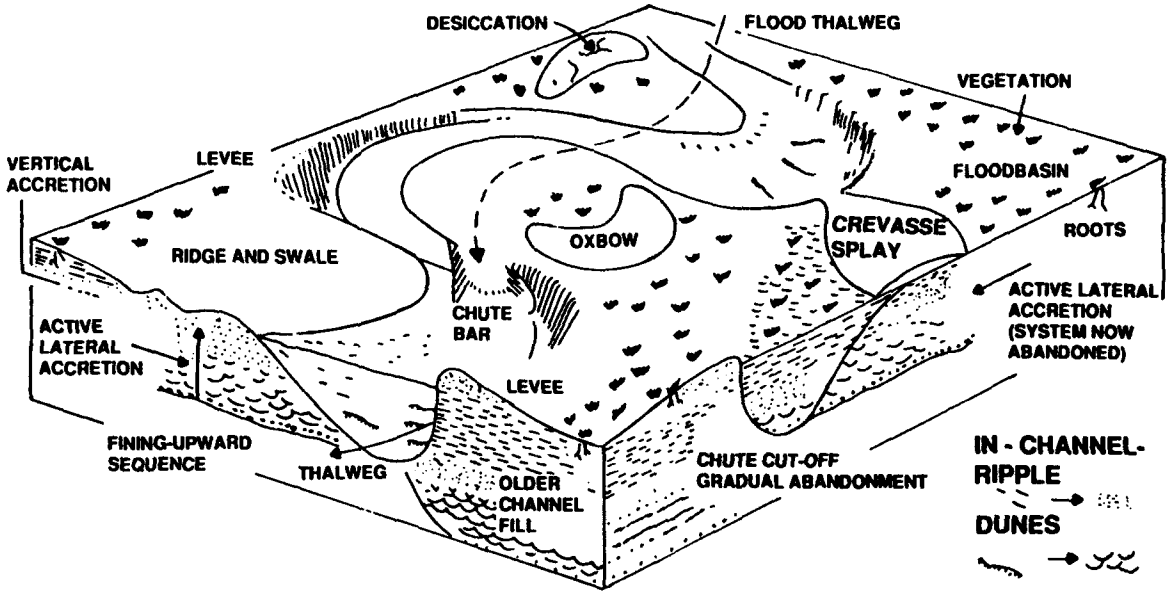

Figure 20. Block Diagram Showing the Major Morphological Elements of a Meandering River System (after Walker, 1979, p. 23).

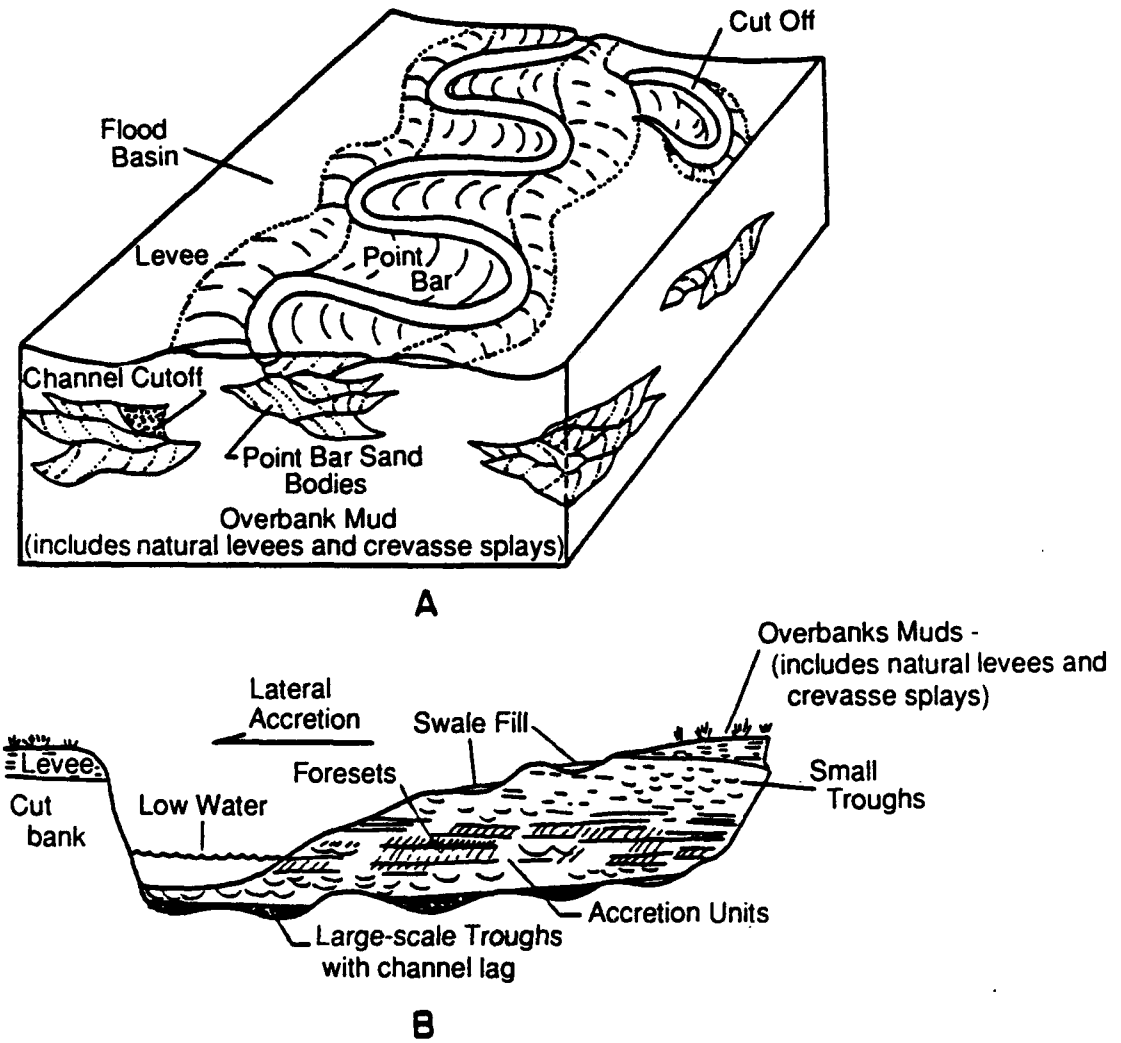

Figure 21. Schematic of Meander Belts and Point Bars (after Brown, et al., 1973, p. 17).

medium-scale, high-angle cross strata to low-angle or horizontal stratification and finally to small-scale, high-angle cross strata. The vertical sequence of these structures and sediments provides the primary basis for the "fining-upward units" in meandering streams. The upper portion of the fining-upward point bar consists of overbank deposits.

TABLE 10. IMPORTANT UNITS IN MEANDERING RIVER SYSTEM

Name	Typical Grain Size(s)	Geometry
Channel	coarse sand to gravel	snake shape
Point bar	fine to medium sand	half-circle moon shape
Overbank or Back Swamp Deposits	silt to clay	sheet blanket
Crevasse Splay	fine sand to silt	lobe shaped sheet
Ox Bow, Clay Plug	fine sand, silt, clay	snake shape

Generally, the channel deposits are the coarse gravels on the channel floor. The inner bend (point bar) consists of coarse sands close to the channel bottom (lower point bar) to fine sands on the upper part of the point bar. On the lower point bar (close to the channel) a bedform of sinuous crested dunes develops with a height ranging from 15 cm to 70 cm. These dunes, called cross beds or fore sets, can be used as an indicator of the local flow direction of the channel. As the main channel is migrating in the direction of its outer bend, the point bar on the inner bend is building itself outward, a process called lateral accretion. As a result, the point bar develops into a half-circular shaped sand body. This migration also results in regular vertical sequence sediments, overlying each other, successively deposited at a larger distance from the main channel. Therefore, a gradually fining upwards sequence can be expected.

Crevasse splay and overbank sands are deposited outside the main channel. The first category is originated by a break in the natural channel dike. The deposits are lobe-shaped sheets, generally fine sands

and silts, coarser towards the feeding point. The overbank deposits occur from flooding at a high stage. Since all coarse material is transported along the bottom of the channel, the overbank deposits consist mainly of silt and clay. Ox bows occur when a meander is cut-off and the main channel takes a shorter track. The old meander, only fed at high flood stage, is filled with fines and clay.

The only quantitative data published about the structural relationships in a meandering stream relates the channel width, the channel depth, and the sinuosity of the meander shape. Depth and width are defined as bankfull depth and width, being the maximum values before general discharge of floodwater occurs into areas outside the channel environment (Leeder, 1973). Sinuosity is defined as the ratio of the thalweg length to the valley length and thus serves as a relative measure of the curvature of the meandering river. Figure 22 (from Leeder, 1973) shows data from 57 measurements of depth and width of modern meandering rivers and a regression line for these data. Except for the channel width and thickness, limited data are available.

c. Braided Systems

Braided streams occur because a combination of hydraulic and topographical conditions cannot support the development of a meandering stream. These conditions include high hydraulic gradients, large sediment and water supply, and/or an easily erodible base. The main channel of the braided stream is typically unstable and from time to time can shift from one area of the river valley to another because of major fluvial activity. Figures 23 and 24 summarize the important structural features often found in braided stream environments.

Figure 23 shows a sequence of channels in the braided Donjek River. In Figure 23 the first order topographic highs are longitudinal bars, separated from one another by large channels that carry most of the water at intermediate- and low-river stage. Because they are primarily a flood stage phenomenon, the internal characteristics of longitudinal bars are: (1) a relatively large mean grain size; (2) relatively poor sorting; (3) crude development of horizontal stratification; and

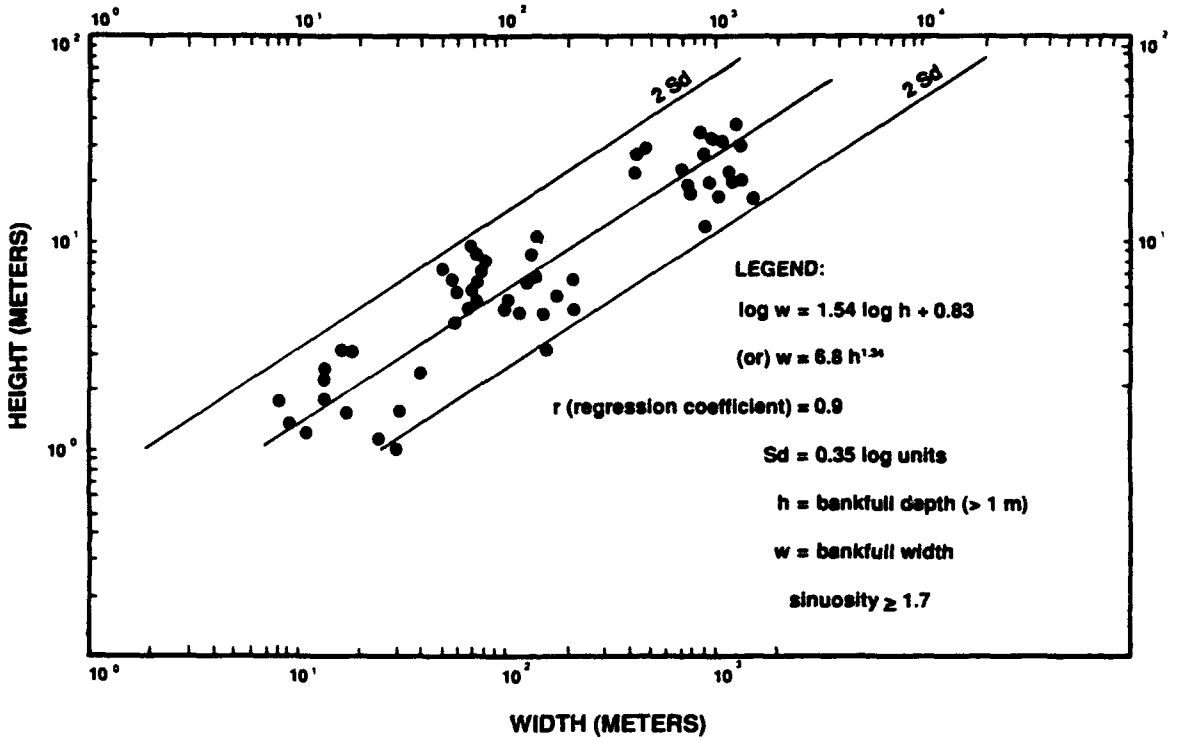

Figure 22. Plot of 57 Measures of Bankfull Depth Against Bankfull Width for Modern Meandering Rivers (after Leeder, 1973, p. 269).

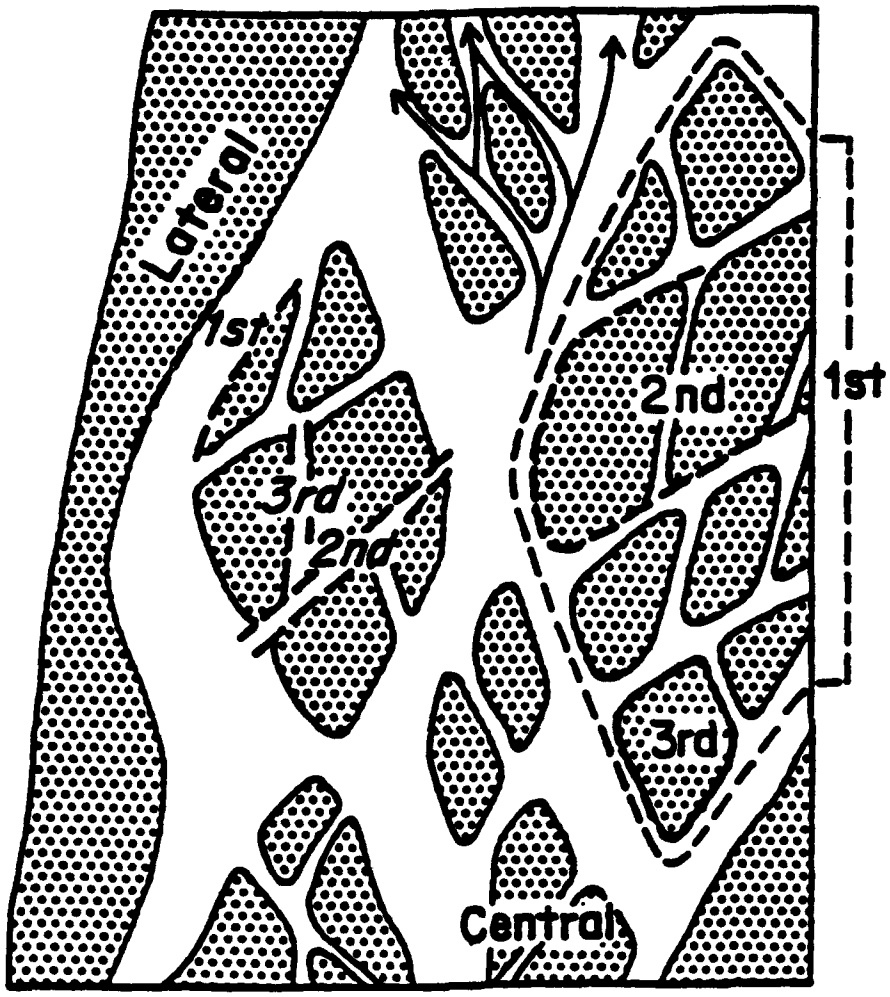

Figure 23. Map Depicting an Hierachal Network of Channel in a Braided Donjek River (after Williams and Rust, 1969).

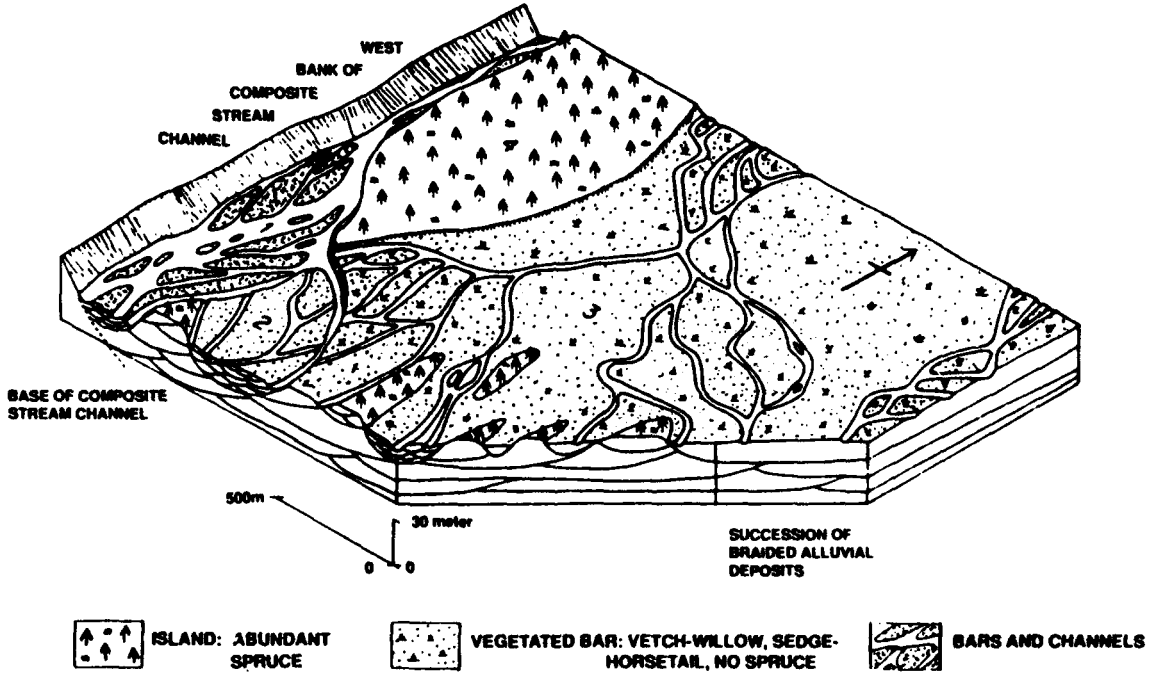

Figure 24. Schematic of the Complex Relationships Among the Different Facies in a Braided Stream Environment (after Williams and Rust, 1969).

(4) trough cross-stratification near the top of the bar (Matthews, 1974). During the low stages of the river, sedimentation on the longitudinal bars becomes negligible but transport and redeposition of sand-sized material continues in the channels and forms transverse bars. As compared to longitudinal bars, transverse bars include: (1) relatively smaller mean grain size; (2) relatively better sorting; and (3) a preponderance of high-angle planar cross-stratification topped by small-scale trough cross-stratification (Matthew, 1974). During periods of low flow, silt and other fine-grained sediments become deposited into the abandoned or inactive stream channels.

As a consequence of its depositional environments, braided streams are characterized by complex interfingering of facies that have horizontal scales of meters to tens of meters and vertical scales of centimeters to a few meters. Even though both upward-fining and upward-coarsing sequences of grain size can be formed within a braided stream, the gross arrangement of subfacies tends to be haphazard.

B. RECONSTRUCTION OF THE DEPOSITIONAL HISTORY AT THE SITE

1. General Overview

Because the CAFB aquifer sediments are relatively close to the Tombigbee River, the terrace aquifer depositional environments were primary fluvial systems. This information alone is enough to indicate that the aquifer is likely to be heterogeneous and that the identification of different facies in the aquifer would likely be difficult. As such, during the project any information about the structure of the local and regional topography, terrain, and aquifer was collected and examined. Table 11 lists the items in this data base.

The information in Table 11 represents a spectrum that includes information from the general to the specific and from the regional to the local scale. The approach was to identify regional trends and then use site-specific information to determine which regional trends were appropriate for the test site.

TABLE 11. TYPES OF INFORMATION COLLECTED TO RECONSTRUCT THE DEPOSITIONAL ENVIRONMENT OF THE CAFB TERRACE AQUIFER

Type of Information	Source
Aerial Maps of the Test Site	U.S. Air Force
Regional Aerial and Topographical Maps	U.S. Geological Survey
Thesis on Geology of County	Mississippi State University
Facies Mapping of CAFB Gravel Pits and CAFB Grain-Size Analyses	Electric Power Research Institute
Study of Depositional Trends in the Tombigbee River Valley	U.S. Army Corps of Engineers
Examples of Modern Braided and Meandering Stream Sediments	Journal Articles and Text Books
Soil Logs and Hydraulic Conductivity Measurements	This Project

2. Archeological Study in the Tombigbee River Valley

Under the supervision of the Army Corps of Engineers (ACE) an archeological study was carried out in the Tombigbee River valley to identify former living sites of ancient man (Muto and Gunz, 1986). It was recognized that the different elements of the surface physiography, as distinguishable from air photographs, were excellent first indicators for selecting the sampling sites. These sampling sites were approximately 50 meters by 150 meters and several of them were located in Columbus, Mississippi. Figure 25 shows the numerous ox bows, recognized from the air photographs, and the selected sampling sites near Columbus, Mississippi. This sampling included auger drilling to sample and describe the soils and depositional history altered and unaltered by human activity.

Figure 26 and Table 12 provide an interpretation of the river valley development from the early Pleistocene to modern times. During the Pleistocene, braided streams dominate the area, eroding the Cretaceous bedrock. The main topography (the Uplands, marked U in Figure 26) was shaped during this period. At the end of the Pleistocene (12,000 B.P.), following an erosional phase, deposits from braided streams and coarse-grained meandering streams are found. Remnants of the Pleistocene have been found in terraces (marked T1 and T2 in Figure 26) higher up in the valley. During the Holocene, uplift continues and

Figure 25. Physiographical Units Recognized From Air Photographs and Sampling Sites Selected by the Corps of Engineers Near the CAFB Aquifer (after Muto and Gunn, 1986).

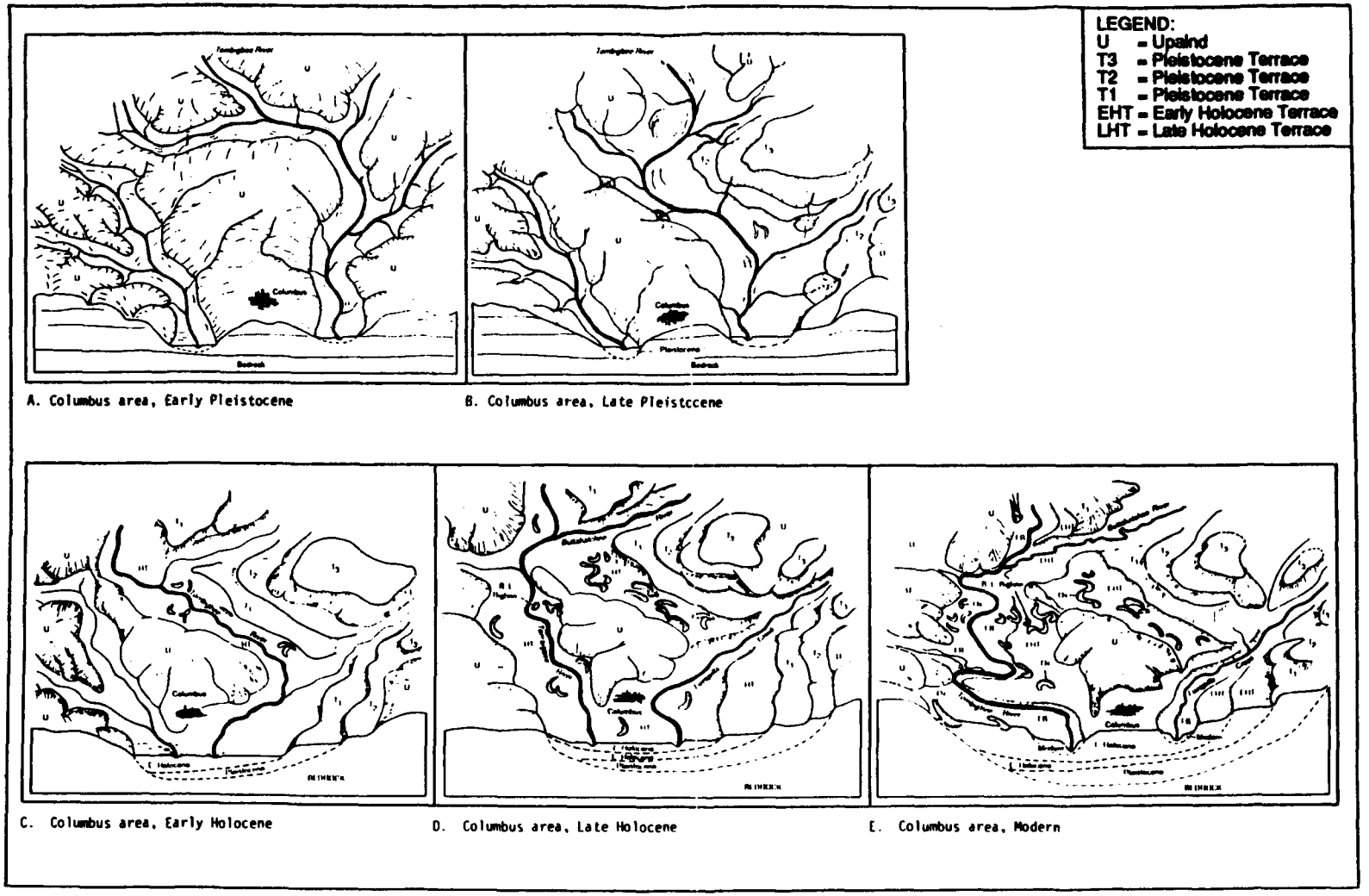

Figure 26. Evolution of the Tombigbee River Valley in the Columbus, Mississippi, Area (after Muto and Gunn, 1986).

terraces were found (EHT and LHT). The Tombigbee River remained metastable until an erosional period began shaping the current physiography in modern times (4,000 B.P.). During this metastable meandering environment, extensive overbank deposits were generated. Also remnants of ox bows (abandoned meanders, clay plugs) are found for this whole period. Appendix D presents a detailed description the river valley's development as provided by Muto and Gunn (1986).

TABLE 12. THE HOMEOSTATIC AND HETEROSTATIC PERIODS ASSOCIATED WITH THE DEVELOPMENT OF THE TOMBIGBEE RIVER VALLEY (after Muto and Gunn, 1986)

SCENARIO 1. PREBRAIDED STREAM PERIOD (> 16,000 B.P.)

I. Homeostatic environment periods
   A. From 19,200 to 18,200
   B. From 17,300 to 15,800

II. Heterostatic environment periods
   A. From 20,000 to 19,200
   B. From 18,200 to 17,300

SCENARIO 2. BRAIDED STREAM OR COARSE-GRAINED MEANDER BELT PERIOD (16,000 - 8,000 B.P.)

I. Homeostatic environment periods
   A. From 12,500 to 9,600

II. Heterostatic environment periods
   A. From 15,800 to 12,500
   B. From 9,600 to 6,400

SCENARIO 3. MEANDER BELT PERIOD (8,000 - 4,000 B.P.)

I. Homeostatic environment periods
   A. From 6,400 to 5,000

II. Heterostatic environment periods
   A. From 5,000 to 4,000

SCENARIO 4. RECENT PERIOD (4,000 B.P. - Present)

I. Homeostatic environment periods
   A. From 4,000 to 3,100
   B. From 2,100 to 1,500

II. Heterostatic environment periods
   A. From 3,100 to 2,100
   B. From 1,500 to Present

3. Aerial Photographs of a River Meander

As shown in Figure 25, numerous outlines of river meanders are visible in aerial photographs in the vicinity of CAFB. Figure 10 shows an aerial photograph of CAFB made in 1956. Aerial photographs taken several years previous show a recently leveled area that lacks any physiographical indication of a river meander. In 1956, however, differences in the growth patterns of newly developed vegetation outlined a former river meander. Photographs taken after 1956 do not show the river meander because of a dense vegetation cover.

Figure 10 shows that the 1-hectare test site includes the river channel in the northwestern and northern areas and the point bar in the southwestern and southern locations. The width of the channel visible in Figure 10 is about 70 meters. According to Figure 22, the channel depth should range between 2.3 and 7 meters. This estimate of the channel depth agrees well with the depths for the lower boundary of the highly permeable gravels at Wells 2, 3, 6, 26, and 9 which range from 4 to 7 meters.

4. Soil Logs From the MADE Site and the Test Site

During the installation of the well network, split-spoon soil samples were collected at 0.61-meter intervals for 10 wells. The samples were collected primarily for locating gravel and clay lenses and for evaluating the ease of soil sampling using different drilling methods. As part of the decisions to use the project's resources to their fullest, a grain-size analysis was not performed on any of the soil samples collected at the test site. Instead, the grain-size information collected from the 214 soil samples were used. Although the MADE soil samples were not collected from the test site, they were collected in the immediate vicinity of the test site and, as shown in Figure 10, the same former river channel that passes through the test site passes through the MADE site.

Based on the soil sampling and drilling activities for the MADE project, a contour map (Figure 27) of the top of the Eutaw clay formation

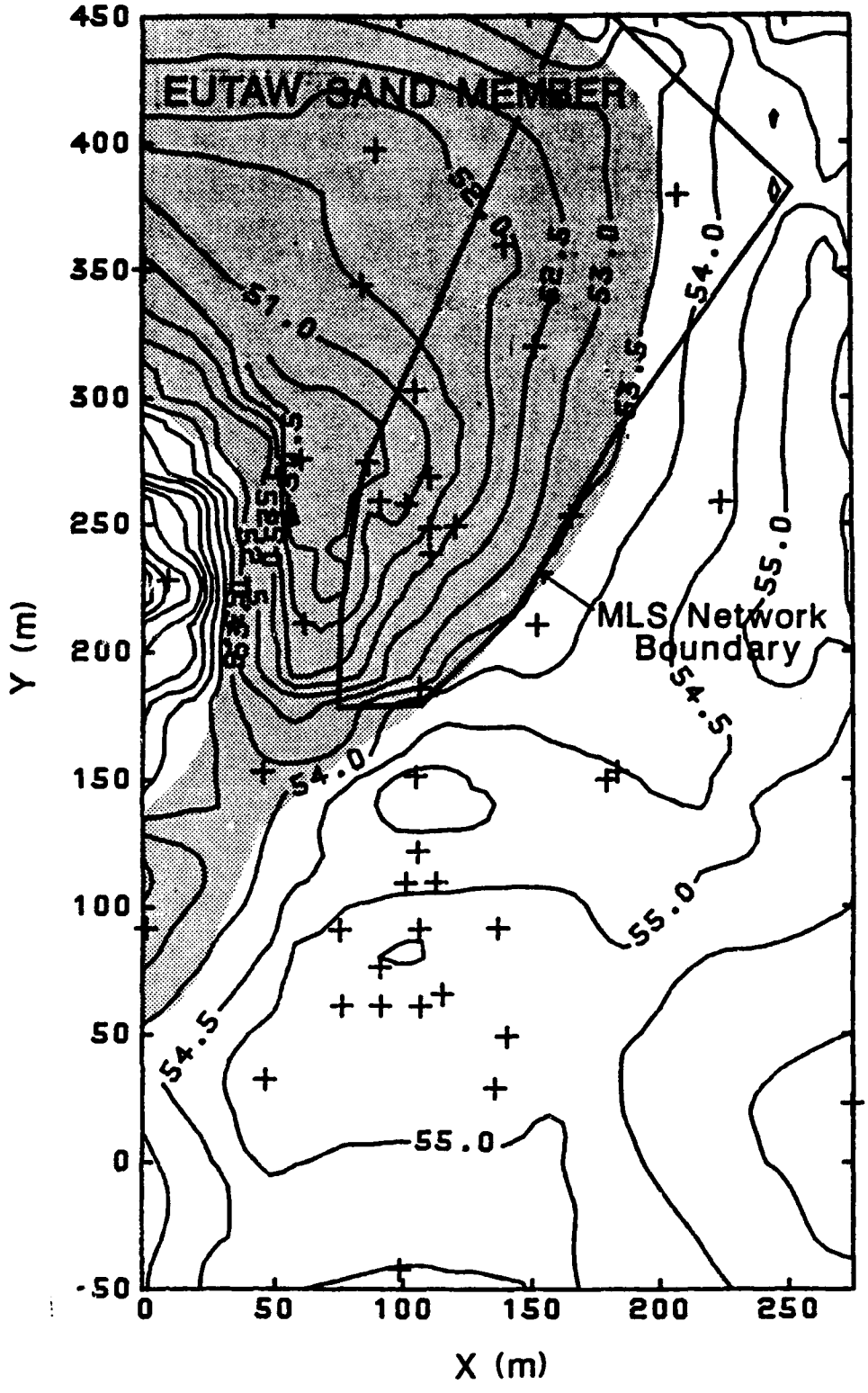

Figure 27. Elevation of Top of Eutaw Formation (Contours in Meters MSL -- after Boggs, et al., 1990).

was constructed. Figure 27 shows the elevation of the erosion surface upon which the terrace sediments are deposited. Over most of the study area, the Eutaw surface is composed of a dense clay which forms an aquitard beneath the terrace deposits. However, fine-grained marine sands, frequently containing thin interbedded clay and silt laminations, form the upper Eutaw in one subregion of the site. This sand unit ranges up to approximately 3 meters thick, and exhibits physical and hydraulic properties similar to those of the terrace deposits.

In Figure 27, the trough-shaped depression in which the Eutaw sand member lies resembles an erosional channel. The marine sands in the channel indicate that an ancient river and not the Tombigbee River scoured the Eutaw sand formation. The importance of the scoured river channel is that it confirms that fluvial depositional environments accounted for the aquifer's sediments.

Figure 28 shows a typical range of grain-size distributions found at the CAFB terrace aquifer. The bimodal distributions shown for Samples C, D, and E are the most frequently encountered distributions. Less common are the well-graded sand and gravel mixtures and uniform sands for Samples A and B. The type of bimodal distributions shown in Figure 28 are more characteristic of a braided rather than a meandering stream environment.

5. Facies Mapping of Outcrops

Approximately 1 km northeast of the test site, Rehfeldt, et al., (1989b) mapped sedimentary features observed in gravel pit exposures. Four major sedimentary facies were observed in the gravel pit exposures: (1) sandy gravel with bimodal mixtures of sand and gravel; (2) well-sorted sand; (3) a highly variable sandy, clayey gravel facies with substantial amounts of clay in pore spaces; and (4) open-work gravel facies of relatively limited horizontal and vertical extent. The sandy gravel facies appeared to be a matrix in which the other facies were embedded. Dimensions of the other facies ranged up to 8 m horizontally and less than 0.5 meter vertically. Figure 29 shows the map of the facies at the gravel exposures.

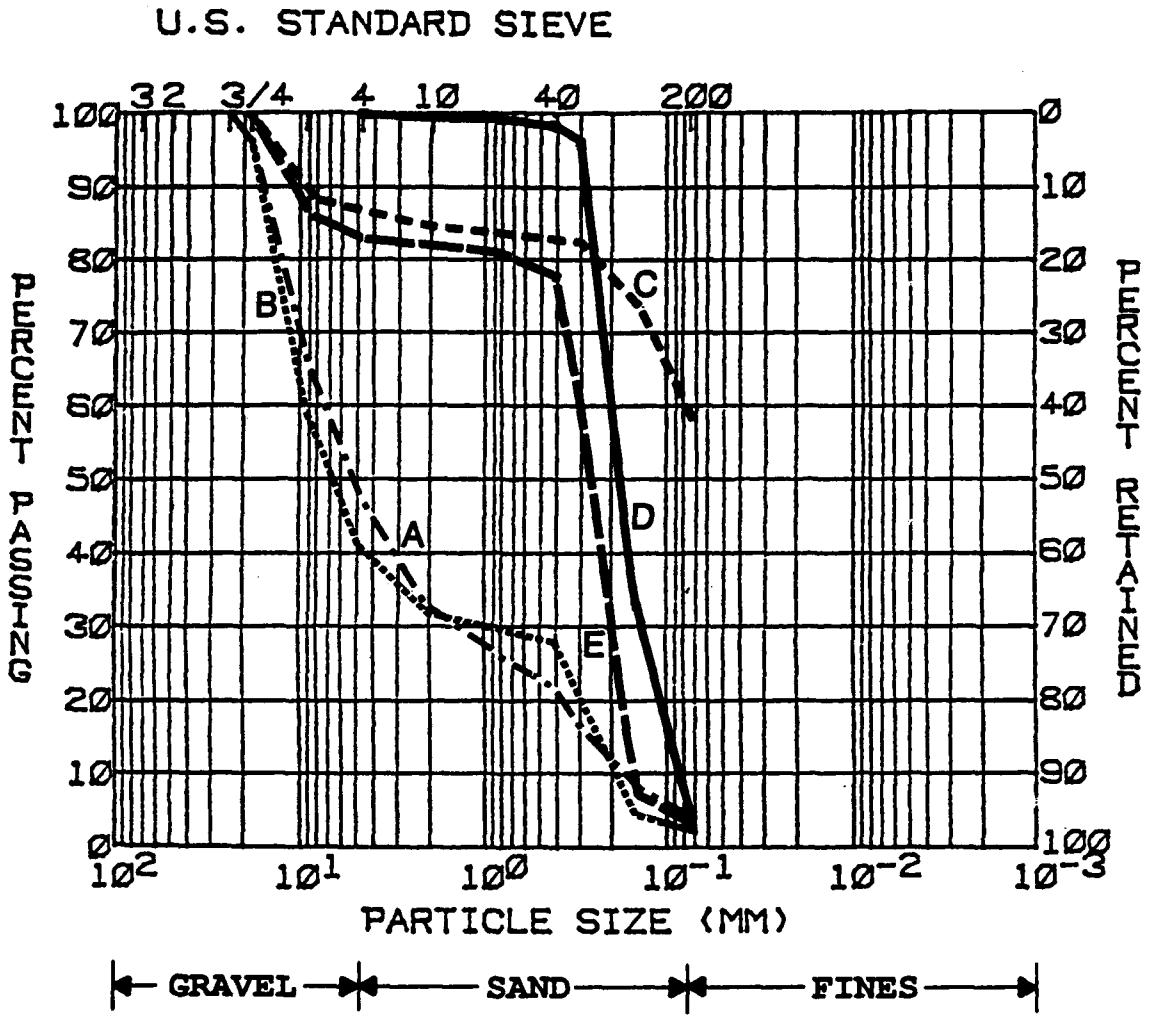

Figure 28. Typical Types of Soil Grain-Size Distribution for the CAFB Aquifer (after Boggs, et al., 1990).

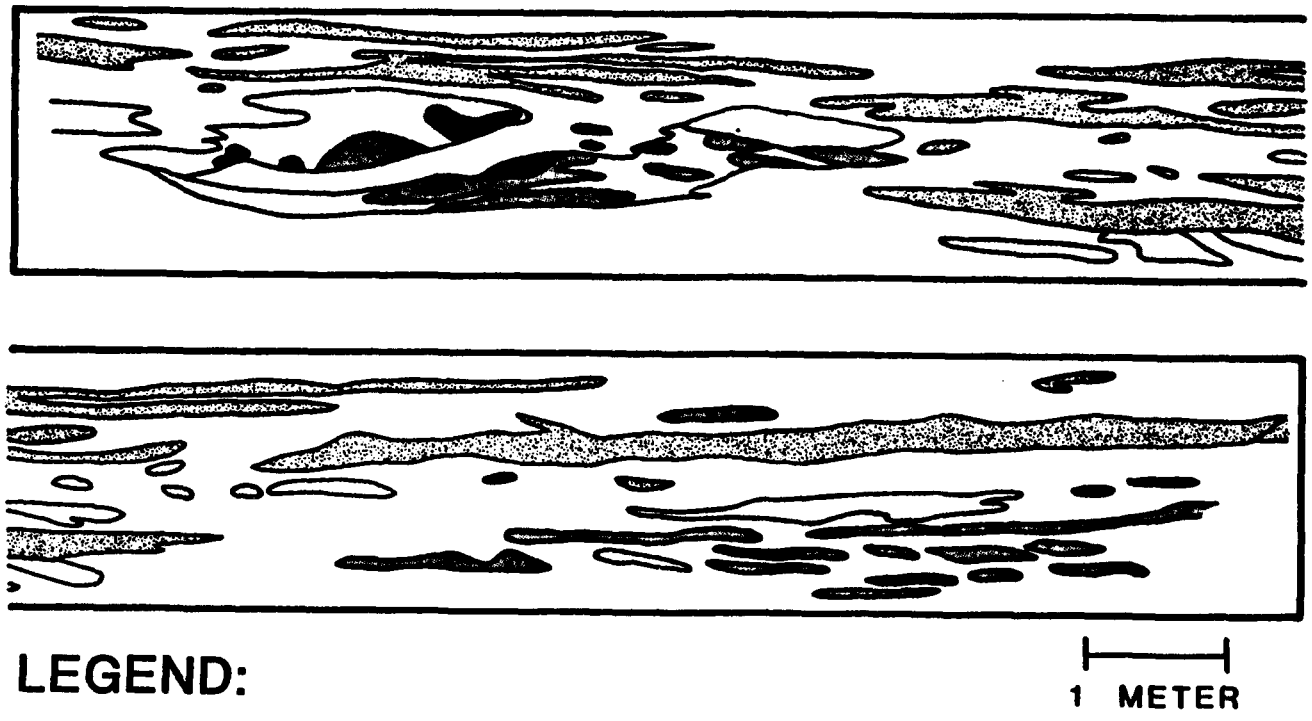

Figure 29. Geological Section of Facies Map at a CAFB Gravel Pit (after Rehfeldt, et al., 1989b).

It is not clear how representative these facies at the gravel pit are of the conditions at the MADE and the USAF test sites. The mapped gravel pit exposures included only the upper three meters of the terrace deposits which lie above the water table. However, similar materials have been found in soil cores at the test site, with the exception of the open-work gravels. This may be due either to the scarcity of the open-work gravels or failure to recognize these features in disturbed soil cores. Rehfeldt, et al. (1989), apparently had difficulty in interpretation of the facies as they state: "Based on unclear criteria the sands are interpreted as deposited by braided streams." Without disagreeing with the conclusion of Rehfeldt, et al. (1989), the author does question the merit of interpreting the facies map without complimentary information.

6. Borehole Flowmeter Data

The flowmeter results in Figure 16 show a zone of high hydraulic conductivity of about 40 meters that crosses the northern and northwestern portion of the site at an elevation of about 61 meters MSL. Within this region are areas several meters to about 20 meters wide with hydraulic conductivities in the range of 0.63 to 3.16 cm/s. These high hydraulic conductivity values are representative of pure gravel. Split spoon soil samples at Wells 2, 3, 6, and 9 have confirmed that gravels are the predominant aquifer material at the upper elevations at these well locations. These gravel deposits probably represent the bedload of the river channel shown in Figure 10.

Based on a 70-meter width for the river meander in Figure 10, Figure 22 indicates that the gravelly bedload of the river should be at a depth between 2.3 and 7 meters. The gravels are at a depth of 4 to 7 meters. At elevations near 61 meters MSL, Figure 16 shows materials of relatively low and moderately high hydraulic conductivity to the northwest and to the southeast of the river channel, respectively. Apparently, the river channel scoured through relatively low hydraulic conductivity material and deposited a material with moderate to moderately high hydraulic conductivity across the point bar.

Near elevation 55 meters MSL, Figure 16 shows a channel of high hydraulic conductivity that lies within a 1-meter trough scoured into the Eutaw clay. Near this river channel, sharp transitions in hydraulic conductivity values occur primarily on the outside of the river meander. An example is the sharp transition near Wells 2, 18, and 19. It is unclear whether the river that formed the channel was characterized more by a meandering or braided river system. On one hand, the higher conductivity material forms a sinusoidal pattern characteristic of meandering rivers. On the other hand, Figures 17 and 18 show that the different hydraulic conductivity units near the base of the channel have an erratic lenticular structure characteristic of longitudinal and transverse bars formed in a braided river.

C. DEPOSITIONAL MODEL

1. General Features

A late Holocene age meandering river, overlying early Holocene meandering rivers and/or late Pleistocene braided rivers is the conceptual model for the deposition of the fluvial terrace deposits at CAFB. In the upper aquifer, the point bar is the southeast and the river channel is in the northwest region of the test site. In the lower aquifer, a river has scoured the Eutaw clay and deposited sediments with a south-north orientation. The grain-size analyses for 214 split-spoon soil samples and a facies map of a gravel pit from sediments near the test site indicate that during the late Holocene, a meandering river removed sediments deposited earlier by a braided river. This scenario is supported by the very irregular lenticular structure of many of the aquifer hydraulic units. It is hypothesized that the late Holocene River is the present Buttahatchee River. Furthermore, the river that existed during the early Holocene or late Pleistocene was either the Tombigbee or the Buttahatchee Rivers or one of the rivers' tributaries.

2. Meandering and Point Bar Deposits

Classically, a well established model exists for the sedimentation of sands on the point bar (the inner meander bend). The

grain size of the deposited sands trends from medium coarse to very fine at a distance from the channel. Due to outward channel migration, a typical vertical sequence at a specific location shows a fining upward trend, with clay drapes occurring in the top half of the sequence. An extensive review of point bar deposition is provided by Reading (1986).

The grain size of the gravelly sands at the test site, of which the upper half evidently were deposited on a point bar, is coarser than would be predicted by the classical point bar model. The observed abrupt changes in the vertical sequence and the absence of the typical fining upward trend, point to more catastrophic depositional events. Such events result in an uneven sand distribution and more chaotic occurrence of gravel lenses and clay drapes (Collinson and Thompson, 1989).

Figure 30 shows a cross section and Figure 31 shows an aerial view of two modern point bars of the Amite River in Louisiana that have been described by McGowen and Garner (1971). The cross section shows a three tier system: channel floor, lower point bar and upper point bar. At low water stage only the channel and a small part of the lower point bar is active and under water. In compliance with the classical point bar model, coarse sand is deposited in the channel and finer sand is deposited on the part of the lower point bar which is active.

During the infrequent high water (flood) stage, the entire point bar becomes active. Small chute channels suddenly break through the upper point bar as catastrophic events, depositing very coarse gravelly material as chute bars, shown in the left of Figure 31. When the flood recedes, the chute channels are abandoned and, from the stagnant water in these chute channels, a clay drape is deposited.

The dimensions of chutes are given by McGowen and Garner (1971) as follows: depth 1.2 to 1.5 meters; width 5 to 7 meters; length 30 to 150 meters. Levey (1978), who investigated similar sediments from the Upper Congaree River in South Carolina, indicates the following dimensions for chute channels: depth 0.3 to 1 meter; width 3 meters; and for chute bars: width 2 to 8 meters; length 10 meters to 100 meters. It is clear that on the scale of the project test site, these deposits are

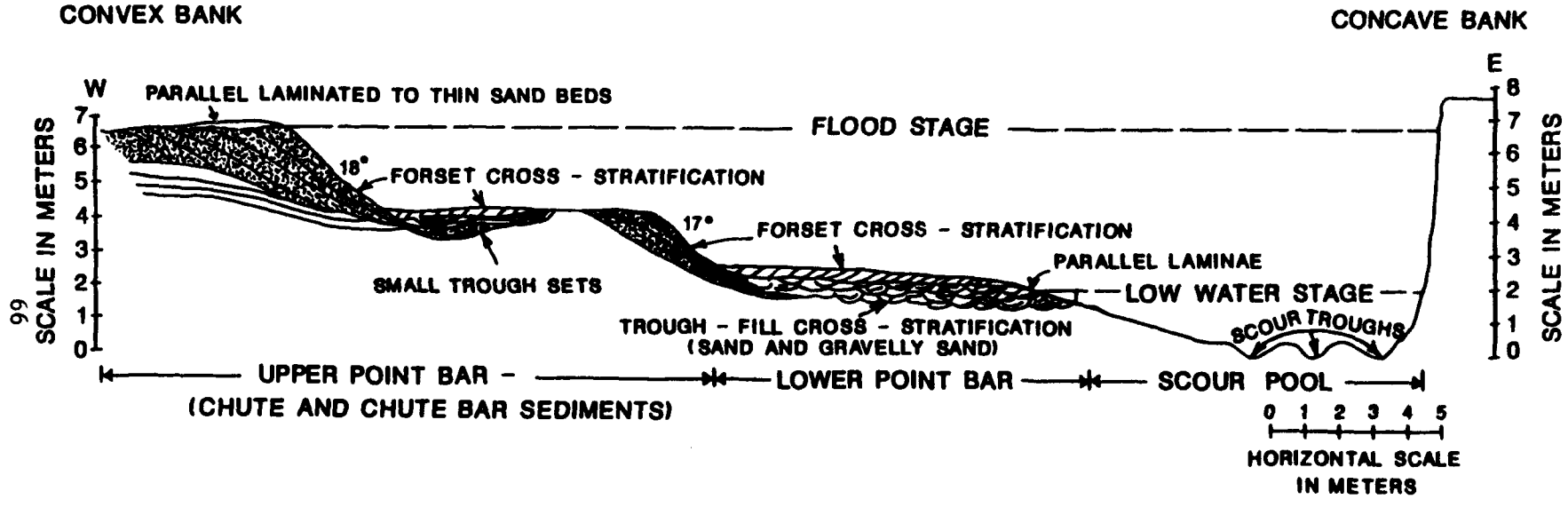

Figure 30. Cross Section of the Modern Amite River as Observed by McGowen and Garner (1971).

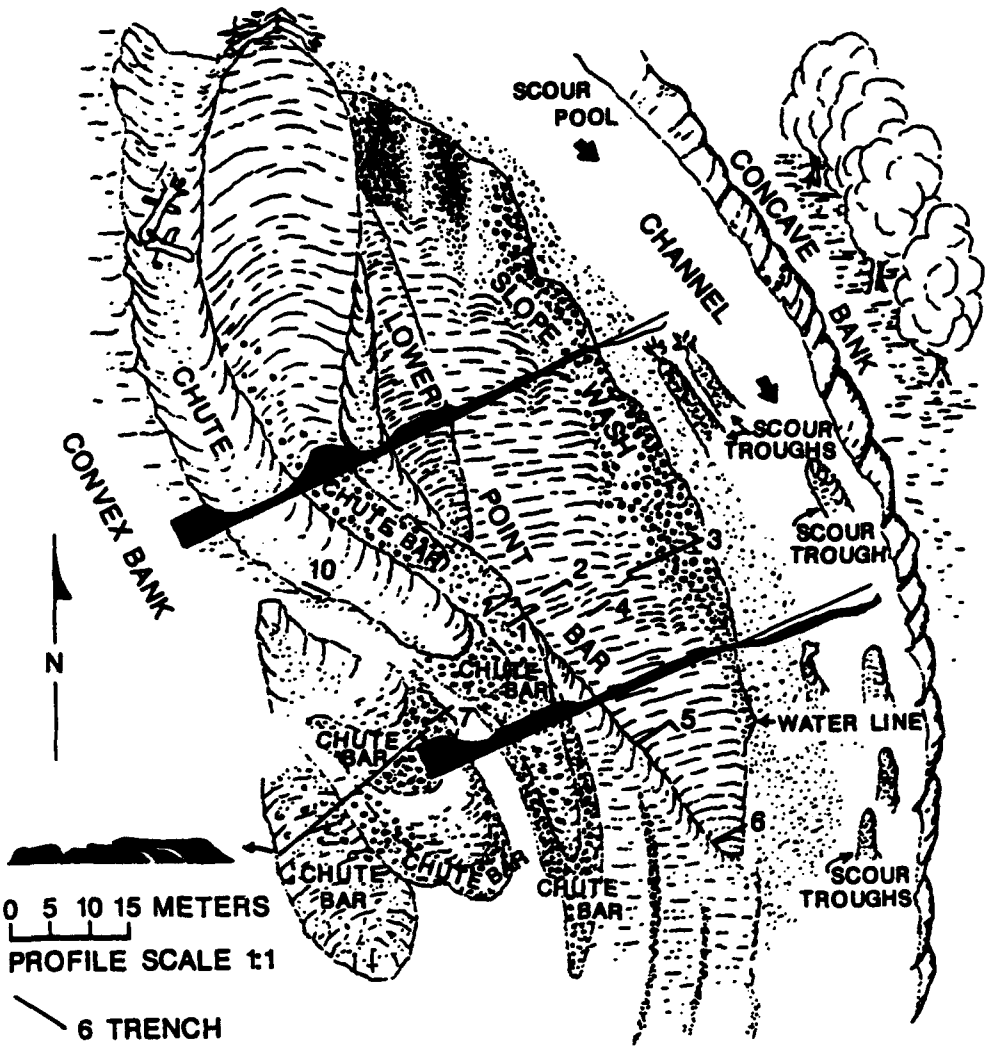

Figure 31. Lateral View of the Modern Amite River as Observed by McGowen and Garner (1971).

major heterogeneities with a large potential impact on groundwater flow and contaminant transport.

3. Braided River Deposits

The lower half of the aquifer is better represented by a braided stream model. This model implies an irregular pattern of coarse gravelly lenses deposited as braid bars at high flow stage, alternating with finer sediments deposited in the channels at low flow stage. Detailed studies of braided stream deposits are less common than those of point bars (Reineck and Sing, 1986). Levey (1978) points out similarities between chute channel and bar deposition on the upper point bar, and braided stream deposition. This supports the gradual transition at the test site from coarse grained point bar sediments to braided stream sediments.

The rapidly changing bar and channel patterns result in units which are laterally smaller than the chute channels and chute bars discussed earlier. As a result, groundwater flow and contaminant transport will be less impacted by these heterogeneities.

4. Implications for a Heterogeneous Aquifer Model

The coarse-grained point bar depositional model for the upper part of the aquifer implies a trend from coarse gravelly sediments in the NW, in the vicinity of the former channel, to slightly finer material in the center and SE area of the site. However, elongated coarse-gravel lenses do occur in the center and SE of the site in the form of chute channels and chute bars. From the meander direction it can be inferred that these lenses are oriented SW to NE. The sedimentological model predicts that the lenses are longer than 10 meters, and 2 to 7 meters wide. The lenses can be capped and tailed (to the NE) by thin clays.

Because the position of the bars and channels is less stable than in meandering river deposits, the braided stream model for the lower half of the aquifer predicts a more regular structure of alternating gravelly lenses (braid bars) and clay/silt infills of the braided channels. These lenses should be laterally less extensive than in the upper part of the aquifer.

SECTION V

DESIGN AND ANALYSIS OF TRACER TESTS

A. OBJECTIVES

Tracer tests include injecting and monitoring the movement of a substance through an aquifer. Tracer tests can provide data useful for evaluating the assumptions and the estimated geohydrological properties that comprise groundwater flow and/or transport models. A series of tracer tests were conducted at CAFB to accomplish the list in Table 13.

TABLE 13. OBJECTIVES FOR TRACER TESTS

1. Collect three-dimensional tracer breakthrough data.
2. Directly show whether three-dimensional transport predictions are necessary for the design of bioreclamation and other pump-and-treat remediation activities in heterogeneous aquifers.
3. Develop a data base from which the accuracy of the borehole flowmeter technique can be evaluated.
4. Develop a data base from which two- and three-dimensional groundwater models can be evaluated.

B. DESCRIPTION OF THE TRACER TESTS

Figure 32 shows the five tracer tests conducted at the test site. For all of the tracer tests, several withdrawal wells were used. The pumping and injection schemes were designed so that Tracer Tests 1, 2, and 5 were five-spot tracer tests (4 withdrawal wells around an injection well) and that Tracer Tests 3 and 4 were a series of simultaneous doublet tracer tests (one withdrawal well and an injection well). The arrangement of the individual pairings of injection and withdrawal wells was selected to maximize the number of tracer tests while maintaining a low risk of cross-contamination among the different tests. Because cross-contamination is unavoidable between the large-scale Tracer Test 5 and other tracer tests, Tracer Test 5 had a different tracer than the others. Appendix E describes the design of the tracer tests and the instrumentation used to conduct the tracer tests.

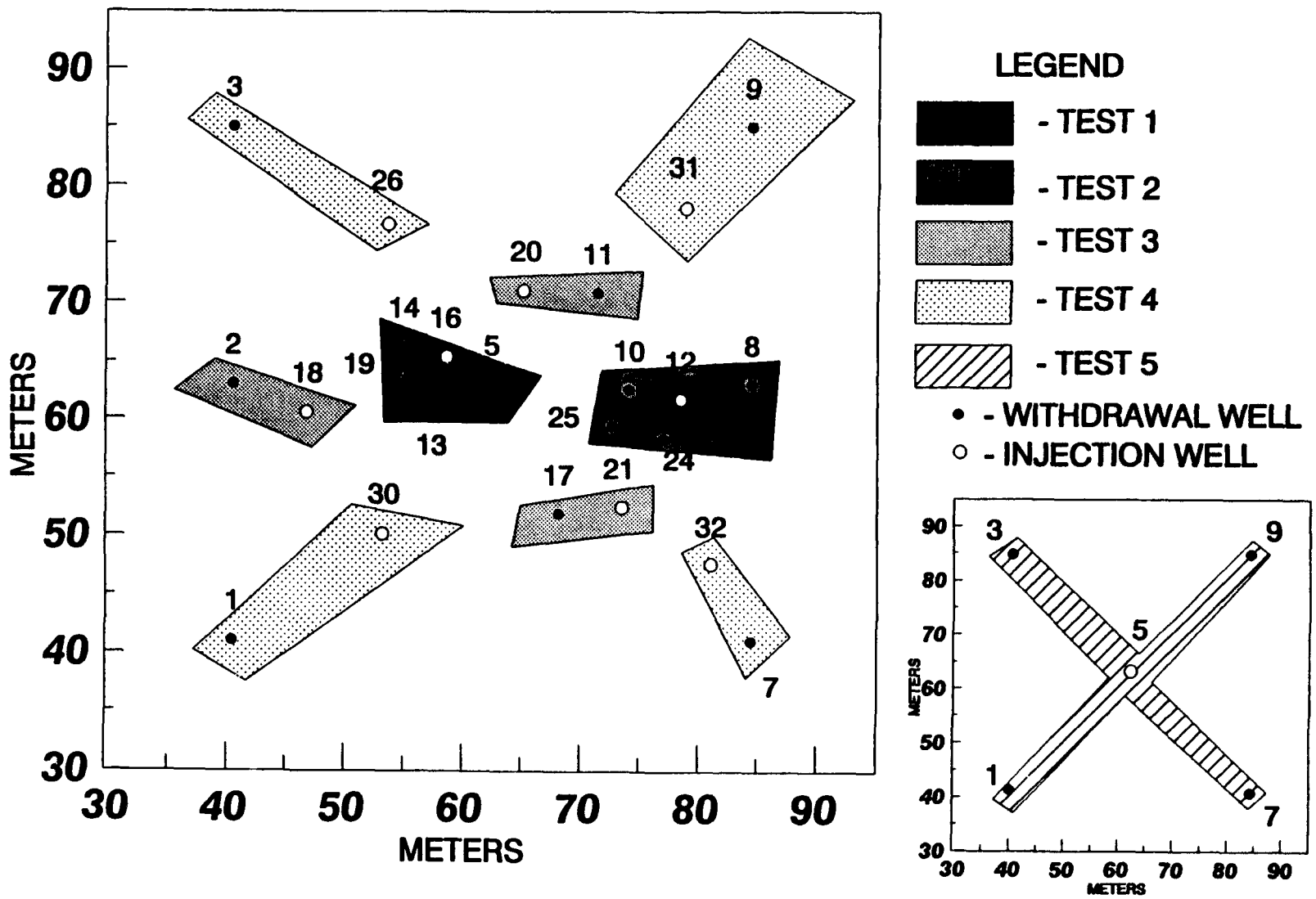

Figure 32. Location of the Tracer Tests Site.

Table 14 provides a brief summary of the injecting and pumping scheme used for the five tracer tests. During each tracer test, as many groundwater samples as possible were collected by a two-man crew. The two-man crew used as many as three sampling carts. Each cart contained three 10-channel peristaltic pumps that could simultaneously sample from all of the ports in the multilevel samplers for both the injection and the withdrawal wells. Each groundwater sample was stored in a 70-mL container. During the day shift, a third crew member measured the electrical conductivity in as many of the samples as possible. At the completion of the tracer tests, the groundwater samples were shipped to TVA Field Operations in Muscle Shoals, Alabama, where specific ion probes were used to measure tracer concentrations. Appendix F provides a detailed description of each of the tracer tests.

TABLE 14. DESCRIPTION OF INJECTION SCHEME FOR TRACER TESTS

Test	Bromide Volume (liters)	Bromide Conc. (mg/L)	Injection Well	Pumping Well(s)
1	1744	800	16 @ 37.8 L/min[1]	5, 13, 14, 19
2	4077	800	12 @ 30.9 L/min[1]	10, 8, 24, 25
3a	1218	800	21 @ 11.4 L/min	17
3b	3247	800	18 @ 18.9 L/min	2
3c	3247	800	20 @ 18.9 L/min	11
4a	2426	1200	32 @ 15.1 L/min	7
4b	4246	1200	30 @ 26.5 L/min	1
4c	4246	1200	26 @ 26.5 L/min	3
4d	3641	1200	31 @ 22.7 L/min	9
5	21238[2]	1500	5 @ 106 L/min	1, 3, 7, 9

[1]Injection rate was divided equally among the pumping wells
[2]Chloride was substituted for bromide as the tracer

Note: For Tracer Tests 1 to 4, no monitoring wells were located between the injection and withdrawal well. For Tracer Tests 1 to 4, all monitoring was conducted at the injection and the withdrawal wells.

C. RESULTS FOR TRACER TESTS 1 TO 4

1. Data Presentation

Important data for each tracer test includes the water table elevations, the vertical distribution of groundwater flow at the wells, and the vertical distribution of the tracer flux and concentration at each of the withdrawal wells. For each tracer test, this information is shown with three figures. For purposes of data analysis, the time required to reach the peak concentration at a well represents the time for the middle of the tracer slug to reach the well. With this assumption, Equation (1) can then be used to calculate the average hydraulic conductivity between two wells given the average hydraulic gradient and the effective porosity of aquifer material.

$$K = \frac{R_d * \eta}{t_p * J} \qquad (1)$$

where: K = average hydraulic conductivity (L/T)
R_d = radial distance between the wells (L)
t_p = time of peak tracer concentration (T)
η = effective porosity (assumed to be 0.3)
J = hydraulic gradient (-)

2. Tracer Test 1

In Figure 33, all of the wells, except for Well 5, have very similar vertical distributions of groundwater flows. The similar patterns indicate that Wells 13, 14, 16, and 19 intersect the same two lenses of relatively high hydraulic conductivity at elevations of about 56 and 59 meters MSL. The profile for Well 5 provides no evidence of a high hydraulic conductivity lens at any depth. The two profiles that are the most similar are Wells 16 and 19. The similar profiles at Wells 16 and 19 may have occurred because they are aligned along the lenses of high hydraulic conductivity.

Figure 34 shows that to reach Wells 13, 14, and 19, the tracer primarily moved through two aquifer lenses located near 56 and 59 meters MSL. Each of the wells shows slightly different results. At Well 19,

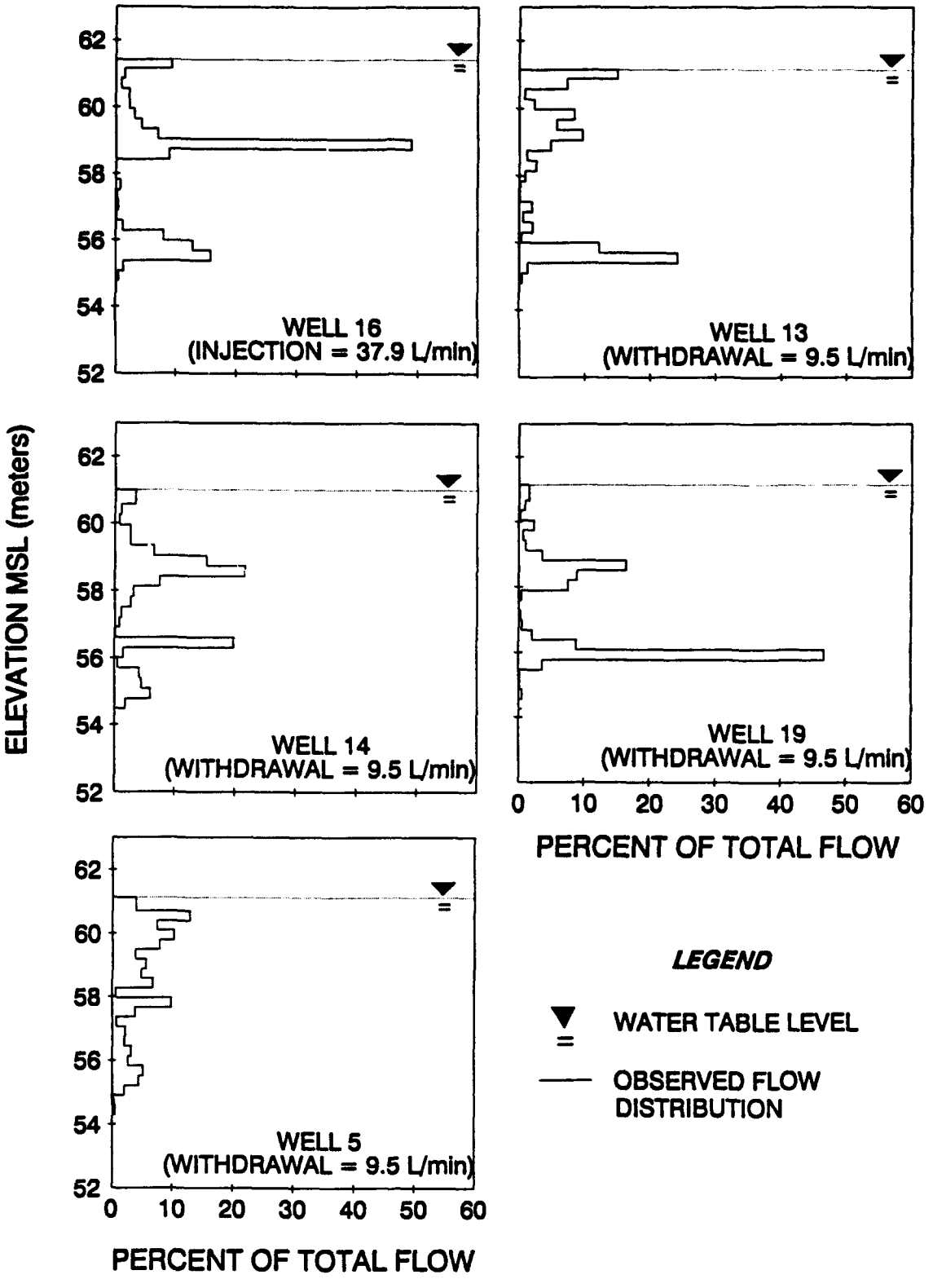

Figure 33. Groundwater Flow Patterns at Wells 16, 13, 14, 19, and Well 5 During Tracer Test 1.

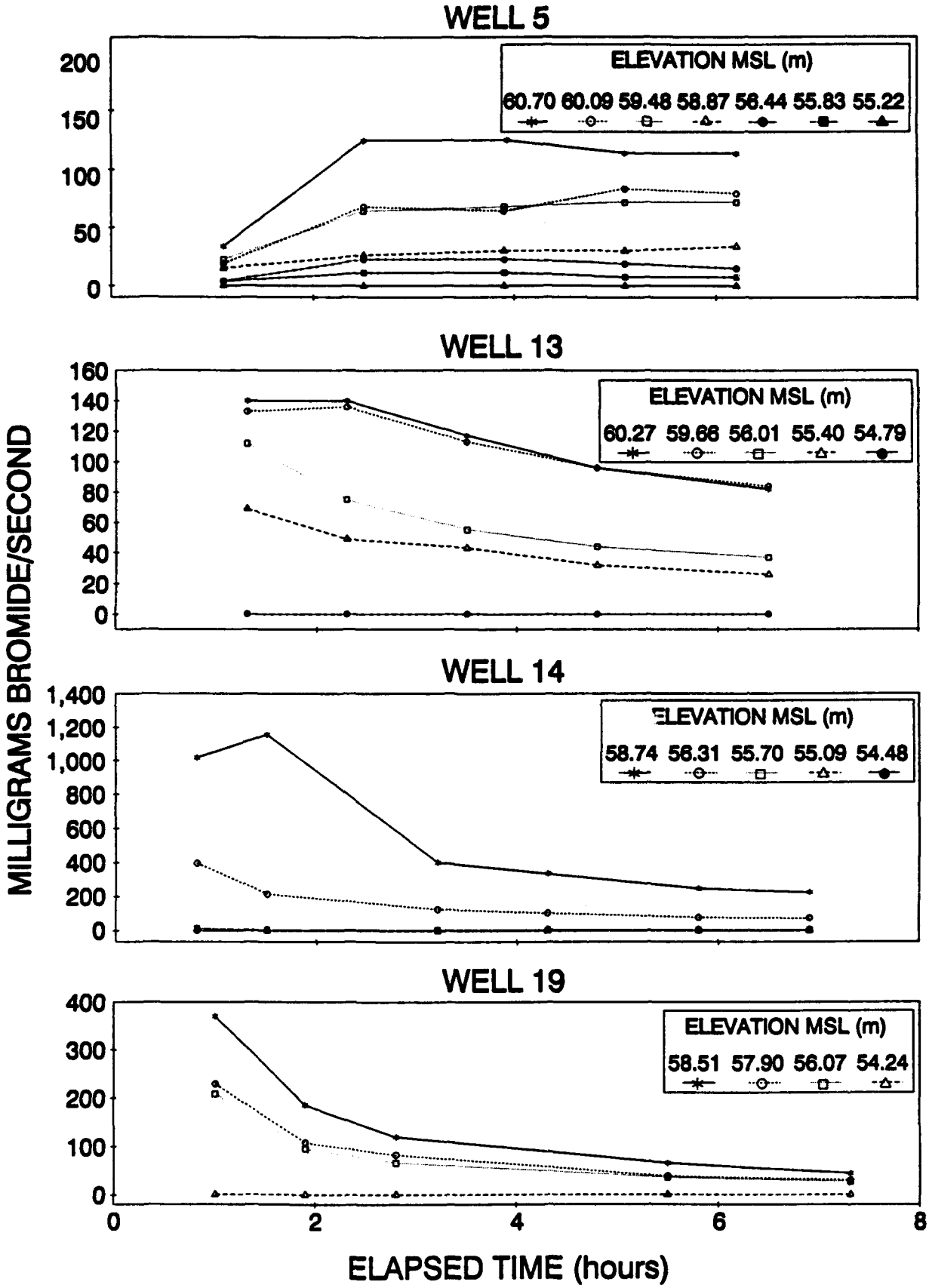

Figure 34. Tracer Flux Patterns at Wells 13, 14, 19, and Well 5 During Tracer Test 1.

most of the tracer arrives from the lower lens. At Well 14, most of the tracer arrives from the higher lens. At Well 13, similar amounts of tracer arrive from the upper and lower lenses. This type of information indicates that two lenses of interest do not have the same areal coverage.

At Well 5, the tracer entered the well primarily at elevations above 59 meters MSL. This indicates that the lower lens does not extend much further east than Well 16 or 13. Figure 35 shows that for some of the tracer breakthrough curves, the peak tracer concentration may have been missed. For these breakthrough curves, Equation (1) can be used only to calculate a lower limit of the hydraulic conductivity. By application of Equation (1), hydraulic conductivities were calculated from the tracer test data. Table 15 compares these values and the borehole flowmeter results. Because the groundwater is traveling from the injection well to the withdrawal well, the hydraulic conductivity value calculated from the tracer test should be compared to both the borehole flowmeter results at the injection and the withdrawal well. In general, favorable agreement was obtained between the two sets of hydraulic conductivity values.

TABLE 15. COMPARISON OF HYDRAULIC CONDUCTIVITY VALUES FROM THE BOREHOLE FLOWMETER AND TRACER TEST 1

Withdrawal Well (W)	Elev (m)	R (m)	Time (min)	V (cm/min)	J	Tracer Test[1] K(cm/s)	Flowmeter[2] Well W K(cm/s)	Flowmeter[2] Well I K(cm/s)
19	58.5	3.66	<60	>6.10	.060	>0.51	1.6	1.5
19	56.1	3.66	<60	>6.10	.060	>0.51	1.7	0.4
14	58.7	3.66	80	4.52	.106	0.21	0.36	1.5
14	56.3	3.66	<48	>7.52	.106	>0.35	0.12	0.4
13	59.6	3.86	<96	4.02	.058	>0.35	0.38	1.5
13	56.0	3.86	96	4.02	.058	0.35	0.61	0.4
5	60.7	4.60	213	2.15	.054	0.20	0.26	1.5
5	59.5	4.60	306	1.51	.054	0.14	0.26	1.5
5	55.8	4.60	171	2.68	.054	0.25	0.12	0.4

[1]From Equation 1
[2]Well W is withdrawal well, Well I is injection Well 16, K is taken from Figures 28-30

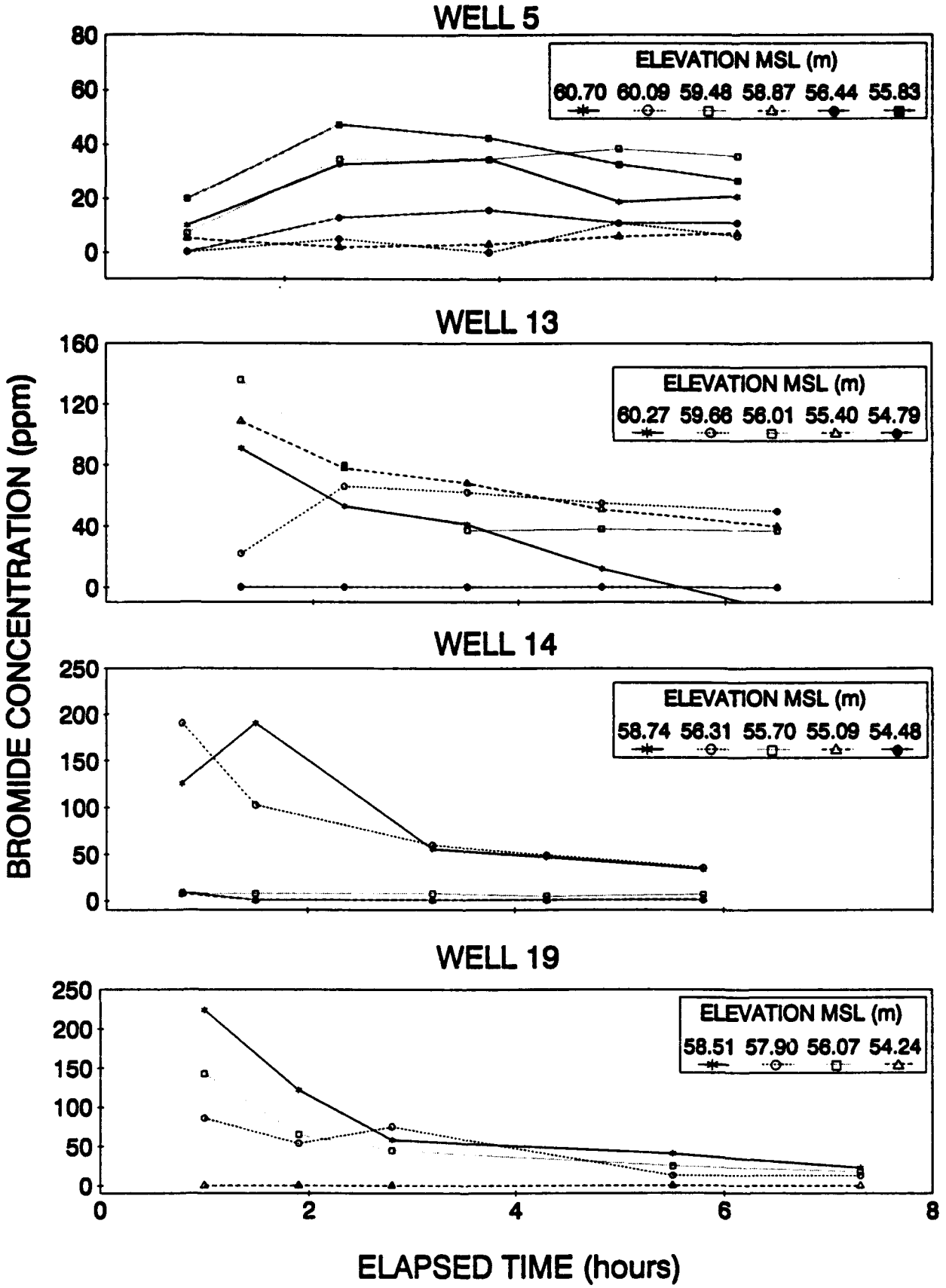

Figure 35. Tracer Concentration Patterns at Wells 13, 14, 19, and Well 5 During Tracer Test 1.

3. Tracer Test 2

Figure 36 shows that each of the wells has a zone of relatively high hydraulic conductivity near elevation 61 meters MSL. In general, all the profiles, with the possible exception of Well 8, exhibit similar patterns. Figure 37 shows that for Wells 8 and 25 the zone of rapid tracer transport is located near 60 meters MSL. Essentially no tracer migration was observed at any elevation less than 59 meters MSL at these wells. At Well 10, the zone of primary tracer transport is located at an elevation near 60 meters MSL but a smaller amount of tracer transport did occur at a lower elevation of 57 meters MSL. The profile for Well 24 shows no tracer transport at elevations higher than 58 meters MSL. Based on Figure 36, one might expect a zone of high tracer transport at an elevation of about 61 meters MSL. However, the sampling ports were not positioned high enough in this well to confirm the expected trend. The zone of moderate tracer transport at elevation 57.6 meters MSL at Well 24 is adequate for the purpose of calculating a hydraulic conductivity value.

Figure 38 shows the observed tracer concentration breakthrough curves for Wells 8, 10, 24, and 25. By applying Equation (1), hydraulic conductivities were calculated for zones of primary tracer transport. Table 16 compares these values and the borehole flowmeter results. Good agreement was found between the two sets of hydraulic conductivity values.

TABLE 16. COMPARISON OF HYDRAULIC CONDUCTIVITY VALUES FROM THE BOREHOLE FLOWMETER AND TRACER TEST 2

Withdrawal Well (W)	Elev (m)	R (m)	Time (min)	V (cm/min)	J	Tracer Test[1] K(cm/s)	Flowmeter[2] Well W K(cm/s)	Flowmeter[2] Well I K(cm/s)
25	60.6	6.13	126	4.87	.155	0.16	0.20	0.43
24	57.0	3.64	951	0.383	.249	0.0079	0.0071	0.022
10	60.2	4.39	<156	>2.81	.292	>0.048	0.27	0.43
8	59.94	6.25	486	1.29	.175	0.037	0.0086	0.43

[1]From Equation 1
[2]Well W is withdrawal well, Well I is injection Well 12, K is taken from Figures 28-30

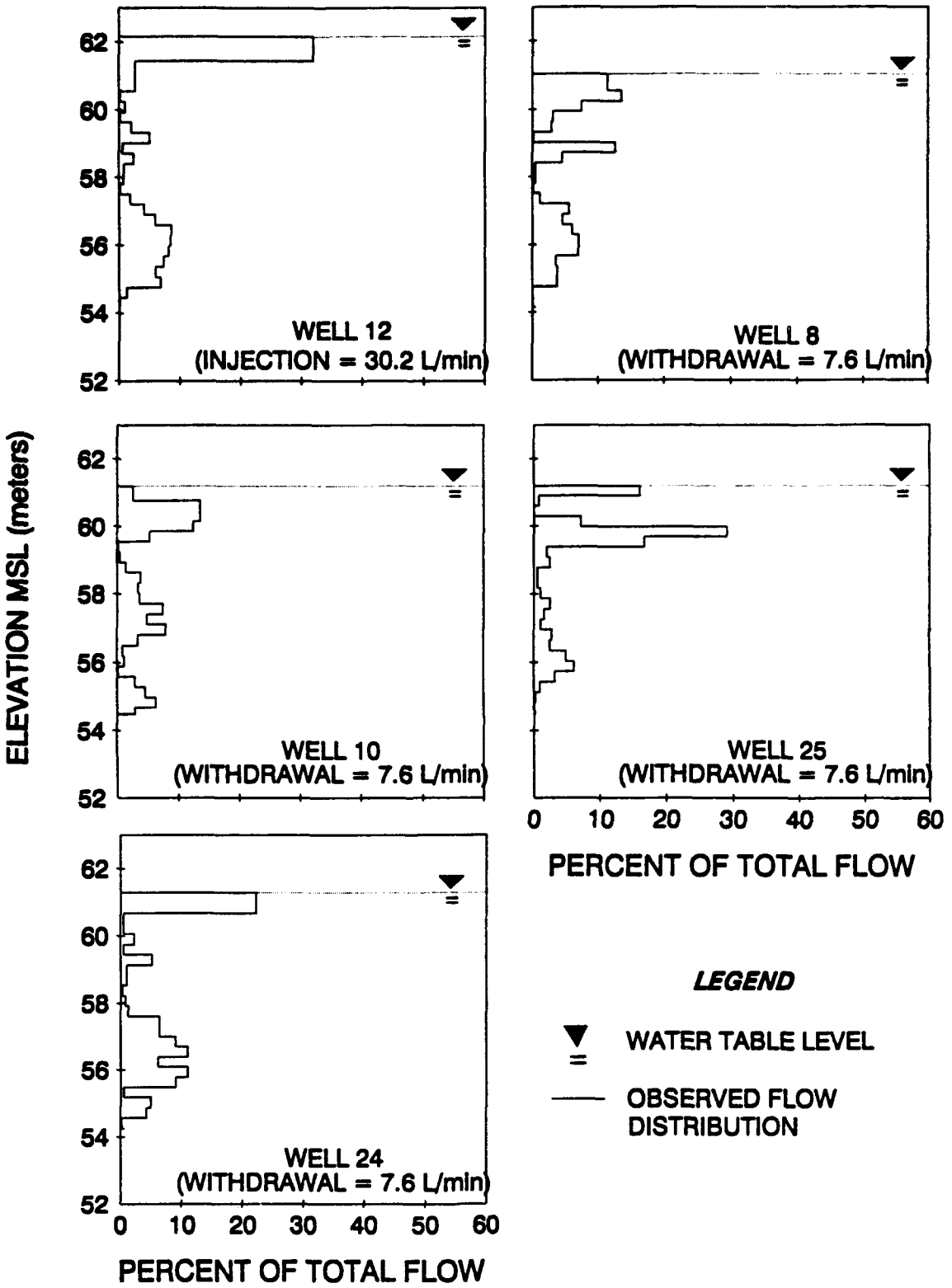

Figure 36. Groundwater Flow Patterns at Wells 8, 10, 12, 24, and 25 During Tracer Test 2.

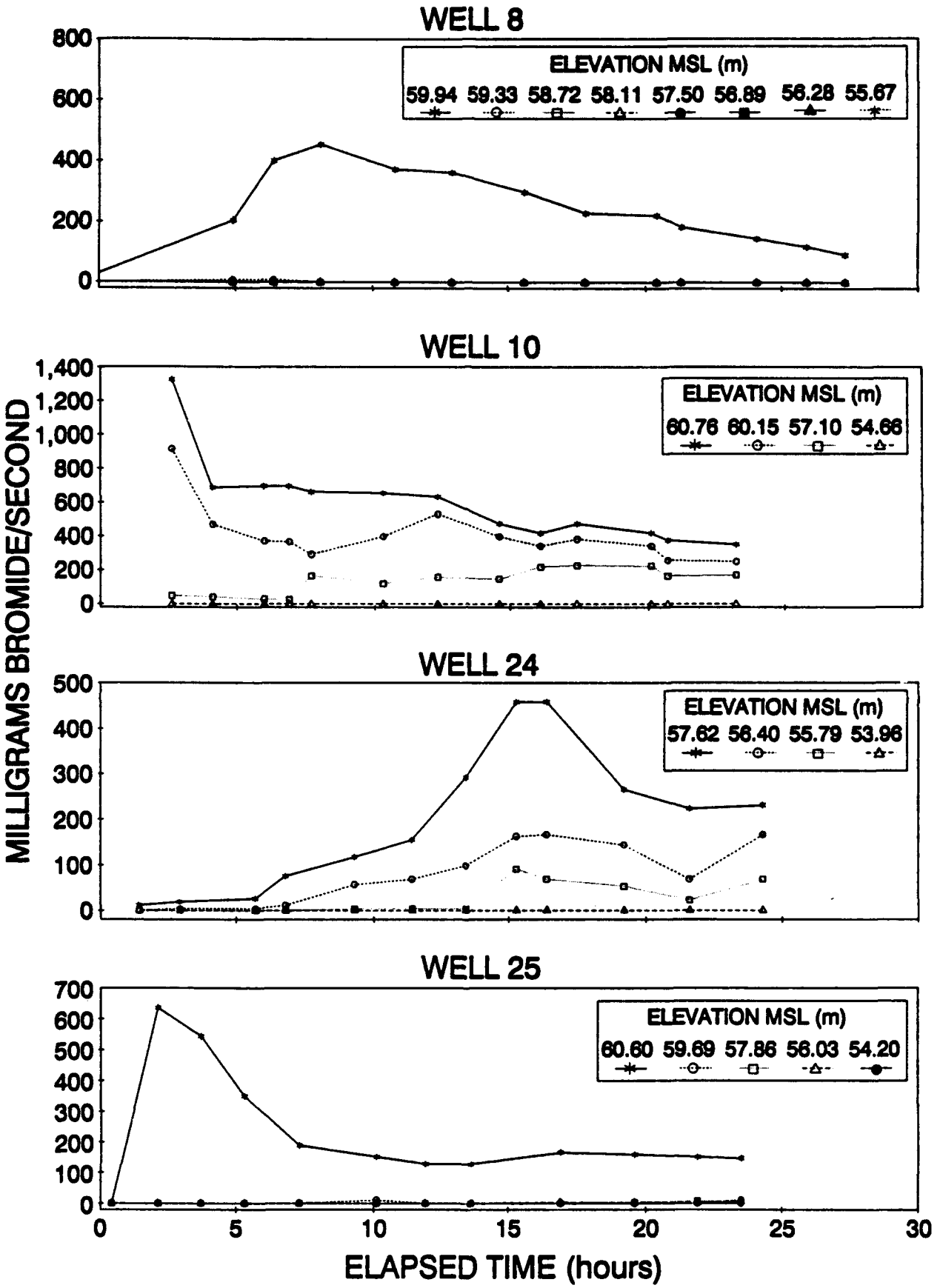

Figure 37. Tracer Flux Patterns at Wells 8, 10, 24, and 25 During Tracer Test 2.

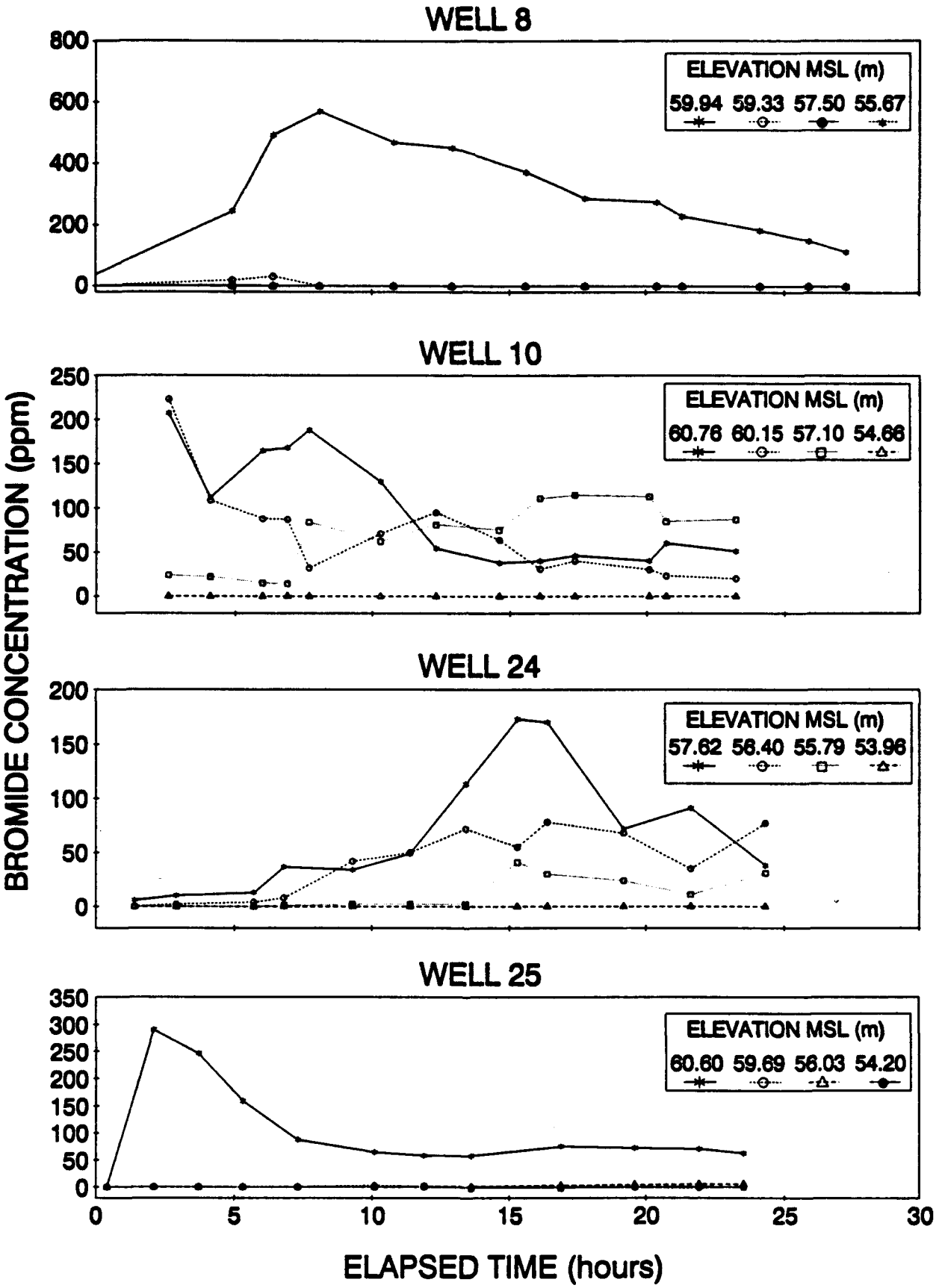

Figure 38. Tracer Concentration Patterns at Wells 8, 10, 24, and 25 During Tracer Test 2.

4. Tracer Test 3

Figure 39 shows the vertical distribution of groundwater flow for three doublet tests. All of the paired flow profiles show noticeable differences. Wells 2 and 18 have very different profiles below 59 meters MSL. Whereas Well 21 has most of its flow located in zones above 59 meters MSL, Well 17 has most of its flow below 59 meters MSL. Below 61 meters MSL, the high flow zones at Well 11 matches the low flow zones at Well 20.

Figure 40 shows well-defined tracer flux breakthrough curves for Wells 2, 11, and 17. For Wells 2 and 11, the plots show that the primary zone of tracer transport is near 59 meters MSL. For Well 17, no information is shown for elevations above 59 meters MSL because above 59 meters MSL there were problems with the tracer test data. Figure 41 shows the calculated tracer concentration breakthrough curves for Wells 2, 11, and 17. By applying Equation (1), hydraulic conductivities were calculated for the zones of primary tracer transport. Table 17 compares these values with the borehole flowmeter results. In general, Table 17 shows an agreement at Wells 17 and 11. At Well 2, the hydraulic conductivity values from the tracer test is about one-fourth of the hydraulic conductivity derived from the borehole flowmeter tests.

TABLE 17. COMPARISON OF HYDRAULIC CONDUCTIVITY VALUES FROM THE BOREHOLE FLOWMETER AND TRACER TEST 3

Withdrawal Well	ELEV (m)	R (m)	Time (min)	V (cm/min)	J	Tracer Test[1] K(cm/s)	Flowmeter[2] Well W K(cm/s)	Flowmeter[2] Well I K(cm/s)
2	59.6	6.72	585	1.14	0.0376	0.153	0.645	0.955
11	58.6	6.15	135	4.55	0.274	0.083	0.148	0.107
17	55.61	5.16	1344	0.384	0.123	0.0156	0.085	0.0093

[1]From Equation 1
[2]Well W is withdrawal well, Well I is the respective injection well, K is taken from Figures 28-30

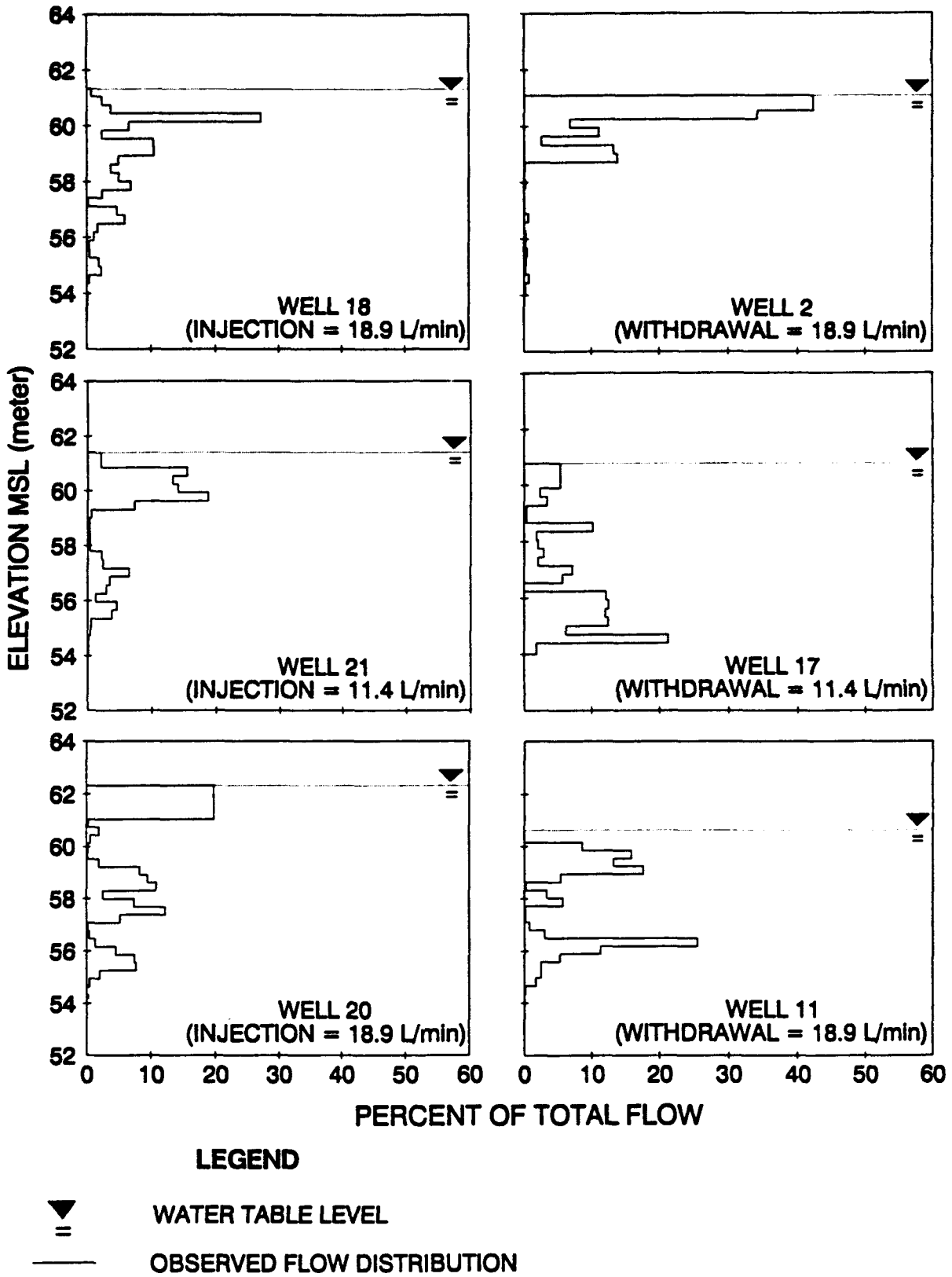

Figure 39. Groundwater Flow Patterns at Wells 2, 11, 17, 18, 20, and 21 During Tracer Test 3.

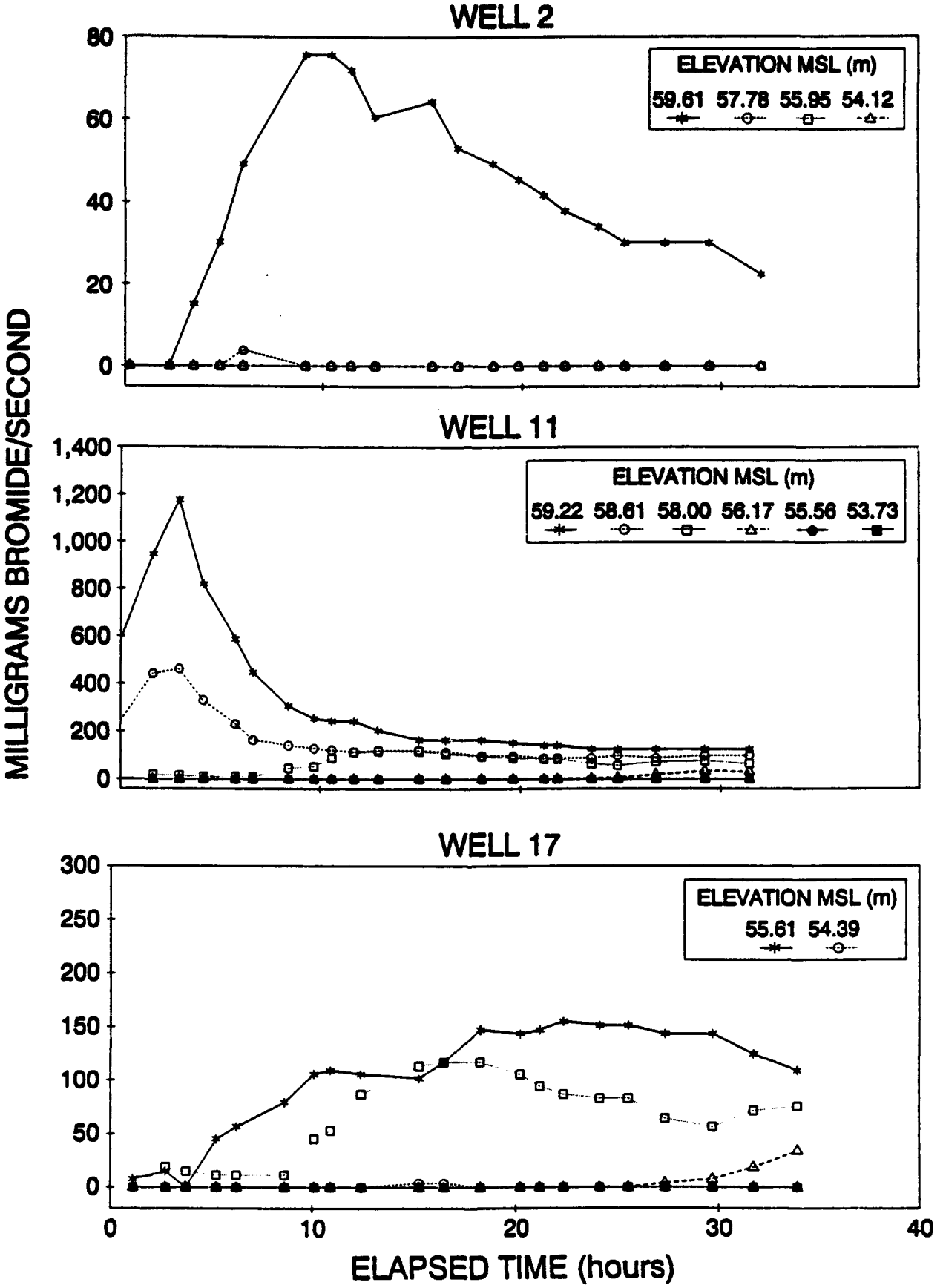

Figure 40. Tracer Flux Patterns at Wells 2, 11, and 17 During Tracer Test 3.

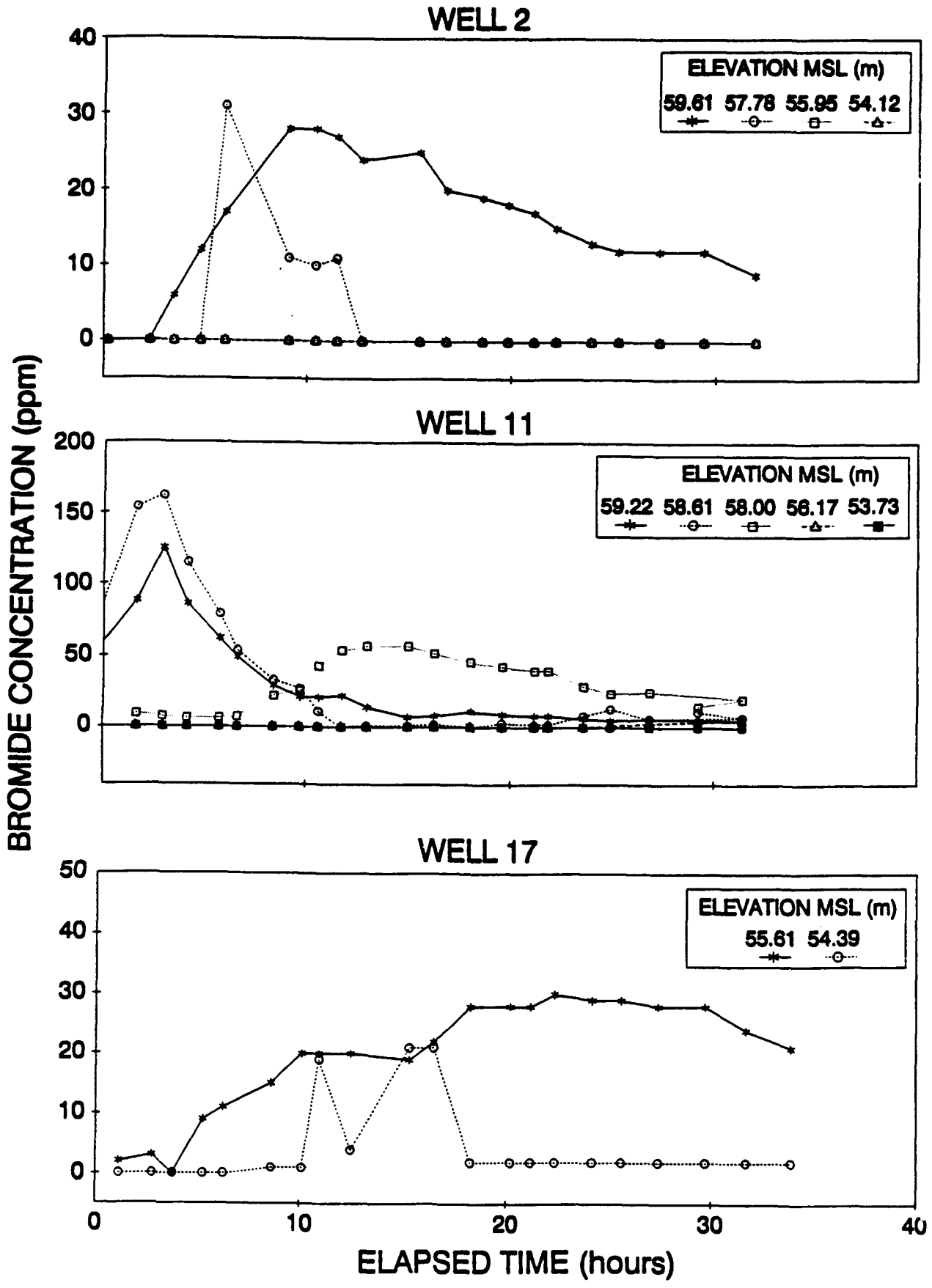

Figure 41. Tracer Concentration Patterns at Wells 2, 11, and 17 During Tracer Test 3.

5. Tracer Test 4

Figure 42 shows that similar flow profiles were obtained for Wells 26 and 3. The profile comparisons for the other well pairs are poor. Figures 43 and 44 show the tracer breakthrough curves for Wells 3, 7, and 9. No data are presented for Well 1 because no tracer curves was observed at the well. The data show that, at Well 3, the primary zone of tracer transport was near 60 meters MSL. Both Wells 7 and 9 show a zone of primary tracer transport near 59 meters MSL and near 55 meters MSL. Although both Wells 7 and 9 have lenses of high conductivity located near the same elevations, there is an important difference between these lenses at the wells. At Well 7, the transport is fastest in the aquifer lens(es) near 55 meters MSL, whereas at Well 13, the transport is fastest in the aquifer lens(es) near 59 meters MSL. By applying Equation (1), hydraulic conductivities were calculated for the zones of primary tracer transport for Wells 3, 7, and 9. Table 18 compares these values and the borehole flowmeter results. In Table 18, the comparisons vary from good (Well 3) to poor (Well 1).

TABLE 18. COMPARISON OF HYDRAULIC CONDUCTIVITY VALUES FROM THE BOREHOLE FLOWMETER AND TRACER TEST 4

Withdrawal Well (W)	Elev (m)	R (m)	Time (min)	V (cm/min)	J	Tracer Test[1] K(cm/s)	Flowmeter[2] Well W K(cm/s)	Flowmeter[2] Well I K(cm/s)
9	59.3	8.87	960	0.923	0.203	0.023	0.22	0.041
9	55.6	8.87	2100	0.422	0.203	0.010	0.30	0.011
7	59.3	7.28	1146	0.63	0.0846	0.037	.11	0.091
7	54.3	7.28	366	1.99	0.0846	0.118	.54	1.75
3	60.33	15.2	900	1.68	0.0249	0.338	0.71	0.125
1	-	15.8	>3,000	<8.8E-5	0.1605	<1.6E-4	0.029[3]	0.077[3]

[1]From Equation 1
[2]Well W is withdrawal well, Well I is injection well, K is taken from Figures 28-30
[3]Average values

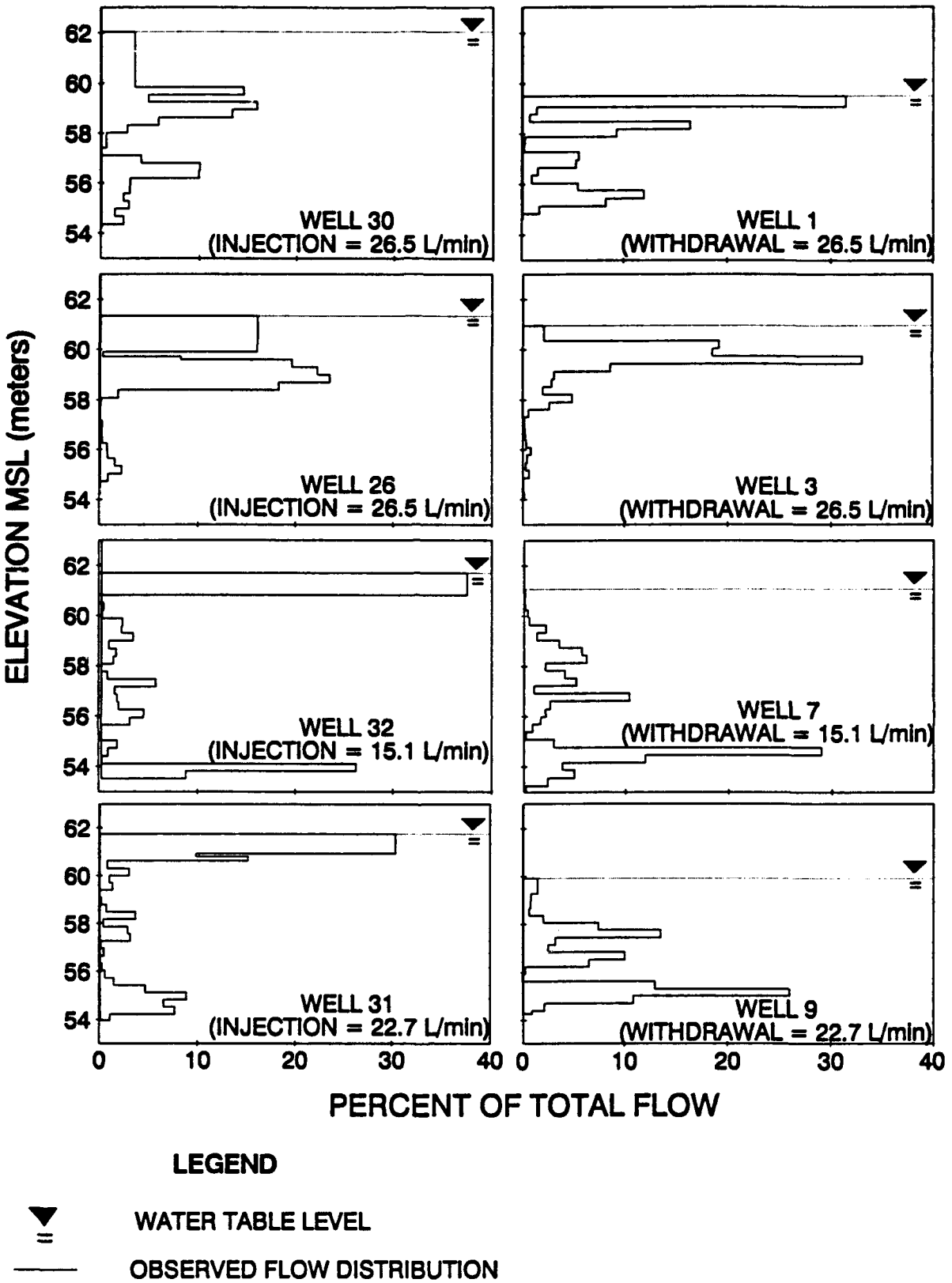

Figure 42. Groundwater Flow Patterns at Wells 1, 3, 7, 9, 26, 30, 31, and 32 During Tracer Test 4.

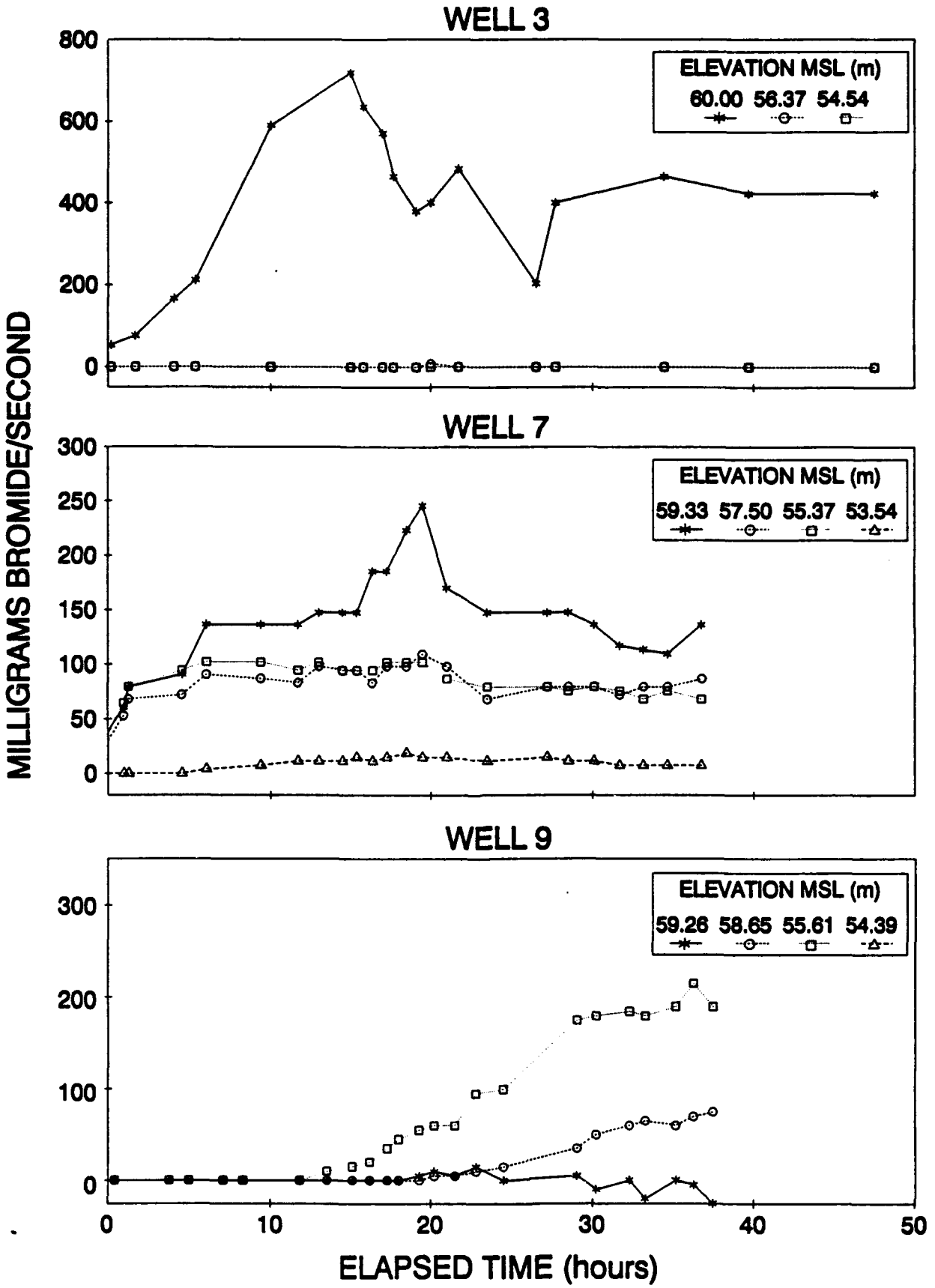

Figure 43. Tracer Flux Patterns at Wells 3, 7, and 9 During Tracer Test 4.

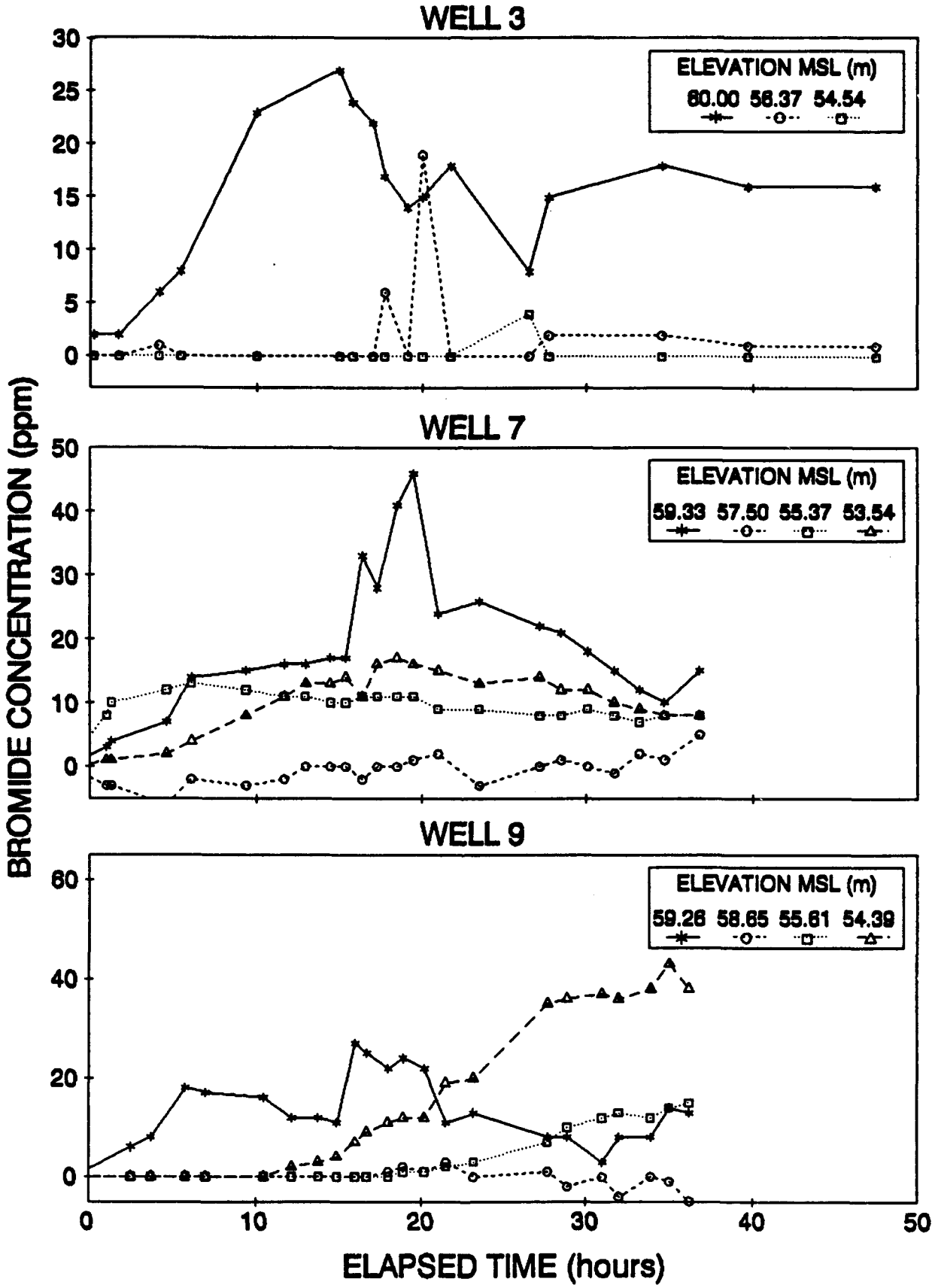

Figure 44. Tracer Concentration Patterns at Wells 3, 7, and 9 During Tracer Test 4.

D. RESULTS FOR TRACER TEST 5

1. Data Presentation

The large-scale tracer test was designed to produce data of sufficient quality and quantity to evaluate the three-dimensional trends in the borehole flowmeter data shown in Figures 16, 17, and 18. As with the other tracer tests, the large-scale tracer test was initiated after a quasi-steady state water table was established. The hydraulic gradients were determined by pumping 26.5 L/min from Wells 1, 3, 7, and 9 and injection of 106 L/min into Well 5. The tracer pulse consisted of 21,238 liters of 1500 mg/L chloride solution and was injected over a 3.4-hour period. For 168 hours after injection, the migration of the tracer pulse was monitored with multilevel samples (see Appendix E) installed in 18 interior wells and the 4 pumping wells. All of the interior wells were used for monitoring except for Wells 14, 15, 19, 12, and 24. Figure 45 shows a schematic for the monitoring and the pumping locations.

The most relevant information from the tracer test for evaluating the trends in the hydraulic conductivity field include the aquifer's hydraulic response to the pumping scheme, the configuration of the water table at steady-state, and the definition of the tracer concentration's breakthrough curves at different elevations. This information was collected and is presented in this section. Before any tracer concentration data is presented, however, one should be aware of several problems with the tracer data. These problems involve the mixing of groundwater in the wells that house the multileveler samplers.

After the steady-state water configuration was achieved, vertical flows were measured by the EM flowmeter inside all of the wells with a multilevel sampler. Because of the absence of any resistance to flow in the wells, the wells had vertical flows orders-of-magnitude greater than the aquifer. A consequence of the vertical flow is that the origin of all the groundwater at a particular elevation was unknown. At any elevation the well water was a mixture of groundwater flowing horizontal and of groundwater flowing vertically through the well. Without a detailed three-dimensional distribution of both the tracer concentrations

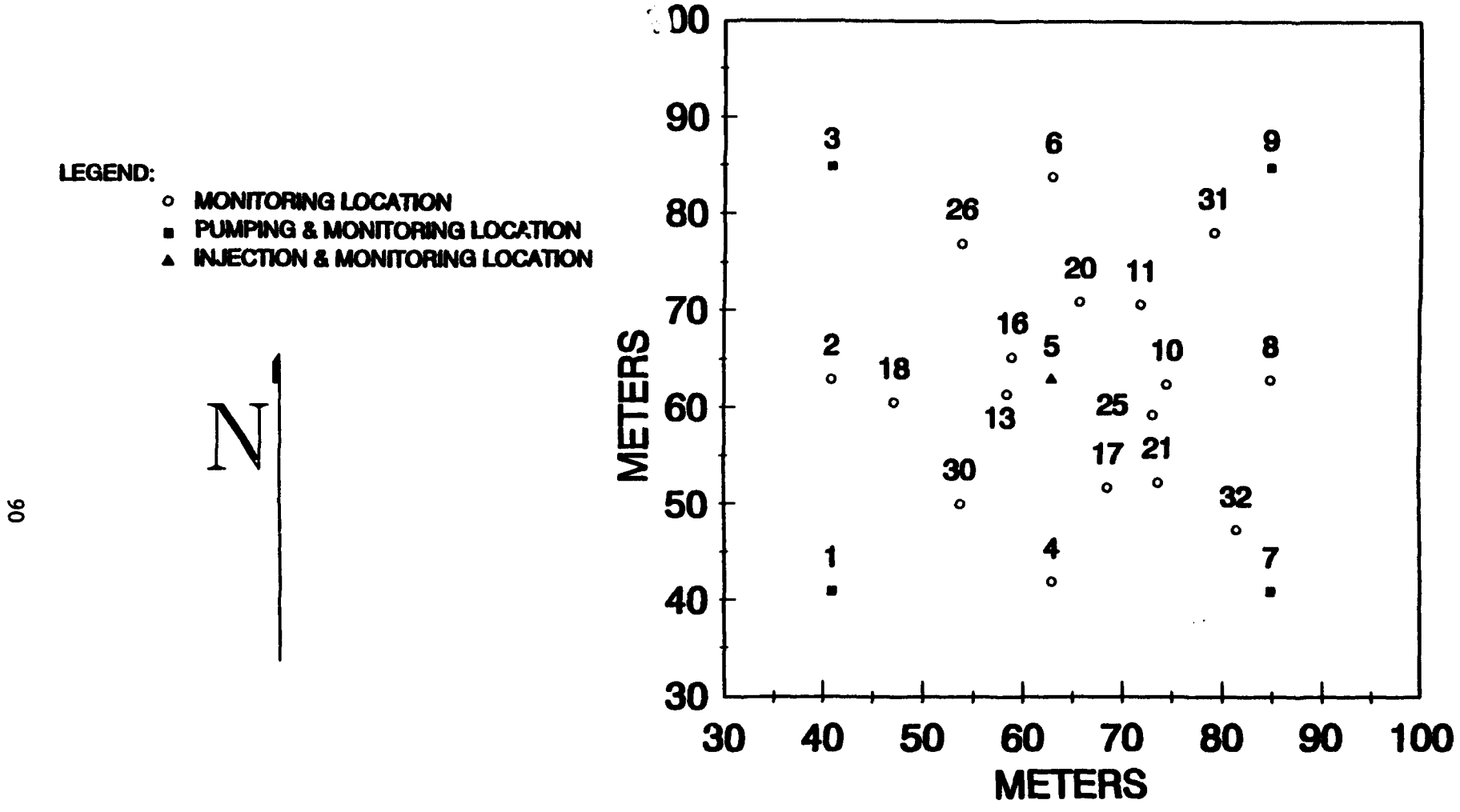

Figure 45. Schematic of Pumping and Monitoring Well Network for Tracer Test 5.

and the horizontal and vertical flowrates in the well, an accurate representation of tracer concentrations inside the aquifer could not be calculated. As discussed in Appendix E, the vertical mixing of groundwater occurred not only inside but also in the annulus of the wells.

In order to help quantify the mixing effect, the profile of the vertical flows were measured inside each well after the multilevel sampler had been removed. By using the concentration data and the vertical flow measurement profiles, one can estimate the upward/downward mass flux of tracer among the different vertical zones in the wells. The flow profiles in the majority of the 27 interior wells had profiles similar to the examples shown in Figure 46. In Figure 46 the flow profiles have unidirectional flows that are less than .4 L/min. At every well, flow measurements were taken at 0.3-m increments.

The vertical mixing in the wells likely caused cross-contamination among the aquifer layers at the well locations. However, the cross-contamination should not have significantly affected the major trends in the tracer movement because the wells intersected only 10^{-5} percent of the aquifer. Because cross-contamination was confined to a relatively small volume, the cross-contamination between the aquifer layers should have quickly dissipated with distance from the wells and have a minor effect on the tracer profiles in the downgradient wells. Because cross-contamination likely occurred, groundwater samples were not taken from wells located immediately downgradient of a well. For this reason, Wells 14, 15, 19, 12, and 24 were not sampled.

Because of the problems associated with the vertical mixing of the well water, the tracer analysis focused on a semi-qualitative analyses. The first question answered was whether the tracer breakthrough occurred in the lower (<56 meters MSL) or the upper zone of the aquifer (>58 meters MSL). The second question answered was the time of the maximum tracer concentrations. At most of the wells, these two questions were easily answered because tracer breakthrough occurred only at the upper portion of the aquifer and the vertical flow field was unidirectionally upward. At these wells, no tracer concentrations were

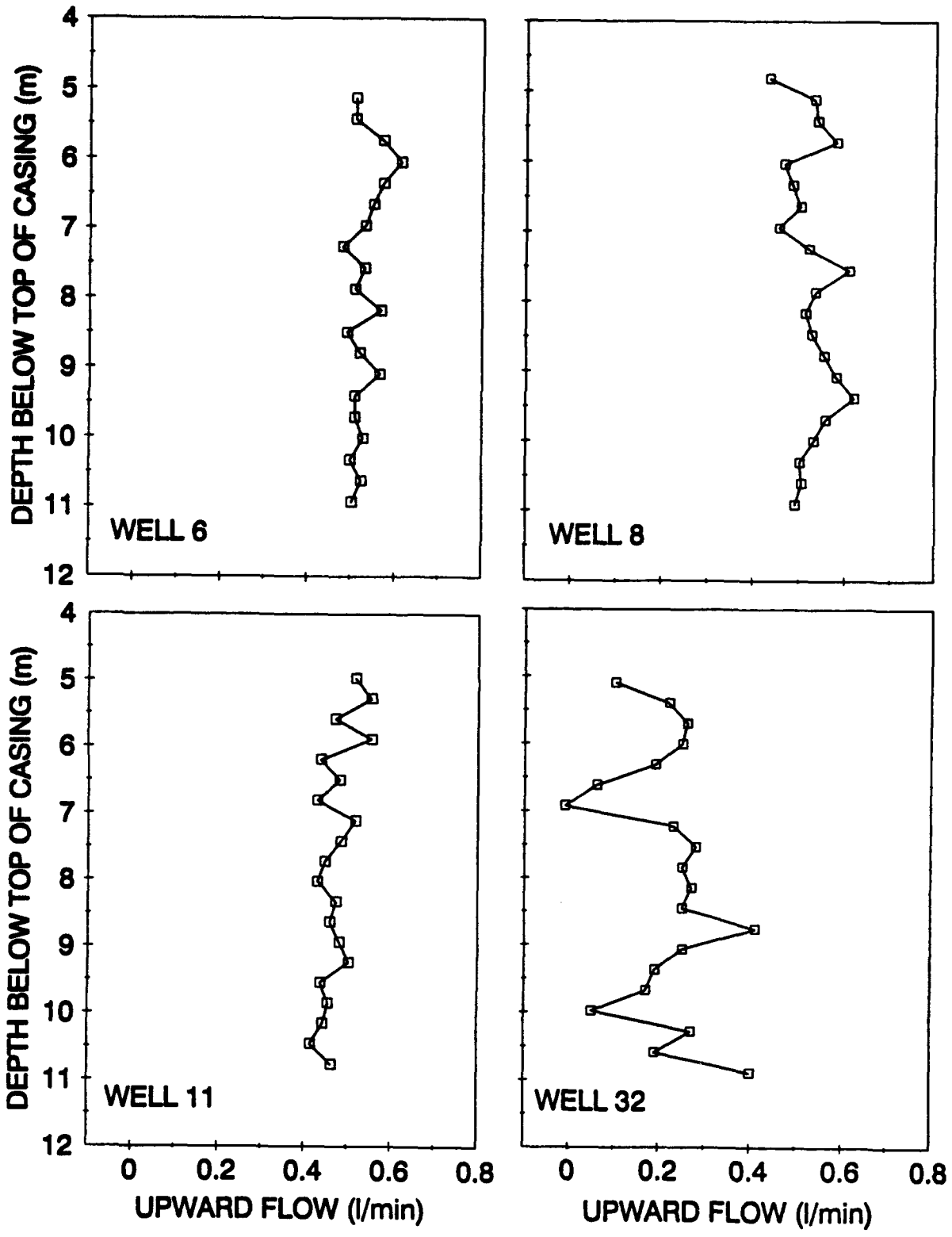

Figure 46. Examples of Vertical Groundwater Flow in Wells During Tracer Test 5.

measured in the lower aquifer and the procedures for characterization of the single tracer breakthrough were straightforward.

At wells with tracer breakthroughs in the lower and the upper portion of the aquifer, the identification of the two breakthrough curves were straightforward but the time of peak tracer concentration was not straightforward. Figure 47 shows an example of tracer data at a well with two tracer breakthrough curves. The well is Well 11. For convenience, only one-third of the electrical conductivity data collected for each time period is shown in Figure 47. At each well, tracer data was collected at 0.3-meter intervals; Figure 47 shows the data for every third interval. Given the vertical flow in Well 11 is unidirectionally upward (see Figure 46), one can reason that: 1) a tracer pulse passed by Well 11 in the upper portion of the aquifer (in this instance above elevation 57.69 meters MSL) sometime between 50 and 75 hours (first hump in Figure 47a); and, 2) a different tracer pulse passed by Well 11 in the lower portion of the aquifer (this instance near 54-55 meters MSL) sometime after 100 hours (see Figure 47c and 47d).

Because of the limitation of the data, one cannot determine whether the second peak in Figure 47a (from time 95 hours to 160 hours) is produced by a second breakthrough curve in the upper aquifer or by the vertical migration of tracer in the well from the tracer pulse that passed through the lower portion of the aquifer. However, such a differentiation was not sought. At Well 11, the goal of the tracer analysis was to determine whether that a tracer pulse passed through the upper and lower zones of the aquifer and to estimate the time of the peak concentration for the first (and perhaps only) tracer pulse at both intervals. For reference, the analysis of the complete set of electrical conductivity values indicated that the times of the peak concentration for the initial (and perhaps only) tracer pulses in the upper and lower aquifer zones at Well 11 were 64 and 124 hours, respectively.

2. Water Table Elevations

Table 19 provides the temporal variations of hydraulic gradients across the entire test area for the tracer test. The data indicates that

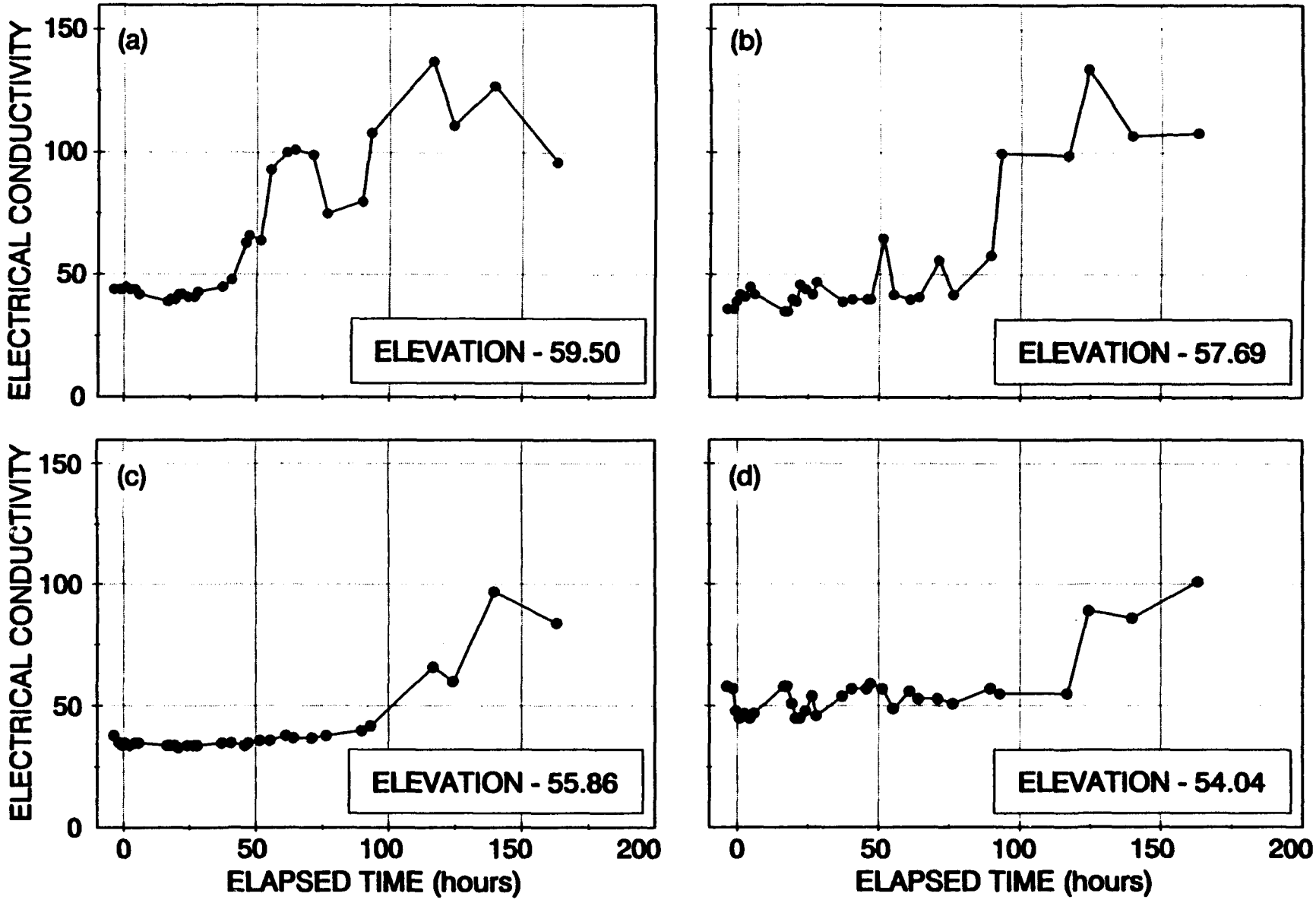

Figure 47. Electrical Conductivity Profile at Well 11 During Tracer Test 5.

TABLE 19. HYDRAULIC GRADIENTS CALCULATED BETWEEN THE MONITORING WELL AND THE INJECTION WELL

Date:	9/13/89	9/14/89	9/14/89	9/15/89	9/17/89	9/18/89	9/19/89	9/20/89
Time:	20:00	00:01	04:00	18:30	10:10	15:00	09:45	17:20
Well								
1	0.14	0.14	0.14	0.14	0.14	0.14	0.15	0.14
2	0.12	0.12	0.12	0.12	0.13	0.12	0.12	0.12
3	0.09	0.09	0.09	0.09	0.09	0.10	0.09	0.09
4	0.12	0.12	0.12	0.12	0.11	0.12	0.12	0.12
6	0.12	0.12	0.12	0.12	NM	0.12	0.12	0.12
7	0.10	0.10	0.10	0.10	0.10	0.10	0.10	0.08
8	0.11	0.11	0.11	0.11	0.11	0.11	0.11	0.11
9	0.13	0.13	0.13	0.13	NM	0.13	0.14	0.13
10	0.21	0.21	0.21	0.21	0.20	0.21	0.21	0.21
11	0.21	0.20	0.20	NM	0.20	0.20	0.20	0.20
12	0.15	0.15	0.15	0.15	NM	0.15	0.15	0.15
13	0.47	0.47	0.46	0.46	0.46	0.46	0.46	0.47
14	0.29	0.29	0.29	0.29	0.29	0.29	0.29	0.29
15	0.19	0.19	0.19	0.18	0.18	0.19	0.19	0.19
16	0.49	0.48	0.48	0.48	0.48	0.48	0.48	0.48
17	0.19	0.19	0.19	0.19	0.19	0.19	0.19	0.19
18	0.16	0.16	0.16	0.16	0.16	0.16	0.16	0.16
19	0.32	0.32	0.32	0.31	0.31	0.31	0.31	0.32
20	0.28	0.28	0.27	0.31	0.27	0.30	0.27	0.27
21	0.16	0.16	0.16	0.16	0.16	0.16	0.16	0.16
22	0.05	0.05	0.05	0.05	0.05	0.05	0.05	0.05
23	NM	NM	NM	NM	0.06	0.06	0.06	0.06
24	0.16	0.16	0.15	0.15	0.15	0.15	0.16	0.15
25	0.22	0.22	0.22	0.22	0.22	0.22	0.22	0.22
26	0.15	0.15	0.15	0.14	0.14	0.15	0.14	0.15
27	NM	NM	NM	NM	0.06	0.06	0.06	0.06
28	NM	NM	NM	NM	0.06	0.06	0.06	0.06
29	NM	NM	NM	NM	NM	0.05	0.05	0.05
30	NM	0.15	0.15	0.15	0.15	0.15	0.15	0.15
31	0.12	0.12	0.12	0.12	NM	0.12	0.12	0.12
32	0.10	0.10	0.10	0.10	0.10	0.11	0.11	0.10
33	NM	NM	NM	NM	0.04	0.04	0.04	0.04
34	NM	NM	NM	NM	0.04	0.04	0.04	0.04
35	NM	NM	NM	NM	NM	0.04	0.04	0.04
36	NM	NM	NM	NM	NM	0.04	0.04	0.04
37	NM	NM	NM	NM	0.06	0.06	0.06	0.0

NM - No Measurement

the aquifer's hydraulic gradients were constant during the total tracer test. Figures 48 and 49 provide a quasi-three-dimensional picture of the aquifer's potentiometric surface. The plots shown in Figures 48 and 49 were produced by an inverse-weighting option in the computer program SURFER (Golden, 1990). The potentiometric contours shown in Figure 48

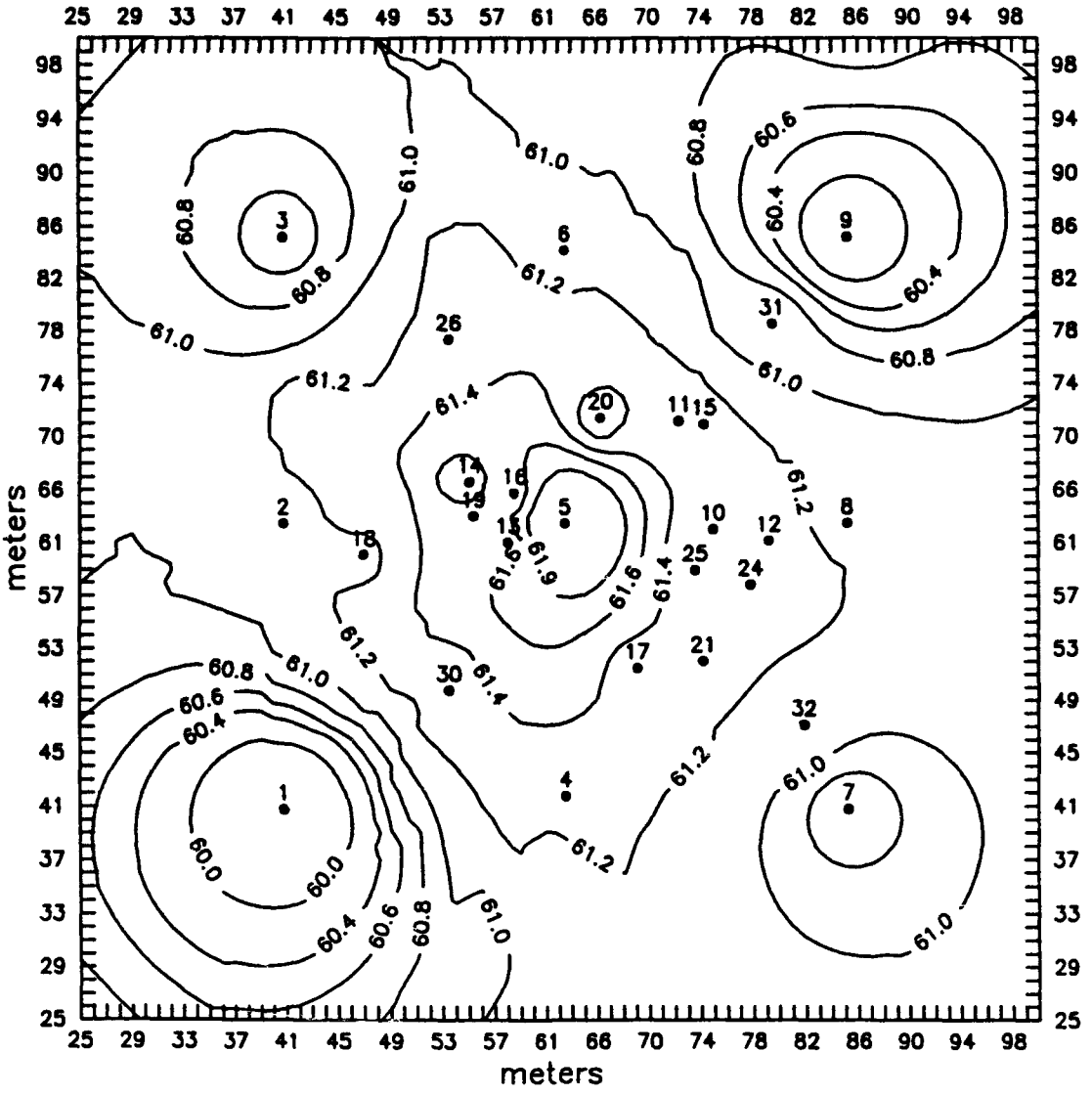

Figure 48. Contours of the Groundwater Potentiometric Surface During Tracer Test 5.

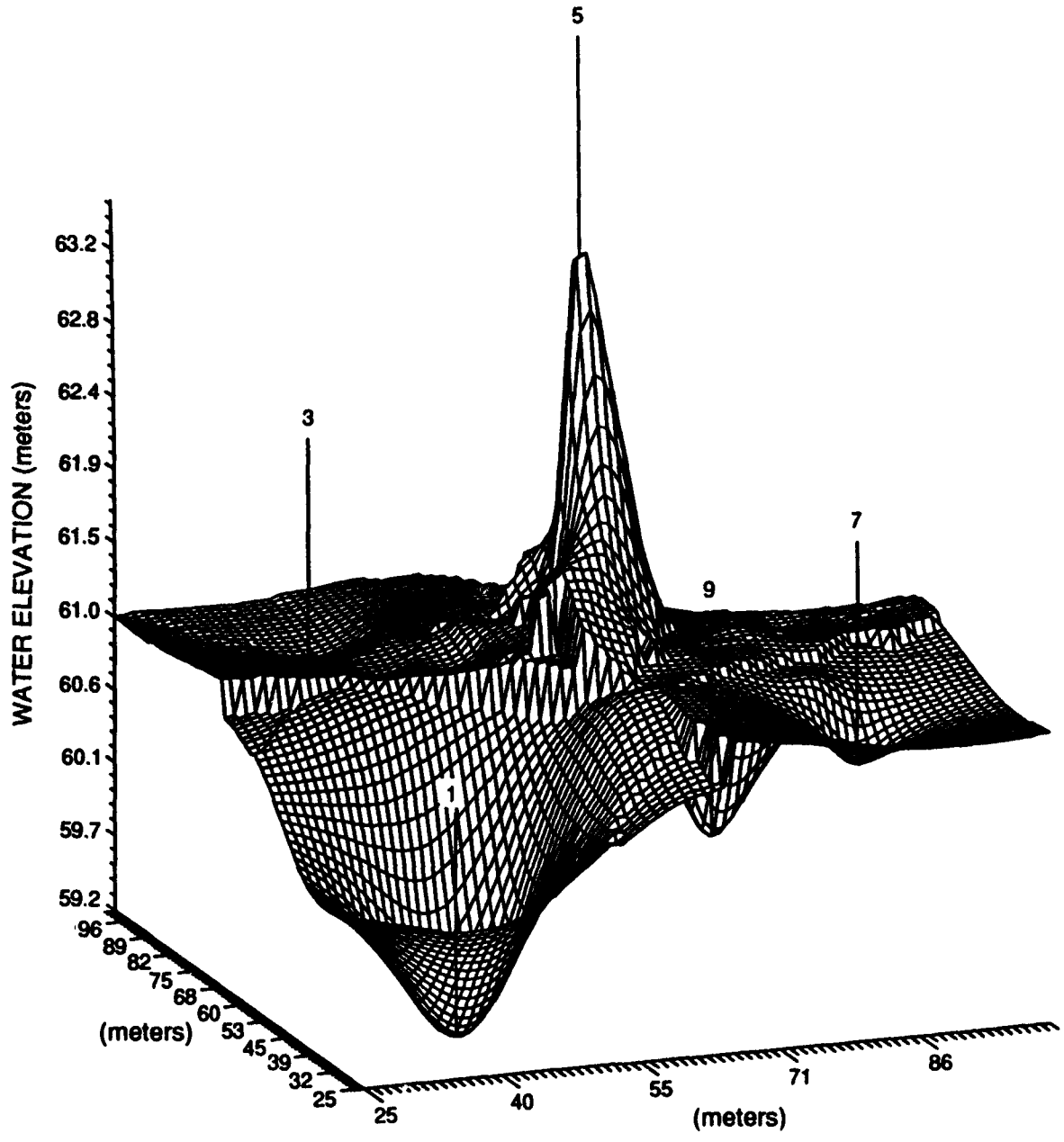

Figure 49. Three-Dimensional Representation of the Groundwater Potentiometric Surface During Tracer Test 5.

indicate that the aquifer material is considerably less resistant to groundwater flow toward Wells 3 and 7, than toward Wells 1 and 9.

3. Tracer Concentrations

As the first half of the groundwater samples were being measured for chloride, problems occurred with adjusting and maintaining the calibration of the specific ion probes. The problems became more frequent and severe until the chloride probes were replaced midway through the chloride measurements. Because the accuracy of this portion of the chloride data was questionable, the electrical conductivity measurements were used to define the shape of the tracer breakthrough curve.

For each of the wells, data similar to those shown in Figures 46 and 47 were collected. The monitoring wells were sampled periodically throughout the duration of the test except for Wells 32 and 7. Unfortunately, the wells were sampled on a regular schedule only until 60 hours into the tracer test. After 60 hours, tracer breakthrough had not begun at Well 32 nor 7. During the tracer test, tracer breakthroughs above 58 meters MSL were observed at 15 wells; no tracer breakthroughs were observed at Wells 1, 9, 8, and 4. Wells 17, 21, 25, 20, and 11 had tracer breakthroughs above 58 meters MSL and below 56 meters MSL. Figure 50 shows the time at which the maximum tracer concentration was achieved in each of these breakthrough curves.

As much as possible, the trends in the electrical conductivity data were compared with trends in the chloride measurements obtained using the specific ion probes. Examination of the two data sets effectively filtered out the potential interferences of bromide except at Wells 13, 16, and 26. At these wells, the tracer breakthroughs occurred during the time period when no reliable chloride measurements were made. The electrical conductivity data appeared sufficiently accurate to depict the time of the maximum tracer concentration in the upper aquifer. However, the electrical conductivity data was not adequate enough to determine whether or not a tracer pulse passed through the lower aquifer near Wells 13, 16, and 26. The problem with the electrical conductivity

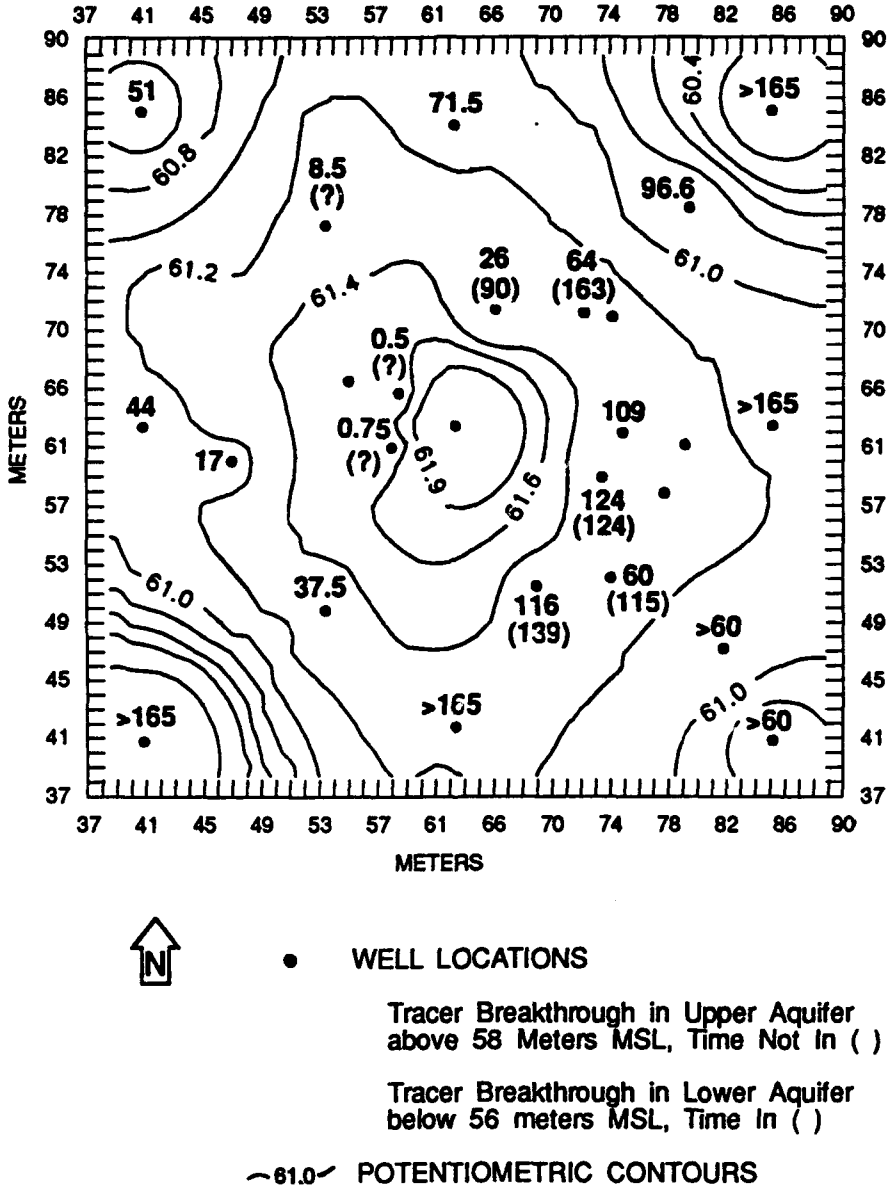

Figure 50. Breakthrough of Peak Concentrations Across the Well Network During Tracer Test 5.

data was that a significant amount of residual bromide from tracer test 1 may have been near the base of the wells at the start of tracer test 5. Consequently, there was uncertainty whether the high electrical conductivity readings were from the chloride from tracer test 5 or from the bromide from tracer test 1. As a result of this uncertainty, Figure 50 has question marks denoting the possible tracer breakthrough times at the base of the aquifer.

A trend in Figure 50 is preferred movement of the tracer from Well 5 in the upper third of the aquifer. The preferred direction is toward Wells 3, 2, and 6. No tracer breakthroughs were observed within 165 hours at Wells 4 and 8 (which mirror Wells 2 and 6, and at Wells 1 and 9, which were withdrawal wells). The skewed distribution of the tracer movement to the northwest indicates that extreme aquifer heterogeneity exists. In general, the type of extreme aquifer heterogeneity shown in Figure 50 agrees with that shown by the borehole flowmeter results (Figure 16).

SECTION VI

EVALUATION OF BOREHOLE FLOWMETER RESULTS

A. LARGE-SCALE TRENDS

1. Aquifer Tests

The results of Aquifer Tests 1, 2, and 3 produce an average/effective transmissivity of the aquifer between 30 and 40 cm^2/s. The actual average of the three transmissivity values is 34.4 cm^2/s. Given the saturated thickness of the aquifer is about 8 meters, the average/effective hydraulic conductivity is approximately 0.043 cm/s. This average value is useful to compare with the geometric mean of the 881 borehole hydraulic conductivity values, which is 0.032 cm/s.

Based on the analysis of three-dimensional flow through heterogeneous aquifers using Monte Carlo techniques, Warren and Price (1961) state: "The most probable behavior of a heterogeneous system approaches that of a homogeneous system with a (hydraulic conductivity) equal to the geometric mean of the individual (hydraulic conductivities)." Relevant to the work of Warren and Price (1961) are the results of stochastic groundwater theory presented by Matheron (1967) and Gutjahr, et al. (1978). For parallel flow conditions (which will be assumed for the large-scale aquifer tests), the average global hydraulic conductivity value lies between the geometric mean, Kag, and the arithmetic mean, Ka, of the punctual hydraulic conductivity values (Matheron, 1967) and is given in first order by Equation (2) (Gutjahr, et al., 1978). Hence, based on the work of Warren and Price (1961), Gutjahr, et al. (1978), and Matheron (1967), the global average hydraulic conductivity for the test site should lie between 0.032 cm/s (the geometric mean) and 0.261 cm/s (the arithmetic mean) and be close to 0.057 cm/s (Kag from Equation 2). The predictions compare favorably to the global average of 0.043 cm/s value calculated from the large-scale aquifer tests.

$$Kag = K_{geo} \ (1 + \sigma^2_{lnk}/6) \qquad (2)$$

where: Kag = global average hydraulic conductivity

K_{geo} = geometric average of punctual hydraulic conductivity values (.032 cm/s from Table 8)

σ^2_{lnk} = variance of the natural logarithm of the punctual hydraulic conductivity values (4.7 from Table 8)

The results of Aquifer Tests 1 and 3 show that the calculated values for transmissivity and the storage coefficient values change with the duration of the period of analysis. Specifically, the calculated transmissivity and the storage coefficient values decrease and increase, respectively, with increases in the duration of each pump test (see Figures 2 and 3). As shown in Figures 2 and 3, the changes include order-of-magnitude differences that occur over relatively long periods of time (>100,000 seconds). Based on the data analyses in Section 6 of Volume 1, the most likely reason for these changes is that significant crossflow occurred whenever the aquifer was hydraulically stressed. Crossflow is groundwater flow perpendicular to the groundwater flow toward a pumped well. The mechanism that drives crossflows are the nonsystematical changes in the hydraulic pressure field created by stressing a heterogeneous aquifer. Crossflow theoretically occurs only if the aquifer has heterogeneities with vertical and/or angular orientations. The borehole flowmeter results shown in Figures 12 to 18 have the three-dimensional hydraulic conductivity spatial variability required to produce crossflow during aquifer tests.

The results of both large- and small-scale tracer tests indicate a trend in the distance between the pumping and observation wells, and the calculated storage coefficient (see Figure 4). At distances near 5 meters, the storage coefficient ranges between 10^{-6} to 10^{-2}. At distances greater than 20 meters, the storage coefficient is greater than 10^{-3}. As discussed in Section II and explained in Volume I, this trend can be explained if the aquifer is heterogeneous and has lenses that: 1) are highly transmissive; 2) have lateral lengths between 3 and 10 meters; and, 3) are deposited in a matrix with a moderately-low hydraulic conductivity. The borehole flowmeter results in Figures 12 to 18 have the three-dimensional hydraulic conductivity spatial variability required to produce the trend in Figure 4.

2. Geological Information

A former river channel lies in the northwestern region of the well network (Figure 10). Existing relationships between the channel depth and width for meandering rivers indicate that the gravels and coarse sands that comprise the bedload of the former river should lie at a depth of 2 to 7 meters beneath the surface of the river channel. Because of their coarseness and lack of fines, these river channel deposits are of high hydraulic conductivity. At an average depth of 4 meters below the surface (i.e., at 61 meters MSL), the borehole flowmeter results (Figure 16) indicate a zone of high hydraulic conductivity values that map the path of the former river channel shown in the 1956 aerial photograph.

The drilling logs of the 37 wells installed at the well network provide evidence of a north-south depression approximately 1 meter deep and 20 meters wide in the Eutaw clay. The most likely explanation of the depression is the existence of another former river channel. If this be true, there should be a path of relatively high hydraulic conductivity materials in the depression. The borehole flowmeter results (Figure 16) show a sinuous path of high conductivity materials within the depression.

3. Tracer Test 5

a. Groundwater Flow Pattern

In a homogeneous aquifer, the pumping and injecting scheme used in Tracer Test 5 would produce identical hydraulic gradients from the injection well to each of the four withdrawal wells. The aquifer's response is a very asymmetrical set of hydraulic gradients. An examination of the borehole flowmeter results provides the reason for asymmetry in the groundwater contours.

Figure 51 shows the hydraulic conductivity profiles and the steady-state water table for selected wells. The position of the water table had a dramatic impact on the direction of groundwater flow. At both Wells 1 and 9 the water table is at about 59 meters MSL and lies

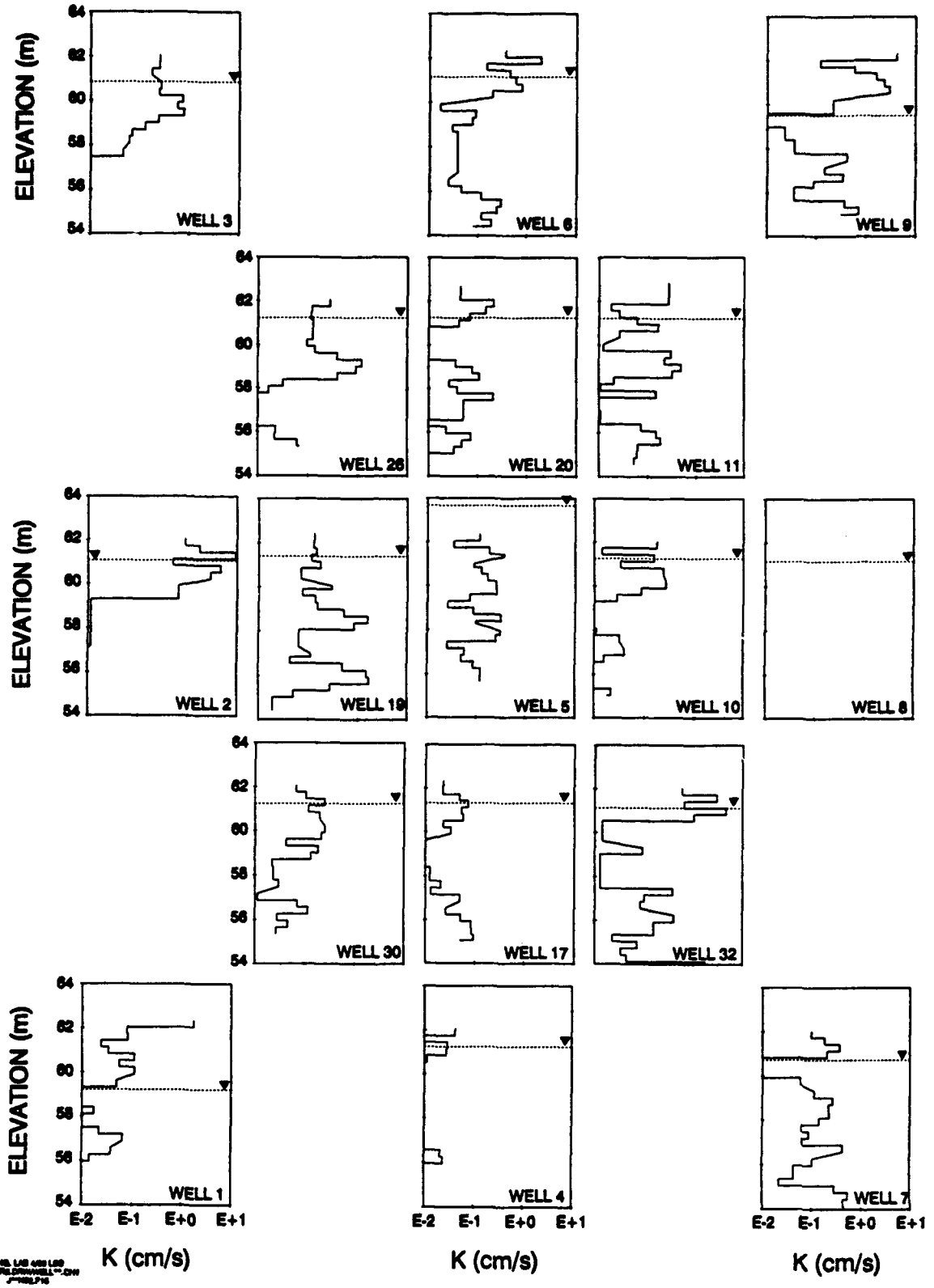

Figure 51. Groundwater Table Elevation During Tracer Test 5 and Hydraulic Conductivity Profiles at Selected Wells.

directly below the most permeable section of the aquifer. When compared to the relatively high water table in April, the water table in September provides fewer numbers of pathways for interconnection between the high hydraulic conductivity near Wells 5, 1, and 9. As shown in Figure 51 and in Figure 16, the relatively low water table of about 61 meters MSL had little effect on the interconnection between the high hydraulic conductivity zones near Wells 5, 3, and 7. The main pathway of groundwater flow to Wells 3 and 7 appears to be the bedload deposits that exists near the top and the base of the terrace aquifer, respectively.

b. Tracer Breakthrough for Tracer Test 5

Figure 50 shows that most of the tracer migrated within the upper third of the aquifer. In the upper layers, the tracer migrated fastest to the northwest, quickly to the north and west, slowly to the northeast and southwest, and slowest to the southeast, east, and south. Given the known hydraulic gradients across the site, borehole flowmeter results (Figure 16) can qualitatively account for trends in the tracer breakthrough times at different wells in the upper third of the aquifer.

B. QUANTITATIVE RESULTS

1. Potential Problems

As illustrated in Figure 11, the hydraulic conductivities calculated from the the borehole flowmeter measurements are based on two important assumptions. The first assumption is that the aquifer is isotropic and perfectly stratified. The second assumption is that the data analysis accounts for the effects of the flowmeter and the well on the flow system. At the CAFB site and at most, if not all, test sites neither of these assumptions are valid. Violations of these assumptions lead to errors in the calculated hydraulic conductivity values.

2. Transmissivity

The transmissivity at a well location is calculated from the time-drawdown curve. In a heterogeneous aquifer, the calculated

transmissivity is sensitive to the selected pumping rate and the method of data analysis. At some well locations, low (i.e., 6 L/min) and high (i.e., 30 L/min) pumping rates led to calculated transmissivity values which were different by orders of magnitude. It was determined that low pumping rates should be used for borehole flowmeter tests. Low pumping rates allow the local aquifer material to exercise primary control over the drawdown rate in the well. However, a question remains regarding the appropriate upper limit for the pumping rates.

Besides the selected pumping rate, differences in the calculated transmissivities can be achieved by using either the Cooper-Jacob equation (1946) or the Cooper-Jacob straight-line method (1946). Neither equation is strictly applicable for heterogeneous aquifers that have large-scale spatial trends in their transmissivity field. The two equations differ primarily in how they weigh the early portion of the drawdown curve, which is significantly affected by skin effects. It was determined that the Cooper-Jacob straight-line method (1946) should be used for borehole flowmeter tests because it best accounts for skin effects. However, some uncertainty still exists in using the Cooper-Jacob straight-line method because aquifer heterogeneities can result in nonideal drawdown curves for which there are no "truly" representative straight-line.

3. Vertical Distribution of Hydraulic Conductivity

The profile of relative hydraulic conductivity is determined directly from the vertical distribution of groundwater and estimates of head losses through and within the well. Sources of errors in the relative hydraulic conductivity profile include vertical flow between different hydraulic units, averaging between different hydraulic units, turbulence and nonuniform flow in the well, and skin effects around the well. Figure 52 illustrates these sources of error.

Because a borehole flowmeter fits snugly into a well, it may partially restrict horizontal flow into the well. If the flowmeter is raised such that it inhibits horizontal flow into the well from a zone of high hydraulic conductivity, then some of the groundwater from the zone

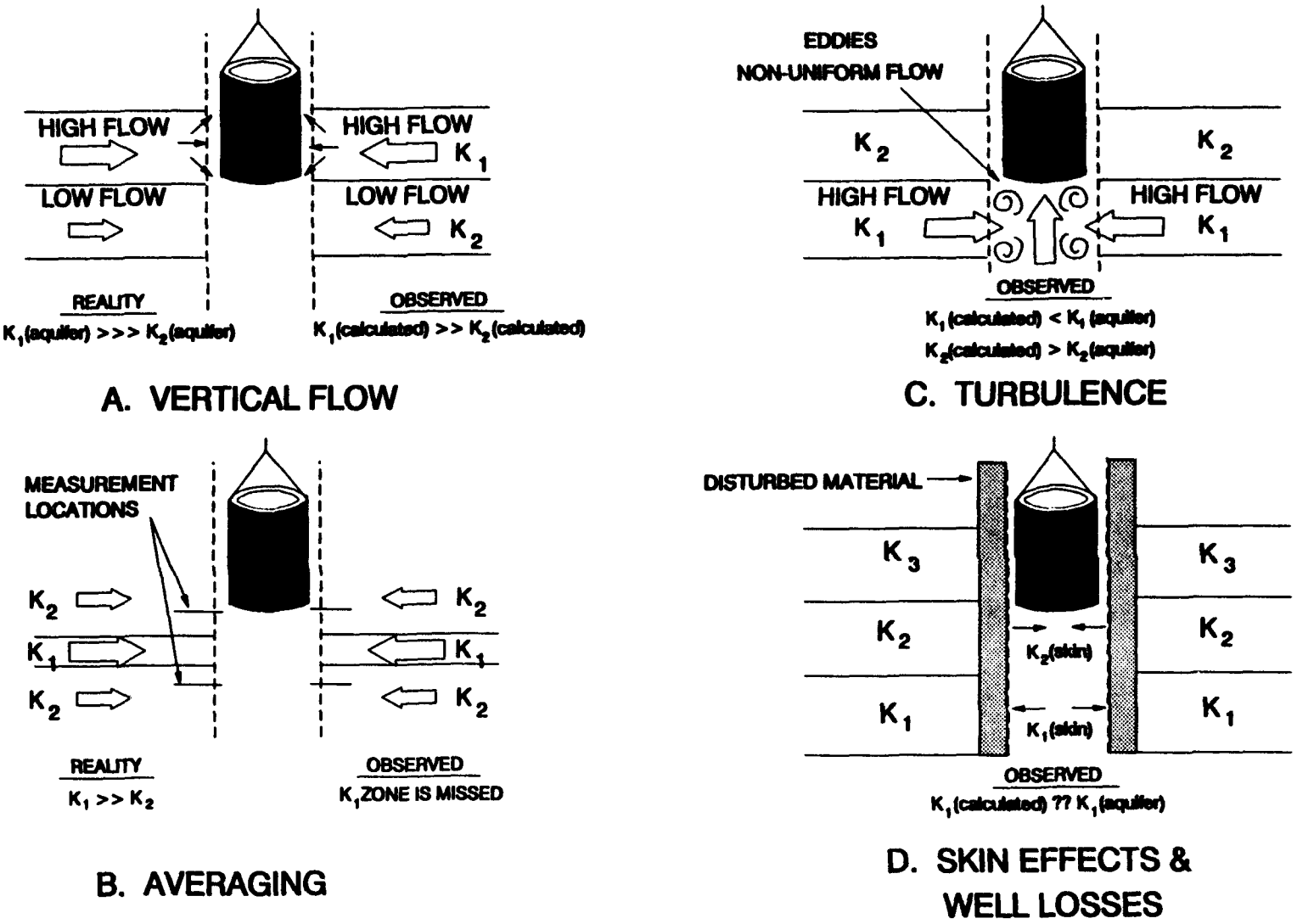

Figure 52. Phenomena that Causes Bias in the Hydraulic Conductivity Profiles.

of high hydraulic conductivity will enter the well around the flowmeter. If a zone of high hydraulic conductivity overlies a zone of low hydraulic conductivity, then this type of rechanneling flow will lead to hydraulic conductivity values that are slightly low for the lenses with high hydraulic conductivity.

The CAFB aquifer does not consist of discretely layered sediments but an almost random arrangement of lenses embedded in a matrix of sands and silts. The flowmeter measurements were taken at regular fixed vertical intervals for convenience and expedience. The disadvantage of fixed intervals is that some of the detailed structure is lost in the flow rates averaging within the fixed vertical intervals.

Immediately upon entering the well, the groundwater flows change from horizontal to vertical. In instances where the incoming groundwater flow rates are relatively high, the flow field within the well will be turbulent and nonuniform. Laboratory data showed that the accuracy of the EM borehole flowmeter is sensitive to the amount of turbulence. From the limited data available (Figure A8) the EM borehole flowmeter appears biased toward low flow measurements in turbulent flow.

At most of the CAFB wells, skin effects need to be accounted for when calculating the transmissivity. At any given well, one would expect the drilling method to disturb portions of the aquifer differently. As a result of a nonuniform vertical distribution of aquifer disturbance, skin effects will affect the vertical groundwater flow distribution into a well. If sufficiently high pumping rates are used then the vertical variation of head loss through the well becomes a concern. This phenomenon should not be ignored even though some algorithms can be used to predict the relationship between head loss and flow rate.

C. TRACER TEST AND BOREHOLE FLOWMETER HYDRAULIC CONDUCTIVITIES

Figures 53 and 54 provide a comparison between the hydraulic conductivity values calculated from the tracer test and the borehole flowmeter test. The information for these graphs came from Figures 12, 13, 14, and 50, and Tables 15, 16, 17, 18, and 19. Figure 53 includes

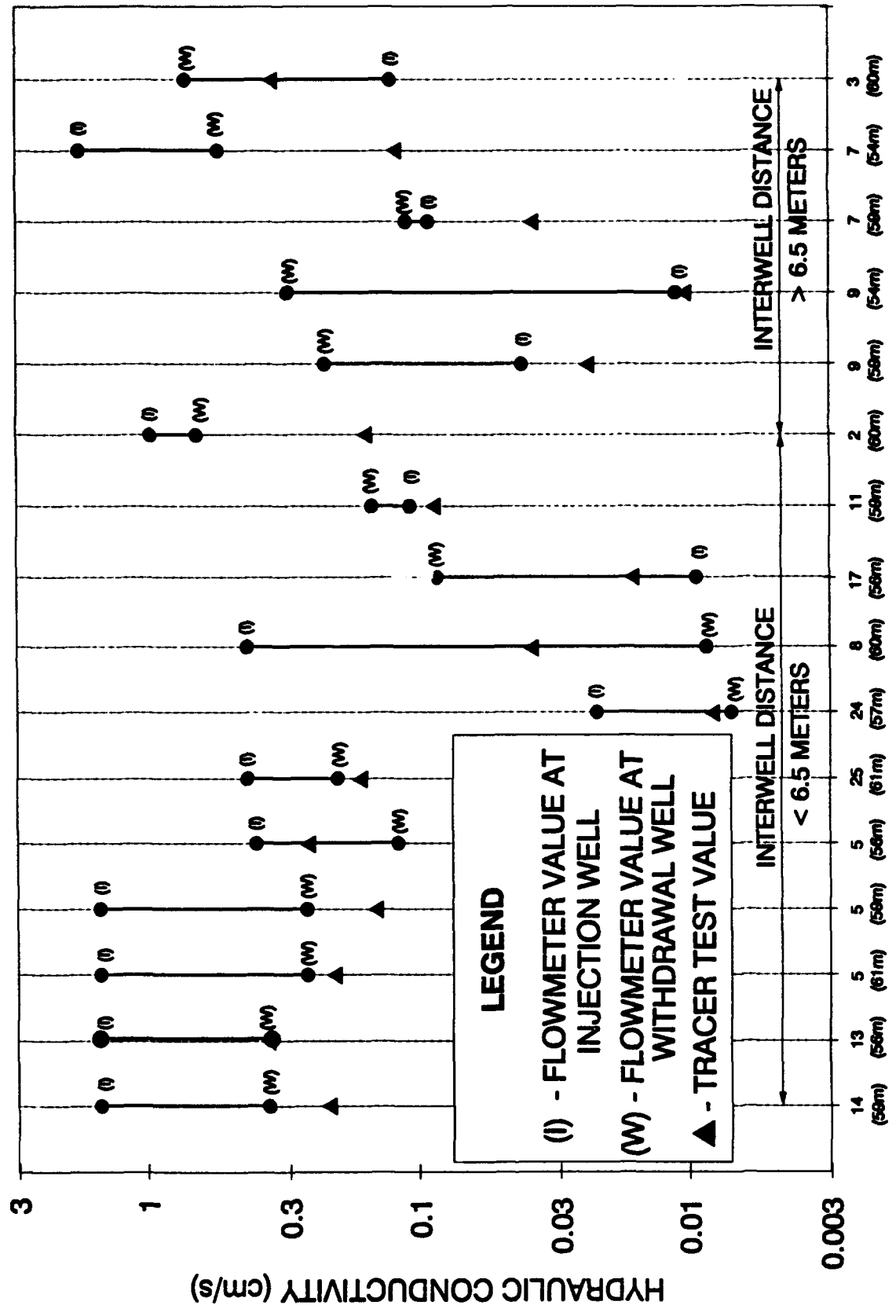

Figure 53. Comparison of Hydraulic Conductivities Calculated From the Borehole Flowmeter and the Tracer Tests 1 to 4 Data.

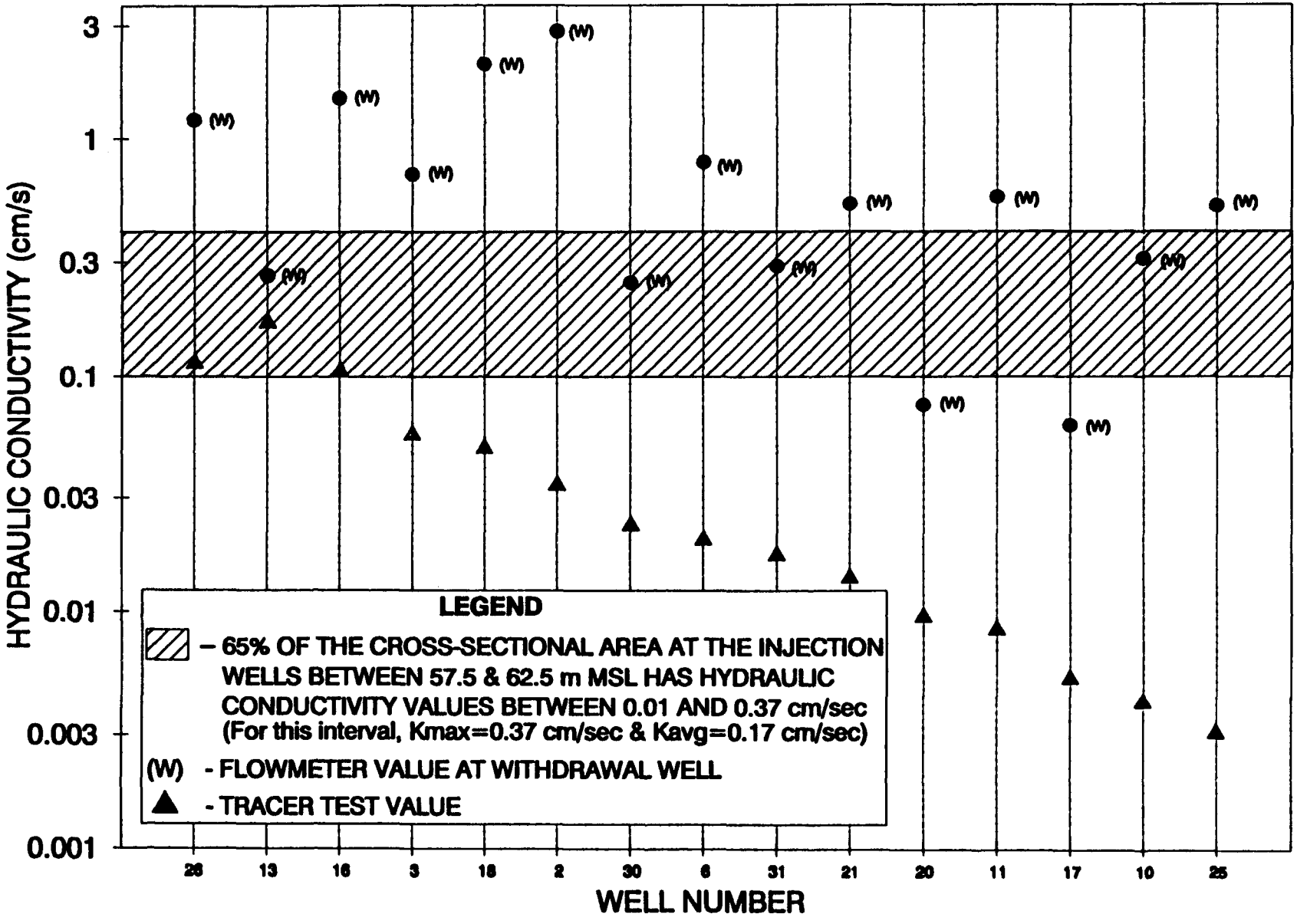

Figure 54. Comparison of Hydraulic Conductivities Calculated From the Borehole Flowmeter and the Tracer Test 5 Data.

only the breakthrough tracer curves for Tracer Test 4 that included at least one point on the rising limb of the curve. In Figure 53 the hydraulic conductivity values calculated from the tracer test data is compared with the values calculated at the tracer test elevation at the injection and the withdrawal wells. Good agreement was achieved between two sets of hydraulic conductivity values when the interwell distance was less than 6.5 meters. In most cases, the "tracer test" hydraulic conductivity value is within a factor of 2 of the hydraulic conductivity value at the withdrawal well. This type of agreement is very encouraging given the very heterogeneous conditions that exist at the site and considering the large difference between the hydraulic conductivity values of the injection and the withdrawal wells.

When the interwell distance becomes greater than 6.5 meters, the match between the hydraulic conductivity values from the tracer and the borehole flowmeter results are typically fair to poor (Figure 53). A trend is supported by Figure 54. Figure 54 presents the data from Tracer Test 5. Figure 54 is similar to Figure 53 except that it shows the range of hydraulic conductivities at the injection well. A single value of hydraulic conductivity was not assigned to the injection well because of the uncertainty regarding the elevation at which the tracer primarily traveled.

D. OVERALL EVALUATION

The CAFB terrace aquifer consists of a heterogeneous mixture of gravels, sands, silts, and clays. The hydraulic and the geological information show that changes in the aquifer types occur both gradually and abruptly; and the numerous lenses within the aquifer have different dimensions and aspect ratios. The importance of the heterogeneity at the CAFB cannot be overstated. A measure of heterogeneity is the variance of the natural logarithm of the hydraulic conductivity measurements, σ_{lnk}. At CAFB σ_{lnk} is 4.7. The estimates of σ_{lnk} for an aquifer composed of coastal sands in Cape Cod, Massachusetts, studied by the United States Geological Survey, and for an aquifer composed of glacial till in Borden, Canada, studied by Stanford and Waterloo Universities, are less than 0.5.

Because of the extreme heterogeneity of the CAFB aquifer, numerous problems were expected with characterizing the hydraulic conductivity field. These problems center on collecting sufficient data to delineate the three-dimensional trends and determining the best hydraulic conductivity value for a location where large differences in the hydraulic properties of the aquifer material change rapidly with distance. Because of these potential problems, the CAFB aquifer is not a good aquifer for ground-truthing the accuracy of the borehole flowmeter technique. No region having little spatial variability in the hydraulic conductivity field could be found for tracer tests and borehole flowmeter tests.

On the other hand, the aquifer heterogeneity created conditions which led to a very rigorous test of the fundamental principles on which the borehole flowmeter is based. To properly evaluate the borehole flowmeter method, several data sets were constructed. These data sets included information related to multiwell aquifer tests, single-well pump tests, geological investigations, and tracer tests. The diversified and extensive data base provided several independent approaches for evaluating the usefulness and accuracy of the EM borehole flowmeter technique. Overall, these evaluations provide a very favorable assessment of the EM borehole flowmeter technique.

Comparison between borehole flowmeter and tracer test hydraulic conductivity data sets shows very good agreement when the interwell distance is less than 6.5 meters. In most cases, the "tracer test" hydraulic conductivity is within a factor of 2 of the borehole flowmeter hydraulic conductivity at the withdrawal well location. This agreement is good considering that observed hydraulic conductivities vary over five orders of magnitude.

As shown in Figures 53 and 54, differences between tracer test and borehole flowmeter hydraulic conductivities become greater when interwell distances increase beyond 6.5 meters. The large differences between the two sets of values indicate that the hydraulic conductivity profiles along the tracer pathway differ from the profiles at the injection and/or withdrawal well locations. Hence, at increasing distances, the

importance of interpolation increases and the type of simple data analyses used in Section V is less and less reasonable.

Overall, the EM borehole flowmeter technique successfully characterizes the three-dimensional hydraulic conductivity field at CAFB at both the regional scale (10-100 meters) and the local scale (1-10 meters). Unfortunately, a more thorough evaluation of these measurements cannot be made as part of this project. Such an evaluation would require that the data be used in a three-dimensional groundwater model to predict the results of the multiwell aquifer tests, the single-well pump tests, and the tracer tests. This task is well beyond the scope and resources of this project and the results of such an exercise is dependent on the interpolation method used to construct the three-dimensional hydraulic conductivity field. Fortunately, that evaluation is not needed to demonstrate that the EM borehole flowmeter technique can characterize an aquifer's hydraulic conductivity field in the detail required to design an optimum network of wells and/or infiltration galleries for bioreclamation systems.

(The reverse of this page is blank.)

SECTION VII

GEOSTATISTICAL ANALYSIS

A. INTRODUCTION

Within the last decade considerable progress has been made in developing stochastic theories/models for problems related to solute transport in groundwater. Many of the stochastic theories assume an intrinsic stationarity hypothesis to extract/simulate attributes of the hydraulic conductivity data. Intrinsic stationarity, in this case, means that the first two moments (i.e., the mean and the variance) of the probability density function for the hydraulic conductivity field are invariant with respect to translation through space. For convenience, stochastic theories will henceforth refer to those theories that assume intrinsic stationarity as defined above.

One of the assumptions in developing and applying stochastic theories is that heterogeneity becomes homogeneous, or spatially periodic, at some scale so that a random variable used to represent hydraulic conductivity exhibits intrinsic stationarity. For those aquifers in which the scale of heterogeneities is large compared to the scale of the problem, the assumption is made that the stochastic theory can be applied after detrending the field and creating a stationary set of residuals. To date, little work has been published that evaluates and/or demonstrates the utility/optimality of these theories in heterogeneous aquifers.

B. INTRINSIC STATIONARITY

As given by Journal and Huijbregts (1978), the random function Z(x) is assumed to satisfy the intrinsic stationarity hypothesis if:

(i) $E[Z(x+h) - Z(x)] = 0$ for all x and h

(ii) $\gamma(h) = 0.5 \text{ var } [Z(x+h) - Z(x)]$ exists and depends only on h where $\gamma(h)$ denotes the variogram as usual.

In the application of stochastic theories, intrinsic stationarity is neither a feature required to be exhibited by the data nor necessarily an intrinsic property of the field, rather it is the property of the theory.

Because the intrinsic stationarity hypothesis cannot be proven and/or disproven, several researchers, notably Philip and Watson (1986), are critical of stochastic theories. Philip and Watson (1986) argue, "with stochastic models, prediction is qualified by hypothesis. It is not prediction in the sense of deduction, unless the hypothesis is proven." In defense of stochastic theories, geostatisticians, notably Srivastava (1986) and Journal (1986), have responded to the criticism and explain that the intrinsic hypothesis is not a scientific theory and therefore requires no a priori justification, and it can only be refuted a posteriori if proven to be inadequate for the goal at hand.

In the mining industry, the goal at hand is the efficient and accurate prediction of the values of a random variable (e.g., ore grades) at each point in a continuous field. In the groundwater industry, the goal at hand is realistic simulations of solute transport through the random variable (e.g., hydraulic conductivity). To accomplish this goal, not only are the values at each point of interest but also the interconnectivity/continuities among the values. The importance of the interconnectivity/continuities, though a minor issue related to selecting which regions contain the best ore grades, are a major issue in predicting solute transport through a hydraulic conductivity field.

The simulation of interconnectivity/continuities are controlled by the probabilistic model assumed for the hydraulic conductivity field. As such, geohydrologists should carefully select the best method to transform and/or to detrend the raw data before determining whether, or if, stochastic theories should be applied. Within the literature, a commonly accepted practice is to apply the logarithmic transformation of the hydraulic conductivity data before data analysis. Within the literature, however, there is no commonly accepted practice regarding the removal of a nonstationarity from the data, much less, a commonly accepted method for detecting and defining a nonstationarity.

C. TRENDS AND DETRENDING

When referring to nonstationarity, the terms "trend" and "drift" are often used in the groundwater literature. In most instances, as in this

case, the term "trend" agrees with its well known usage in the context of trend surface analysis wherein a model like Equation (3) is used. The term "drift" refers to a trend characterized by a polynominal of zero order.

$$Z(x) = Y(x) + m(x) \tag{3}$$

The delineation of a trend is accomplished objectively by some type of mathematical function. Within the literature several methods have been proposed for detrending nonstationary fields so that the structure, the variance, and the properties of the stationary portion of the field can be determined. Table 20 lists the methods.

TABLE 20. SIX METHODS FOR DETRENDING DATA (from Rehfeldt, et al., 1989a)

1. Ordinary Least Squares (OLS) to remove the trend and calculate the covariance of the residuals.
2. Iterative Generalized Least Squares (IGLS) to remove the trend and calculate the covariance of the residuals.
3. Maximum Likelihood (ML) to simultaneously estimate the trend and the covariance.
4. Restricted Maximum Likelihood (RML) to estimate the covariance without having to estimate the trend first.
5. Minimum-Variance Unbiased Quadratic Estimation.
6. Generalized Covariances.

Russo and Jury (1987) have investigated the question of which is the best method for removing the trend and obtaining the correlation length and the variance of the underlying stationary field. In their study, they generated a theoretical two-dimensional stationary field and then tainted the field by adding a deterministic trend. The authors then applied the OLS, IGLS, ML, and RML methods to detrend the data and obtain the variances and correlation lengths listed in Table 21.

Of the six methods shown in Table 21, the OLS method is by far the simplest to implement. A criticism of the OLS method is that the method assumes that all of the residuals are independent and uncorrelated when, in fact, the reason for using the OLS method is to better define the correlated nature among the residuals. However, the results of Russo and Jury (1987) indicate that, even with this potential problem, the OLS method is as good,

TABLE 21. SUMMARY OF COVARIANCE PARAMETER ESTIMATES FOR SYNTHETIC NONSTATIONARY RANDOM FIELD (from Russo and Jury, 1987)

Linear Trend #1
with 72 sampling points

Method	Variance (σ^2)	Correlation Length (λ)
Input	1.0	0.07
OLS	1.267	0.062
ML	1.365	0.174
RML	1.615	0.223

Linear Trend #2 with 72 sampling points

	Field 1		Field 2	
Method	Variance (σ^2)	Correlation Length (λ)	Variance (σ^2)	Correlation Length (λ)
Input	1.0	0.07	1.0	0.28
OLS	1.267	0.062	0.703	0.17
IGLS	1.272	0.062	0.728	0.17
ML	1.375	0.174	1.154	0.443
RML	1.614	0.223	2.916	1.414

Non Linear Trend with 288 sampling points

	Field 1		Field 2	
Method	Variance (σ^2)	Correlation Length (λ)	Variance (σ^2)	Correlation Length (λ)
Input	1.0	0.07	1.0	0.28
OLS	1.097	0.170	1.006	0.187
IGLS	1.170	1.170	1.209	0.259
RML	5.845	0.989	5.265	1.386

if not better, than other methods. For the present study, the OLS method was used in conjunction with polynomial expressions of different orders to fit three-dimensional trends through the logarithms of the hydraulic conductivity data.

The results of Russo and Jury (1987) indicate that if the trend is linear and significant, the trend can be easily diagnosed by the variograms. However, when the trend is not strong, or if it is nonlinear, then identifying the presence of a trend from the sample variogram is, for all practical purposes, highly uncertain. An estimate of the importance

of this uncertainty is well summarized by the concluding remarks of Russo and Jury (1987):

> "In the case of nonlinear drift the values of λ=0.259 and σ^2=1.209 provided by the IGLS procedure and the values of λ=1.386 and σ^2=5.265 provided by the RML procedure are associated with the values of the Akaike Information Criterion, 185.5 and 185.6, respectively, and hence by the criteria, represent equally valid estimates of the parameters [Original values are λ=0.358 and σ^2=2.9151]. Note however, that the difference between the estimates b=6.6 and 5.4, respectively, of the "slopes" of the variogram, $b=\sqrt{2\ \sigma^2/\lambda}$ in this example are not very large. The parameter b is, as discussed in the work by Russo and Jury (this issue), all that is required for application of conditional probability such as kriging. However, for applications of unconditional probability such a stochastic transport modeling, both λ and σ^2, must be estimated individually. For example, longitudinal macrodispersivity (Gelhar and Axness, 1983) is proportional to the product and λ and σ^2 of the logarithm of the hydraulic conductivity. For the nonlinear drift example above, the two cases with essentially identical values of the AIC have values of the product $(\lambda)(\sigma)^2$ equal to 0.31 and 7.3."

In order to estimate values for λ and σ^2 for the theory of Gelhar and Axness (1983) at the EPRI-MADE site, which is less than 200 meters from the USAF test site, Rehfeldt, et al. (1989b), applied ordinary least squares regression to remove polynomial trends of orders 1, 2, and 3 from a data set of 1242 logarithmic values of hydraulic conductivity. One of the most fundamental questions of this investigation is the definition of what is a trend and what is random. For the stochastic transport theory, Rehfeldt, et al. (1989b), assumed that the variation in the hydraulic conductivity field with scales on the order of the size of the plume are regarded as a trend and variations in hydraulic conductivity with scales on the order of 10 percent of the plume are treated as random. Based on this premise, Rehfeldt, et al. (1989b), acknowledge that "even within the same aquifer, the definition of what is trend and what is random will change depending on the time and space scales of the problem at hand."

Rehfeldt, et al. (1989b), state "the variograms of the residuals 'look' more like the variogram of stationary random processes, the larger the order of the polynominal, (and that) one would be hard pressed to

defend a trend of order 1, 2, or 3 as being the best based on the variograms." In order to select the most appropriate trend, Rehfeldt, et al. (1989b), used information from a natural gradient tracer test and the local geology. In short, they recommend that the "third order trend surface should be rejected because it is physically inconsistent with the other known information at the EPRI-MADE site. Second order is the highest order trend that is compatible with the other data on site."

Boggs, et al. (1990), reevaluate the detrending of the MADE site after augmenting Rehfeldt's data set by 1114 hydraulic conductivity values, most of which are from locations in the previously untested far-field, which is about 80 to 150 meters downgradient of the tracer injection location. Boggs, et al. (1990), state that "the third-order polynominal trend was judged the best representation of the conductivity drift based on its compatibility with the groundwater flow field as inferred from observation of the tracer plume during the natural-gradient test." Table 22 shows the significant differences in the variance and the correlation scales from the original data and the residuals created by the third-order detrending.

TABLE 22. COVARIANCE PARAMETER ESTIMATES FOR LOGARITHMIC HYDRAULIC CONDUCTIVITY DATA AT THE EPRI-MADE SITE

	σ^2	λ_h	λ_v
Original Data	4.5	12.0	1.5
Third-Order Residuals	2.8	5.3	0.7

Inasmuch as Russo and Jury (1987), Rehfeldt, et al. (1989a, b), and Boggs, et al. (1990), illustrate the considerable uncertainty and problems with estimating the covariance parameters in a nonstationarity field, they have understated the problem by implicitly assuming that detrending is best accomplished by only using some type of continuous mathematical function. In reality, heterogeneous aquifers contain geological facies. At the MADE and the USAF site, these facies include chutes, channels, point bars, etc. Each of these facies have different orientations, dimensions, and probability density functions for their hydraulic conductivity field. Some of the interfacies transitions are

gradual, while others are abrupt. Clearly, if such facies are distinguishable, then the approach of representing each of the facies in the aquifer by the same trend and the same covariance parameter is highly questionable and not optimal.

D. FACIES AND FACIES MODELING

The term facies can be defined as the combination of the physical, hydrological, and/or mineralogical properties exhibited by a geological formation in a designated volume. With regard to modeling the flow patterns in petroleum reservoirs, numerous articles have advocated the stochastic modeling of facies to generate the architecture of the petroleum reservoir. Haldorsen and Damsieth (1990) and Haldorsen and MacDonald (1987) provide a review of these articles. Stochastic facies models focus on generating synthetic geological architecture and/or hydraulic conductivity fields that are conditioned to observations.

In stochastic modeling of facies, a point in space belongs to only one of a limited number of classes (or groups), and the model controls how the class values at each point interact. Implicit in these models is that the facies are discrete units and the reservoir construction is driven by geological depositional history. For many groundwater problems, facies modeling may not realistically generate spatial variability at the micro-scale. However, facies models and the basis for the models can provide information on: (1) the underlying structure and cause of a nonstationarity at the macro- and meso-scale, and; (2) insight into the spatial variability in the hydraulic conductivity field for each facies.

At the test site, several different facies exist. These facies include a coarse-grain meander channel, coarse-grain point bar, chute bars within the point bar, a cutbank, and a braided channel. Each facies is characterized by lenses with different orientations, dimensions and hydraulic properties. The transition between the different facies will be abrupt at some locations but gradual at other locations. In such a heterogeneous aquifer, a stochastic model that assumes intrinsic stationarity is not realistic. Moreover, problems exist with using many types of continuous mathematical functions to detrend because the basic

structure of the mathematical function and the hydraulic conductivity field are different.

An understanding of the depositional environment and the facies for a test site is important because it provides insight and direction into how to subdivide and detrend the hydraulic conductivity field. The importance of facies is well illustrated by the trend selected by the third-order trend by Boggs, et al. (1990), for the EPRI-MADE hydraulic conductivity field. The trend shows a zone of high hydraulic conductivity throughout the thickness of the aquifer and aligned longitudinally with the orientation of the MADE sampling network (see Figure 6). The trend starts near the middle of the network where Figure 6 shows the former river channel crossing the network. In short, the trend is inconsistent with the meander, as it is perpendicular to it. The inconsistency between the structure in the trend and the structure in the depositional model casts uncertainty on the usefulness of variograms for the residuals produced by the third-order polynomial fit at the EPRI-MADE site.

Russo and Jury (1987) indicate that visual inspection of variograms may detect a nonstationary trend when a significant linear trend exists, but will not detect a nonlinear trend. Based on these results, one may expect that an investigation into nonstationarity requires more than a visual inspection of the variograms. Hence, one should recall that Russo and Jury had the same trend across the field. Based on the type of geological facies in fluvial environments, one expects that the facies in the aquifer have significantly different trends in their hydraulic conductivity fields. A visual inspection of variograms in the aquifer may indicate whether each region has similar or dissimilar structures. Similar structures would support the intrinsic and stationary hypothesis; and dissimilar would support a nonstationary hypothesis.

E. HORIZONTAL AND VERTICAL VARIOGRAMS

In order to evaluate the merit of the intrinsic stationarity probabilistic model at the test site, the vertical and horizontal variograms were calculated for six subsets and the complete set of the natural logarithms of the hydraulic conductivity values. From the

comprehensive borehole flowmeter data set, the six smaller data sets were created by partitioning the comprehensive data set into an upper zone and a lower zone, by partitioning the comprehensive data set into an east zone and a west zone, and by partitioning the comprehensive data set into a north zone and a south zone. Table 9 provides a statistical comparison of the first two moments among the data sets.

Figure 15 shows the probability distribution function, pdf, of Ln(K) for each of the seven data sets. For each of the three-paired sets of hydraulic conductivity data (i.e., north-south), the probability is less than 6 percent that each of the two data sets was generated by the same pdf based on the Kolmorgorv-Smirnov's limiting distribution (Feller, 1948; Smirnov, 1948). The low percentages support that strict stationarity would be a poor probabilistic model for the hydraulic conductivity field.

Figures 55 and 56 show the vertical and the horizontal variograms calculated for seven data sets. For each variogram, a theoretical exponential variogram (Equation (4)) was fitted to the data to estimate the correlation length. The vertical and the horizontal variograms for the total region appear well-behaved and do not indicate a nonstationarity. The significant differences in the variograms for the different regions in the aquifer, however, indicate that a nonstationarity exists. Within the variograms for the north, west, and upper regions

$$\lambda(h) = \sigma^2_{lnk} \ (1 - \exp \ (-h/\lambda)) \qquad (4)$$

where: $\lambda(h)$ = stationary negative-exponential variogram
λ = lag or separation distance between measurement couples
σ^2_{lnk} = sill (assumed equal to the sample variance)

F. DETRENDING WITH POLYNOMIAL EXPRESSIONS

The global logarithmic hydraulic conductivity field was detrended by polynomial expressions of orders one to six. The results of the OLS trend analysis are presented in Figures 57 through 62. These trends are

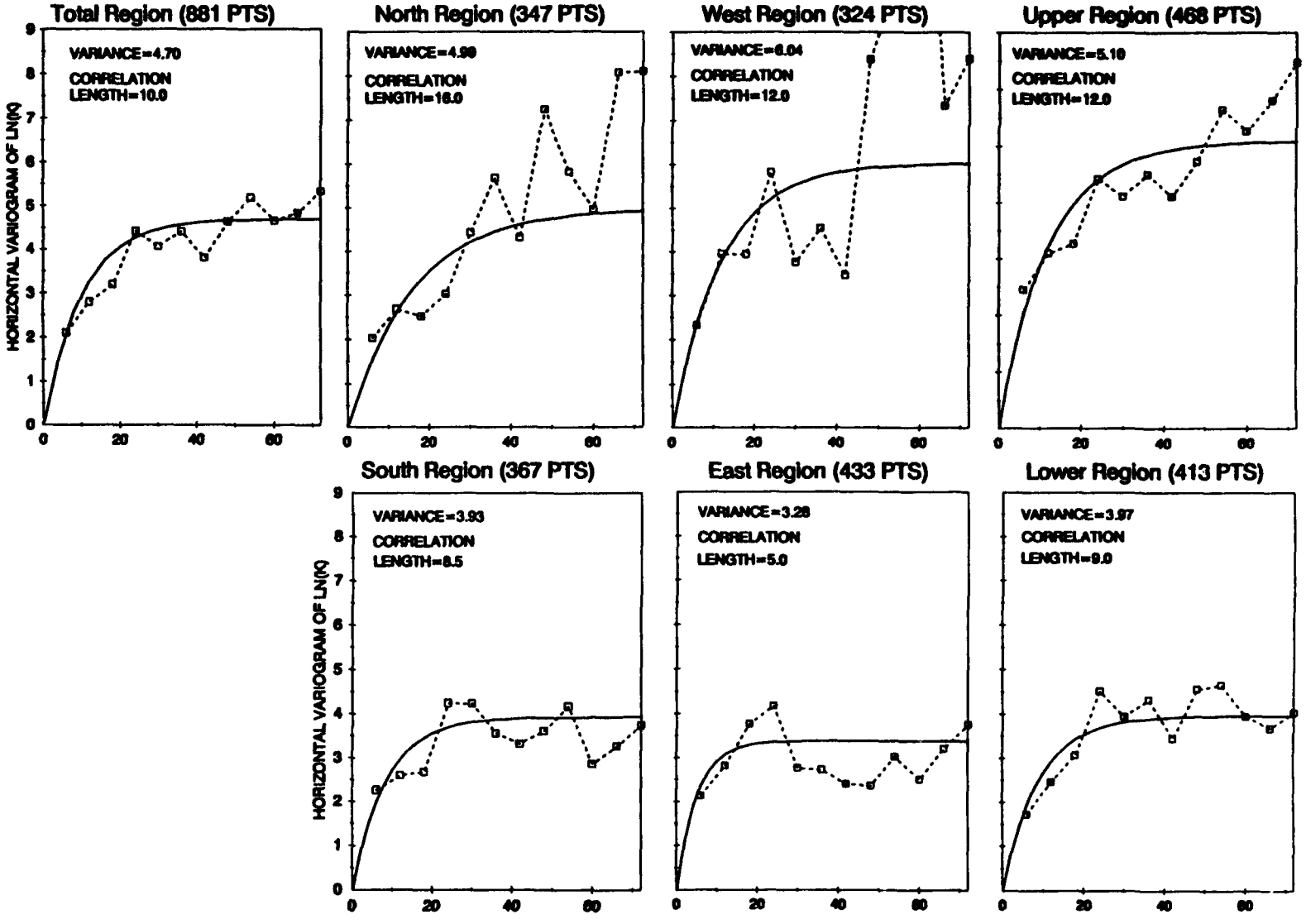

Figure 55. Horizontal Variograms for the Different Regions in the Test Site.

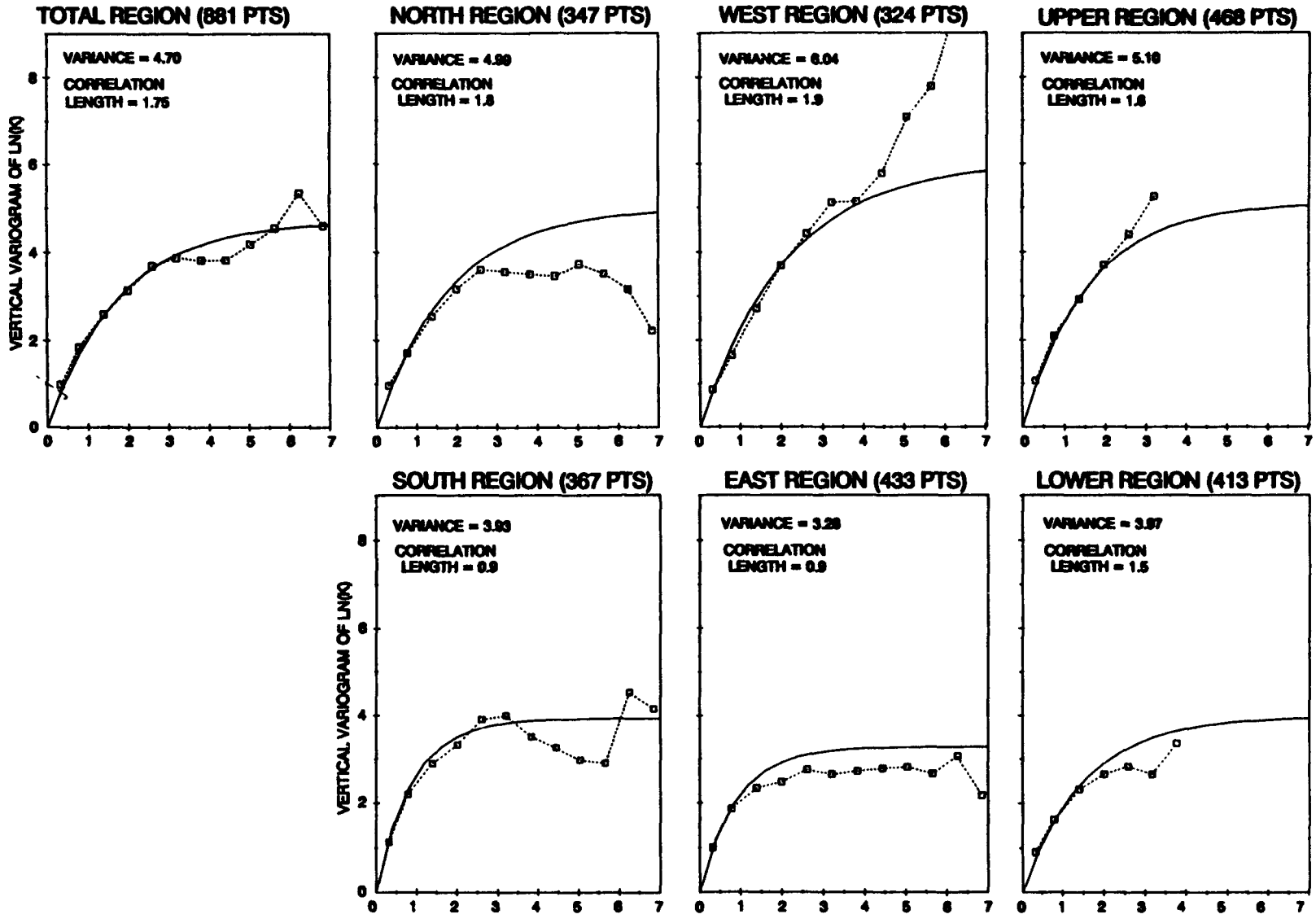

Figure 56. Vertical Variograms for the Different Regions in the Test Site.

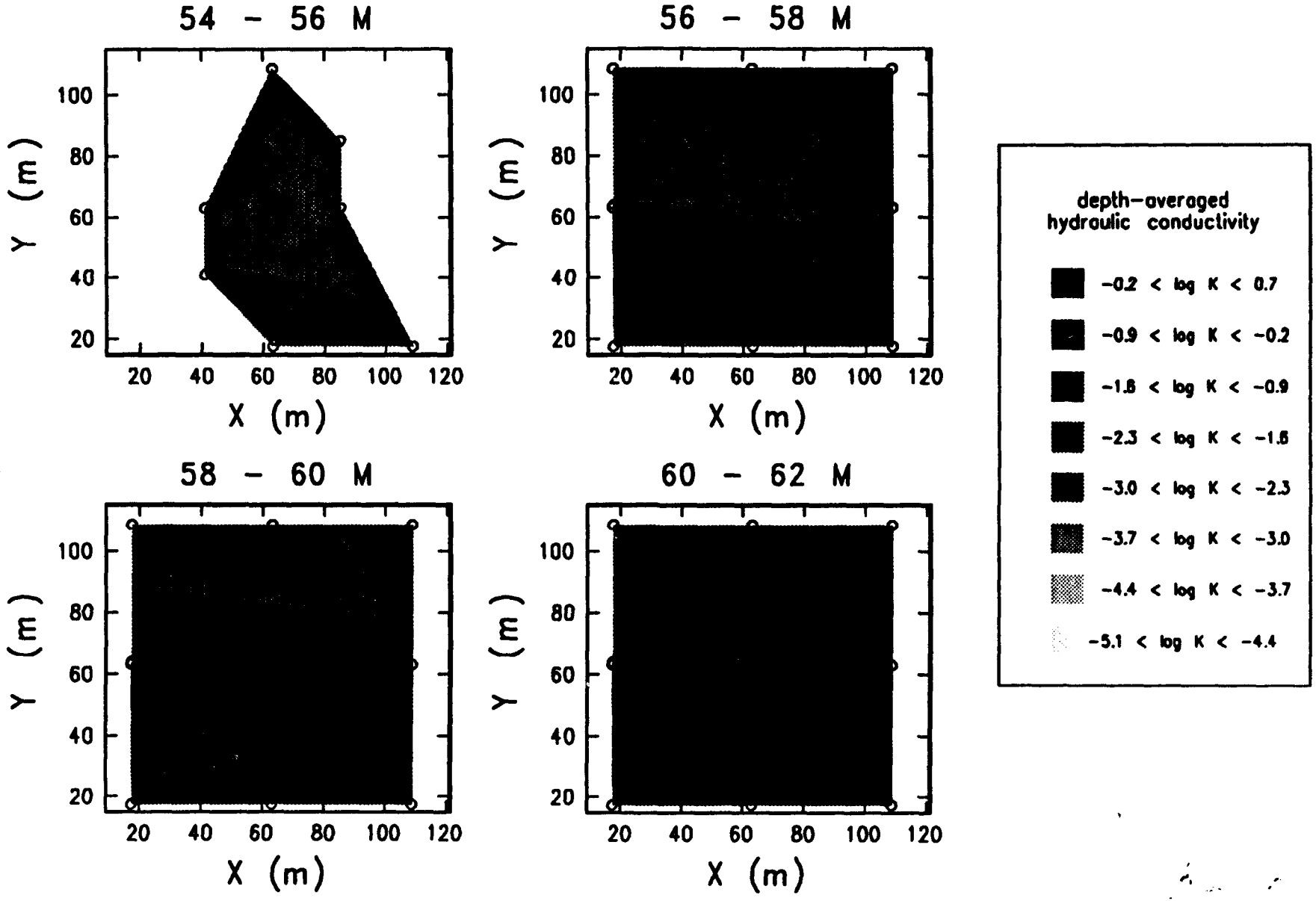

Figure 57. Depth-Averaged Hydraulic Conductivity Cross Sections of the First Order Polynomial Used to Detrend the Hydraulic Conductivity Field.

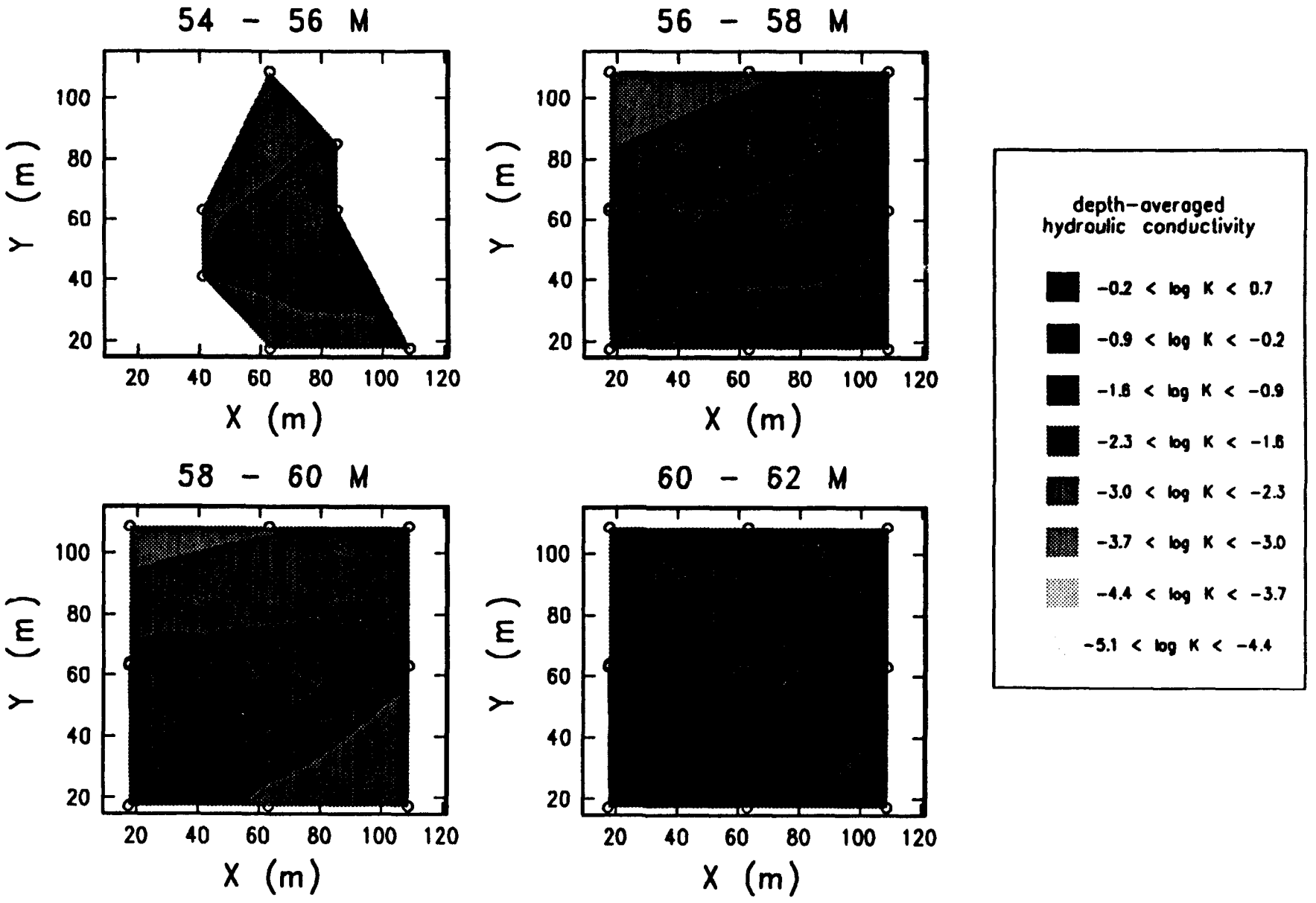

Figure 58. Depth-Averaged Hydraulic Conductivity Cross Sections of the Second Order Polynomial Used to Detrend the Hydraulic Conductivity Field.

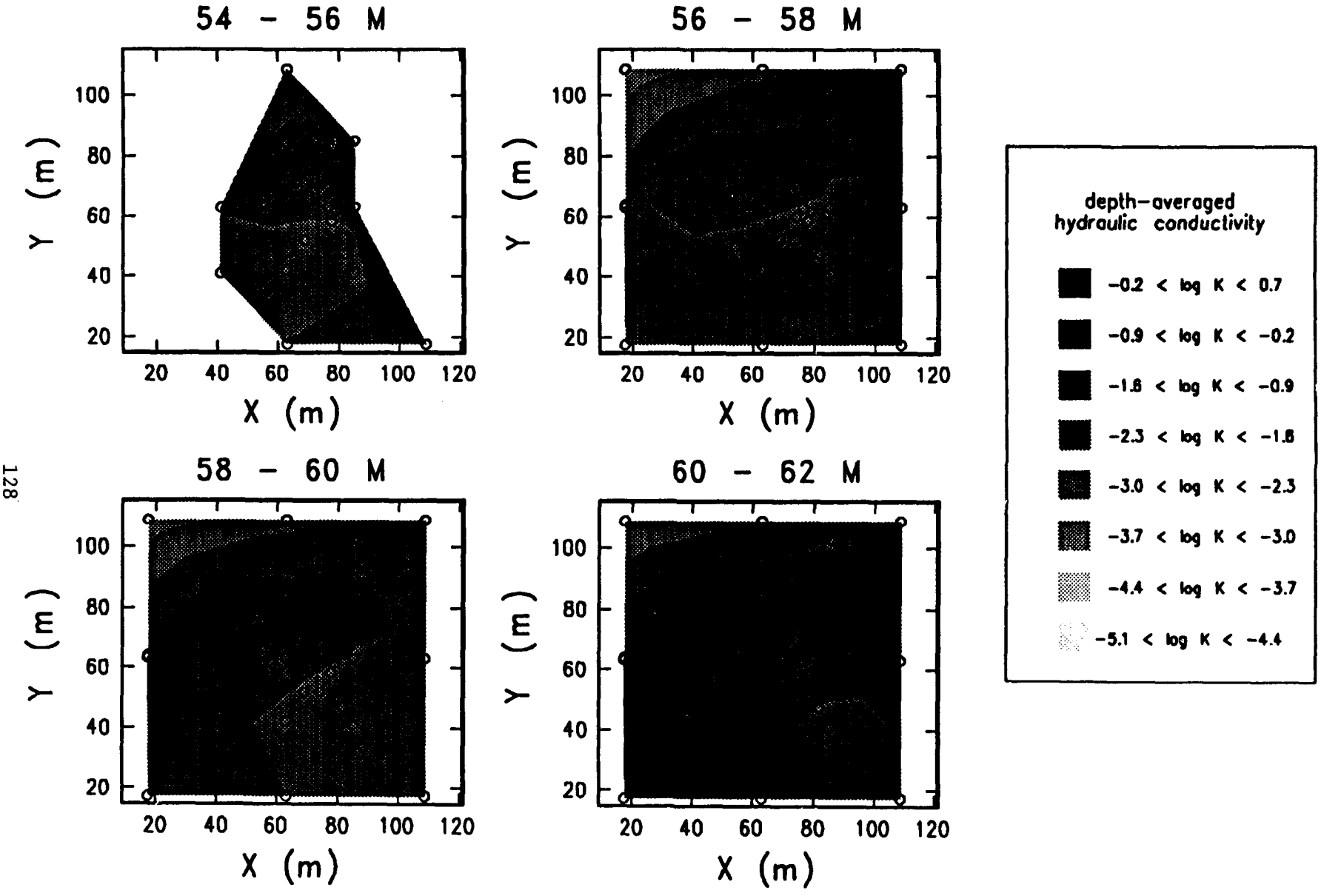

Figure 59. Depth-Averaged Hydraulic Conductivity Cross Sections of the Third Order Polynomial Used to Detrend the Hydraulic Conductivity Field.

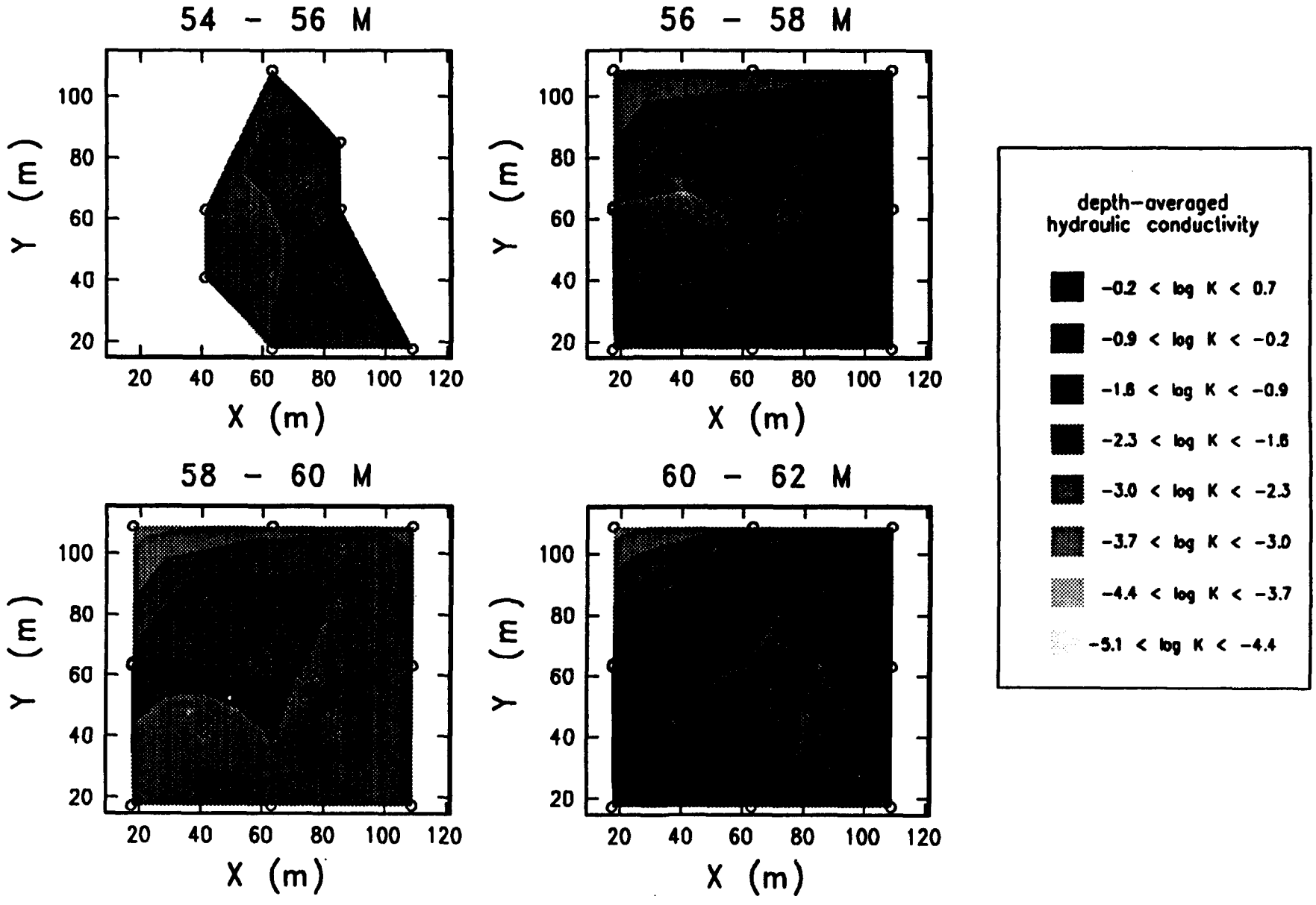

Figure 60. Depth-Averaged Hydraulic Conductivity Cross Sections of the Fourth Order Polynomial Used to Detrend the Hydraulic Conductivity Field.

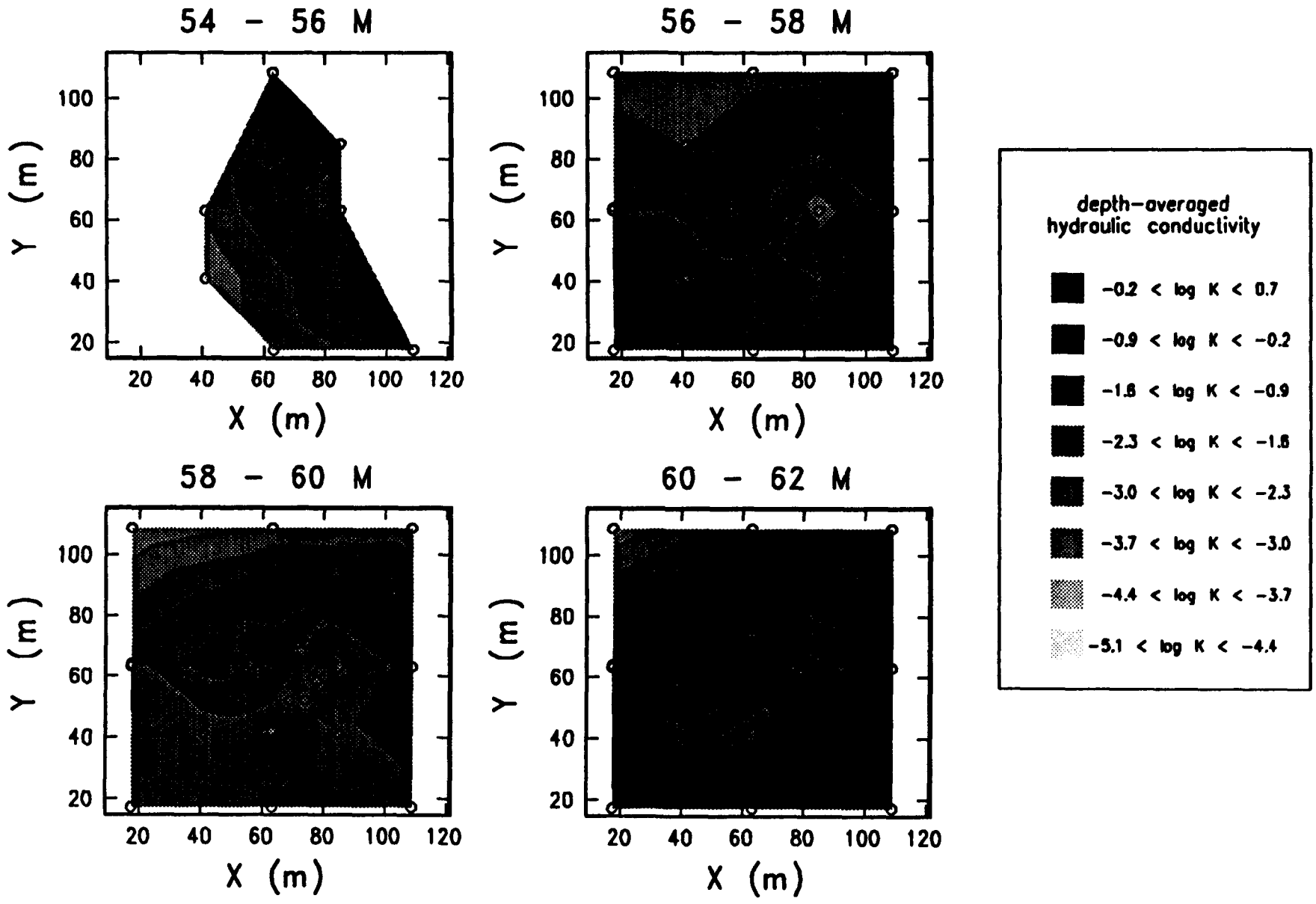

Figure 61. Depth-Averaged Hydraulic Conductivity Cross Sections of the Fifth Order Polynomial Used to Detrend the Hydraulic Conductivity Field.

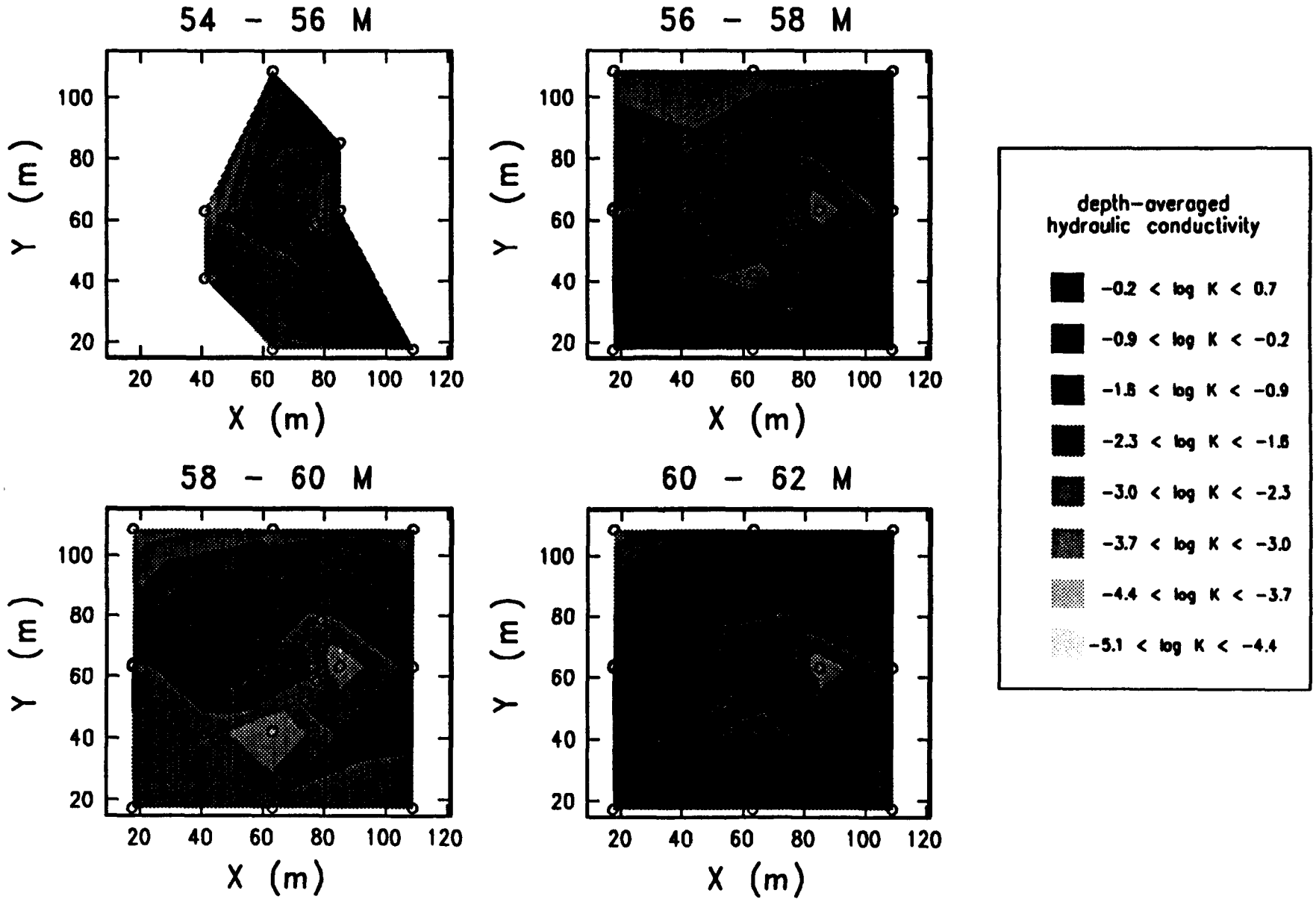

Figure 62. Depth-Averaged Hydraulic Conductivity Cross Sections of the Sixth Order Polynomial Used to Detrend the Hydraulic Conductivity Field.

presented in the same format as the actual data in Figure 16. For each of the six polynomial equations, a set of residuals was calculated by subtracting the value of the trend from the data at each measurement location. Figure 63 shows that as one fits trends of increasing order to the data, the detrended data shows decreasing variance and correlation scales with respect to the untrended data. Figures 64 and 65 show the effects of detrending on the variance and the correlation scales for the different regions across the site. The effects of detrending are significant; however, there is considerable uncertainty about which polynomial expression best detrends the data. Although the absolute values of the statistical quantities shown in Figures 64 and 65 decrease with higher order trends, the relative difference among most of these statistical quantities for each detrending remains similar. This phenomena occurs because the structure of the polynomial expressions and of geological facies, which control the heterogeneity, are different. The trends that make the hydraulic conductivity nonstationary do not extend across the whole test site but are limited to the geological facies that created it. Hence, because the polynomial fits try to fit the same trend through a field, and because the geological facies produce trends that are limited in their influence, polynomial expressions are not well-suited for detrending the hydraulic conductivity field at CAFB.

G. IMPLICATIONS FOR STOCHASTIC MODELS

An analysis of the variograms for different regions of the test site indicates that the logarithmic hydraulic conductivity field is poorly represented by a probabilistic model that assumes intrinsic stationarity. Nonstationarity occurs at CAFB because several different geological facies exist within the sediments. Several different polynomial expressions of different orders one to six were used to detrend the hydraulic conductivity field.

Although the effects of detrending had a very large impact on both the variance and the correlation scales of the residuals, no criteria appeared reasonable for determining the point at which optimum detrending had occurred. An examination of the statistical properties of the residuals from different regions show that although the absolute

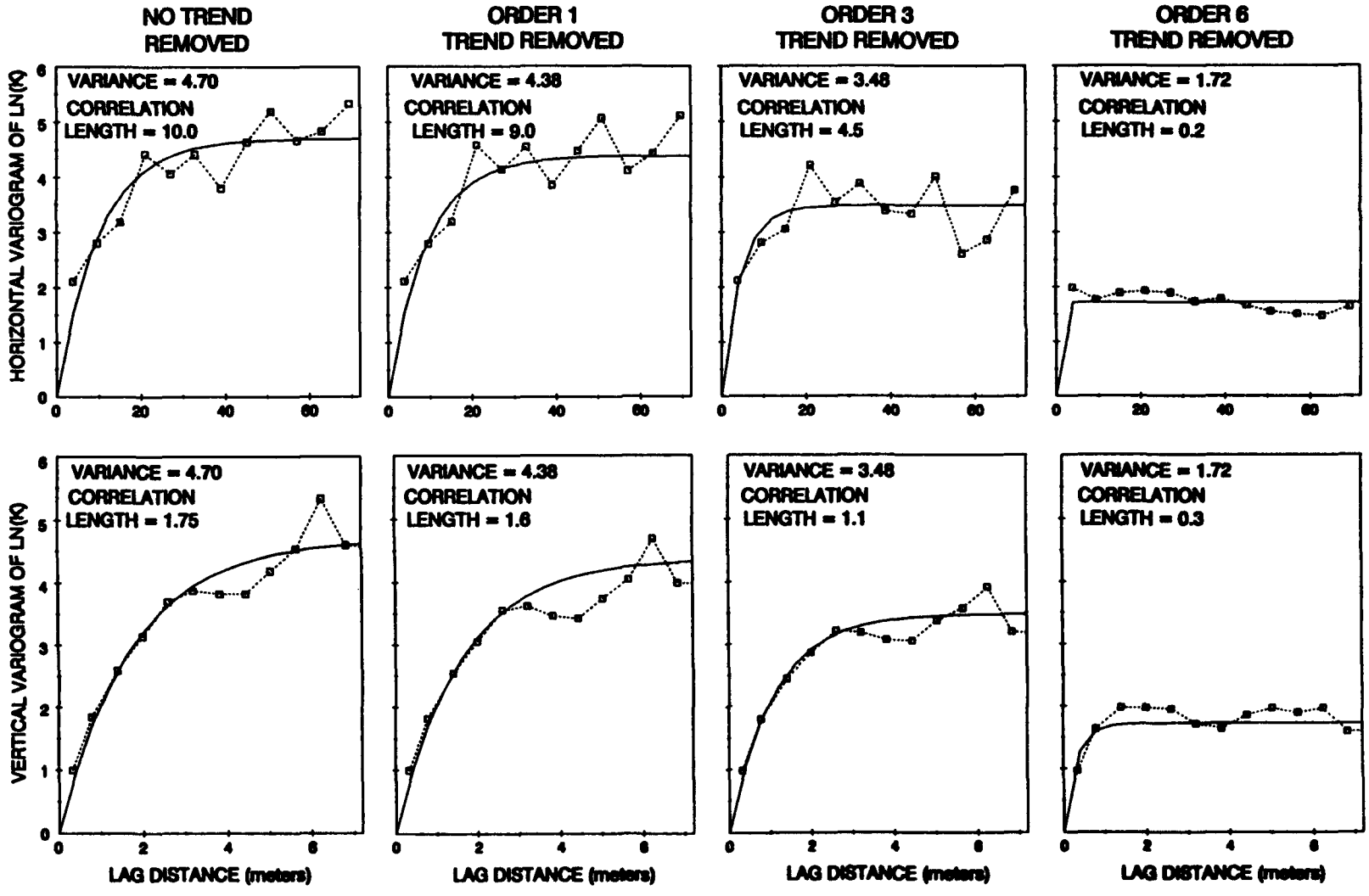

Figure 63. Horizontal and Vertical Variograms for the Residuals.

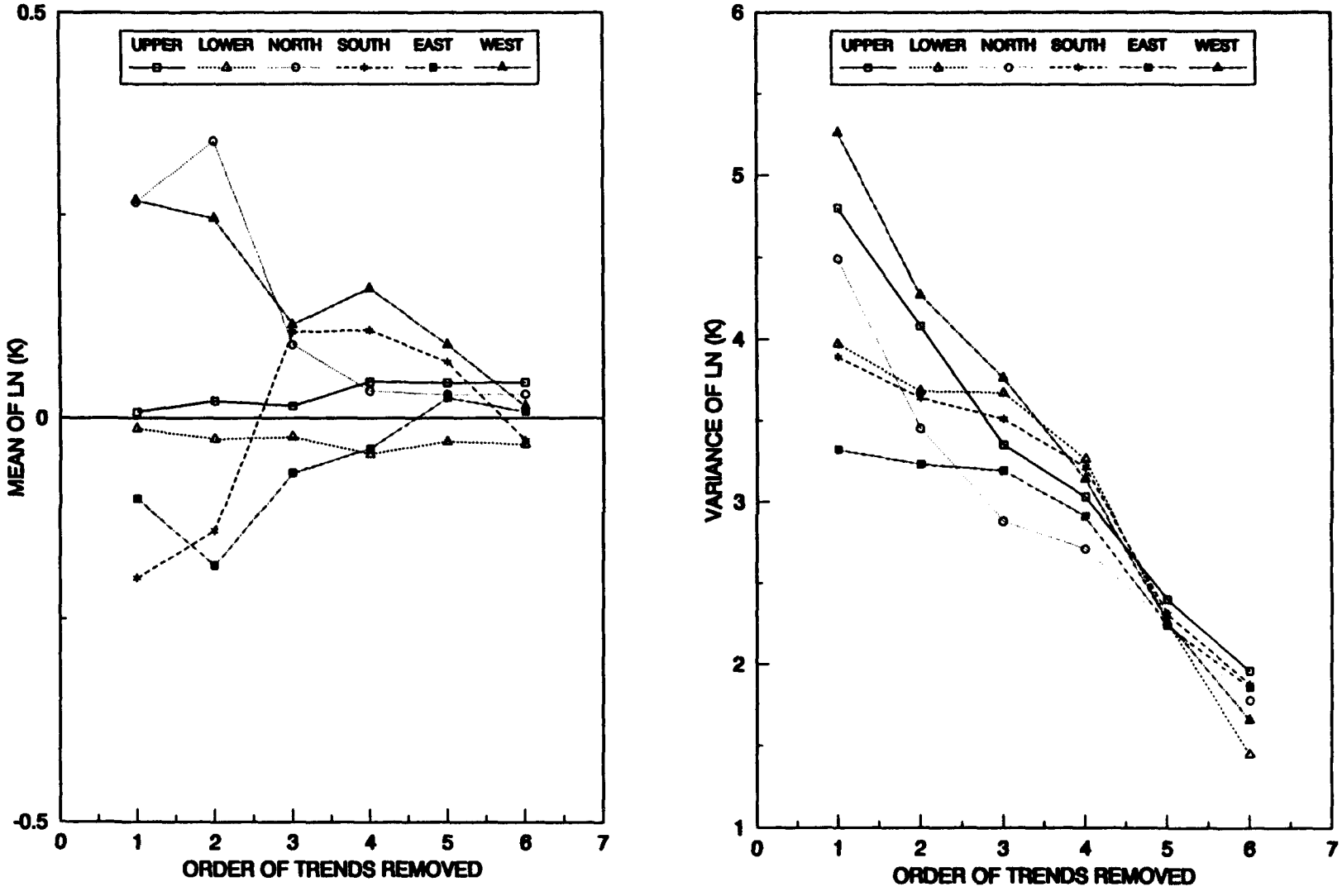

Figure 64. The Effect of Detrending on the Mean and the Variance of the Residuals.

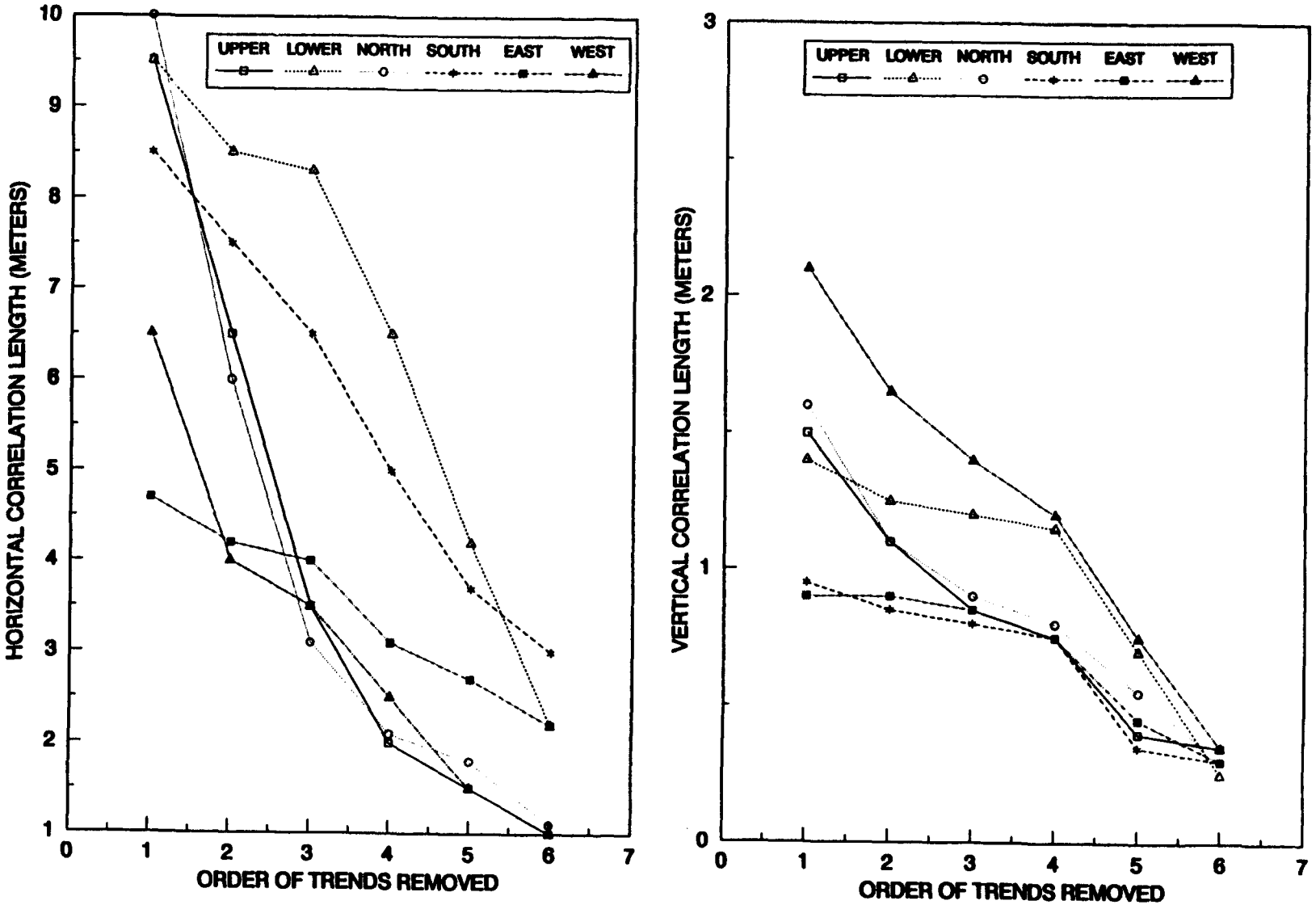

Figure 65. The Effect of Detrending on the Horizontal and Vertical Correlation Lengths for the Residuals.

differences in the values significantly decreased with high-order polynomials, the relative differences increased or remained about the same. The results indicate polynominal expressions are not well-suited for detrending the hydraulic conductivity data because they fit the same trend through a whole area; whereas the geological facies, which are responsible for the trends in the field, are limited to specific regions.

Detrending with a stochastic facies model may appear as an appealing alternative to detrending by ordinary least-squares or an equivalent mathematical technique. However, the following skeptical remarks should be made. Generally the data availability allows, as in our case, development of a conceptual facies model. Some indications are available where boundaries between facies are, but large uncertainties remain. In our case, for example, the aerial photograph clearly defines a facies boundary at the surface, but how exactly to project this boundary in depth is unknown. The amount of data needed to develop a quantitative facies model to be used for detrending, goes beyond what is generally feasible to collect in the field. And if such an amount of detailed data is available, the question arises whether some type of a deterministic approach, based on this vast quantity of data, should not be preferred above the stochastic approach.

SECTION VIII

SITE CHARACTERIZATION METHODOLOGY

A. OVERVIEW OF PROJECT

The project characterized the geohydrology for the CAFB aquifer in the detail required to evaluate a well network design for remediation of a contaminant spill by bioreclamation. The project included well network design, single-well and multiwell aquifer pump tests, borehole flowmeter tests, geological investigations, tracer tests, and geostatistical analyses. These investigations demonstrate that solute movement cannot be accurately predicted in the CAFB aquifer without characterizing the hydraulic conductivity field in three dimensions.

A major portion of the project centered on borehole flowmeter tests for measuring horizontal hydraulic conductivity variation in three dimensions. The project led to significant advances in the borehole flowmeter technique described by Rehfeldt, et al. (1989). Included are the development of an electromagnetic borehole flowmeter, use of the Cooper-Jacob straight-line equation for calculating transmissivity from drawdown data, and use of a low pumping rate so that the calculated transmissivity reflects the aquifer properties near the well.

Different types of investigations were conducted to evaluate the representativeness of the borehole flowmeter hydraulic conductivity values. The investigations show that the trends in the borehole flowmeter hydraulic conductivity values and/or the values themselves: (1) compare favorably with the results of the tracer tests with interwell distances less than 6.5 meters; (2) produce a geometric mean consistent with the results of the large-scale pump tests; (3) map the abandoned channel and point bar of a former meandering river; and (4) agree with the zones of high and low transmissivities indicated by the large-scale pump and tracer test results. The investigations indicate that the borehole flowmeter technique provided hydraulic conductivity fields in the detail required to accurately predict tracer movement in aquifers.

Although significant advancements of the borehole flowmeter technique were accomplished, several areas of uncertainty still exist. These areas include the process of selecting the proper pumping rate, impact of skin effect on vertical distribution of flow to a well, and appropriateness of using a data analyses technique that assumes horizontal flow to the well. To a large extent, these areas of uncertainty need to be addressed on a site-by-site basis. Although these uncertainties may be important in particular situations, the analysis of the three-dimensional hydraulic conductivity field at CAFB indicates that the uncertainty associated with calculating the values is less than the problems associated with interpolating between the values. Hydraulic conductivity values show that order-of-magnitude differences exist over distances as short as 0.3 meters vertically and 3 meters horizontally. Sharp contrasts in aquifer properties occur because of the lenticular structure of aquifer materials created by different geological facies.

The importance of proper spatial interpolation of the hydraulic conductivity values is shown by the tracer test results. When the interwell distances were less than 6.5 meters, the hydraulic conductivity values from the tracer and the borehole flowmeter tests were within a factor of two. When the interwell distances were greater than 6.5 meters, the differences between the hydraulic conductivity values from the tracer and the borehole flowmeter tests typically varied between a factor of 10 and 100. Hence, in predicting tracer migration over distances greater than 6.5 meters in heterogeneous aquifers, linear interpolating of hydraulic conductivity values will likely provide an incorrect analysis. A review of the project's diversified and extensive investigations makes it clear that in order to model tracer migration accurately in heterogeneous aquifers, the method of spatial interpolation needs to adequately reproduce the following: (1) dimensions, aspect ratio, and orientation of the different lenses; (2) the interconnectiveness among the lenses; and (3) the hydraulic conductivity contrasts among the different aquifer lenses and the aquifer matrix.

Because of their general popularity in the hydrosciences, geostatistical techniques were selected a priori as the method for spatially interpolating the hydraulic conductivity field. One of the

keystones for geostatistical analyses is the assumption of intrinsic stationarity. Intrinsic stationarity, in our case, means that the first two moments (i.e., the average and the variance) of the probability density function for the hydraulic conductivity field are invariant with respect to translation through space. The assumed probabilistic model of intrinsic stationarity is important because it justifies the universal application of the same variogram across the aquifer. Because of the relatively large number of hydraulic conductivity values measured at the site, the appropriateness of an intrinsic stationarity model could be evaluated by calculating a variogram for different regions across the test site. A comparison of the regional variograms shows that intrinsic stationarity is a highly questionable and, perhaps a poorly-suited, probabilistic model for the hydraulic conductivity field.

At the test site, the nonstationarities in the hydraulic conductivity field represent important geological facies. The geological investigation indicates that two former river channels and at least one point bar exist across the site. Each geological facies was formed by different climate, flow patterns, and sediments. Consequently, each geological facies has different patterns in the hydraulic conductivity fields. In an attempt to remove the nonstationary features from the hydraulic conductivity field, trend analyses were conducted by fitting polynomial expressions to the data by least-squares regression. For each trend, a set of residuals was created by subtracting the simulated value from the data at each measurement location.

An examination of statistical properties of residuals from different regions shows that, although absolute differences in the values decreased significantly with high order polynomials, the relative differences remained about the same. Results indicate polynomial expressions are not well-suited for detrending the CAFB hydraulic conductivity field because they fit the same trend through a whole area; whereas geological facies, which are responsible for trends in the field, are limited to specific regions. Because nonstationary features could not be removed from the hydraulic conductivity field, significant problems may occur with using geostatistical techniques for spatial interpolating of the hydraulic conductivity field in heterogeneous aquifers.

B. NUMERICAL MODELING OF HETEROGENEOUS AQUIFERS

Many of the groundwater codes for modeling flow and/or solute transport in groundwater systems are based on the Finite Difference Method (FDM), the Finite Element Method (FEM), or the Integrated Finite Difference Method (FDM). All of these numerical methods solve partial differential equations that describe groundwater processes over a given domain by the integration of fluxes over small, but finite, intervals of time across a single discrete surface segment of chosen subdomains or elements. Pinder (1988) briefly describes the advantages and disadvantages of each numerical method.

The numerical solution to the equations that describe groundwater flow are relatively straightforward (Huyakorn and Pinder, 1983). Problems that typically arise are related to computer storage and time limitations for large-scale three-dimensional simulations in heterogeneous aquifers. A practical and proven approach to modeling groundwater flow is with the finite difference or the integrated finite difference methods (McDonald and Harbaugh, 1984; Ababou, et al., 1988). For modeling saturated groundwater flow, the author recommends the United States Geological Survey three-dimensional finite difference MODFLOW model (McDonald and Harbaugh, 1984). The model is commonly used, well documented, and supported by an array of pre- and post-processors.

Numerical modeling of groundwater solute transport is considerably more difficult than numerical modeling of groundwater flow. The difficultly arises primarily because of the hyperbolic character (e.g., both an advective and a dispersive term) of the transport equation. Although both FDM and FEM codes can solve three-dimensional solute transport problems, they are not well-suited to model solute transport in heterogeneous aquifers dominated by advective flow. The solution to such problems can require unrealistic refinements in the spacing of both the grid network and the time steps in order to prevent numerical dispersion and/or oscillations. Guidelines for these refinements are ambiguous but are related to the conceptual approach (e.g., Eulerian, Langrangian) of the numerical method and the concepts associated with Courant and Peclet numbers. For a simple one-dimensional solute transport problem, the

Peclet and the Courant numbers are given in Equations (5) and (6), respectively.

$$\text{(Peclet Number)}\ \frac{\bar{V}\,x}{D} < 2 \qquad (5)$$

$$\text{(Courant Number)}\ \frac{\bar{V}\Delta t}{x} < 1 \qquad (6)$$

where: $\bar{V}$ = mean velocity (L/T)
x = dimension of grid (L)
D = dispersion coefficient (L^2/T)
Δt = time step (T)

The conceptual approach used by most numerical methods for solving the groundwater transport equation can be classified as Eulerian, Langrangian, or mixed Eulerian-Langrangian (Neuman, 1984). Zheng (1990) provides a good overview of the advantages and disadvantages of each. The following discussion of the approaches is based on Zheng (1990). In the Eulerian approach, the transport equation is solved with a fixed grid method. All of the terms of the equation are discretized together and the resulting algebraic equations are solved simultaneously in one step. The Eulerian approach offers the advantage and convenience of a fixed grid, and handles dispersion and reaction dominated problems effectively. For advective-dominated problems which exist in heterogeneous aquifers, however, Eulerian methods are suspectible to excessive numerical dispersion or oscillation, and limited by small grid spacing and time steps.

In the Langrangian approach, the transport equation is solved in either a deforming grid or deforming coordinate in a fixed grid. The Langrangian approach provides an accurate and efficient solution to advection-dominated problems with sharp concentration fronts. However, without a fixed grid or coordinate, a Langrangian method can lead to numerical instability and computational difficulties in nonuniform media with multiple sinks/sources and complex boundary conditions (Yeh, 1990). The mixed Eulerian-Langrangian approach attempts to combine the advantages of both the Eulerian and the Langrangian approaches by solving the advection term with a Langrangian method and the dispersion and reaction terms with a Eulerian method.

Reviews of the Eulerian-Langrangian approaches are presented by Cady and Neuman (1987), Hauguel (1985), and Baptista, Adams, and Stolzenbach (1985). According to how the advective transport is taken into account, the Eulerian-Langrangian approaches can be grouped into three classes: one class makes use of particle tracking and relates the concentration at a grid node to the solute mass associated with each particle and the particle density around the node; while the second class treats concentration directly as a primary variable throughout the calculations without resorting to the use of any particles; and the third class consists of models in which the first and second approaches are used together in an adaptive manner depending on the steepness of the concentration gradient (Molz, et al., 1990). The first class has been called the Method of Characteristics (MOC) (Konikow and Bredehoeft, 1978). The second class has been called the "single-step reverse particle tracking" method by Neuman (1984) and the "Modified Method of Characteristics (MMOC)" by Ewing, Russell, and Wheeler (1984). The third class can be called a hybrid MOC/MMOC technique and has been discussed by Neuman (1984), Neuman and Cady (1987) and Farmer (1987).

In previous attempts to model groundwater flow in heterogeneous aquifers, the author has relied on discrete particle-tracking (DPT) methods in order to avoid problems with numerical dispersion and oscillations. Recently, several DPT models that interface with the output from MODFLOW have become commercially available. Two such codes are PATH3D (Zheng, 1990) and MODPATH (Pollock, 1990). Both of these codes are well documented and easily used. An attractive graphic enhancement to MODPATH is GeoTrack (GeoTrans, 1989). Based on the author's experience with the DPT methods, both of these codes are well-suited for simulating advective transport in heterogeneous aquifers.

In several situations, the DPT codes will not be adequate. These situations occur when large numbers of particles are required to create well-defined concentration distribution or when some type of chemical reactions is needed. In these situations, and perhaps in general, the model MT3D may be the type code of choice. MT3D uses a modular structure similar to that implemented in MODFLOW and has the capability to implement any of the three classes of mixed Eulerian-Langrangian

approaches. The author has yet to use MT3D, but the availability of both the MOC, the MMOC, and the hybrid MOC/MMOC options should make MT3D suitable for a wide range of field problems.

C. SPATIAL INTERPOLATION OF HYDRAULIC CONDUCTIVITY MEASUREMENTS

The application of groundwater solute transport models include three major preliminary tasks. The first task is measuring the aquifer hydraulic properties. The second task is developing a conceptual model of the aquifer and creating a continuous three-dimensional field of the aquifer properties from the field data. The third task is establishing the type of boundary and initial conditions for the problem and predicting solute transport with a numerical computer model. Given the borehole flowmeter technique to measure horizontal hydraulic conductivities and the coupled MODFLOW - MT3D codes to simulate solute transport, the major obstacle to modeling solute transport in heterogeneous environments is developing a representative continuous three-dimensional hydraulic conductivity field from point measurements.

Over the last decade, attention has focused on using stochastic techniques to develop hydraulic conductivity fields for five major reasons: (1) incomplete information about dimensions and internal (geometric) architecture; (2) complex spatial deposition of reservoir building blocks or facies; (3) difficult-to-capture aquifer-property variability and variability structure; (4) unknown relationships between property value and the volume of aquifer used for averaging (the scale problem); and, (5) convenience and speed (Haldorsen and Damsieth, 1990). These stochastic models can be divided into discrete models and continuous models.

Discrete models describe geological features of a discrete nature such as the location and dimensions of sand bodies in a fluvial depositional environment (Bridge, 1979; Haldorsen, et al., 1988; and King, 1989); distribution, orientations, and lengths of fractures and faults (Long and Witherspoon, 1985); and facies modeling (Matheron, et al., 1987; and Farmer, 1989). If discrete models are used to generate aquifer architectures for solute transport modeling, then hydraulic

conductivity values are assigned to each geological unit. Traditionally, this step involves assigning a constant hydraulic conductivity value to each geological unit.

Continuous models describe properties of the aquifer that vary continuously across the aquifer. The continuous models determine a distinct value at each point or area by using algorithms that contain information related to: (1) the mean level, or possible lateral or vertical trends, for the variable; (2) the variability about the mean; (3) how strongly neighboring points tend to have similar values; and (4) the covariation of the variable. Traditionally, these models are based on geostatistical techniques and assume some type of stationarity.

In general, discrete models are not well-suited for reproducing small-scale heterogeneities within individual facies and continuous models are not well-suited for reproducing meso-scale heterogeneities among different facies. As a result, neither model is well-suited for creating hydraulic conductivity fields for aquifers that include several geological facies that contain important micro-scale heterogeneities. Haldorsen and Damsieth (1990) acknowledge the problems with both the discrete and continuous models and propose a hybrid model. The hybrid model is a two-stage model with the best from the discrete and the continuous models. Stage 1 includes a discrete model to describe the large-scale heterogeneities (i.e., geological facies) in the aquifer. Stage 2 includes a continuous model to describe the small-scale variation within each geological feature.

For the hydraulic conductivity field at CAFB, there is no spatial interpolation method that can create a continuous three-dimensional hydraulic conductivity field from field data representative of both the micro- and the meso-scale aquifer heterogeneities. Until such interpolation capabilities are available, geologists should conduct numerous field tests aimed at providing data with which to validate the structure of the hydraulic conductivity field used in the numerical groundwater model.

D. RECOMMENDED SITE CHARACTERIZATION METHODOLOGY

Based on the information in Volumes I and II, a methodology has been developed for measuring the aquifer hydraulic properties in the detail required to evaluate alternative well designs for bioreclamation of a contaminated area. The site characterization methodology includes designing a well network, preparing a preliminary assessment of the site's heterogeneity, measuring vertical variation of horizontal hydraulic conductivity values, and collecting calibration data for groundwater flow models.

An outline of the site characterization methodology and a description of the major tasks associated with the site characterization methodology are given in the flowchart and Tables 23 and 24, respectively. Before these tasks are discussed, one should note that near the beginning and near the end of the flowchart (Figure 66), assessments are made regarding the feasibility of in-situ bioreclamation. Based on geohydrological considerations, the chance for successful bioreclamation remediation is dependent on the heterogeneity of the aquifer. If the aquifer is very heterogeneous, two problems may arise.

The first problem related to heterogeneity occurs when the vertical profiles of horizontal hydraulic conductivity at the well locations are very different. In these instances, no validated procedures exist for the proper interpolation among the profiles. As a result, the representativeness of the interpolated three-dimensional hydraulic conductivity field is unknown. This uncertainty becomes interbedded into the groundwater modeling results and leads to uncertainty in the evaluation of the hydraulic design of the bioreclamation system. The second problem related to heterogeneity occurs when the variations among the hydraulic conductivity of the aquifer materials are very large. There, it may be too costly to install a system of wells and/or infiltration galleries to deliver an adequate flow rate to less permeable target zones of the aquifer material.

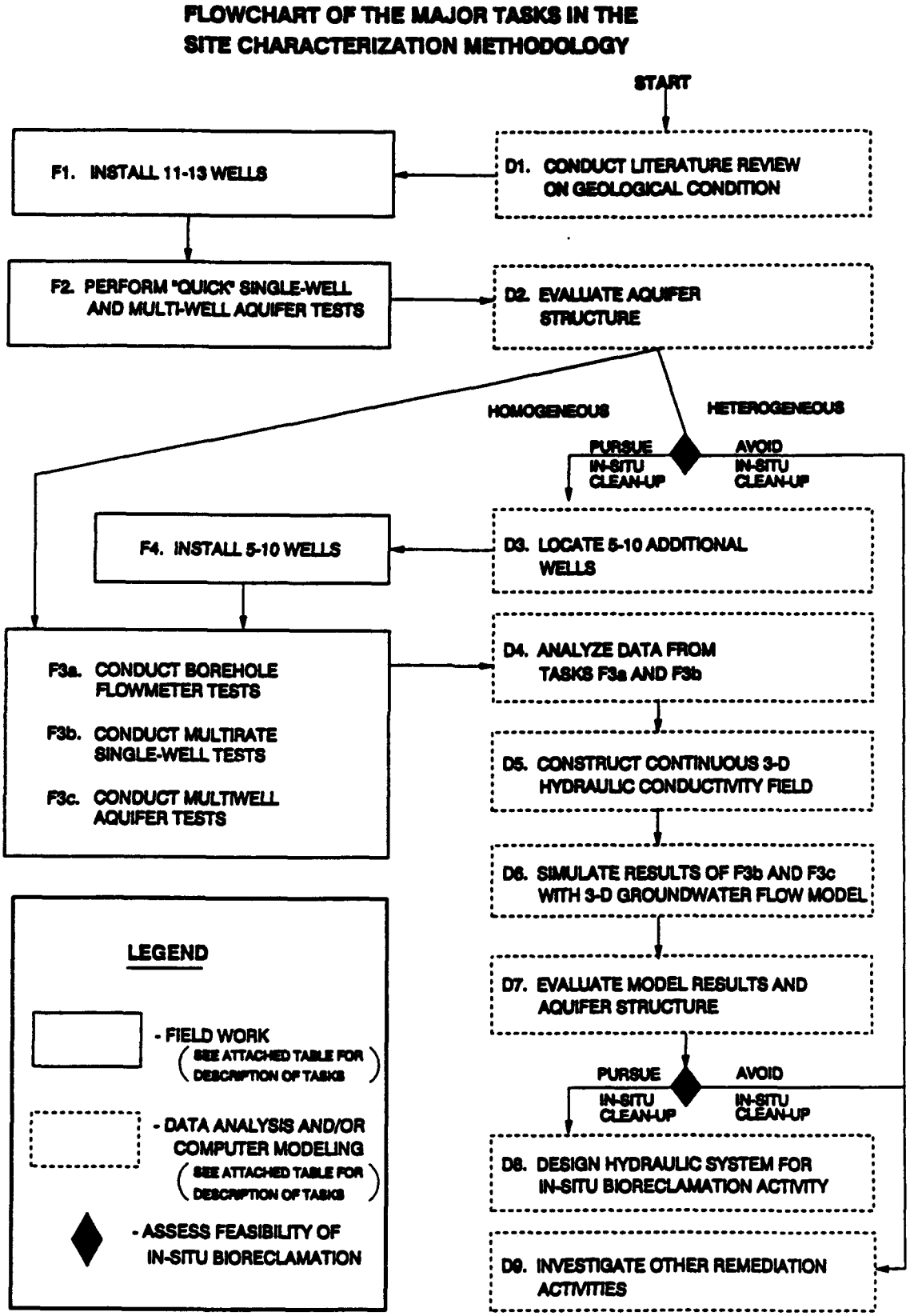

Figure 66. Flowchart of the Major Tasks in the Site Characterization Methodology.

TABLE 23. DESCRIPTION OF THE TASKS ASSOCIATED WITH FIELDWORK

Task		Description
F1.	Install 11-13 wells	Use a Hollow-Stem Auger to install 11 to 13 fully screened wells. Nine of these wells should be placed on a regular grid; the remaining wells should be placed 2 to 4 meters from a well near the interior of the well network. (Volume I, Section II)
F2.	Perform "Quick" Single-Well and Multiwell Aquifer Tests	Conduct 10- to 40-minute moderate to low flow single-well tests at each well to determine the transmissivity pattern. Slug-tests should not be conducted because they are strongly affected by the disturbed zone around the wells. During the single-well tests monitor the drawdown in any close wells to determine values for storage coefficients and hydraulic conductivity. Note whether large vertical variations of hydraulic conductivity exist. (Volume I, Sections V, VI, VII, and VIII)
F3a.	Conduct Borehole Flowmeter Tests	While pumping/injecting at a low rate, perform borehole flowmeter tests to determine transmissivity and three-dimensional hydraulic conductivity patterns. Conduct a separate borehole flowmeter test at high injection rates if large portions of the unsaturated zone need to be characterized. Each test should last 40 to 90 minutes. (Volume II, Section III)
F3b.	Conduct Multirate Single-Well Tests	Conduct the necessary single-well tests to determine how sensitive the calculated transmissivity value is to the pumping rate. Results from the borehole flowmeter tests may be acceptable for inclusion in the data base. If the aquifer is rather homogeneous only several of these tests are needed. (Volume I, Sections VII and VIII)
F3c.	Conduct Multiwell Aquifer Tests	During Tasks F3a and F3b, monitor the drawdown in nearby wells. (Volume I, Sections V and VI)

TABLE 24. DESCRIPTION OF TASKS ASSOCIATED WITH DATA ANALYSIS AND/OR COMPUTER MODELING

Task		Description
D1.	Conduct Literature Review on Geological Conditions	Obtain information on the type of depositional environments responsible for the aquifer material. Extract any information about the structure of the hydraulic conductivity field. (Volume II, Section IV)
D2.	Evaluate Aquifer Structure	Determine whether bioreclamation appears to be a viable remediation approach, given the known trends in the hydraulic conductivity field. (Volume I, Sections VI and VIII, and Volume II, Section III)
D3.	Install 5-10 Additional Wells	Install wells in areas where the greatest differences occur in the transmissivity field and/or where improvements can be made in the variogram calculations. Use program similar to WELPLAN. (Volume I, Section II)
D4.	Analyze Data from Tasks F3a and F3b	Determine vertical variations of hydraulic conductivity at each well site. Determine whether calculated transmissivities are sensitive to pumping rate. (Volume I, Sections V, VI, VII, and VIII, and Volume II, Section III)
D5.	Construct Continuous 3-D Hydraulic Conductivity Field	From three-dimensional hydraulic conductivity data, construct a continuous three-dimensional grid. The method for doing this is beyond scope of this report. (Volume II, Sections VI and VII, discusses some options)
D6.	Simulate Results of F3b and F3c with Three-Dimensional Groundwater Flow Model	If the aquifer is heterogeneous, transmissivities and storage coefficients will be sensitive to the pumping rates, test duration, and orientation/distance between the pumped and the observation well. The appropriateness of a groundwater flow model's accuracy is to reproduce the drawdowns observed during Tasks F3a and F3b (Volume I, Section VI, and Volume II, Section VIII)
D7.	Evaluate Model Results and Aquifer Structure	Based on the comparison between the predicted and the observed well responses determine whether to pursue in-situ bioreclamation.

TABLE 24. DESCRIPTION OF TASKS ASSOCIATED WITH DATA ANALYSIS AND/OR COMPUTER MODELING (CONCLUDED)

Task	Description
D8. Design Hydraulic System for In-Situ Bioreclamation	Use groundwater model to evaluate alternative designs for bioreclamation systems. (Volume II, Section VIII discusses some approaches)

(The reverse of this page is blank.)

SECTION IX

REFERENCES

Ababou, R., L.W. Gelhar, and D. McLaughlin, 1988, "Three-Dimensional Flow in Random Porous Media," Report No. 318, Ralph M. Parsons Laboratory, Department of Civil Engineering, Massachusetts Institute of Technology, Cambridge, Massachusetts.

Baptista, A.M., E.E. Adams, and K.D. Stolzenbach, 1985, "Comparison of Several Eulerian-Langrangian Models to Solve the Advection Diffusion Equation," Proceedings of the International Symposium on Refined Flow Modelling and Turbulence Measurements, Iowa Institute of Hydraulic Research, The University of Iowa, Iowa City, Iowa, September 16-18, Vol 1.

Betson, R.P., J.M. Boggs, S.C. Young, and L.W. Gelhar, 1985, Macrodispersion Experiment (MADE): Design of a Field Experiment to Investigate Transport Processes in a Saturated Groundwater Zone, EPRI Interim Report, EA-4082, Electric Power Research Institute, Palo Alto, California.

Boggs, J.M., S.C. Young, D.J. Benton, and Y.C. Chung, 1990, Hydrogeologic Characterization of the MADE Site, EPRI Interim Report, EN-6915, Palo Alto, California.

Bridge, J.S., and M.R. Leeder, 1979, "A Simulation Model of Alluvial Stratigraphy," Sedimentology, Vol. 26, pp. 617-644.

Cady, R., and S.P. Neuman, 1987, "Advection-Dispersion With Adaptive Eulerian-Langrangian Finite Elements," in: Advances in Transport Phenomena in Porous Media, edited by J. Bear and M.Y. Coropcioglu, NATO ASI Series E: Applied Sciences, No. 128, Dordrecht, The Netherlands: Martinus Nijhoff Publishers.

Collinson, J.D., and D.B. Thompson, 1989, Sedimentary Structures, Unwin Hyman, p. 16.

Cooper, H.H., and C.E. Jacob., 1946, "A Generalized Graphical Method for Evaluating Formation Constants and Summarizing Well-Field History," Transactions of the American Geophysical Union, 217, pp. 626-534.

Ewing, R.E., T.F. Russell, and M.F. Wheeler, 1984, "Convergence Analysis of an Approximation of Miscible Displacement in Porous Media by Mixed Finite Elements and a Modified Method of Characteristics," Computer Methods in Applied Mechanics and Engineering, 47, 73-94.

Farmer, C.J., 1989, "The Mathematical Generation of Reservoir Geology," Paper presented at the European Conference on the Mathematics of Oil Recovery, Cambridge, Massachusetts, July.

Farmer, C.L., 1987, "Moving Particle Techniques," in: Advances in Transport Phenomena in Porous Media, edited by J. Bear and M.Y. Coropcioglu, NATO ASI Series E: Applied Sciences, No. 128, Dordrecht, The Netherlands: Martinus Nijhoff Publishers.

Feller, W., 1948, "On the Kolmogorov-Smirnov Limit Theorems for Empirical Distributions," Annuals of Math. Stat., Vol. 19, pp. 177-189.

Gelhar, L.W., and C.L. Axness, 1983, "Three-Dimensional Analysis of Macrodispersion in Aquifer," Water Resources Research, Vol. 19, No. 1, pp. 161-180.

GeoTrans, 1989, GeoTrack: A Computer Program to Display Particle Pathlines Generated From Groundwater Flow Simulations, Prepared for the Westinghouse Savannah River Company, Herndon, Virginia.

Gutjahr, A.L., L.W. Gelhar, A.A. Bakr, and J.R. McMillan, 1978, "Stochastic Analysis of Spatial Variability in Subsurface Flow, Part 2: Evaluation and Application," Water Resources Research, Vol. 14, No. 5, pp. 953-960.

Haldorsen, H.H., P.J. Brand, and C.J. MacDonald, 1988, "Review of the Stochastic Nature of Reservoirs," Mathematics in Oil Production, S. Edwards and P. King (eds), Oxford Science Publications, Clarendon Press, Oxford, pp. 109-209.

Haldorsen, H.H., and E. Damsieth, 1990, "Stochastic Modeling," Society of Petroleum Engineers, April, pp. 404-412.

Harper, W., 1990, "Program GCONT," TVA Engineering Laboratory Unpublished Report, Tennessee Valley Authority, Norris, Tennessee.

Hauguel, A., 1985, "Numerical Modelling of Complex Industrial and Environmental Flows," Proceedings of the International Symposium of Refined Flow Modelling and Turbulence Measurements, Iowa Institute of Hydraulic Research, The University of Iowa, Iowa City, Iowa, September 16-18, Vol 1.

Hess, K.M., 1989, "Use of the Borehole Flowmeter to Determine Spatial Heterogeneity of Hydraulic Conductivity and Macrodispersion in a Sand and Gravel Aquifer Cape Cod, Massachusetts," Conference Proceedings for New Field Techniques for Quantifying the Physical and Chemical Properties of Heterogeneous Aquifers, Water Well Journal Publishing Company, Dallas, Texas, pp. 497-508.

Hufschmied, P., 1983, "Die Ermittlung der Durchlassigkeit von Lockergen-steins-Grundwasserleitern, eine vergleichende Untersuchung verchiedener Felmethoden," Doctoral Dissertation No. 7397, ETH Zurich, Switzerland.

Huyakorn, P.S., and G.F. Pinder, 1983, Computational Methods in Subsurface Flow, Academic Press, New York.

Golden Software, Inc., SURFER, Version 4, Golden, Colorado.

Javandel, I., and P.A. Witherspoon, 1969, "A Method of Analyzing Transient Flow in Multilayered Aquifers," Water Resources Research, Vol. 5, pp. 856-869.

Journal, A.G., and C. T. Huijbregts, 1978, Mining Geostatistics, London, Academic Press.

Journal, A.G., 1986, "Geostatistic Models and Tools for the Earth Sciences," Mathematical Geology, Vol. 18, No. 1, pp. 119-140.

King, P.R., 1989, "The Connectivity and Conductivity of Overlapping Sandbodies," Paper presented in Intl. Conference on North Sea Oil and Gas Reservoirs, Trondheim, May 8-11.

Konikow, L.F., and J.D. Bredehoeft, 1978, "Computer Model of Two-Dimensional Solute Transport and Dispersion in Groundwater Techniques," Water Resources Investigations of the United States Geological Survey, NTIS, Washington D.C., Book 7, Chapter C2.

Leeder, M.R., 1973, "Fluviatile Fining-Upward Cycles and the Magnitude of Palechannels," Geol. Mag., Vol. 110, No. 3, pp. 265-76.

Levey, R.A., 1978, "Bed-Form Distribution and Internal Stratification of Coarse Grained Pointbars, Upper Congaree River, S.C.," in: Fluvial Sedimentology (ed. A.D. Miall), Canadian Society of Petroleum Geologists, pp. 105-127.

Liffiefors, H.W., 1967, "On the Kolmogorov-Smirnov Test for Normality With the Mean and Variance Unknown," American Statistical Association Journal, pp. 399-402.

Long, J.C.S., and P.A. Witherspoon, 1985, "The Relationship of the Degree of Interconnection to Permeability in Fracture Networks," J. Geophy. Res., Vol. 90, No. B4, pp. 3087-98.

Matheron, G., 1967, Elements pour une Theorie des Milieux Poreux, Masson Ed., Paris.

Matthews, R.K., 1974, Dynamic Stratigraphy, Chapter 10, Prentice Hall, New Hall, New Jersey.

McDonald, M.G., and A.W. Harbaugh, 1984, A Modular Three-Dimensional Finite Difference Ground-Water Flow Model, United States Geological Survey, Reston, Virginia.

McGowen, J.H. and L. E. Garner, 1971, "Physiographic Features and Stratification Types of Coarse Grained Pointbars: Modern and Ancient Examples," Sedimentology, v. 14, pp. 77-111.

Molz, F.J., R.H. Morin, A.E. Hess, J.G. Melville, and O. Guven, 1989, "The Impeller Meter for Measuring Aquifer Permeability Variations: Evaluation and Comparison with Other Tests," Water Resources Research, Vol. 25, No. 7, pp. 1677-1683.

Molz, F.J., O. Guven, J.G. Melville, I. Javandel, A.E. Hess, and F. L. Paillet, "A New Approach and Methodologies for Characterizing the Hydrogeologic Properties of Aquifers," EPA/600/2-90/002, Robert S. Kerr Laboratory, U.S. Environmental Protection Agency, Ada, Oklahoma.

Morin, R.H., A.E. Hess, and F.L. Paillet, 1988, "Determining the Distribution of Hydraulic Conductivity in Fractured Limestone Aquifers by

Simultaneous Injection and Geophysical Logging," Groundwater, Vol. 26, pp. 587-595.

Muto, G.R., and J. Gunn, 1986, A Study of Late Quaternary Environments and Early Man, Phase I Final Report, Project Narrative and Appendices A-D, U.S. Army Corps of Engineers, Mobile and Nashville Districts, Appendix C, Geosciences Documentation.

Neuman, S.P., 1984, "Adaptive Eulerian-Langrangian Finite Element Method for Advection-Dispersion," International Journal for Numerical Methods in Engineering, 20, 321-337.

Olea, R.A., 1984, Systematic Sampling of Spatial Functions, Kansas Geological Survey: Series on Spatial Analysis, No. 7.

Philip, G.M., and D. F. Watson, 1986, "Matheronian Geostatistics - Quo Vadis?," Mathematical Geology, Vol. 18, No. 1, pp. 93-117.

Pinder, G.F., 1988, "An Overview of Groundwater Modeling," in: Groundwater Flow and Quality Modeling, edited by E. Custodio, A. Gurgui, J.P. Lobo Ferreira, NATO ASI Series C: Mathematical and Physical Sciences, Dordrecht, Holland: D. Reidel Publishing Co., Vol. 224, pp. 119-134.

Pollock, D.W., 1990, A Graphical Kernel System (GKS) Version of Computer Program MODPATH-PLOT for Displaying Path Lines Generated From the U.S. Geological Survey Three-Dimensional Ground-Water Flow Model, USGS OFR 89-622, 49 pp.

Reading, H.G., 1986, Sedimentary Facies and Environments, Blackwell, pp. 36-37.

Rehfeldt, K.R., P. Hufschmeid, L.W. Gelhar, and M.E. Schaefer, 1989a, Measuring Hydraulic Conductivity with the Borehole Flowmeter, EPRI Topical Report EN-6511, Palo Alto, California.

Rehfeldt, K.R., L.W. Gelhar, J.B. Southard, and A. Dasinger, 1989b, Estimates of Macrodispersivity Based on Analyses of Hydraulic Conductivity Variability at the MADE Site, EPRI Interim Report EN-6405, Palo Alto, California.

Reineck, H.E., and I.B. Sing, 1986, Depositional Sedimentary Environments, Springer-Verlag, pp. 274-284.

Russo, D., and W. A. Jury, 1987, "A Theoretical Study of the Estimation of the Correlation Scale in Spatially Variable Fields; 2. Nonstationary Fields," Water Resources Research, Vol. 23, No. 7, pp. 1269-1279.

Srivastava, R.M., 1986, "Philip and Watson - Quo Vadunt?," Mathematical Geology, Vol. 18, No. 1, pp. 141-146.

Smirnov, N., 1948, "Table for Estimating the Goodness of Fit to Empirical Distributions," Annuals of Math. Stat., Vol. 19, pp. 279-281.

Wagner, B.J., and S.M. Gorelick, 1989, "Reliable Aquifer Remediation in the Presence of Spatially Variable Hydraulic Conductivity: From Data to Design," Water Resources Research, Vol. 25, pp. 1111-1115.

Warrick, A.W., and D.E. Myers, 1987, "Optimization of Sampling Locations for Variogram Calculations," Water Resources Research, Vol. 23, No. 3.

Yeh, G.T., 1990, "A Eulerian-Langrangian Method With Zoomable Hidden Fine-Mesh Approach to Solving Advection-Dispersion Equations," Water Resources Research, Vol. 26, No. 6, pp. 1133-1144.

Young, S.C., and J.M. Boggs, 1988, "Development of a Driven Multilevel Groundwater Sampling Well and Instrumentation for Measuring Vertical Hydraulic Gradients Over Short Distances," DOE Model Conference, Oak Ridge, Tennessee.

Young, S.C., and W.R. Waldrop, 1989, "An Electromagnetic Borehole Flowmeter for Measuring Hydraulic Conductivity Variability," Conference Proceedings for New Field Techniques for Quantifying the Physical and Chemical Properties of Heterogeneous Aquifers, Water Well Journal Publishing Company, Dallas, Texas, pp. 497-508.

Young, S.C., and J.M. Boggs, 1989, "Observed Migration of a Tracer Plume at the MADE Site," EPA and EPRI Environmental and Research Conference: Groundwater Quality and Waste Disposal, Washington D.C., May.

Zheng, C., 1990, PATH3D - A Ground-Water Path and Travel-Time Simulator, S.S. Papadolpulos & Associates, Inc., Rockville, Maryland.

Zheng, C., 1990, "MT3D A Modular Three-Dimensional Transport Model for Simulation of Advection, Dispersion and Chemical Reactions of Contaminants in Groundwater Systems," prepared for the U.S. Environmental Protection Agency, Robert S. Kerr Laboratory, Ada, Oklahoma.

(The reverse of this page is blank.)

APPENDIX A

IMPELLER AND ELECTROMAGNETIC BOREHOLE FLOWMETER COMPARISON

A. DESCRIPTION OF FLOWMETERS

Impeller meters have been used for several decades in the petroleum industry, but only a few such instruments have suitable specifications for groundwater applications. Three of the most suitable impeller meters were used in the studies of Molz, et al. (1989), and Rehfeldt, et al. (1989). Of these three meters the most accurate is an impeller flowmeter manufactured by Haferland Geophysical, Hanover, West Germany. A schematic of the Haferland impeller meter is shown in Figure A1.

The impeller flowmeter contains a lightweight impeller that spins in response to the vertical movement of water in a well. The impeller is aligned by two adjustable needles made of hardened steel. On the top of the impeller are 10 equally spaced pins that fit into a circular groove in the shaft of the flowmeter. Situated on the inside and the outside of the groove are two pairs of optical sensors that record the movement of the pins attached to the impeller. The electronics attached to the optical sensors generate a square wave excitation at a frequency directly proportional to the rotational speed of the pins.

The electromagnetic (EM) flowmeter, shown in Figure A2, was developed at the TVA Engineering Laboratory in Norris, Tennessee. The flowmeter consists of an electromagnet and two electrodes (placed 180 degrees apart) that are cast in a durable epoxy. The epoxy is molded to a cylindrical shape that minimizes the turbulence associated with channeling the water past the electrodes and electromagnets. The flowmeter has no moveable parts. The flowmeter operates according to Faraday's Law of Induction, which states that the voltage induced by a conductor moving at right angles through a magnetic field is directly proportional to the velocity of the conductor through that field. The flowing water is the conductor, the electromagnet generates the magnetic field, and the electrodes measure the induced voltage. The electronics attached to the electrodes will transmit a voltage that is directly proportional to the velocity of the water.

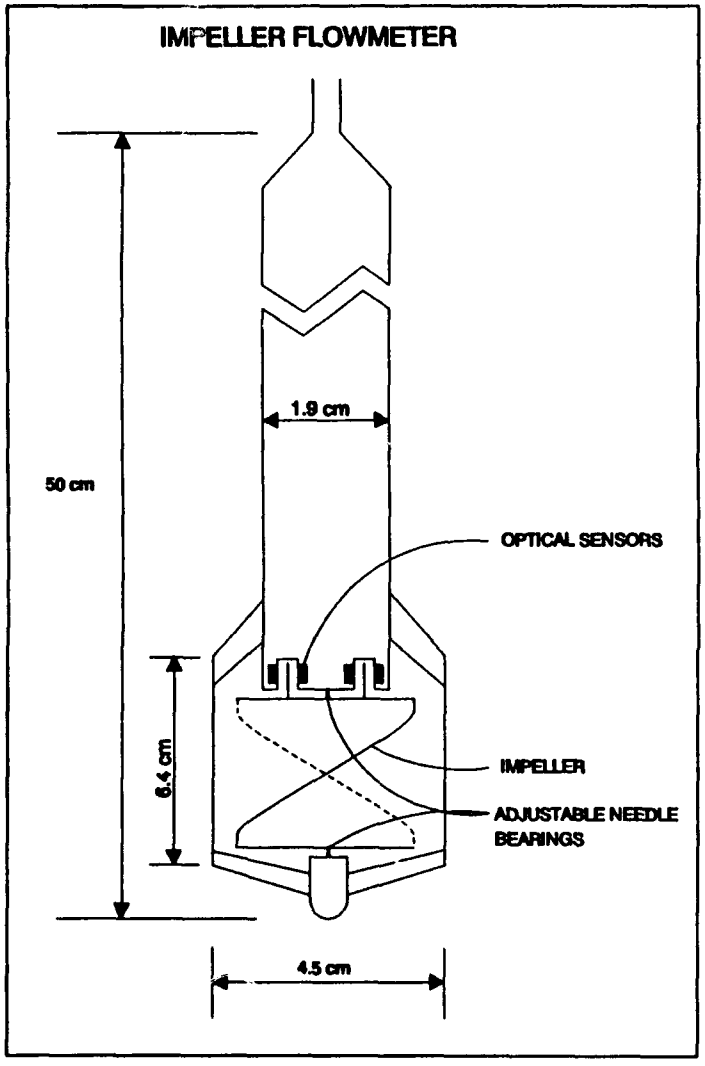

Figure A1. Schematic of Haferland Impeller Borehole Flowmeter.

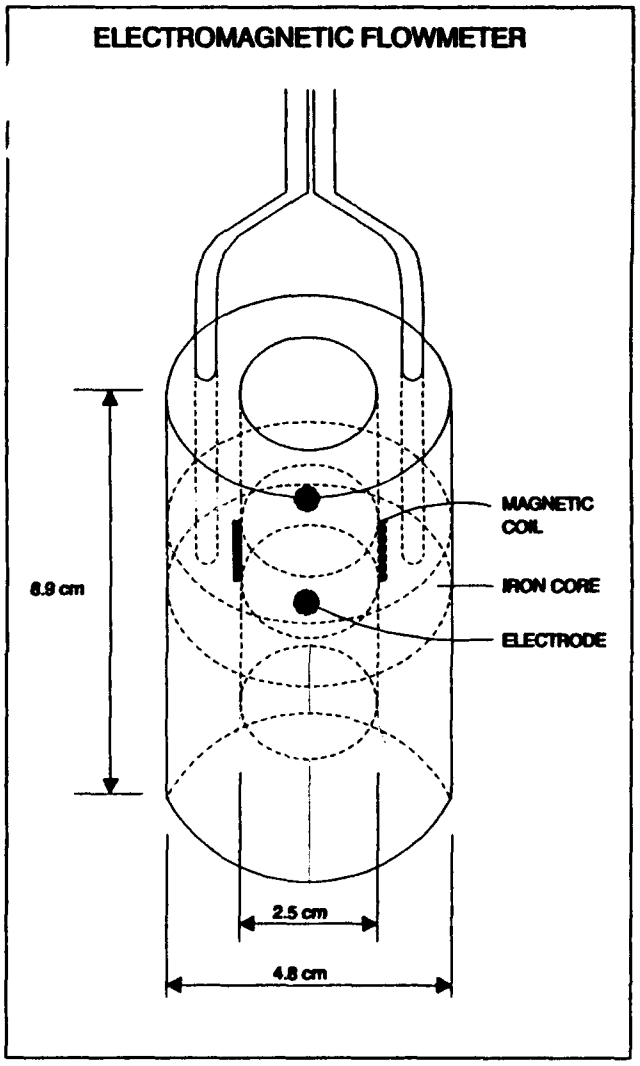

Figure A2. Schematic of TVA Electromagnetic Borehole Flowmeter.

B. CALIBRATION RESULTS

1. Setup

Figure A3 is a schematic of a typical calibration setup. The water enters and leaves the pipe through one of the two attached hoses. The flow direction is controlled by attaching the water supply to either the upper or lower hose. The flow rate through the pipe can be adjusted and is carefully measured in the hose with an in-line meter and at the discharge point with a stopwatch and a calibrated bucket.

2. Impeller Flowmeter Calibration

TVA received the impeller meter from the Massachusetts Institute of Technology in June 1988. During the first week of testing, it became clear that the flowmeter's performance is dependent on the amount of friction between the impeller and the needle bearings. In turn, the amount of friction between the impeller and the needle bearings depends on the vertical adjustment of the bearing needles, the amount of rust on the bearing needles, and the sharpness of the bearing needles.

In July 1988, TVA used the impeller flowmeter for testing five wells at CAFB. The borehole flowmeter tests included both injecting water and pumping water from the wells. The pumping rates ranged from 7.5 to 26 L/min. The injection rates ranged from 23 to 26 L/min. For the July 1988 field test, a pre- and post-calibration was made for upward flow. Figure A4 shows a difference of about 1.0 L/min between the two calibrations.

During August and September 1988, the impeller meter was frequently calibrated during three flow tests. The first test consisted of 10 days of constant (day and night) 15 L/min upward flow. The second test consisted of 7 days of intermittent (days only) 15 L/min upward flow. For the second test, the flowmeter was dried after each day and set aside for the next day. The third test consisted of 5 days of 15 L/min downward flow. During these tests the flowmeter was calibrated a total of 19 times for upward flow. The calibrations were conducted on

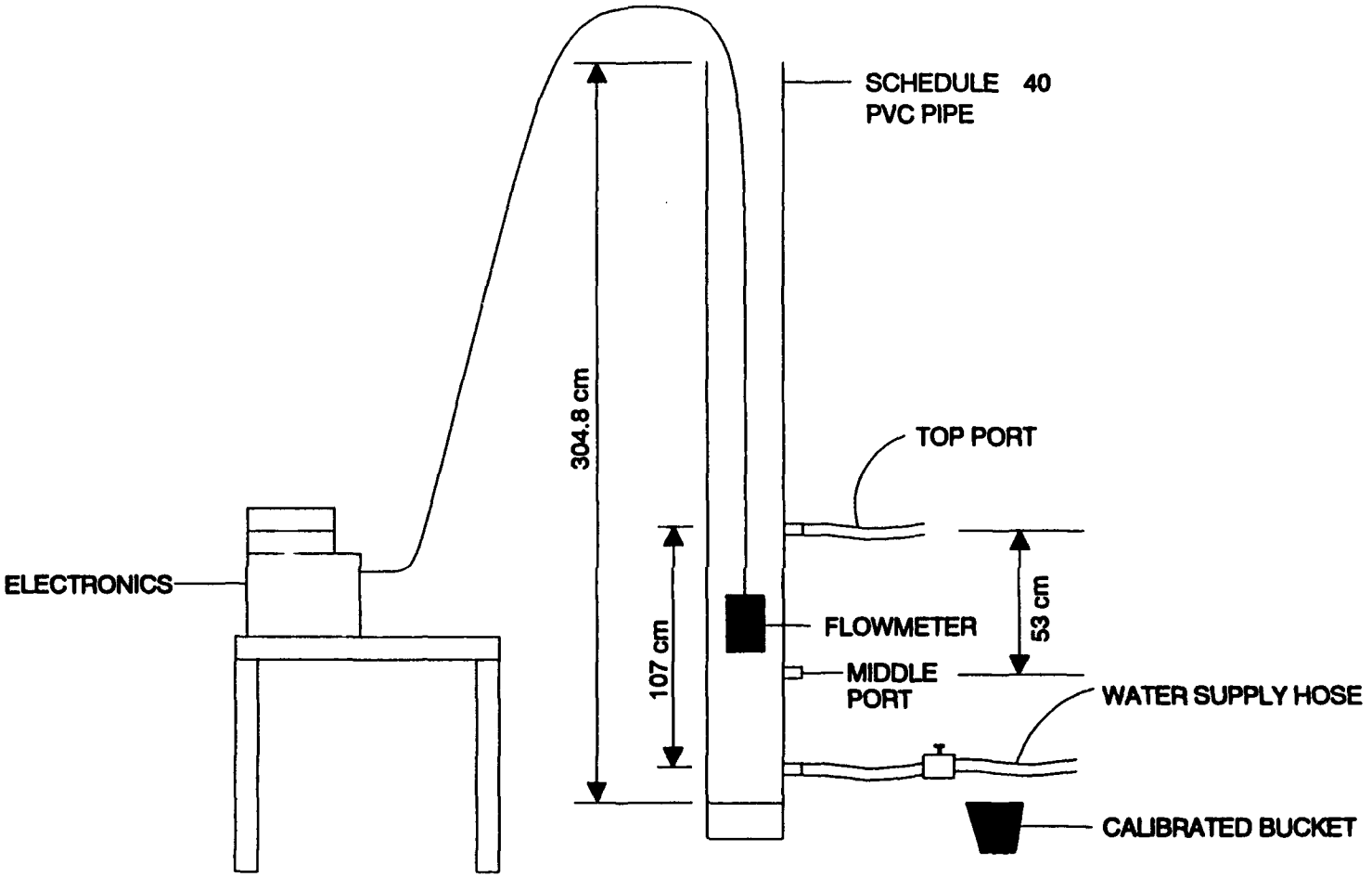

Figure A3. Schematic of Flow Calibration System.

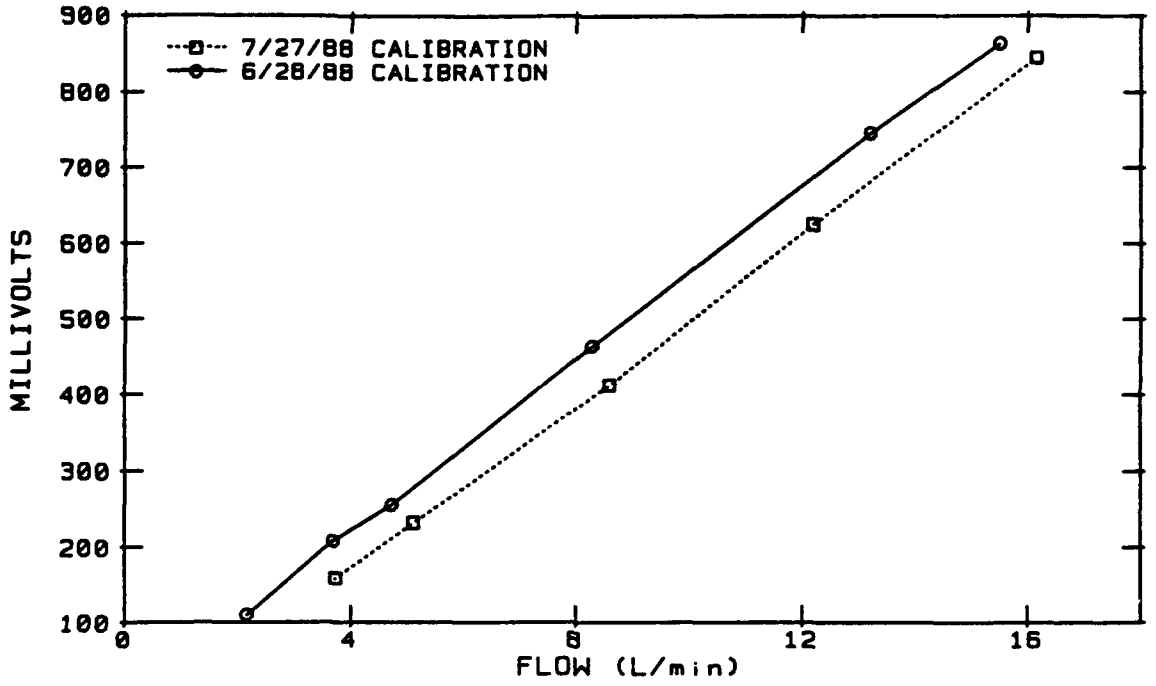

Figure A4. Calibrations for the Impeller Flowmeter Before and After a Field Test.

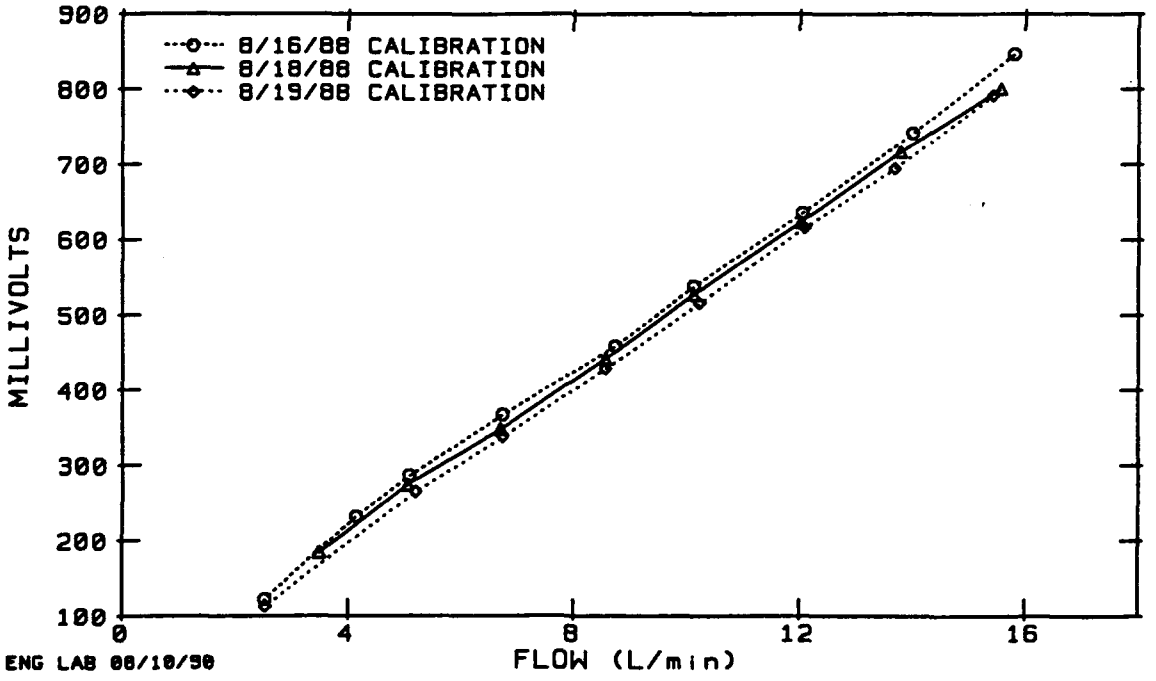

Figure A5. Calibrations for the Impeller Flowmeter During a 15 (L/min) Laboratory Test.

different days and included about nine points. After each flow test, the flowmeter's needle bearings were reconditioned and resharpened.

Figure A5 shows three of the calibration curves for the first test. The results indicate that upward flow can cause enough wear on the bearing needles to change the calibration curves, but the change is gradual. Over approximately 4 days of 15 L/min upward flow, the calibration curves shifted about 0.4 L/min. The results of the second test indicate that alternating the flowmeter in and out of the water does not affect the rate at which the calibration curve shifts. The results of the third flow test showed that 18 hours of 15 L/min downward flow caused enough wear on the bearings to shift the calibration for the upward flow by about 0.4 L/min.

The analysis of the impeller borehole flowmeter calibration data indicates the following: (1) the calibration curve for the meter is sensitive to the condition of the bearing needles; (2) frequent maintenance and calibrations are required to insure proper interpretation of field data; and (3) although the meter can respond to flow rates near 1 L/min, the meter does not accurately (10 percent precision) measure flows below 0.5 L/min.

3. Electromagnetic Flowmeter Calibration

The prototype EM meter was built in November 1988. In December the meter was used to log 20 wells at the CAFB site. Between November 1988 and March 1989, the flowmeter response was calibrated several times. Calibrations showed that the EM flowmeter consistently provided a linear response for discharges down to 0.10 L/min. At 0.10 L/min, a 10 percent deviation typically existed between the flowmeter response and a linear response. Figure A6 provides the pre- and post-calibration of the EM meter for the April 1989 tests in 5.2-cm well pipe. The 5 percent difference in the calibration curves resulted from a change that occurred in the flowmeter's hand-wired circuitry during the fieldwork. Since April 1989, TVA has developed printed circuit boards for the EM flowmeter to greatly reduce the possibility of the flowmeter's calibration curves changing during fieldwork.

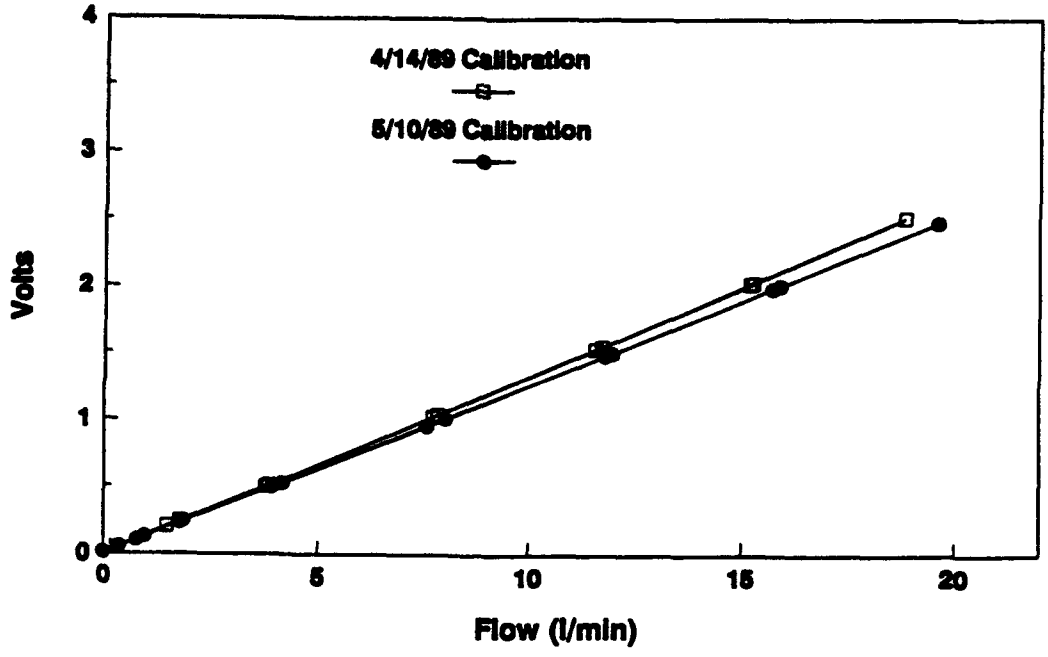

Figure A6. Calibrations for the Electromagnetic Flowmeter Before and After a Field Test.

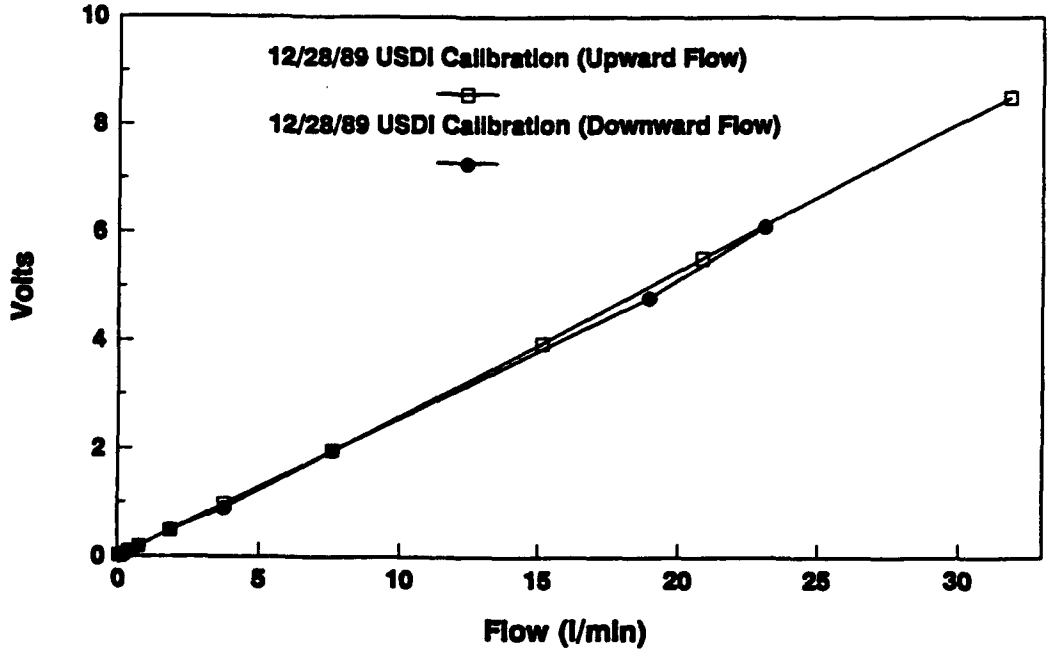

Figure A7. Calibrations for the Electromagnetic Flowmeter During a United States Department of Interior Laboratory Test.

The results of TVAs calibrations have been checked by Dr. Alfred E. Hess, an instrumentation engineer with the United States Department of the Interior (USDI). Figure A7 shows the results of the independent evaluation of the EM flowmeter. The USDI calibrations were conducted with a 7.6-cm PVC pipe and showed that at a flow rate of 0.04 L/min, the accuracy of the EM flowmeter was about 20 percent. The USDI calibration results show that for flow rates of about 0.1 L/min the flowmeter was typically accurate to within 1 to 5 percent.

C. EFFECTS OF TURBULENCE ON THE ACCURACY OF THE FLOWMETERS

The turbulence and nonuniform flow caused by the transition of horizontal flow to vertical flow in the well may affect the response of a borehole flowmeter. A simple but very extreme test of this effect was conducted with the calibration set-up shown in Figure A3. A constant flow was injected at the middle hose and discharged at the top hose. The relatively short distance of 53 cm between the two ports was selected to promote nonuniform flow in the pipe. Although this test may not represent how the inflow radially enters a borehole, it will show if a flowmeter's response depends on the nature of the flow patterns and whether different flowmeters have different sensitivities to uniform and nonuniform flow fields.

Before the test, calibrations were done on both the EM flowmeter and the EPRI impeller meter. The impeller meter was on loan for approximately 7 months and had just been returned. The calibration data for the EM flowmeter looked good but the data looked poor for the impeller meter. After sharpening the bottom bearing needle and polishing the upper bearing needle, the calibration data for the impeller meter was greatly improved and looked acceptable.

At the beginning of the test, the top of each flowmeter was placed below the midpoint of the inflow and raised at 2.54-cm increments after each flow measurement. The distance between the flowmeter and the inflow was measured between the midpoint of the inflow and the bottom of the flowmeter. As the flowmeter is raised past the inflow, the meter obstructs the pathway of the injected water. During this obstruction,

some of the inflow may be diverted downward and return as upward flow on the other side of the pipe. Results are shown in Table 6 and Figure A8.

Table A1 and Figure A8 show that the EM meter can provide misleading results in the vicinity of high horizontal inflows. These results are believed to occur from two sources of error. The first source occurs when the meter partially blocks the inflow and causes some of the inflow to spread vertically downward. This effect is expected to become much less important when the incoming flow is controlled by the pressure head at the top of the well and not from the pressure behind the inflow. The second source occurs when the flowmeter has passed the inflow but remains in the turbulence caused by the inflow. The data indicates turbulence will cause an underestimate of the flow rate. Fortunately, the effects of turbulence decline rapidly with distance from the inflow.

TABLE A-1. EFFECT OF HORIZONTAL INFLOW ON FLOWMETER RESPONSE

Electromagnetic Meter (Inflow = 8.32 L/min)			Impeller Meter (Inflow = 7.30 L/min)		
Distance from BOM (cm)*	Distance from TOM (cm)**	Mean Flow (L/min)	Distance from BOM (cm)*	Distance from TOM (cm)**	Mean Flow (L/min)
-15.8	-5.1	0.0	-11.4	-5.1	2.42
-10.7	-2.5	0.26	-8.9	-2.5	4.57
- 8.3	0.0	0.83	-6.4	0.0	4.53
- 5.7	2.5	2.34	-3.8	2.5	1.89
- 3.2	5.1	2.49	-1.3	5.1	1.89
- 0.6	7.6	3.78	1.3	7.6	13.00
1.9	10.2	4.76	3.9	10.2	14.97
4.4	12.7	6.08	6.4	12.7	3.02
7.0	15.2	7.03	8.9	15.2	7.71
9.5	17.8	7.56	11.4	17.8	7.90
12.1	20.3	8.05	14.0	20.3	7.52
14.6	22.9	8.31	16.6	22.9	7.25
17.1	25.4	8.31	19.1	25.4	7.00
19.7	27.9	8.31	21.5	27.9	6.80
22.2	30.5	8.31	24.0	30.4	6.57

* Distance measured from midpoint of inflow and lower inlet of the meter.
** Distance measured from midpoint of inflow and upper inlet of the meter.

Note: A negative distance indicates a distance below the inflow source. A positive distance indicates a distance above the inflow source. The estimated error associated with these measurements is 1 cm.

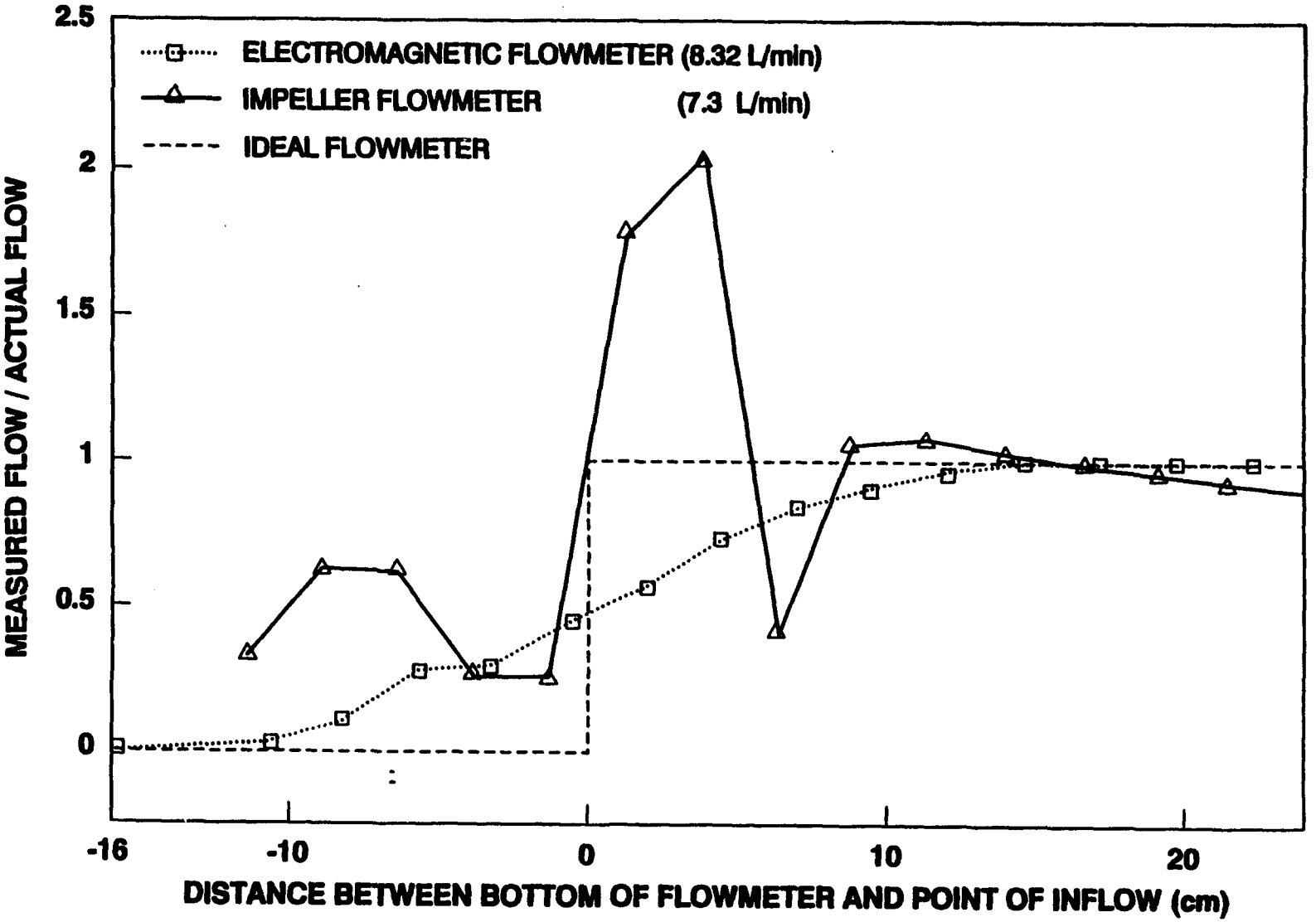

Figure A8. The Effect of Non-Uniform Flow on the Response From the Electromagnetic and the Impeller Flowmeters.

Table A1 and Figure A8 show that the impeller flowmeter appears to be more likely to provide misleading results in the vicinity of high horizontal flows than the EM flowmeter. The combined effects of the turbulence and nonuniform flow have an unpredictable effect on the impeller flowmeter response until the flowmeter's bottom is about 15 cm above the inflow. In the zone of high turbulence, it appears that the eddies can either increase or decrease the spin of the impeller. The lack of a constant flow rate at a distance of 20 to 30 cm from the inflow is believed to be caused by nonuniform flow effects on the impeller meter.

One of the implications of Table 6 and Figure A7 is that the flow measurements near zones of relatively high transmissivity or numerous fractures will have more uncertainty associated with them than the other flow measurements. In such instances, several flow measurements, taken several centimeters apart from each other, should be made to help locate the zone and determine if any effects of turbulence can be detected. A detailed investigation into the importance of the uncertainty with the flow measurements near highly transmissive zones was not conducted as part of this study. However, from the calibration data, one should note that this uncertainty is a lesser concern with an EM flowmeter than an impeller meter.

D. FINAL EVALUATION

Throughout the project, the EM flowmeter consistently performed better than the impeller meter with respect to precision, accuracy, and durability. One of the main advantages of the EM flowmeter is the range of flows for which the meter provides accuracy and precision. The low detection limit of less than 0.05 L/min and the high precision of the EM prototype flowmeter makes it well-suited for aquifers with large variability in their hydraulic properties. The EM flowmeter will lead to more detailed measurements or to fewer flow tests than a less sensitive flowmeter. If the borehole flowmeter technique is used in or close to contaminated aquifers, the capability of the EM flowmeter to measure small flow is desirable in order to minimize the pumping or injection rates. Similarly, in aquifers of relatively low transmissivity, the low flow rates at which the EM flowmeter can operate may make the borehole

flowmeter technique possible where it otherwise might not be with a less sensitive flowmeter.

Another attractive feature of the EM prototype flowmeter is that it is well designed for field use. The meter has no moving parts that may suffer from everyday wear and tear, and has no adjustable parts that affect its calibration. The meter also has no parts that can corrode or react with solutes in the groundwater. For protection during fieldwork, the meter is encased in a stainless steel housing.

APPENDIX B

WELL EQUATIONS FOR CALCULATING HYDRAULIC CONDUCTIVITY PROFILES FROM BOREHOLE FLOWMETER DATA

A. REVIEW OF METHODS FOR CALCULATING HYDRAULIC CONDUCTIVITY PROFILES

1. Basic Assumptions

Recall from Figure 11 that in the analysis of the borehole flowmeter data, one assumes the water flows to (or from) the pumped well in an idealized horizontally layered aquifer. This assumption permits a hydraulic conductivity to be calculated for each layer based on the incremental thickness, Δz_i; the incremental flow, ΔQ_i; and the incremental drawdown, Δs_i, in each layer.

In order to calculate the hydraulic conductivity values, accurate and representative measurements are needed for the time-drawdown response and the vertical distribution of the discharges to and/or from the well. The proper measurement of the vertical flow distribution requires that the pumping rate does not create undesirable vertical gradients at the well-aquifer interface and that any ambient vertical flow in the well is properly accounted for. The proper measurement of the time-drawdown response requires that the head losses through the well and through the disturbed portion of the aquifer (e.g., the skin effect) be properly accounted for.

2. Cooper-Jacob Equation for Layered Flow

Numerous researchers (Rehfeldt, et al., 1989; Molz, et al., 1989; Morin, et al., 1988, and Boggs, et al., 1990) have used the Cooper-Jacob equation (1946) to calculate the hydraulic conductivity profile from borehole flowmeter data. Equation (B1) is a form of the Cooper-Jacob equation, which is based on horizontal and unbounded flow through the aquifer to the well. In order to apply Equation (B1) to each layer, an assumption is required about the relationship between the transmissivity, T, and the storage coefficient, S, in each aquifer layer. Two simple assumptions are: (1) S is constant and does not vary with T (see Morin,

et al., 1988; Molz, et al., 1989) and (2) S varies with T such that the diffusivity (i.e., T/S) remains constant (see Rehfeldt, et al., 1989; Boggs, et al., 1990). It can be shown that the first and second assumptions lead to Equations (B2) and (B3), respectively.

$$T = \frac{Q}{4 \pi s} \ln \left[\frac{2.25 T t}{r_w^2 S}\right] \quad \text{(B1)}$$

$$K_i = \frac{q_i}{4 \pi s_i z_i} \ln \left[\frac{2.25 T t}{r_w^2 S}\right] \quad \text{(B2)}$$

$$K_i = \frac{q_i}{4 \pi s_i z_i} \ln \left[\frac{2.25 K_i z_i t}{r_w^2 z_i S_s}\right] \quad \text{(B3)}$$

where: Q = total discharge (L^3/T)
s = drawdown in well (L)
T = aquifer transmissivity (L/T)
S = storage coefficient for the aquifer = $S_s \times \Sigma(z_i)$ (-)
K_i = hydraulic conductivity for layer i (L/T)
z_i = thickness of layer i (L)
q_i = flow to (or from) layer i (L^3/T)
S_s = specific storage for the aquifer (-)
r_w = effective radius of well (L)
t_i = elapsed time (T)
s_i = drawdown in layer i (L)
B = aquifer thickness (L)
S_i = storage coefficient for layer i

At the project test site, the borehole flowmeter measurements were made at each well during ambient and pumping conditions at 0.3-meter increments. Figure B1(a) shows the discharge profile for Well 2 during a constant pumping rate of about 23 L/min. Figure B1(b) shows the profiles hydraulic conductivity as calculated from Equations (B2) and (B3) given the same drawdown at a specified time, the same storage coefficient for the total aquifer, and the same effective radius. Figure B1(b) shows that the ratio of the hydraulic conductivity values from Equation (B3) to the values from Equation (B2) range from 1.2 to 0.4.

Figure B1(c) shows the radius-of-influence of the designated aquifer layers at Well 2 as defined by Equation (B4). For each aquifer layer, the radius-of-influence represents a radial distance over which the the well drawdown affects the hydraulic pressure gradient. The same

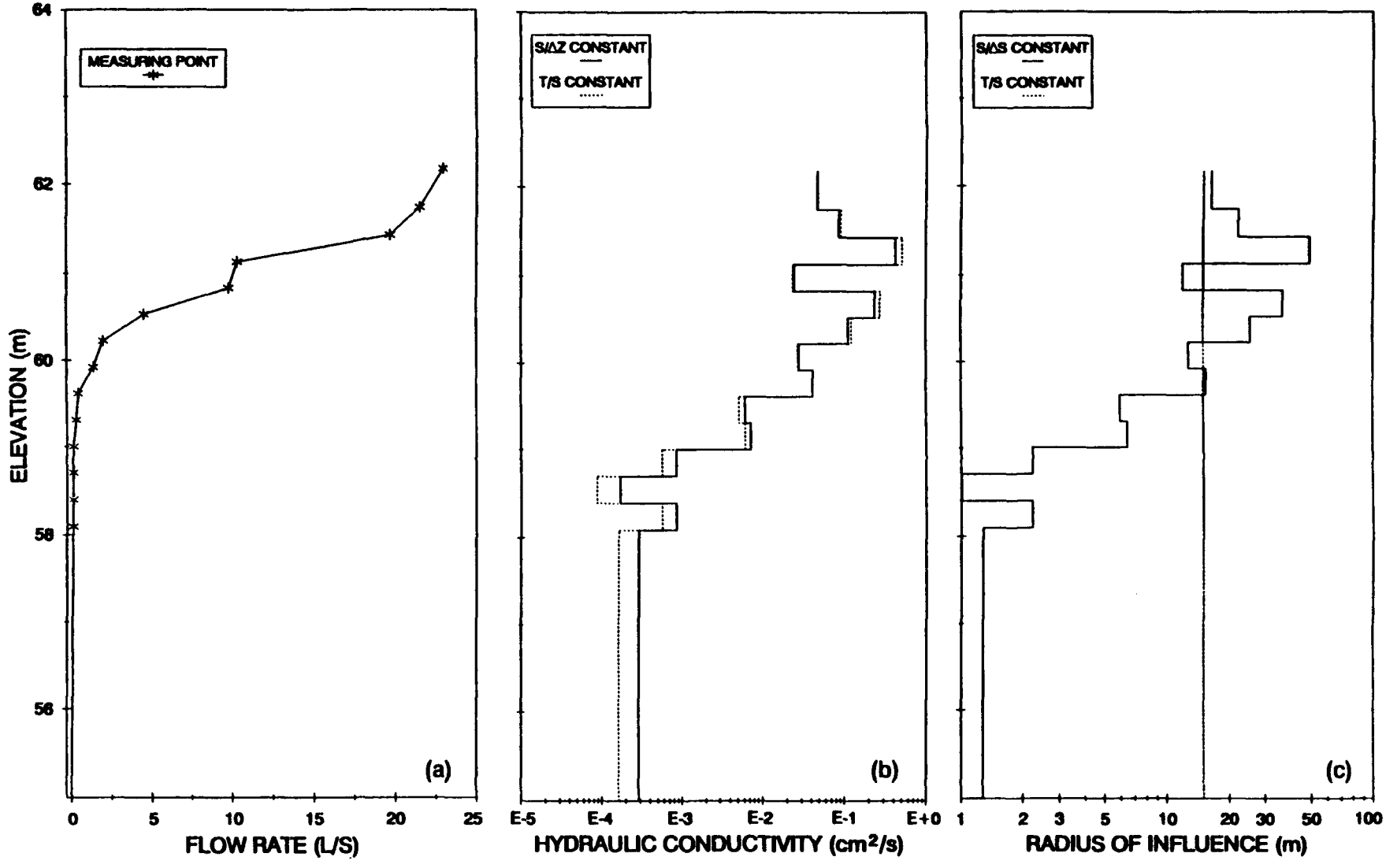

Figure B1. Vertical Profiles at Well 2: (a) Measured Flow; (b) Hydraulic Conductivity; (c) Radius of Influence.

radius-of-influence values produced by Equation (B2) for each aquifer layer implies that the horizontal hydraulic pressure gradient in every layer is the same. Thus, no vertical hydraulic gradients exist between the layers. The different radius-of-influence values produced by Equation B3 for each aquifer layer implies that different horizontal hydraulic pressure gradients exist at fixed radial distances near the well in each aquifer layer. Thus, vertical hydraulic gradients and therefore vertical flow exist between the aquifer layers. The result of Equation (B3) is contrary to the assumption of horizontal flow to the well used as justification for applying the Cooper-Jacob equation to analyze borehole flowmeter data.

$$R = \left[\frac{2.25\ K_i\ z_i\ t_i}{S_i}\right]^{1/2} \qquad \text{(B4)}$$

3. Steady Flow in Stratified Aquifers at the Well Bore

Support for using Equation (B2) over (B3) comes from the results of a computer modeling study conducted by Javandel and Witherspoon (1969). This two-dimensional modeling study showed that in an idealized, layered aquifer with a constant storage coefficient, flow to a well bore rapidly becomes horizontal, even for relatively large contrasts in hydraulic conductivities among the layers. Horizontal flow occurs because crossflow between the different layers reduces the vertical gradients between the layers. The implication of the work of Javandel and Witherspoon is Equation (B5).

$$Q_i = (\alpha)\ z_i\ K_i \qquad \text{(B5)}$$

where: α = a constant of proportionality that is calculated by dividing the total pumping rate by the well transmissivity (i.e., $\alpha = Q/T$)

Both Equations (B2) and (B5) indicate that the incremental discharge for any layer i is directly proportional to the transmissivity of the layer. A difference between the two equations is that Equation (B5) permits the aquifer's transmissivity to be calculated by any method, whereas Equation (B2) requires that the aquifer

transmissivity be calculated by the Cooper-Jacob equation. Another difference is that Equation (B2) provides a way to correct for well head losses (i.e., different s_i values) whereas Equation (B5) does not.

B. RECOMMENDED METHOD FOR BOREHOLE FLOWMETER DATA ANALYSIS

1. General Approach

Based on the review of the Cooper-Jacob equation (1946) and the modeling results of Javandel and Witherspoon (1969), a three-step procedure is used to analyze the borehole flowmeter data. This procedure is similar to the approach advocated by Molz, et al. (1989). The first step is to determine the ratio of the hydraulic conductivity values (i.e., K_i) at each layer to the depth-averaged hydraulic conductivity (K) from the distribution of groundwater. The second step is to determine the value of K from a Cooper-Jacob straight-line analysis of the time-drawdown curve for the pump test. The third step is to determine the absolute value of K_i for each layer by multiplying K_i by the value of K.

2. Profile of Relative Hydraulic Conductivities for Each Layer

The K_i/K profile for each well was calculated by a computer program that solves Equation (B2). This program was originally written by Dr. Peter Hufschmied (1983), extensively modified by Dr. Kenneth Rehfeldt (Rehfeldt, et al., 1989a), and slightly modified by the author. Although simple, the program has several helpful features such as: (1) correction for head losses in the well screen and pipe at different layers; (2) a detailed output of the calculated head losses; (3) a methodology to handle nonscreened sections of pipe near the coupling of the well sections; (4) corrections for different water temperatures; and (5) vertical flow in the well caused by ambient geohydrological conditions in the aquifer.

A potentially important aspect in determining the K_i/K profile is the distribution of groundwater flow in the well under ambient conditions. Ambient groundwater flow occurs in the fully screened wells

because of the vertical gradients in the aquifer. By applying the principles of superpositioning as discussed by Rehfeldt et. al. (1990), the effect of the ambient flow in the flow distribution in the well during the pump test can be accounted for in determining the K_i/K profile. Six of the wells tested in July had locations where the ambient flow was greater than 1.0 L/min. Table B1 lists the maximum value of groundwater flow measured in each of the 37 wells tested in April 1990.

TABLE B-1. MAXIMUM VALUE OF GROUNDWATER FLOW MEASURED AT EACH WELL DURING APRIL 1990

Well	Flow (L/min)	Well	Flow (L/min)	Well	Flow (L/min)	Well	Flow (L/min)
1	0.261	11	0.193	21	0.322	31	0.742
2	0.428	12	0.322	22	0.223	32	0.208
3	1.529	13	0.840	23	0.950	33	0.000
4	0.496	14	0.159	24	0.473	34	0.246
5	0.129	15	0.136	25	1.200	35	0.261
6	0.061	16	1.230	26	0.681	36	0.848
7	0.216	17	1.741	27	2.945	37	0.322
8	0.201	18	0.352	28	0.481		
9	0.360	19	0.397	29	0.511		
10	0.367	20	1.317	30	0.129		

3. The Depth-Averaged Hydraulic Conductivity from the Cooper-Jacob Straight-Line Method

As shown in Volume I, Section VII, the Cooper-Jacob equation is inappropriate for calculating K because of the skin effects at the wells. Figure 5 shows that negative skin effects at some of the test wells have led to order-of-magnitude differences between Cooper-Jacob straight-line and Cooper-Jacob based transmissivities.

Figure B2 compares the Cooper-Jacob based transmissivities calculated from drawdown values at the inflection point (see Figure 5) and at the end of the test. The comparison shows relatively little difference between the two transmissivities. One explanation of the results presented in Figure B2 is that the amount of drawdown required to move the cone-of-influence through the skin effect is large enough such that the additional drawdown occurring after the inflection point has a minimal effect on the calculated transmissivity. As a result, one might

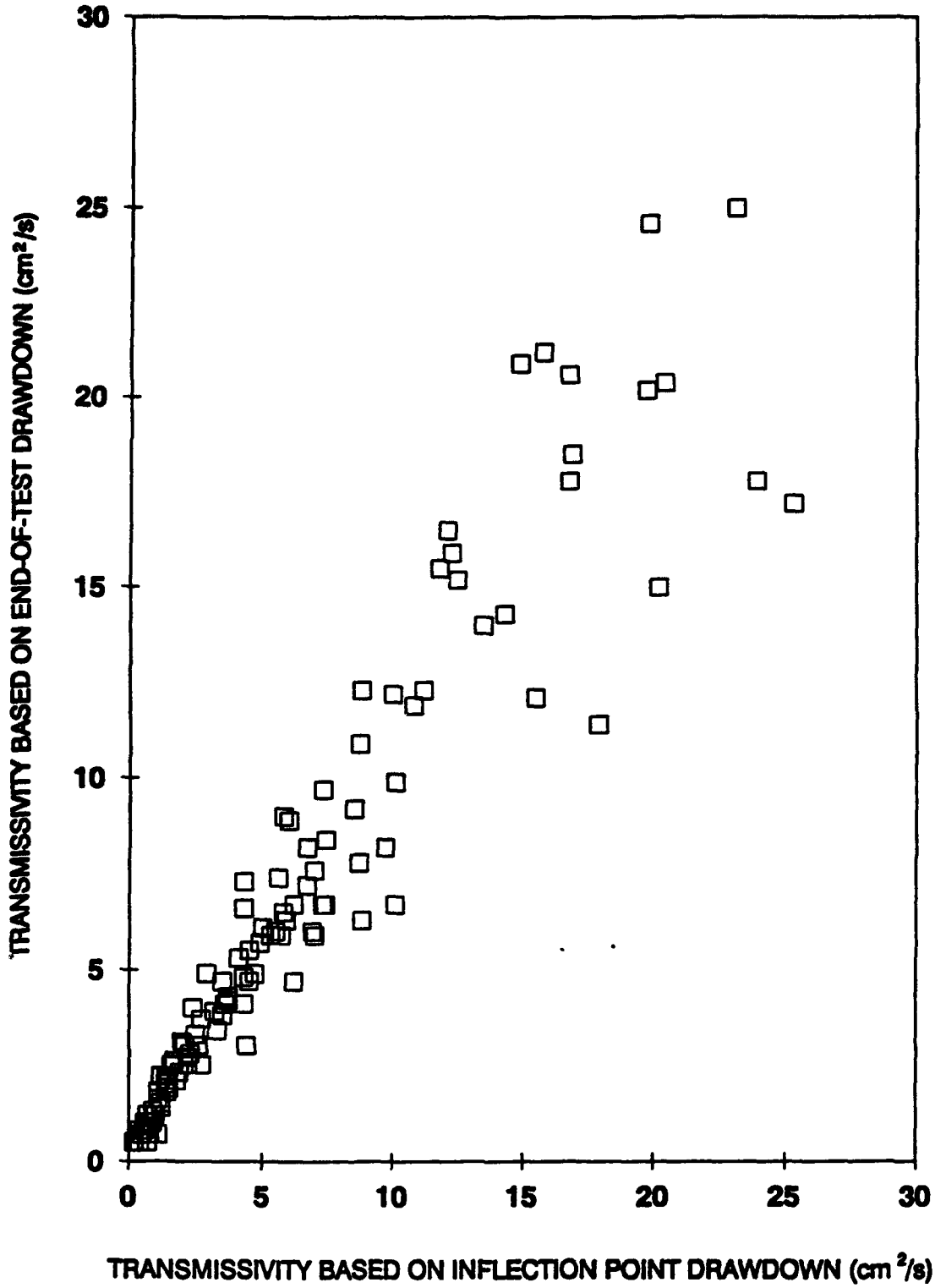

Figure B2. Comparisons of Transmissivity Values Calculated at the Inflection Point (about 1 minute) and at the End (about 20 minutes) of the Pumping Test.

speculate that the sensitivity of the Cooper-Jacob straight-line transmissivities to the pumping rate (as summarized in Figure 7) would not exist for the Cooper-Jacob based transmissivities. Figure B3 confirms this speculation.

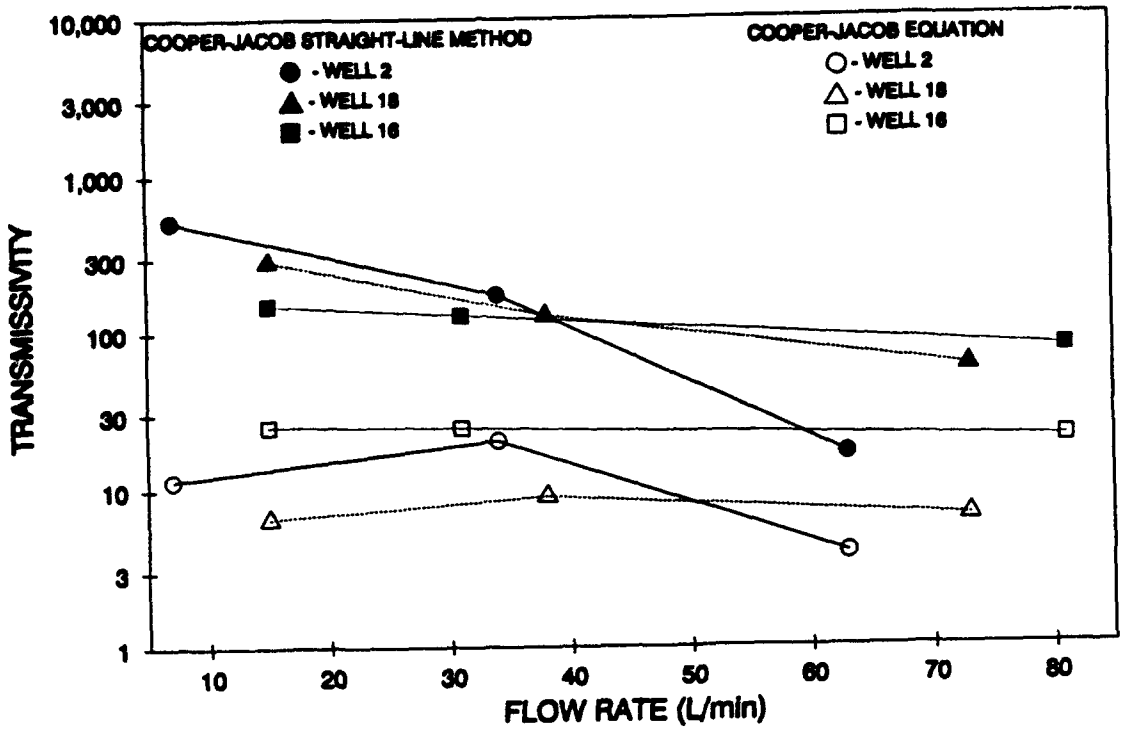

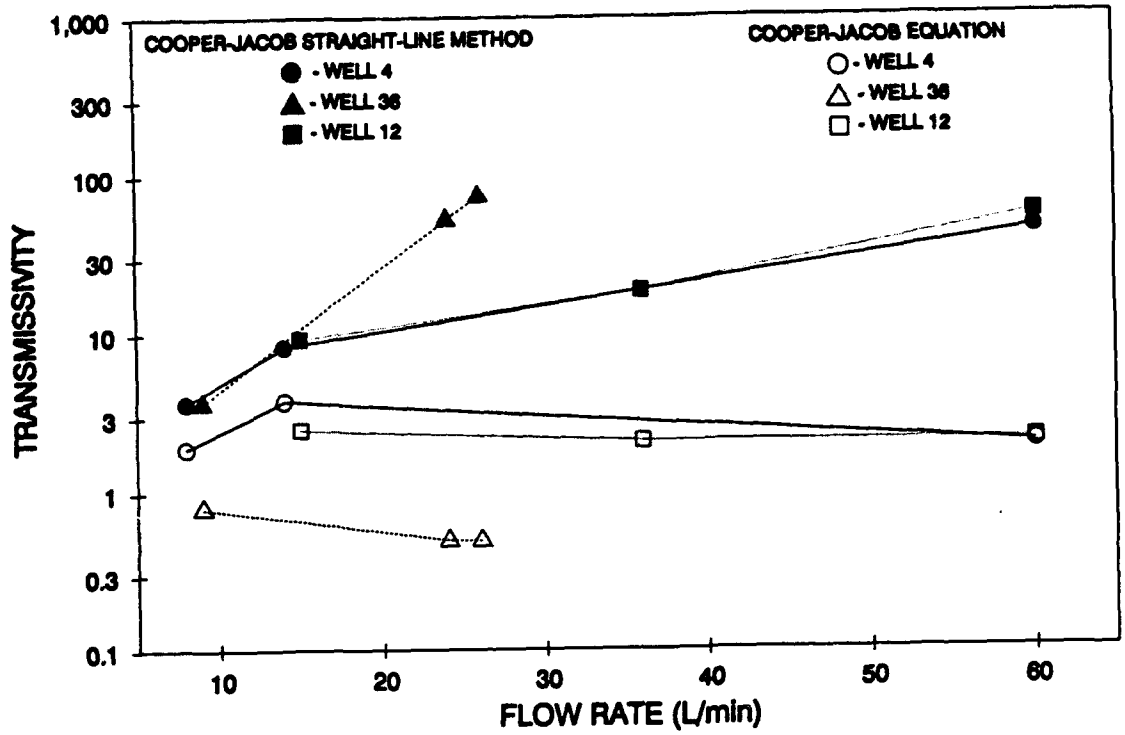

Figure B3. The Sensitivity of the Cooper-Jacob and the Cooper-Jacob Straight-Line Equation Transmissivity Values to Different Pumping Rates.

(The reverse of this page is blank.)

APPENDIX C

FLOW DISTRIBUTIONS FOR DIFFERENT FLOWMETER TESTS AT THE SAME WELL

The equations used to analyze the borehole flowmeter data assume that given negligible well head losses the pumping rate does not affect the normalized distribution of horizontal flow to a well. This assumption was checked by comparing borehole flowmeter results from December 1988 and April 1989. In December 1988, borehole flowmeter measurements were made at 21 wells during moderate (i.e., 20-30 L/min) and low (i.e., 6-12 L/min) pumping rates. In April 1989, borehole flowmeter measurements were made at all 37 wells during moderate (i.e., 20-25 L/min) injection rates. Figures C1 to C4 compare the flow distributions for these three flowmeter tests. For several of the tests, well head losses were not negligible and corrections in flow distributions were made to reflect the effects of different pressures inside the well on the flow distributions.

Figures C1 to C4 show that, for each well, the general features of the flow profile are the same. For many of the wells, the differences in the flow profiles would be greatly reduced if the increment of any of the comparisons were increased from 0.3 meter to 0.6 meter. The differences between the flow profiles are attributed to the different vertical hydraulic gradients acting during the different pumping and injection tests. These vertical gradients cause groundwater to deviate from strictly horizontal flow. This hypothesis is supported by two trends. The first trend is an increase in differences in the flow profiles for the two pump tests with greater differences in the drawdown produced by the pump tests. The second trend is that the differences in the flow profiles are much greater between the injection test and either one of the pump tests than the differences between the two pump tests.

The results in Figures C1 to C4 show that the pumping rate does affect the normalized distribution of horizontal flow to a well. However, this effect does not appear to be significant. A statistical analysis of all the flow profile data shows that over 80 and 60 percent of the normalized discharge measurements taken at the same location at different pumping rates are within a factor of two for the pumping tests and the injection test and the high-rate pumping test, respectively.

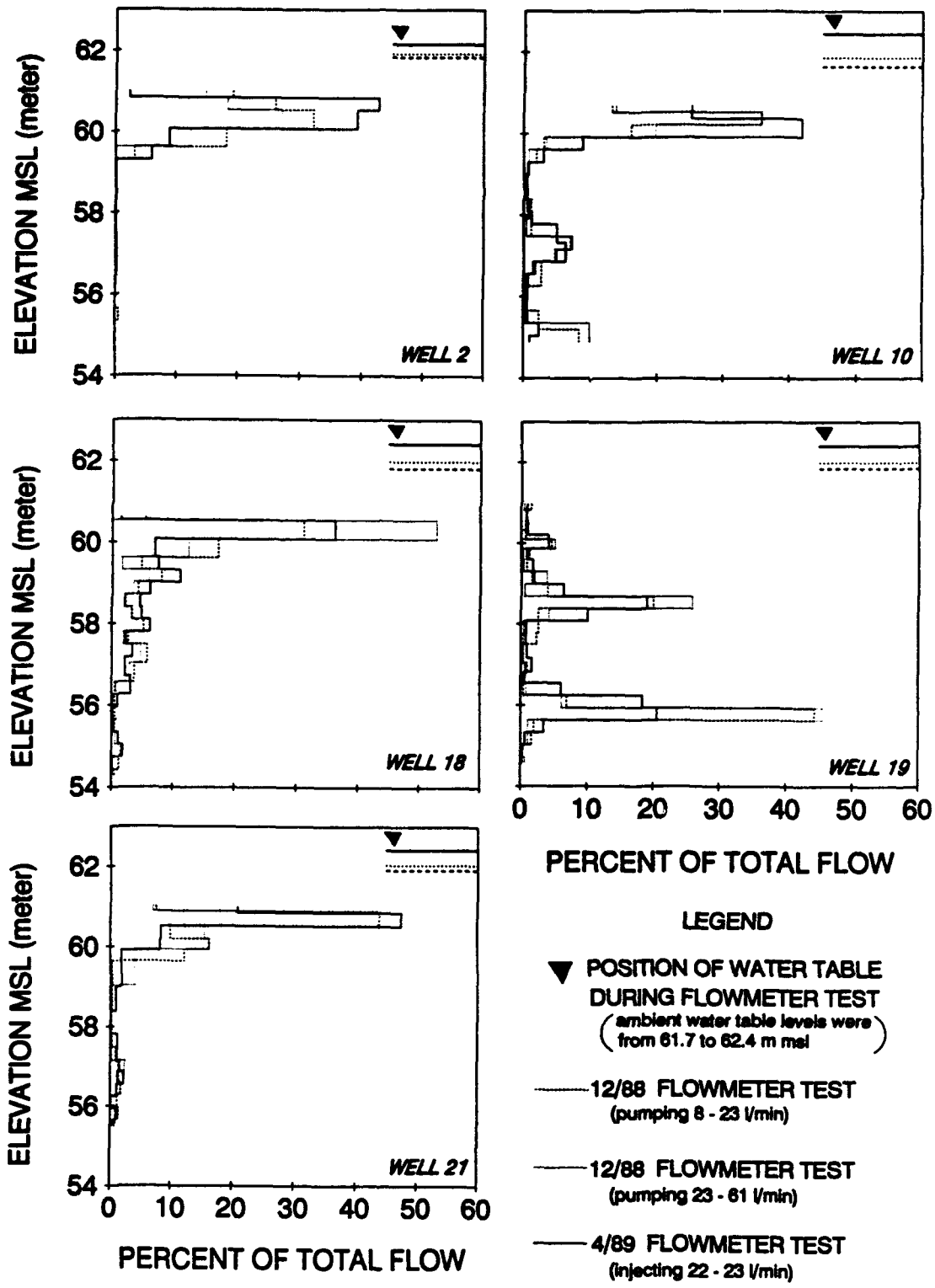

Figure C1. Comparisons Among Different Borehole Flowmeter Test Results for Predicting the Relative Distribution of Flow Over a Specific Vertical Interval for Wells 2, 18, 21, 10, and 19.

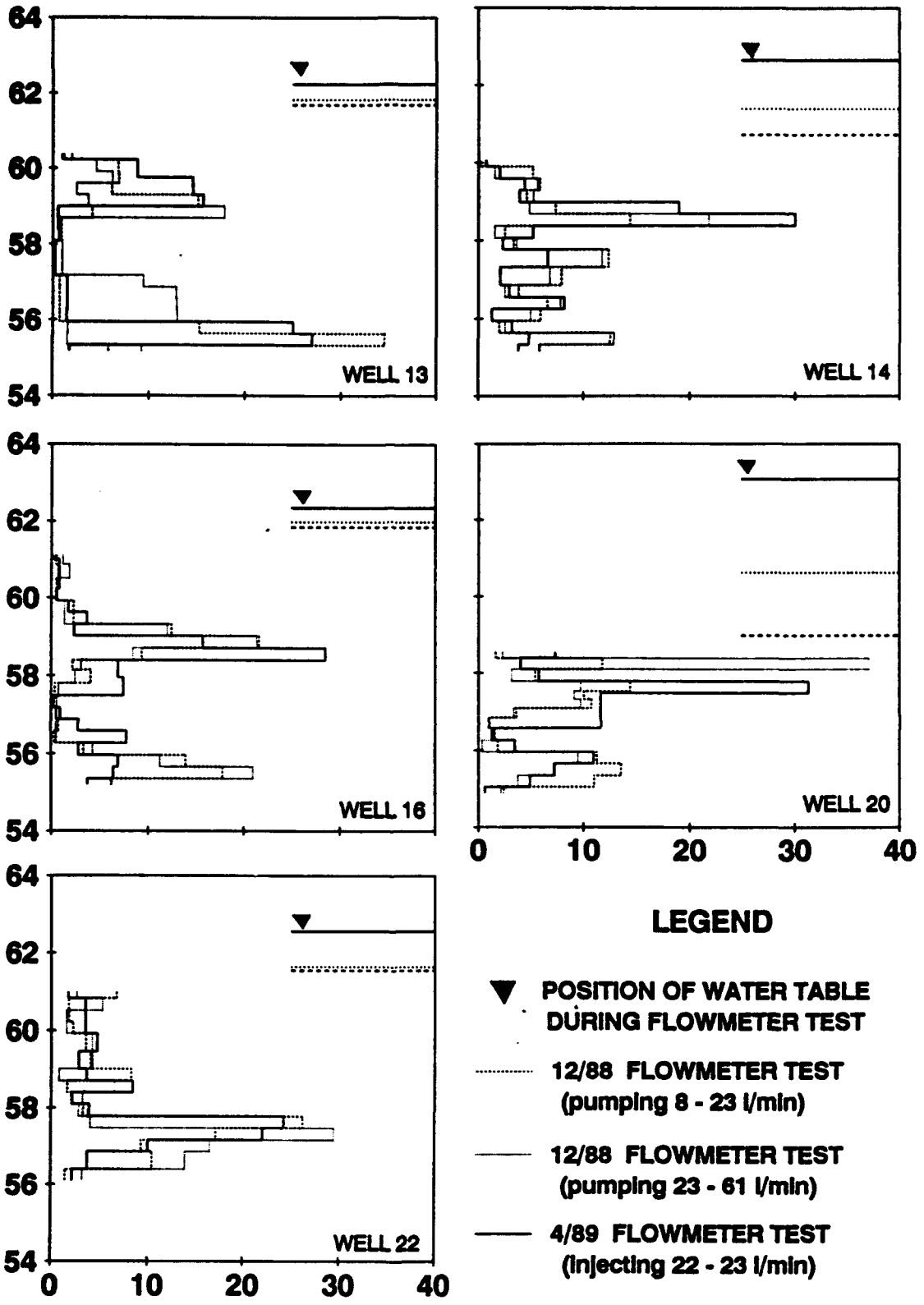

Figure C2. Comparisons Among Different Borehole Flowmeter Test Results for Predicting the Relative Distribution of Flow Over a Specific Vertical Interval for Wells 13, 16, 22, 14, and 20.

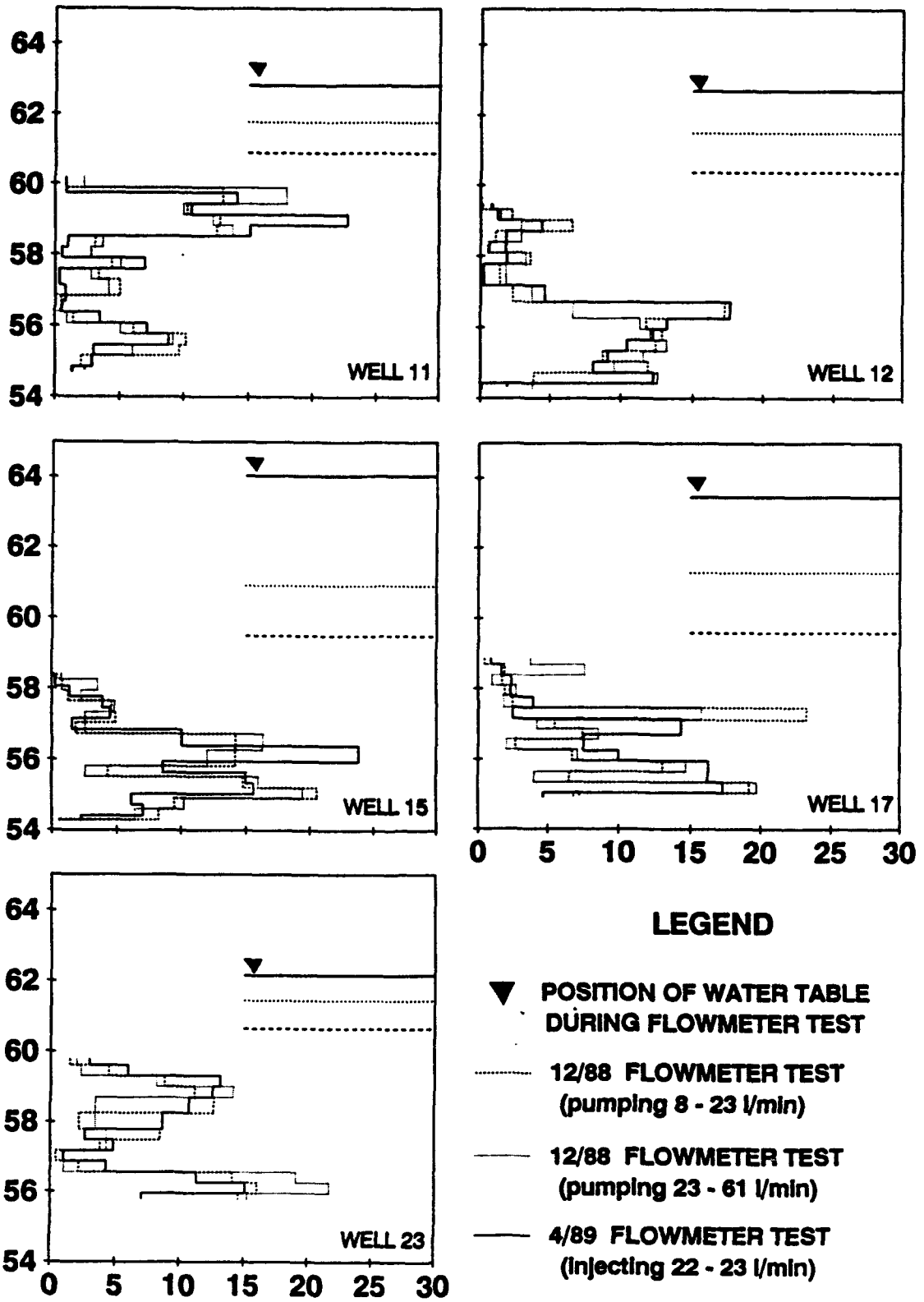

Figure C3. Comparisons Among Different Borehole Flowmeter Test Results for Predicting the Relative Distribution of Flow Over a Specific Vertical Interval for Wells 11, 15, 23, 12, and 17.

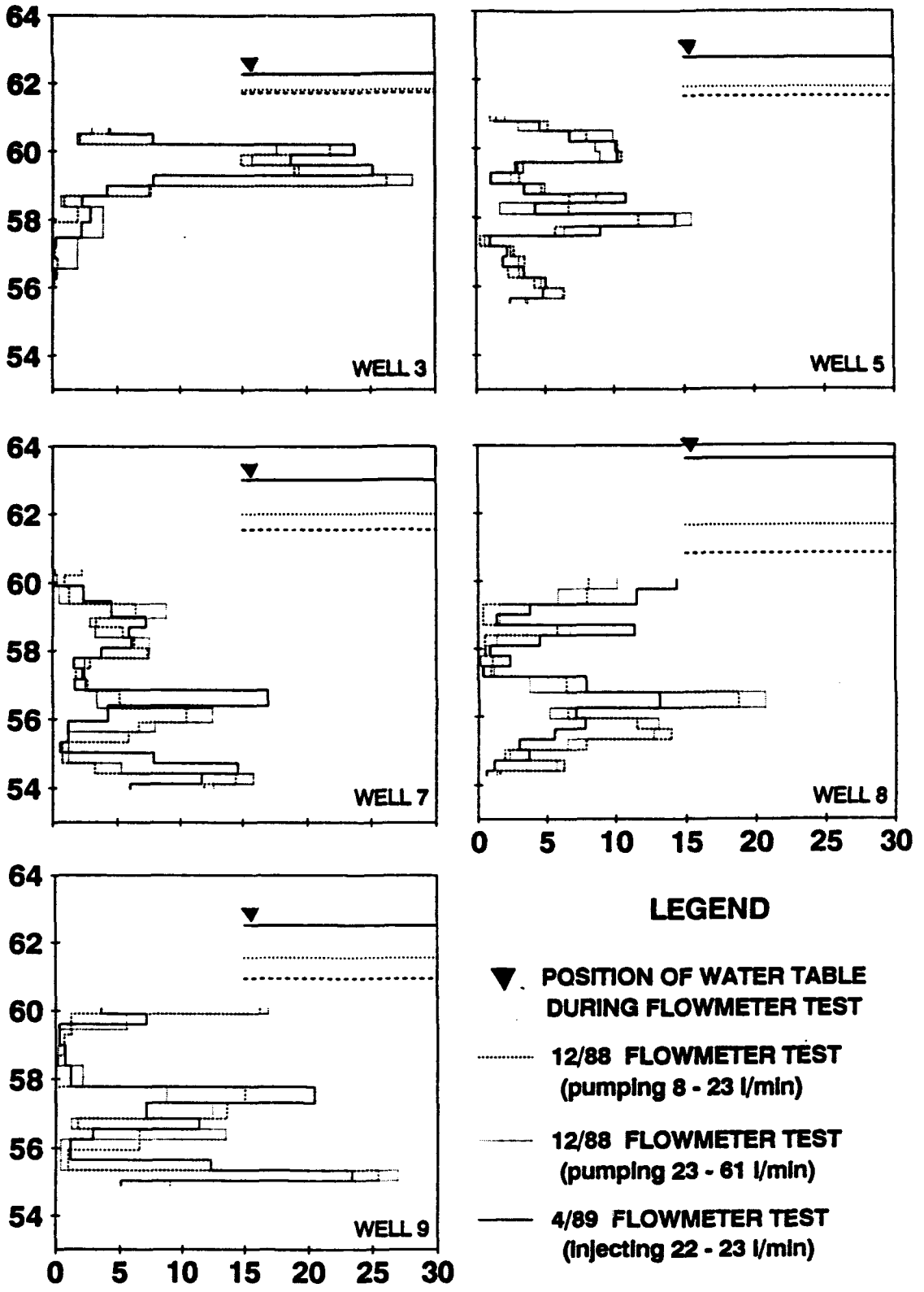

Figure C4. Comparisons Among Different Borehole Flowmeter Test Results for Predicting the Relative Distribution of Flow Over a Specific Vertical Interval for Wells 3, 7, 9, 5, and 8.

(The reverse of this page is blank.)

APPENDIX D

HISTORY OF THE GEOLOGICAL DEPOSITIONAL ENVIRONMENT

The segment of geologic time pertinent to this study with a widespread erosion of bedrock (Eutaw formation) was more than 40,000 years ago. This episode possibly occurred 100,000 years ago, especially considering the structural development of the sedimentary soils overlying this bedrock. A second widespread erosional episode occurred between 40,000 and 12,000 years ago. This episode may have marked the end of the Pleistocene and signal the beginning of Holocene times. We suggest a date of 18,000-20,000 years ago for this second erosional episode.

The basal depositional unit of Holocene times appears to have been a series of cross-bedded gravels fining upward to clean quartz fluvial sands. This unit was deposited in post-Pleistocene times, but more than approximately 12,000 years ago. During this depositional episode, there was both local erosion and soil development in areas above the flood limits of the floodplain. It appears that inception of the post-Pleistocene fragipans also occurred during this interval. In those areas away from the main channel, deposition took place. During this time, the Tombigbee River probably was in a braided or coarse-grained meander belt condition. Typical topographic features for this type of regime include distributary channels, braided channels, anastomotic streamlets, and various sand and gravel bars.

It appears that between 11,000 B.P. and 12,000 B.P. the Tombigbee River (at least locally) consisted of meandering channels. By that time the formation of most of the high Holocene terrace was completed. Continued formation of both high and low Holocene terrace levels persist until approximately 5,000 B.P. The abandonment of B. L. Bigbee ox bow occurred by approximately 11,000 B.P., and stable portions of the high Holocene terrace began weathering to form the Early-Holocene soil.

A period of extensive overbank deposition occurred between 11,000 and 5,000 B.P. During this time, the Tombigbee River exhibited dynamic metastable conditions that permitted stability of some topographic features and (on the other hand) rapid formation and eradication of

others. Those topographic features that have survived exhibit time-transgressive facies of the Mid-Holocene soil.

Judging from the geologic soils and B. L. Bigbee ox bow sediments, a change in deposition occurred between approximately 8,000 B.P. and 6,000 B.P. Either a depositional hiatus or marked slowing of the rate of deposition occurred. During this interval a greater extent of geomorphic floodplain may have been stable for longer periods than during the previous several millennia. The maturation of the meandering river regime also took place during this interval (7,500 B.P.-5,000 B.P.).

The geologic record may be interpreted to indicate that a widespread erosional episode occurred after 5,000 B.P. B. L. Bigbee sediments and pollen spectra indicate down cutting within the main geological sections. This erosional episode signals the end of Mid-Holocene soil formation. By 4,000-3,000 B.P., stable surfaces began the Late-Holocene soil-forming process. These events represent the outline of paleoenvironmental processes documented by our Phase I research.

APPENDIX E

THE DESIGN OF THE TRACER TESTS

A. THE TRACER TEST DESIGN

1. Potential Problems

The complex and heterogeneous hydraulic conductivity field at the site poses several problems associated with the monitoring and the interpretation of the three-dimensional tracer concentration data. Monitoring of the three-dimensional tracer concentrations is complicated by the large vertical hydraulic gradients. These vertical gradients can cause mixing of the tracer concentration fronts near the well if the disturbed zone around the wells is different from the structure of the undisturbed aquifer. The use of the tracer data to validate the borehole flowmeter hydraulic conductivity values is complicated by the differences in the hydraulic conductivity profiles at the monitoring well locations. The spatial variability in the hydraulic conductivity field introduces uncertainty in defining the pathways of solute transport. This results in an uncertainty with respect to the values of hydraulic conductivity calculated from the tracer tests.

Across the EPRI-MADE and the USAF test site, vertical hydraulic gradients from 2 to 10 percent are common in the aquifer (Boggs, et al., 1990). Because of these vertical gradients, the potential exists for mixing to occur alongside the annulus of multilevel samplers as shown in Figures E1 and E2. Figure E1 shows a hypothetical cross section of an aquifer before and after a well installation. Near the well a vertical column of relatively moderate hydraulic conductivity disturbed material has been created. At some locations, this disturbed material has replaced material of relatively low hydraulic conductivity that maintained a pressure differential between the lower and the upper portions of the aquifer.

Figure E2 shows the type of multilevel sampler installation used at the EPRI-MADE site and how the disturbed zone around these multilevel samplers can lead to mixing of the concentration fronts near the well

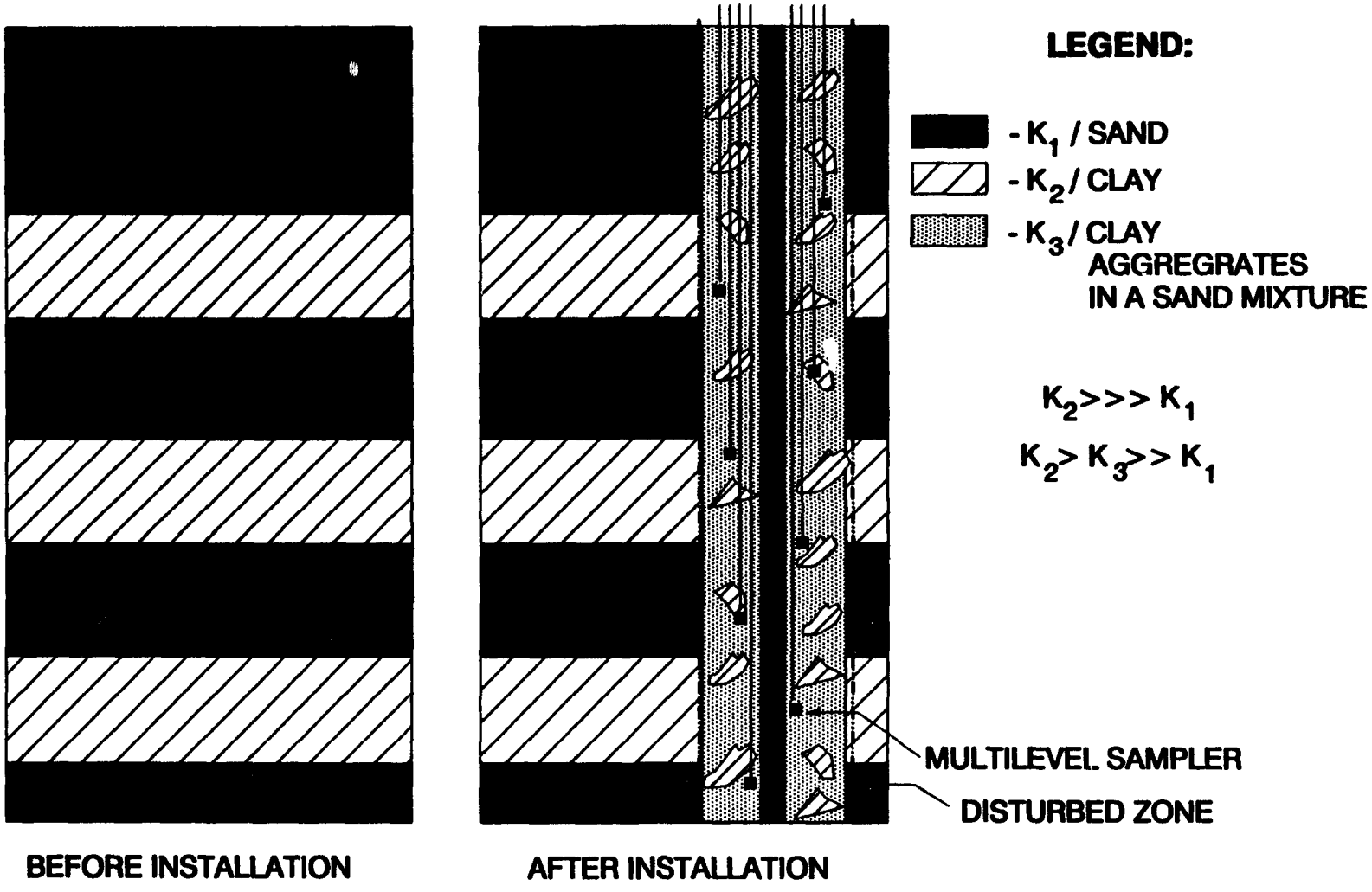

Figure E1. A Conceptual Disturbed Zone Around Groundwater Wells.

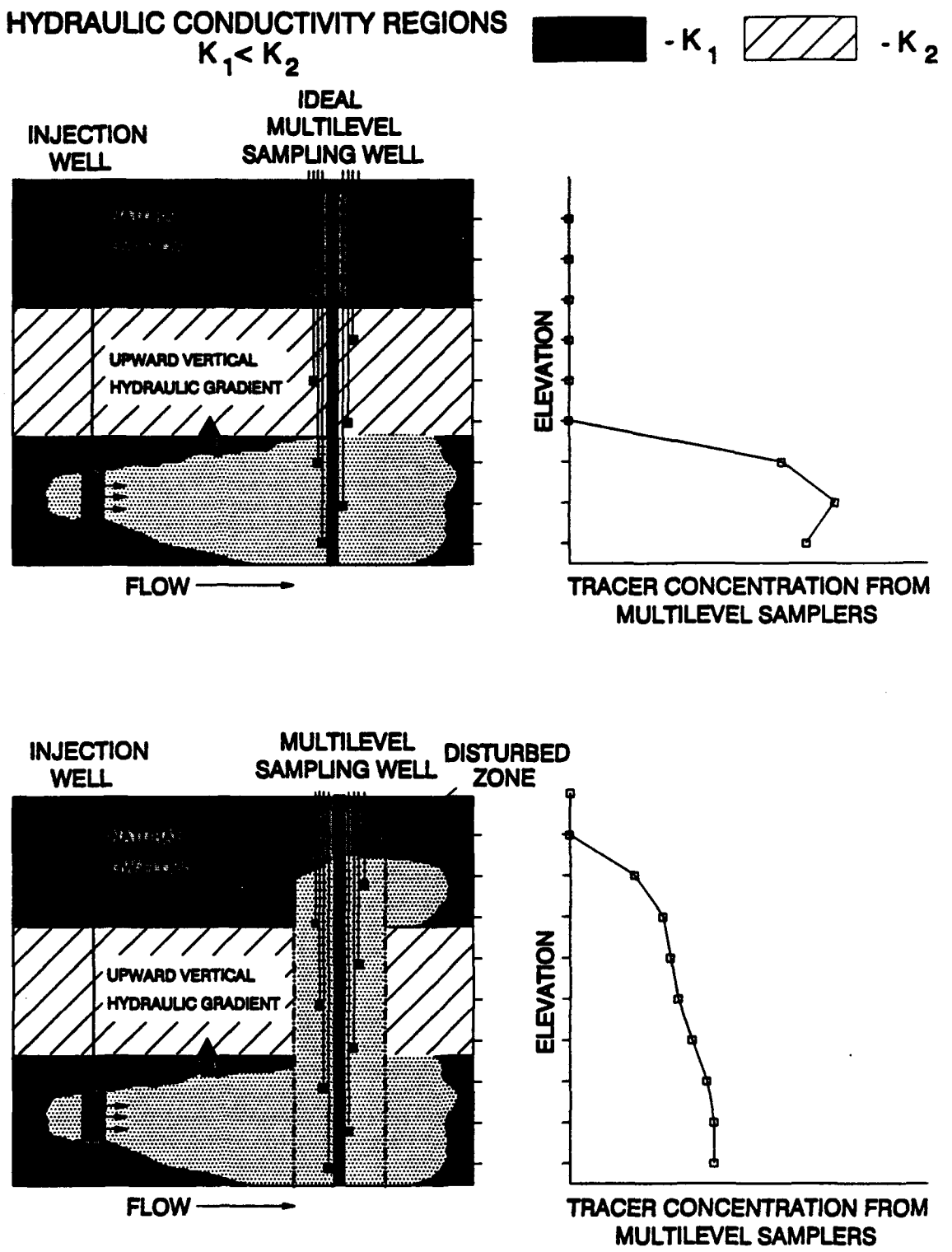

Figure E2. Potential for Mixing of Concentration Fronts in the Annulus of Multilevel Samplers.

installation. This mixing prevents multilevel samplers from obtaining representative groundwater samples from specific elevations in the aquifer. The fact that vertical flows as high as 2.9 L/min (see Appendix B) have been measured in some of the fully screened wells during ambient conditions indicates a potential for mixing (Figure E2). The fact that some type of vertical mixing could occur in the annulus of the wells was demonstrated by a series of small-scale tracer tests in the well annulus by Boggs, et al. (1989). As discussed by Young and Boggs (1989), this mixing in the well annulus has adversely affected the representativeness of groundwater samples from the multilevel samplers.

An important goal for the tracer tests is to demonstrate that the borehole hydraulic conductivity values can be used to accurately predict solute transport. However, this demonstration may be difficult because of the problems with a complex aquifer structure. Over large distances, and perhaps even over short distances, accurate solute transport predictions for the CAFB aquifer will require not only accurate hydraulic conductivity values but also accurate interpolation among the hydraulic conductivity values. In instances where the aquifer structure is different at the tracer injection and the withdrawal locations, it may be difficult to determine whether the differences between the observed and the predicted tracer breakthrough curves resulted from errors in the measurement, or from the interpolation of the hydraulic conductivity field. The problems associated with the spatial variability in the hydraulic conductivity field can be minimized by aligning the tracer injection and withdrawal points with the principal axes of the aquifer lenses, by keeping the distance between the points of tracer injection and withdrawal small relative to the dimensions of the lenses, and by placing the points of tracer injection and withdrawal in an area where no major changes in geological facies occur.

2. General Approach

a. Tracer(s)

Chloride and bromide were selected as tracers because: (1) they are believed to be conservative tracers (Betson, et al., 1985);

(2) their background concentrations are relatively low; (3) their relative concentrations can be measured quickly and accurately in the field with an electrical conductivity meter; and (4) their absolute concentrations can be measured relatively quickly and accurately in the laboratory with specific-ion probes.

b. The Flow Field

For the tracer tests, the groundwater flow patterns were controlled by a system of injection and withdrawal wells. By using a network of wells, a flow field was created so that the rate and the direction of tracer movement could be controlled. In order to mimic flow fields used in bioreclamation activities, the groundwater was recirculated from the withdrawal wells to the injection well(s). For each tracer test, accurate measurements of water table levels and flow rates were made to determine when the hydraulic pressure field stabilized. Once quasi-steady-state flow conditions were achieved, the tracer solution was injected.

c. Monitoring Approach and Equipment

Because of concerns about the performance of the multilevel samplers, none of them were installed. Instead, a procedure was developed to use the injection and withdrawal wells to monitor the three-dimensional tracer flux. Figure E3 shows the set-up used to monitor the three-dimensional tracer flux at the withdrawal and the injection wells. The set-up requires taking both concentration and groundwater flow measurements at the same elevations in the wells. Because both the tracer concentration and the vertical groundwater flow at designated elevations are known, the amount of tracer mass entering the designated layers can be calculated.

A multilevel sampler was placed inside each well. Figures E4 and E5 show the type of multilevel samplers installed in the tracer injection wells and withdrawal wells, respectively. During the tracer test, groundwater samples were collected simultaneously from all of the sampling tubes by using the appropriate number of peristaltic pumps. To

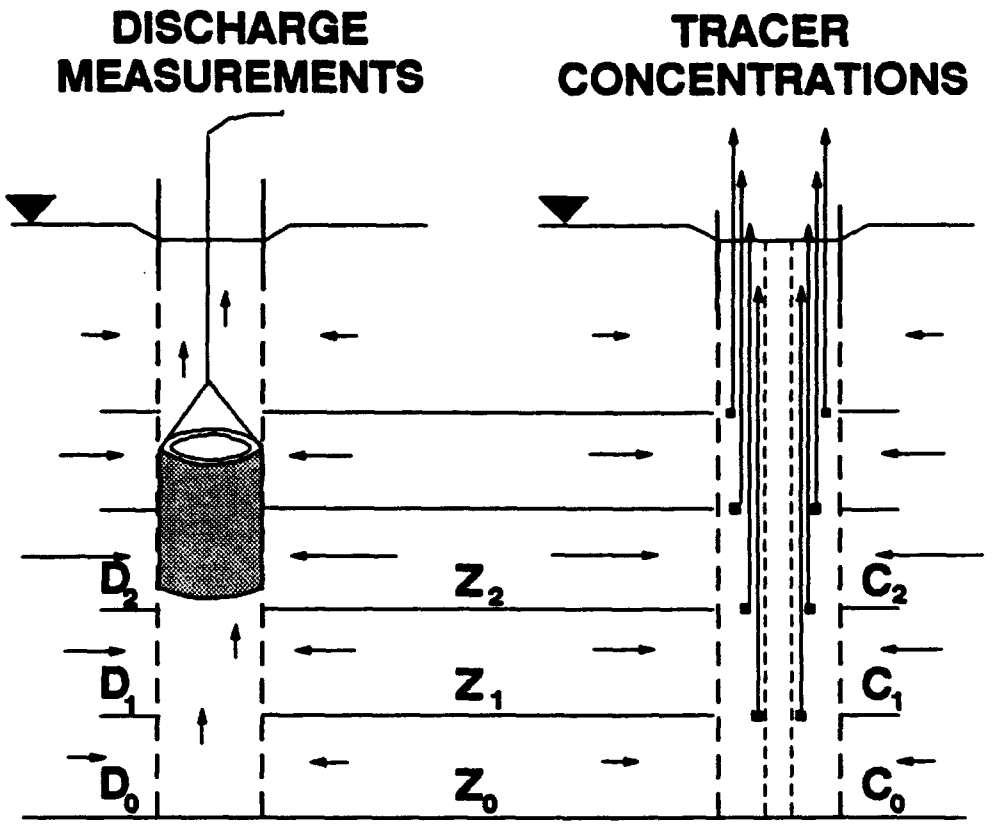

LEGEND:

Z_I - LOCATION OF LAYER I

D_I - DISCHARGE FROM LAYER I

C_I - AVERAGE TRACER CONCENTRATION IN LAYER I

EXAMPLE CALCULATION OF MASS FLUX

INTERVAL	VERTICAL DISCHARGE	TRACER CONCENTRATION	CUMULATIVE MASS FLUX OF TRACER	INCREMENTAL MASS FLUX OF TRACER
Z_0	D_0	C_0	D_0*C_0	D_0*C_0
Z_1	D_1	C_1	D_1*C_1	$D_1*C_1-(D_0*C_0)$
Z_2	D_2	C_2	D_2*C_2	$D_2*C_2-(D_1*C_1)$
Z_I	D_I	C_I	D_I*C_I	$D_I*C_I-(D_{I-1}*C_{I-1})$

Figure E3. Borehole Flowmeter and Tracer Concentration Measurements at the Injection and Withdrawal Wells.

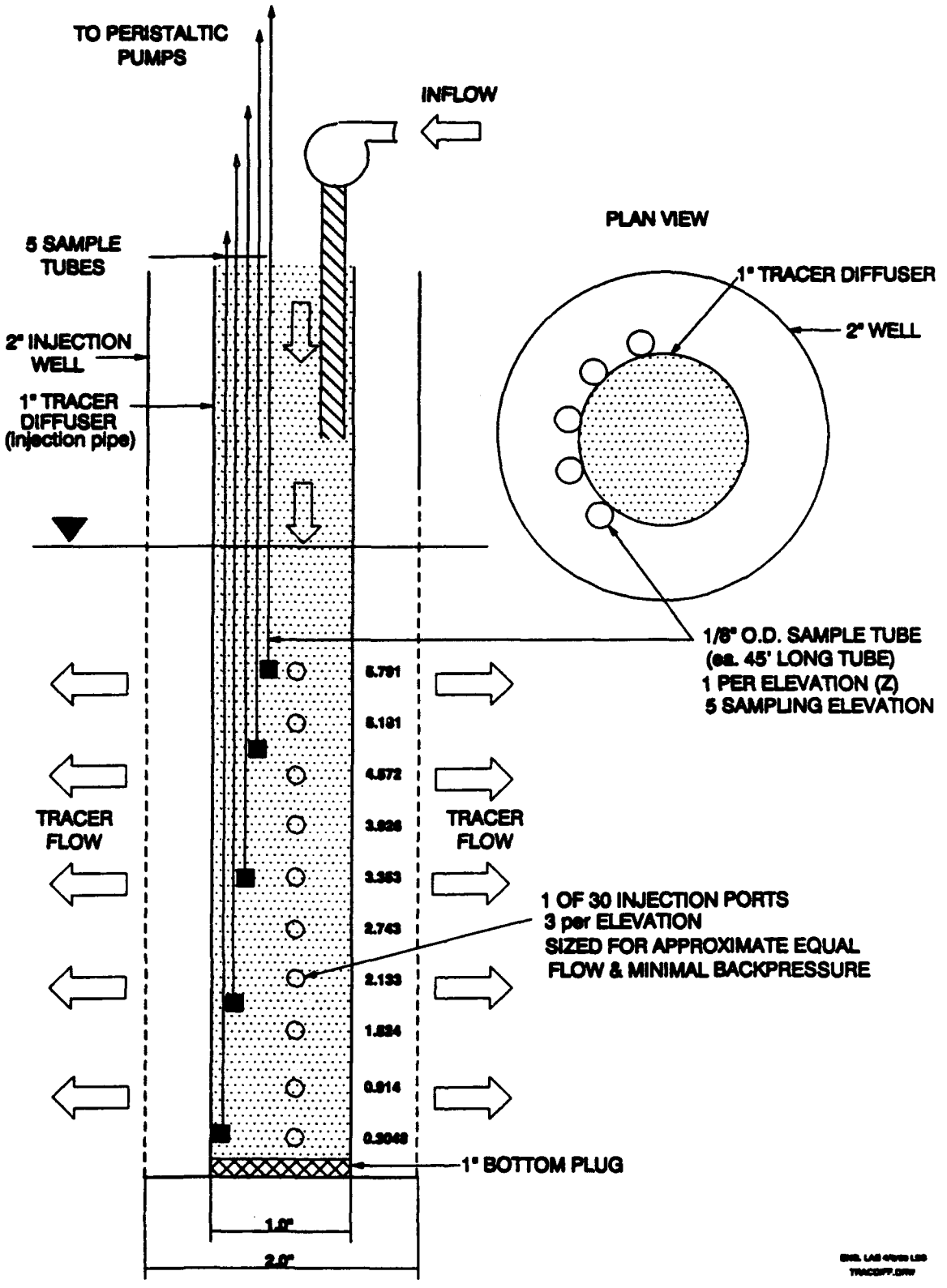

Figure E4. Multilevel Sampler for Collecting Groundwater Samples From Inside the Injection Wells.

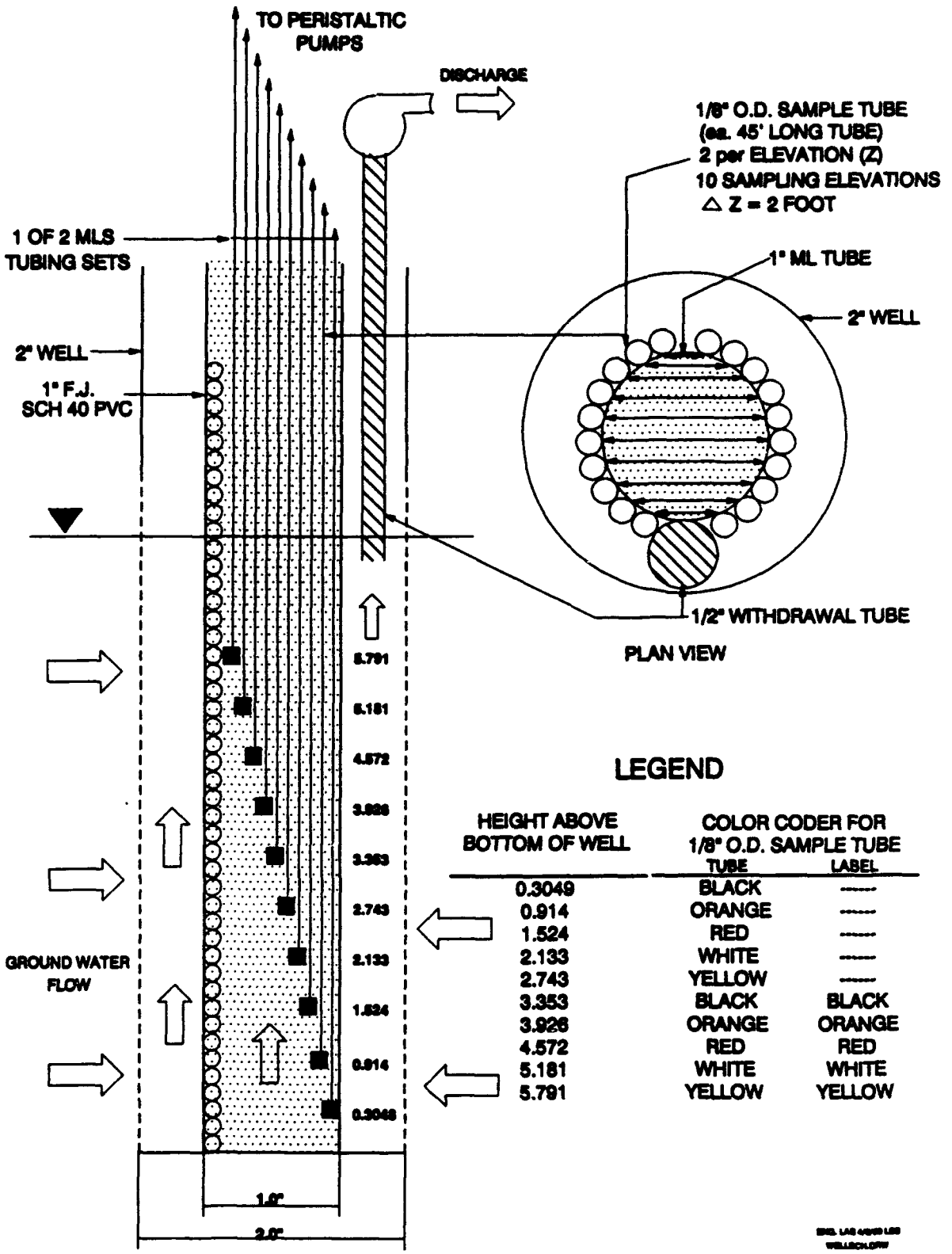

Figure E5. Multilevel Sampler for Collecting Groundwater Samples From Inside the Withdrawal Wells.

avoid problems with sample collection, all of the sample tubing and peristaltic pump connections were color-coded. As shown in Figure E5, two samples were collected at each elevation of the withdrawal wells. At the surface, these two samples were mixed into a single composite sample.

Two sets of borehole flowmeter measurements were taken for each tracer test. The first set was taken after the steady-state flow field had been established but before the tracer was injected; the second was taken after the last set of groundwater samples was collected from the multilevel samplers. For the purpose of characterizing the flow field during the tracer test, flow rates from the two data sets were averaged.

d. The Location and Number of Tracer Tests

Several tests are required to independently evaluate the validity of calculated hydraulic conductivity values and the validity of interpolation among point measurements of hydraulic conductivities. To collect as much information as possible about solute transport in the aquifer, small-scale (3-5 meters), intermediate-scale (7-15 meters), and large-scale (31 meters) tracer tests were conducted. Figure E6 shows the locations of injection and withdrawal wells for all of the tracer tests.

e. Type of Tracer Injection

In order to ensure timely and cost-effective tracer testing, tracer solutions were introduced as a slug source. Advantages of finite duration instead of a continuous tracer injection include: (1) better tracer breakthrough curve for calculating average velocity of the tracer; (2) lower costs; (3) minimum contamination of the aquifer; and (4) lower risk of cross-contamination between different tracer tests. A possible disadvantage of a finite duration test is that an inadequate amount of tracer may be added to provide a well-defined breakthrough curve.

f. Surface Piping Network

Figure E7 presents a general schematic of the piping system used to regulate the pumping of water from the withdrawal wells to the

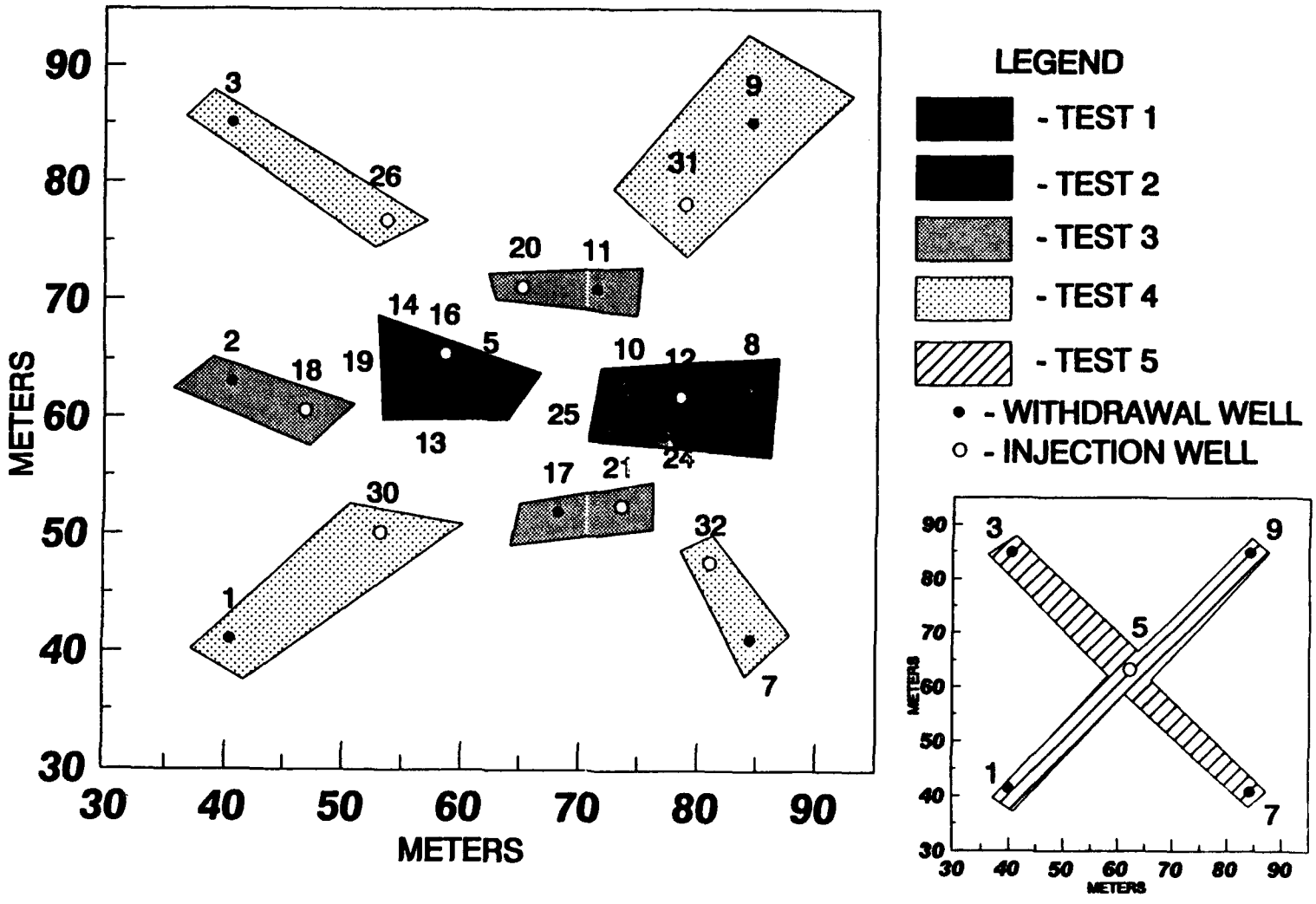

Figure E6. Location of the Tracer Tests.

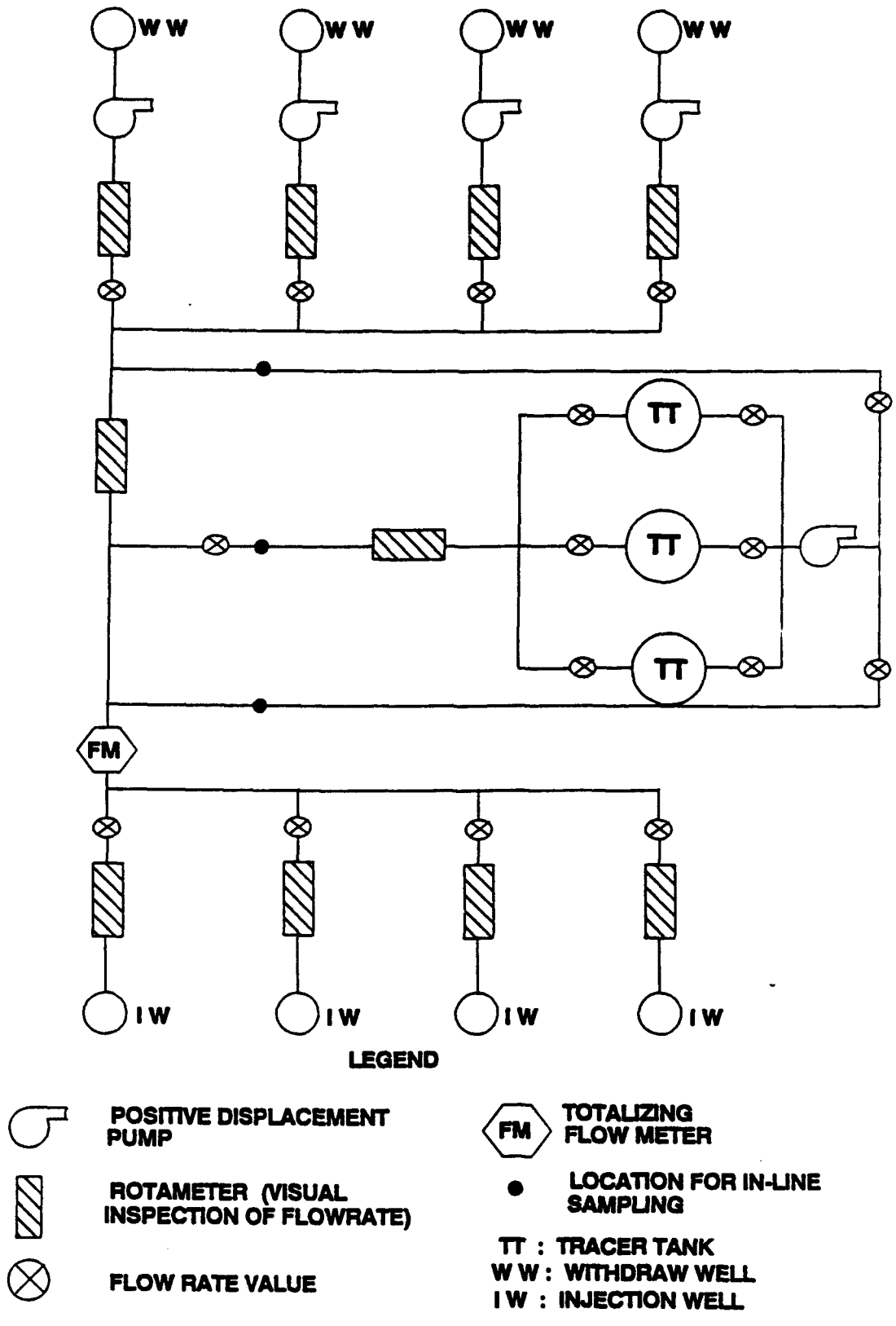

Figure E7. Setup for the Tracer Injection and Recirculation of Groundwater From the Withdrawal Well(s) to the Injection Well(s).

injection wells. The system is designed to accommodate up to four injection wells, four withdrawal wells, and three tracer tanks. The piping arrangement provided the capability to conduct several tracer tests simultaneously. To monitor the flow through the pipes, numerous rotameters were installed in-line to provide quick visual checks of the flow rates.

As shown in Figure E7, the piping arrangement permits pumping from the tracer tank to the injection wells while another tracer tank is filled. During the start of the tracer tests, the tracer solution was pumped from the tracer tanks to the injection wells. After the tracer slug was injected, the groundwater was then pumped directly from the withdrawal wells to the injection wells.

APPENDIX F

DESCRIPTION OF THE FIVE TRACER TESTS

A. TRACER TEST 1

Tracer Test 1 included pumping Wells 5, 13, 14, and 19 at approximately 9.5 L/min and injecting the total discharge into Well 16. The pumping began at 1552 on August 29 and the initial borehole flowmeter survey was conducted at all of the withdrawal wells on August 30 from approximately 1050 to 1550. On August 31 from 0000 to 0047, a tracer slug of 1,781 liters of 800 ppm bromide solution was injected into Well 16. Groundwater samples were collected at 0.6-meter vertical intervals from the withdrawal wells for about 7 hours after the tracer midpoint of the tracer injection. A final borehole flowmeter survey of all the wells was conducted on August 31 from 1355 to 1740.

B. TRACER TEST 2

Tracer Test 2 included pumping Wells 8, 10, 24, and 25 at approximately 7.6 L/min and injecting the total discharge into Well 12. The pumping began at 0015 on September 1 and the initial borehole flowmeter survey was conducted at all of the withdrawal wells on September 1 from approximately 0840 to 1433. A slug of 4,077 liters of 800 ppm bromide solution was injected into Well 12 from 2330 on September 1 to 0145 on September 2. Groundwater samples were collected at 0.6-meter vertical intervals from the withdrawal wells for about 26 hours after the tracer midpoint of the tracer injection. A final borehole flowmeter survey of all the wells was conducted on September 2 from 0840 to 1650.

C. TRACER TEST 3

Tracer Test 3 was designed to simulate three recirculating doublet tests. The withdrawal wells were Wells 2, 11, and 17; the injection wells were Wells 18, 20, and 21. Figure E6 shows the well locations and Table 14 provides the approximate pumping or injecting rates for each well. The initial borehole flowmeter survey was conducted at Wells 2,

11, and 17 on September 4 from 0920 to 1415. A slug of 7,712 liters of 800 ppm bromide solution was partitioned into all three injection wells in amounts proportional to their respective flow rates between 2230 on September 4 and 0200 on September 5. Groundwater samples were collected at 0.6-meter vertical intervals from the withdrawal wells for about 34 hours. A final borehole flowmeter survey of all of the wells was conducted from 1115 to 2215 on September 6.

D. TRACER TEST 4

Tracer Test 4 was designed to simulate four recirculating doublet tests. The withdrawal wells were Wells 1, 3, 7, and 9; the injection wells were Wells 30, 26, 32, and 31. Table 14 provides the approximate pumping or injection rate for each well. The pumping began at 0500 on September 8 and the initial borehole flowmeter survey was conducted at all of the withdrawal wells from 1805 to 2250 on September 8. A slug of 14,559 liters of 1200 ppm bromide solution was partitioned into all three injection wells in amounts proportional to their respective flow rates between 1840 and 2120 on September 9. Groundwater samples were collected at 0.6-meter vertical intervals from the withdrawal wells for about 50 hours. The final borehole flowmeter survey was conducted at Wells 3, 26, 32, 30, 31, and 7 on September 12 from 0905 to 1930. The final borehole flowmeter survey was conducted at Wells 9 and 1 from 0830 to 1026 on September 13.

E. TRACER TEST 5

Tracer Test 5 included pumping Wells 1, 3, 7, and 9 at approximately 26.5 L/min and injecting the total discharge of 106 L/min into Well 5. The pumping began at 1330 on September 13. The injection of 21,238 liters of a chloride solution occurred between 1130 and 1450 on September 14. No initial borehole flowmeter survey was conducted before the tracer injection. Throughout the entire tracer test, groundwater samples were taken from most of the 27 wells with the type of multilevel sampler shown in Figure E5. During the tracer test, borehole flowmeter surveys were conducted in the monitoring wells. Tracer Test 5 lasted for approximately 170 hours and ended on September 21 at 0900.